

MASTER OF SCIENCE THESIS

AE5810

Air Launch versus Ground Launch: a Multidisciplinary Design Optimization Study of Expendable Launch Vehicles on Cost and Performance

M.W. van Kesteren

November 18th, 2013

Faculty of Aerospace Engineering · Delft University of Technology

Air Launch versus Ground Launch: a Multidisciplinary Design Optimization Study of Expendable Launch Vehicles on Cost and Performance

MASTER OF SCIENCE THESIS

For obtaining the degree of Master of Science in Aerospace
Engineering at Delft University of Technology

M.W. van Kesteren

November 18th, 2013

M.W. van Kesteren
Study number: 1356763

DELFT UNIVERSITY OF TECHNOLOGY
DEPARTMENT OF
ASTRODYNAMICS AND SPACE MISSIONS

The undersigned hereby certify that they have read and recommend to the Faculty of Aerospace Engineering for acceptance a thesis entitled “**Air Launch versus Ground Launch: a Multidisciplinary Design Optimization Study of Expendable Launch Vehicles on Cost and Performance**” by **M.W. van Kesteren** in partial fulfillment of the requirements for the degree of **Master of Science**.

Dated: November 18th, 2013

Head of department:

Prof. Ir. B.A.C. Ambrosius

Supervisor:

Ir. M.C. Naeije

Supervisor:

Ir. B.T.C. Zandbergen

Member, Thesis Committee:

Ir. A.J.P. van Kleef

Abstract

This work reports a thesis research done in the field of air launch at TU Delft's faculty of Aerospace Engineering. During the entire era of space flight air launch is seen as a very promising concept. Despite its claimed advantages, air launch is up till now only a marginal success with the Pegasus launch vehicle from Orbital Sciences. In this study is investigated for which conditions expendable air launched vehicles can achieve a performance gain compared with expendable ground launched vehicles. The scope of this study is limited to near-term feasible concepts. Therefore, only existing carrier aircraft that require minimum modifications are evaluated. Solid propelled rockets are more promising for air launch than liquid rockets, therefore, only solid propelled rockets are considered during this study. Potential markets for launch vehicles with a 10 kg and 2,000 kg payload capability to low earth orbit are identified. The influences of different launch parameters and the presence of a wing on the potential performance gain of air launch are investigated.

A Multidisciplinary Design Optimization (MDO) is deemed the most suitable approach for the comparison between air launch and ground launch. In earlier thesis work performed at the TU Delft an MDO tool in the Tudat framework is developed by Jan Vandamme. This tool is used as a starting point for this work but is heavily modified and expanded. For the typical disciplines of launch vehicle design models are developed and validated. The Multidisciplinary Design Analysis (MDA) and MDO validation tested the ability of the tool to model the design and the trajectory of launch vehicles. During the MDA validation it is shown that the tool is capable to do this for the design as well as for the trajectory. From the MDO validation it can be concluded that the optimized designs have realistic configurations and a lower cost per flight than the designs for the MDA validation.

Air launch can provide a reduction in the cost per flight between 26.9 and 31.3%. For a payload of 10 kg the gross take-off weight (GTOW) of the launch vehicle can be reduced with 63.5-70.1% while this is 33.6-47.4% for the 2,000 kg payload class vehicles. Moreover, air launch reduces the amount of ΔV required to orbit with between 935 and 1,225 $\text{m}\cdot\text{s}^{-1}$ compared to ground launch for a 10 kg payload for subsonic launch conditions. The ΔV advantage of air launch for the 2,000 kg payload class is between 302 and 797 $\text{m}\cdot\text{s}^{-1}$. A three stage launch vehicle is deemed the most suitable for the 10 kg payload class.

Decreasing the release altitude from 15.0 to 10.0 km increases the amount of ΔV that has to be provided with $270 \text{ m}\cdot\text{s}^{-1}$ and results in a higher GTOW and cost per flight. For a wingless launch vehicle horizontal launch is less advantageous than a launch under a positive release flight path angle. The difference in the cost per flight and the GTOW for optimized air launched vehicles for various positive release flight path angles is limited. For the release conditions that are considered for this study small variations in the release velocity do not lead to an additional increase or reduction in velocity losses. Similar trends are observed for the 2,000 kg payload class, however, the relative differences in the cost per flight, GTOW and the ΔV are smaller.

Winged vehicles provide a small cost advantage (2.45%) compared to wingless vehicles for horizontal launch as well as an advantage for the GTOW (19.9%) and the required amount of ΔV to orbit (4.60%). As soon as a winged launch vehicle will be released under a positive flight path angle the cost advantage and the ΔV advantage of the winged configuration will diminish quickly.

For the 10 kg payload class the introduction of the absolute error, E , for the different models causes the largest change in payload mass when E is introduced for the propulsion models and the mass model for the vehicle equipment bay (VEB). The payload mass is the most sensitive to changes in the inert mass and the sliver fraction of the upper stage, the propulsion characteristics and the mass of the VEB. From the Monte-Carlo analysis follows an overprediction of the payload mass as well as the cost per flight for both payload classes.

It can be concluded that for the models used in this tool a regressive burning grain does not enhance the performance of the launch vehicle in terms of the cost per flight, the GTOW and the required amount of ΔV . A constraint for the ratio between web thickness and case diameter is required in order to get a realistic configuration. The introduction of this constraint results in an increase in the cost per flight between 2.34% and 2.47% and the GTOW between 8.51% and 9.00% for the optimized air and ground launched vehicle for the 10 kg payload case. For the 2,000 kg payload most unconstrained designs do not violate this constraint.

Preface

This document concludes my final thesis research that is required to complete my MSc curriculum in the field of Aerospace Engineering. I could have again refer to Blais Pascal as I have done in the preface of my literature study: "I would have written a shorter letter, but I did not have the time". I could also have written here a paeon to the effects of coffee on your productivity or a reflection to the last year where I tried to find a balance between study, work and fun things. The final thing that crossed my mind to write here is the anecdote why the size of a horse determined the width of launch vehicles. I will save you from this dull story and use the rest of this preface to thank the people that supported me during the past year.

I would like to take this moment to thank my supervisors Marc Naeije and Barry Zandbergen who always kept the door open for questions, and helped me to stay focused on the larger picture. The first time I spoke with Barry about a possible subject for a thesis research was early as November 2010. Even before I started my MSc I made clear for myself that I would like to do my thesis research in the field of launch vehicles. After three years nothing is left of my original plan but the fascination for launch vehicles is still there. It is a honor for me that Prof. Ir. Ambrosius will be the head of my examination committee. A word of thanks is reserved for the NLR and especially for Arnaud van Kleef. I would like to thank Arnaud for his enthusiasm, the data he provided and that he offered to be part of the examination committee. I need to thank as well the students (Jan Vandamme and Roel Eerkens), who performed research in the field of air launch before, for their time to talk with me about their work.

A special thanks goes out to my parents, family and friends for supporting me and for helping me enjoy life outside of the study.

Menno van Kesteren

Delft, November 18th, 2013

Contents

Abstract	vii
Preface	viii
List of Figures	xix
List of Tables	xxiv
Nomenclature	xxiv
1 Introduction	1
1.1 Scope Thesis Research	2
1.2 Introduction to Air Launch	4
1.3 Research Question and Objectives	7
1.4 Outline Thesis Research and Report	8
2 Multidisciplinary Design Optimization and Tool Architecture	9
2.1 General Optimization Problem	9
2.2 Multidisciplinary Design Optimization	10
2.3 Optimization Algorithms	12
2.4 Objective Function and Constraint Handling	13
2.5 Tool Architecture	14
3 Flight Mechanics	17
3.1 State Variables	17
3.2 Reference Frames	19
3.3 Equations of Motion for a Launch Vehicle	21

4	Environment	23
4.1	Gravitational Model	23
4.2	Atmospheric Model	24
5	Propulsion	27
5.1	Thrust Model	27
5.2	Modeling Solid Rocket Propulsion	29
5.3	Validation Propulsion Model	32
5.4	Propulsion Constraints	36
6	Launch Vehicle Modeling	37
6.1	Geometry Models	37
6.2	Mass Models	42
6.3	Launch Vehicle Constraints	52
7	Aerodynamics	53
7.1	Aerodynamic Model	53
7.2	Missile Datcom	54
7.3	Validation Aerodynamic Model	57
8	Trajectory	61
8.1	Trajectory Optimization with Heuristic Algorithms	61
8.2	Velocity Losses	63
8.3	Numerical Integration	63
8.4	Validation Trajectory Model	65
8.5	Trajectory Constraints	68
9	Cost	71
9.1	Cost Model	71
9.2	Development Cost	73
9.3	Production Cost	75
9.4	Operations Cost	77
9.5	Validation Cost Model	79
10	Verification and Validation	81
10.1	Validation ALOSS Launch Vehicle	81
10.2	Multidisciplinary Design Analysis Validation	83
10.3	Multidisciplinary Design Optimization Validation	88
11	Results	95
11.1	10 kg Payload Class	95
11.2	2,000 kg Payload Class	105
11.3	Application of the Tool: Launch from Andøya	109

12 Sensitivity Analysis	113
12.1 One-at-a-time Approach	113
12.2 Monte-Carlo Analysis	125
12.3 Effects of a Regressive Burning Grain	130
12.4 Effect of the Implementation of a Constraint for the Web Thickness Case Diameter Ratio	131
12.5 Different Heuristic Optimization Algorithms	133
13 Conclusions and Recommendations	135
13.1 Conclusions	135
13.2 Recommendations	138
A Original Thesis Research Proposal	141
A.1 Research Question and Objectives	141
A.2 Preliminary Architecture Multidisciplinary Design Optimization	142
A.3 Assumptions and Limitations for this study	145
A.4 Thesis Work Packages and Schedule	145
B ALOSS Launch Vehicle Characteristics	149
C Thermodynamic Properties of Solid Propellants	151
D Solid Rocket Stage Database	153
E Propulsion Validation Data	157
F Launch Vehicle Validation Data	159
G Aerodynamic Launcher Configuration Database	163
H Cost Model Validation Data	165
I Multidisciplinary Design Optimization Validation Data	169
I.1 Taurus	169
I.2 Pegasus XL	171
J Appendix to the Results	175
J.1 10 kg Payload Class	175
J.2 2,000 kg Payload Class	186
J.3 Launch from Andøya	195
J.4 Effects of a Regressive Burning Grain	199
J.5 Effect of the Implementation of a Constraint for the Web Thickness Case Diameter Ratio	201
References	205

List of Figures

1.1	Captures from the shuttle launches in "Superman Returns" and "Moonraker".	1
1.2	Comparison of nozzle expansion behavior [78].	5
1.3	F-16 External 370 gallon fuel tank [106]	6
2.1	Classical decomposition of the different disciplines in launch vehicle design [5].	11
2.2	Top level overview of the MDO tool used for this thesis research.	16
3.1	Spherical coordinates [69].	18
3.2	Orbital elements [21].	19
3.3	Relation between the inertial and rotating geocentric frame (I and R) and the vertical frame (V) [69].	20
3.4	Rotation from reference frame A to reference frame B [70].	21
3.5	Earth-centered, Earth-fixed reference frame (adapted from [5]).	22
5.1	Relation between the propulsion frame (index P) and the body frame (index B). All angles are indicated in positive direction [69].	29
5.2	Thrust and pressure over burn time for the Star 26 and CASTOR 120 SRM [4].	30
5.3	Absolute error [%] in calculated vacuum thrust compared with the actual vacuum thrust.	34
5.4	Absolute error [%] in calculated vacuum Isp compared with the actual vacuum Isp.	34
5.5	Absolute error [%] in calculated propellant mass compared with the actual propellant mass.	35
6.1	Impression of the launch vehicle model.	37
6.2	Schematic of the nozzle convergent (left) and nozzle divergent (right) for a conical nozzle [120].	38

6.3	Absolute mean error [%] in calculated length of the stage compared with the actual length.	39
6.4	Geometry of a non-winged three stage launch vehicle (not to scale). . . .	40
6.5	Geometry of a tangent ogive nose cone [73].	41
6.6	Impression of the P-POD and the fairing of VEGA.	41
6.7	Geometry model winged launch vehicle (only the first stage is shown). . .	42
6.8	Mass breakdown structure of the launch vehicle.	43
6.9	Correlation between nozzle mass and vacuum thrust for large SRMs ($T_{vac} > 200\text{kN}$).	44
6.10	Correlation between nozzle mass and vacuum thrust for small SRMs with TVC ($T_{vac} < 200\text{kN}$).	44
6.11	Correlation between nozzle mass and vacuum thrust for small SRMs without TVC ($T_{vac} < 200\text{kN}$).	45
6.12	Absolute error [%] in calculated nozzle mass compared with actual nozzle mass.	45
6.13	Geometry of the motor case.	46
6.14	Absolute error [%] in calculated motor case mass compared with the actual motor case mass.	47
6.15	Simplified geometry of the fairing for the mass calculations.	49
6.16	Correlation between the mass of the VEB and the total inert vehicle mass. .	50
6.17	Absolute error [%] in calculated total inert mass compared with the actual total inert mass.	52
7.1	Aerodynamic reference frame (angles are indicated positive) [31].	54
7.2	The different geometry and flights conditions that can be evaluated by Missile Datcom [111].	55
7.3	Overview of methods used for axisymmetric body-alone aerodynamics by Missile Datcom [111].	55
7.4	Predicted drag coefficient at various Mach numbers by Missile Datcom at $\alpha=0^\circ$ for Vega's actual shape and for a vehicle with an uniform diameter. .	56
7.5	Wind tunnel results versus Missile Datcom and Aeroprediction 98 predictions for a body alone configuration for Mach 2.0 [95].	58
7.6	Predicted drag coefficient at various Mach numbers by the NLR and Missile Datcom at $\alpha=0^\circ$ for the ALOSS launch vehicle.	58
7.7	Wind tunnel results versus Missile Datcom predictions for Pegasus for Mach 2.0 (reference area is the wing area of Pegasus). Wind tunnel data from [66].	59
8.1	The parametric control law for the pitch angle for the MDA validation of Taurus for the first three stages.	62
8.2	Visualization of the four slopes used for the Runge-Kutta 4 integrator [76]. .	65
8.3	Comparison of the thrust and mass versus time of the tool and NLR's tool for the ALOSS F-16 case.	66

8.4	Comparison of the drag force and angle of attack of the tool and NLR's tool for the ALOSS F-16 case.	66
8.5	Comparison of the altitude and velocity versus time of the tool and NLR's tool for the ALOSS F-16 case.	67
8.6	Comparison of the pitch and flight path angle of the tool and NLR's tool for the ALOSS F-16 case.	67
9.1	TransCost Model breakdown [99].	72
9.2	Breakdown of the final cost model.	73
9.3	Correlation between propellant mass and TFU production cost for small SRMs.	75
9.4	Production cost TFU as function of propellant mass using the three different CERs.	76
9.5	Comparison between several cost for conventional and horizontal launch [19].	78
9.6	The advertised cost per flight, and the estimated cost by TransCost, Martino's model and the final model.	79
9.7	Error in estimated cost per flight for TransCost, Martino's model and the final model.	80
11.1	GTOW versus cost per flight for all valid optimized vehicles for the ALOSS case.	96
11.2	Burn time versus vacuum thrust for all valid optimized vehicles for the ALOSS case.	97
11.3	Inert mass versus propellant mass for all valid optimized vehicles for the ALOSS case.	97
11.4	Altitude and velocity versus time for the several ALOSS cases.	98
11.5	Pitch angle and flight path angle for several ALOSS cases.	99
11.6	Drag and lift force for several ALOSS cases.	99
11.7	Pitch angle and angle of attack for the first 100 seconds for the optimized ground launched vehicle and optimized air launched vehicles for various release flight path angles.	101
11.8	Drag and lift force for the optimized ground launched vehicle and optimized vehicles for various release flight path angles.	101
11.9	Thrust force and pitch angle versus time for the optimized air launched vehicles for different release altitudes and velocities.	103
11.10	Final value for the semi-major axis and eccentricity for all optimized two stage vehicles (green area indicates the tolerances for orbit).	104
11.11	Pitch angle and flight path angle for the three and four stage optimized air launched vehicle.	105
11.12	Angle of attack and bending load versus time for the optimized vehicles or ground launch and horizontal and vertical air launch for the 2,000 kg payload case.	106

11.13	Dynamic pressure and angle of attack versus time for the optimized winged air launched vehicles for the 2,000 kg payload class.	108
11.14	Drag and lift force versus time for the optimized winged air launched vehicles for the 2,000 kg payload class.	109
12.1	Cost per flight versus the total number of launches and learning factor, p , for the optimized air launched and optimized ground launched vehicle for the 10 kg payload class.	120
12.2	Cost per flight versus the total number of launches and learning factor, p , for the optimized wingless and winged air launched and optimized ground launched vehicle for the 2,000 kg payload class.	125
12.3	Scatter plot for the outcomes of the Monte-Carlo analysis for 150 runs for the cost per flight, payload mass and GTOW for the 10 kg payload class.	126
12.4	Scatter plot for the outcomes of the Monte-Carlo analysis for 150 runs for the cost per flight, payload mass and GTOW for the 2,000 kg payload class.	128
12.5	Thrust force and acceleration versus time for the optimized air launched vehicles with constant and regressive thrust.	130
12.6	Evolution of burning area over time [120].	132
12.7	Evolution of the average and best fitness value for different heuristic algorithms over 2,500 generations.	134
A.1	Overview preliminary architecture MDO for the thesis research.	143
A.2	Thesis schedule.	148
B.1	Impression of the ALOSS launch vehicle [106]	149
C.1	Input file CEA	151
I.1	Comparison of the altitude and velocity versus time for the MDA and MDO validation of Taurus.	170
I.2	Comparison of the thrust and acceleration versus time for the MDA and MDO validation of Taurus.	170
I.3	Comparison of the pitch and flight path angle versus time for the MDA and MDO validation of Taurus.	170
I.4	Comparison of the altitude and velocity versus time for the MDA and MDO validation of Pegasus XL.	173
I.5	Comparison of the thrust and acceleration versus time for the MDA and MDO validation of Pegasus XL.	173
I.6	Comparison of the pitch and flight path angle versus time for the MDA and MDO validation of Pegasus XL.	173
J.1	Thrust force and acceleration versus time for the optimized vehicles for the ALOSS case.	176
J.2	Dynamic pressure and angle of attack versus time for the optimized vehicles for the ALOSS case.	176

J.3	Bending load and mass versus time for the optimized vehicles for the ALOSS case.	176
J.4	Altitude and velocity versus time for the optimized ground launched vehicle and optimized air launched vehicles for various release flight path angles.	178
J.5	Pitch angle and flight path angle for the optimized ground launched vehicle and optimized air launched vehicles for various release flight path angles.	178
J.6	Altitude and velocity versus time for the optimized ground launched vehicle and optimized air launched vehicles for various release flight path angles.	179
J.7	Dynamic pressure and angle of attack versus time for the optimized ground launched vehicle and optimized air launched vehicles for various release flight path angles.	179
J.8	Bending load and mass versus time for the optimized ground launched vehicle and optimized air launched vehicles for various release flight path angles.	179
J.9	Altitude and velocity versus time for the optimized air launched vehicles for various release altitudes and velocities.	181
J.10	Drag and lift force for the optimized air launched vehicles for various release altitudes and velocities.	181
J.11	Flight path angle and acceleration versus time for the optimized air launched vehicles for various release altitudes and velocities.	182
J.12	Dynamic pressure and angle of attack versus time for the optimized air launched vehicles for various release altitudes and velocities.	182
J.13	Bending load and mass versus time for the optimized air launched vehicles for various release altitudes and velocities.	182
J.14	Altitude and velocity versus time for the three and four stage optimized air launched vehicle.	185
J.15	Drag and lift force for the three and four stage optimized air launched vehicle.	185
J.16	Thrust force and acceleration versus time for the three and four stage optimized air launched vehicle.	185
J.17	Dynamic pressure and angle of attack versus time for the three and four stage optimized air launched vehicle.	186
J.18	Bending load and mass versus time for the three and four stage optimized air launched vehicle.	186
J.19	Altitude and velocity versus time for the optimized vehicles for ground launch and horizontal and vertical air launch conditions for the 2,000 kg payload class.	188
J.20	Pitch angle and flight path angle for ground launch and horizontal and vertical air launch conditions for the 2,000 kg payload class.	188
J.21	Drag and lift force for the optimized vehicles for ground launch and horizontal and vertical air launch conditions for the 2,000 kg payload class.	188
J.22	Thrust force and acceleration versus time for the optimized vehicles for ground launch and horizontal and vertical air launch conditions for the 2,000 kg payload class.	189

J.23	Dynamic pressure and mass versus time for the optimized vehicles for ground launch and horizontal and vertical air launch conditions for the 2,000 kg payload class.	189
J.24	Altitude and velocity versus time for the optimized air launched vehicles for various release altitudes and velocities for the 2,000 kg payload class. .	190
J.25	Drag and lift force versus time for the optimized air launched vehicles for various release altitudes and velocities for the 2,000 kg payload class. . . .	190
J.26	Pitch angle and flight path angle versus time for the optimized air launched vehicles for various release altitudes and velocities for the 2,000 kg payload class.	190
J.27	Thrust force and acceleration versus time for the optimized air launched vehicles for various release altitudes and velocities for the 2,000 kg payload class.	192
J.28	Dynamic pressure and angle of attack versus time for the optimized air launched vehicles for various release altitudes and velocities for the 2,000 kg payload class.	192
J.29	Bending load and mass versus time for the optimized air launched vehicles for various release altitudes and velocities for the 2,000 kg payload class. .	192
J.30	Altitude and velocity versus time for the optimized winged air launched vehicles for the 2,000 kg payload class.	193
J.31	Pitch angle and flight path angle versus time for the optimized winged air launched vehicles for the 2,000 kg payload class.	193
J.32	Thrust force and acceleration versus time for the optimized winged air launched vehicles for the 2,000 kg payload class.	195
J.33	Bending load and mass versus time for the optimized winged air launched vehicles for the 2,000 kg payload class.	195
J.34	Altitude and velocity versus time for the optimized vehicles for the launch from Andøya.	196
J.35	Drag and lift force versus time for the optimized vehicles for the launch from Andøya.	196
J.36	Pitch angle and flight path angle versus time for the optimized vehicles for the launch from Andøya.	196
J.37	Thrust force and acceleration versus time for the optimized vehicles for the launch from Andøya.	198
J.38	Dynamic pressure and angle of attack versus time for the optimized vehicles for the launch from Andøya.	198
J.39	Bending load and mass versus time for the optimized vehicles for the launch from Andøya.	198
J.40	Altitude and velocity versus time for the optimized air launched vehicle with a regressive burning third stage.	199
J.41	Pitch angle and flight path angle for the optimized air launched vehicle with a regressive burning third stage.	199
J.42	Drag and lift force for the optimized air launched vehicle with a regressive burning third stage.	200

J.43	Dynamic pressure and angle of attack versus time for the optimized air launched vehicle with a regressive burning third stage.	201
J.44	Bending load and mass versus time for the optimized air launched vehicle with a regressive burning third stage.	201
J.45	Altitude and velocity versus time for the optimized vehicles with or without the $\frac{2 \cdot w}{D_{case}}$ constraint.	202
J.46	Drag and lift force versus time for the optimized vehicles with or without the $\frac{2 \cdot w}{D_{case}}$ constraint.	202
J.47	Pitch angle and flight path angle versus time for the optimized vehicles with or without the $\frac{2 \cdot w}{D_{case}}$ constraint.	202
J.48	Thrust force and acceleration versus time for the optimized vehicles with or without the $\frac{2 \cdot w}{D_{case}}$ constraint.	204
J.49	Dynamic pressure and angle of attack versus time for the optimized vehicles with or without the $\frac{2 \cdot w}{D_{case}}$ constraint.	204
J.50	Bending load and mass versus time for the optimized vehicles with or without the $\frac{2 \cdot w}{D_{case}}$ constraint.	204

List of Tables

1.1	Release conditions that are investigated in this thesis research.	8
4.1	Reference heights and temperature gradients for the different layers of the US Standard Atmosphere 1976 (adapted from [20]).	25
5.1	Design variables for the SRM.	30
5.2	Statistical figures of the error in the estimation of the most relevant parameters for the propulsion model.	36
6.1	Statistical figures of the error in the estimation of the stage's length. . . .	39
6.2	Statistical figures of the error in the estimation of the nozzle mass.	45
6.3	Statistical figures of the error in the estimation of the motor case mass. . .	48
6.4	Statistical figures of the error in the estimation of the interstage mass. . .	49
6.5	Statistical figures of the error in the estimation of the fairing mass.	50
6.6	Statistical figures of the error in the estimation of the VEB mass.	51
6.7	Statistical figures of the error in the estimation of the total inert mass. . .	51
7.1	Mach numbers and angles of attack evaluated in Missile Datcom for this study.	57
8.1	Final altitude of the ALOSS F-16 case for different step sizes for the Runge-Kutta 4 integrator.	68
9.1	Development system engineering correction factor, f_0 , for different launch vehicle configurations.	74
9.2	Development standard factor, f_1 , for different project types [61].	74
9.3	Estimated cost for the acquisition, modification and testing of a Boeing 747-400F to a carrier aircraft [6].	74

9.4	Statistical figures of the error in the estimation of the launch cost for the three different cost models.	80
10.1	Characteristics of the stages for MDA validation for the ALOSS launch vehicle.	82
10.2	Mass properties for MDA validation for the ALOSS launch vehicle (all data from [106]).	83
10.3	Summary of the MDA vehicle output parameters for Taurus compared with the actual values for Taurus.	84
10.4	Summary of the MDA trajectory parameters for Taurus compared with the actual values for Taurus.	85
10.5	Summary of the MDA vehicle output parameters for Pegasus XL compared with the actual values for Pegasus XL.	87
10.6	Summary of the MDA trajectory parameters for Pegasus XL compared with the actual values for Pegasus XL.	88
10.7	Summary of the MDO vehicle output parameters for Taurus compared with the MDA vehicle output parameters.	89
10.8	Summary of the MDO trajectory parameters for Taurus compared with the MDA trajectory parameters.	90
10.9	Summary of the MDO vehicle output parameters for Pegasus XL compared with the MDA vehicle output parameters.	92
10.10	Summary of the MDO trajectory parameters for Pegasus XL compared with the MDA trajectory parameters.	93
11.1	Summary of the most important characteristics for the optimized ALOSS case.	98
11.2	Summary of the most important characteristics for the optimized ground launched vehicle and the optimized vehicles for various release flight path angles.	100
11.3	Summary of the most important characteristics for the optimized air launched vehicles for various release altitudes and velocities.	102
11.4	Summary of the most important characteristics for the optimized three and four stage air launched vehicles.	104
11.5	Summary of the most important characteristics for the optimized vehicles for ground launch and horizontal and vertical air launch for the 2,000 kg payload case.	106
11.6	Summary of the most important characteristics for different release altitudes and velocities for the 2,000 kg payload class.	107
11.7	Summary of the most important characteristics for optimized winged air launched vehicles for various release flight path angles.	108
11.8	Summary of the most important characteristics for the optimized air and ground launched vehicle with a payload mass of 12.5 kg from a launch from ARR to a 500 km polar orbit.	110
11.9	Vehicle characteristics for a launch vehicle consisting of COTS SRMs. . .	111

12.1	Results of the OAT approach for the best air launched vehicle for $+E$. . .	114
12.2	Results of the OAT approach for the best air launched vehicle for $-E$. . .	115
12.3	Results for OAT approach for different materials for the motor case. . . .	117
12.4	Results sensitivity analysis of the OAT approach for the 10 kg payload class with a 10% deviation for the linear varying parameters in the cost model.	118
12.5	Results sensitivity analysis for a change in the annual launch rate for the 10 kg payload class.	119
12.6	Results sensitivity analysis for a change in the total number of launches for the 10 kg payload class.	119
12.7	Results sensitivity analysis for a change in the learning factor, p	120
12.8	Results of the OAT approach for the best air launched vehicle for the 2,000 kg payload class for $+E$	121
12.9	Results of the OAT approach for the best air launched vehicle for the 2,000 kg payload class for $-E$	122
12.10	Results sensitivity analysis of the OAT approach for the 2,000 kg payload class with a 10% deviation for the linear varying parameters in the cost model.	123
12.11	Results sensitivity analysis for a change in the annual launch rate for the 2,000 kg payload class.	123
12.12	Results sensitivity analysis for a change in the annual launch rate for the 2,000 kg payload class.	124
12.13	Results sensitivity analysis for a change in the learning factor, p , for the 2,000 kg payload class.	124
12.14	Results for Monte-Carlo analysis for 150 runs for the design parameters.	126
12.15	Results for Monte-Carlo analysis for the cost parameters that are different for air and ground launch for varying deviations for the mean.	127
12.16	Results for Monte-Carlo analysis for 150 runs for the design parameters for the 2,000 kg payload class.	128
12.17	Results for Monte-Carlo analysis for the cost parameters that are different for wingless air launched, winged air launched and ground launched vehicles for the 2,000 kg payload class for varying deviations for the mean.	129
12.18	Summary of the most important characteristics for the optimized vehicles with or without the $\frac{2 \cdot w}{D_{case}}$ constraint.	133
12.19	Comparison of the cost per flight obtained for different weights and crossover probabilities of the DE.	134
B.1	Characteristics of the stages for ALOSS (all data from [106]).	150
C.1	Thermodynamic properties of the HTBP1912 propellant for various chamber pressures.	152
D.1	Solid Rocket Stage Database (1/2).	154
D.2	Solid Rocket Stage Database (2/2).	155

E.1	Validation data for the propulsion elements of the SRM stages.	157
F.1	Validation data for the fairing mass model.	159
F.2	Validation data for the interstage mass model.	159
F.3	Validation data for the VEB mass model.	160
F.4	Validation data for the total length of the stages.	160
F.5	Validation data for the masses of the different SRM stage components. . .	161
G.1	Configuration matrix Missile Datcom for small launch vehicles.	163
G.2	Configuration matrix Missile Datcom for large launch vehicles.	164
G.3	Configuration matrix Missile Datcom for winged large launch vehicles (diameters in the database are the same as in Table G.2).	164
H.1	Cost data used for the development of a CER for the production cost of small SRMs [107, 94].	165
H.2	Launch vehicle characteristics for the validation of the cost model.	166
H.3	Correction factors and additional elements used for the validation of the cost model.	166
H.4	Outcome of the validation of the three cost models for existing launch vehicles.	167
I.1	Input parameters MDA validation Taurus.	169
I.2	Vehicle characteristics for the MDO validation for Taurus.	171
I.3	Input parameters MDA validation Pegasus XL.	171
I.4	Vehicle characteristics for the MDO validation for Pegasus XL.	172
J.1	Characteristics for the optimized vehicles for the ALOSS case.	177
J.2	Characteristics for the optimized ground launched vehicle and the optimized vehicles for various release flight path angles.	180
J.3	Characteristics for the optimized vehicles for different release altitude and velocities.	183
J.4	Characteristics for the optimized four stage air launched vehicle.	184
J.5	Characteristics for the optimized vehicles for ground launch and horizontal and vertical air launch conditions for the 2,000 kg payload class.	187
J.6	Characteristics for the optimized air launched vehicles for different release altitudes and velocities for the 2,000 kg payload class.	191
J.7	Characteristics for the optimized winged air launched vehicles for the 2,000 kg payload class.	194
J.8	Characteristics for the optimized vehicles for the launch from Andøya. . .	197
J.9	Characteristics for the optimized air launched vehicle with a regressive burning third stage.	200
J.10	Characteristics for the optimized vehicles with the $\frac{2 \cdot w}{D_{case}}$ constraint.	203

Nomenclature

Latin Symbols

a	Semimajor axis	[m]
A_e	Exit area of the nozzle	[m ²]
a_x	Axial acceleration	[m s ⁻²]
b	Layer in US 1976 Standard Atmosphere	[-]
c^*	Characteristic velocity	[m s ⁻¹]
C_D	Drag coefficient	[-]
C_F°	Thrust coefficient	[-]
C_L	Lift coefficient	[-]
C_S	Side force coefficient	[-]
D	Drag force	[N]
D_{case}	Diameter motor case	[m]
D_{exit}	Diameter nozzle exit	[m]
E	Absolute mean error	[%]
e	Eccentricity	[-]
F	Objective function	[-]
\mathbf{F}_G	Gravitational force	[N]
f	Correction factor for cost	[-]
g_0	Gravitational acceleration on Earth	[m s ⁻²]
G	Universal gravitational constant	[m ³ kg ⁻¹ s ⁻²]
H	Geopotential altitude	[m']
H_b	Geopotential altitude of layer b	[m']
i	Inclination	[deg]

$I_{sp_{vac}}$	Vacuum specific impulse	[s]
j	Number of inequality constraints	[-]
k	Boltzmann constant	[Nm K ⁻¹]
k	Correction factor for the material of the interstage	[-]
L	Annual launch rate	[-]
L	Lift force	[N]
L_{case}	Length motor case	[m]
L_{con}	Length nozzle convergent	[m]
L_{div}	Length nozzle divergent	[m]
$L_{fairing}$	Length fairing	[m]
L_{in}	Length interstage	[m]
l	Total number of launches	[-]
$L_{M,b}$	Gradient of molecular temperature in layer b	[K km ⁻¹]
L_{tot}	Total length launch vehicle	[m]
\dot{m}	Mass flow	[kg s ⁻¹]
M	Molecular mass	[kg mol ⁻¹]
M_E	Mass Earth	[kg]
M_e	Burn-out mass	[kg]
M	Mass	[kg]
M	Mean anomaly	[deg]
N_A	Avogadro's constant	[mol ⁻¹]
n	Burning rate exponent	[-]
n	Number of motors evaluated	[-]
p	Learning factor	[-]
p_a	Ambient pressure	[bar]
P_b	Pressure of layer b	[Pa]
p_e	Exit pressure	[bar]
q	Mass flow rate	[kg s ⁻¹]
\dot{Q}	Heat flux	[W m ⁻²]
Q_i	Complexity of stage i	[-]
q_{max}	Maximum dynamic pressure	[kPa]
\mathbf{r}	Distance vector	[m]
R_A	Universal gas constant	[J kg ⁻¹ mol ⁻¹]
R	Specific gas constant	[J kg ⁻¹ mol ⁻¹]
r	Distance	[m]
r	Regression rate	[mm s ⁻¹]
R_u	Longitudinal radius of the throat	[deg]
S	Side force	[N]

S_{ref}	Aerodynamic reference surface	[m ²]
T	Temperature	[T]
T	Thrust force	[N]
T_c	Chamber temperature	[K]
T_M	Molecular temperature	[K]
$T_{M,b}$	Molecular temperature in layer b	[K]
T_{vac}	Thrust force in vacuum	[N]
U_{eqvac}	Equivalent exhaust velocity in vacuum	[m s ⁻¹]
U_e	Exhaust velocity	[m s ⁻¹]
V_G	Ground speed	[m s ⁻¹]
w	Web thickness	[mm]
\mathbf{x}	Vector of independent variables	[-]
Z	Geometric altitude	[m]

Greek Symbols

α	Angle of attack	[deg]
α_{max}	Maximum angle of attack	[deg]
β	Nozzle convergent half angle	[deg]
Γ	Vandenkerckhove function	[-]
γ	Ratio of specific heats	[-]
γ	Flight path angle	[deg]
δ	Latitude	[deg]
ϵ	Expansion ratio	[-]
ϵ_T	Elevation angle thrust force	[deg]
θ	Pitch angle	[deg]
θ	True anomaly	[deg]
$\dot{\theta}_{max}$	Maximum pitch rate	[deg s ⁻¹]
θ	Nozzle divergent half angle	[deg]
λ	Taper ratio	[-]
μ	Bank angle	[deg]
μ	Mean error	[%]
ξ	Correction factor for the thrust	[-]
ρ	Density	[kg m ⁻³]
σ	Standard deviation of the error	[%]
τ	Longitude	[deg]
χ	Heading	[deg]

ψ_T	Azimuth angle thrust force	[deg]
Ω	Longitude of the ascending node	[deg]
ω_E	Angular velocity of the Earth	[deg s ⁻¹]
ω	Argument of perigee	[deg]

Abbreviations

ALOSS	Affordable Launch Opportunities for Small Satellites
AP	Ammonium perchlorate
ARR	Andøya Rocket Range
CEA	NASA Glenn Equilibrium Program
CER	Cost Estimation Relationship
CFRP	Carbon Fibre Reinforced Plastic
CONOPS	Concept of Operations
COTS	Commercial of-the-shelf
DA	Direct ascent
DoD	Department of Defence
DoF	Degree of Freedom
ECTS	European Credit Transfer System
EPDM	Ethylene-Propylene-Diene Copolymer
ESA	European Space Agency
FF	Filling Factor
FFI	Norwegian Defence Research Establishment
FY	Fiscal Year
GTOW	Gross Take-Off Weight
HLS	Horizontal Launch Study
HPA	High Performance Aircraft
HTA	Hohmann Transfer Ascent
HTPB	Hydroxyl terminated polybutadiene
ICBM	Intercontinental Ballistic Missile
ITAR	International Traffic in Arms Regulations
LEO	Low Earth Orbit
MDF	Multi Discipline Feasible
MDO	Multidisciplinary Design Optimization
MER	Mass Estimation Relationship
MoD	Ministry of Defence
MYr	Man-Years
NASA	National Aeronautics and Space Administration

NLR	Nationaal Lucht- en Ruimtevaartlaboratorium
OAT	One-at-a-time
ORS	Operationally Responsive Space
PaGMO	Parallel Global Multiobjective Optimizer
P-POD	Poly Picosatellite Orbital Deployer
PSO	Particle Swarm Optimization
RLV	Reusable Launch Vehicle
SEE	Standard Error of Estimate
SQP	Sequential Quadratic Programming
SRM	Solid Rocket Motor
SSTO	Single-stage-to-orbit
TFU	Theoretical First Unit
Tudat	TU Delft Astrodynamics Toolbox
TVC	Thrust Vectoring Control
US	United States
VEB	Vehicle Equipment Bay

Chapter 1

Introduction

For many decades the movie industry is highly interested in air launch. Air launch is the launch of a rocket from an aircraft or other reusable platform. Every James Bond fan remembers the air launch of a Space Shuttle from a Boeing 747 during the opening scene of the Bond movie "Moonraker". A more recent example can be found in the movie "Superman Returns" where a small shuttle is launched from the back of a Boeing 777. The fact that during the era of spaceflight at least 136 studies to air launch were conducted [6] and currently still a lot of concepts are in development show that air launch is also seen as a promising concept in the scientific world. Two examples of recent concepts are the GOLauncher from Generation Orbit, which has very recently been selected to launch a group of three 3U CubeSats to orbit for NASA [25, 68], and the massive Stratolauncher from Stratolaunch Systems [97]. This is because besides the initial altitude and velocity for the launch vehicle air launch provides additional advantages (see Section 1.2). Over the last 23 years the expendable air launched vehicle Pegasus completed 37 successful missions. The question rises why air launch, despite its promising elements, is up till now only a marginal success. Since there is only one operational air launched vehicle and Pegasus is one of the most expensive ways to orbit in terms of €/kg payload [9].



Figure 1.1: Captures from the shuttle launches in "Superman Returns" and "Moonraker".

This report presents the work done for the 42 ECTS (1,176 hours) AE5810 Master Thesis and concludes the MSc curriculum of Aerospace Engineering at the TU Delft. As prede-

cessor for this thesis research a 12 ECTS (336 hours) literature study about air launch has been conducted [103]. In this work is often referred to this literature study and the original thesis research proposal can be found in Appendix A.

This chapter starts with the scope of this thesis research. Next a brief introduction to air launch is given. After that the research question and objectives for this thesis research are identified. The last section of this chapter provides the outline for this thesis research and this report.

1.1 Scope Thesis Research

Air launch spans a variety of concepts: from expendable to reusable launch vehicles, from rocket propulsion to airbreathing, from balloons to hypersonic waves-riders as carrier vehicles. Investigating all these concepts during a single thesis research is too much. Therefore, during the development of the initial research plan [104] and literature study [103] it was decided to limit this study to near term (1-3 years) feasible concepts for expendable launch vehicles. According to the recently conducted Horizontal Launch Study (HLS) from NASA there are three air launch concepts that show near term feasibility [6]. The first one is a modified fighter jet that carries a small multistage solid rocket (payload mass less than 250 kg) to high subsonic or supersonic release conditions. The second and third option are a modified commercial jet that carries respectively a multistage solid or liquid rocket (payload mass 250 kg to 4,500 kg) to subsonic release conditions.

This study will be limited to the use of solid rockets. The first reason for this is that solid rockets are in general cheaper than liquid rockets [52]. Next the higher accelerations of solid rockets in comparison to liquid rockets increase the significance of drag and, therefore, solid rockets would have more benefit from air launch than liquid rockets [116]. Also the boil-off¹ problem of cryogenic propellants is a disadvantage for (cryogenic) liquid propelled rockets. In addition solid rockets have shown to be able to withstand the sideways g-forces and the high aerodynamic pressure of a horizontal air launch with little increase in weight [89]. This is due to the fact that the motor case of a solid rocket must be sized to withstand the internal pressure of combustion [120]. Also the solid propellant itself provides some structural strength [89].

1.1.1 Potential markets for Air Launch

For the two remaining options different potential markets for air launch are identified in [103]. The first one is the emerging market for nano and microsatellites (1-50 kg)² that is seen by many people as the potential prime market for air launched vehicles [18]. Microsatellites are often launched together with larger satellites because a dedicated launch would be too expensive. However, for the small satellite a major disadvantage is that the primary client dictates the final destination and launch date. This leads to various limitations such that the full potential of the small satellite's mission is not always exploited. Furthermore, at this moment one of the main concerns for nano- and micro satellites is to find a piggyback ride or a spot on a shared launch [38]. Market

¹Boil-off is the vapor loss that happens when the cryogenic propellant is heated.

²There is no universal definition in terms of mass for microsatellites, so, everywhere in this report the applicable mass range is indicated.

analysis for the microsatellite market shows a significant growth in the number of nano- and microsatellite (1-50 kg) [18]. The most recent projections indicate continued growth in the of nano- and microsatellite market, with an estimated number between 121 and 188 nano- and microsatellites that have to be launched in 2020 [24]. In [46] several experts from industry and governmental organizations identify the need of a dedicated nano launch vehicle. In order to make a dedicated launch vehicle competitive with ride shares the cost per flight should be in the order of 1-2 \$M per launch [46].

The second potential market is the market for operationally responsive space (ORS). ORS is the capability to develop satellites within a couple of months and launch them almost instantaneously on demand [39]. Currently, the development time of a conventional satellite is 4-10 years and for a microsatellite (10-100 kg) 1-4 years [40]. The lead times for launch vehicles are between 12 and 36 months [47] and for ride shares these are sometimes even longer. The U.S. DoD does not like this and is therefore investigating ORS. Recently the Dutch Ministry of Defense (MoD) announced that it is investigating ORS in an international context [102]. Air launch removes the need for cumbersome launch facilities and, therefore, fits perfectly for ORS.

The last potential market would be that of the small launch vehicles. According to NASA small launch vehicles have a smaller maximum payload mass than 2,200 kg to low earth orbit (LEO). The main competitors in this market are Dnepr, Minotaur, Rockot, PSLV and the recently introduced Vega. Dnepr, Minotaur and Rockot rely on the use of decommissioned intercontinental ballistic missile engines (ICBM) and therefore can be launched at very competitive prices [115]. However, the stock and lifetimes of those ICBM engines is limited [115]. Hence in the future there will be space for competitors for this class of launch vehicles [36].

In order to estimate the cost of a launch, information about the expected launch rate is required. Based on literature a total number of 120 launches over a period of 20 years (6 launches per year) is considered as the baseline for this study [6, 15].

1.1.2 Research to Air Launch within the Netherlands

In 2011 the Nationaal Lucht- en Ruimtevaartlaboratorium (NLR) conducted the Affordable Launch Opportunities for Small Satellites (ALOSS) study that investigated if the use of an air launched platform for a dedicated launch for nano- and microsatellites (1-20 kg) can fulfill the market needs for a competitive price [106]. A conceptual design for a multistage launcher system was performed using the F-16 fighter jet and the LynX space plane as air launched platforms. The objective for the conceptual design was to put a 10 kg satellite in LEO. The technical details for the analysis of the LynX space plane were omitted from the publicly available report because these contain confidential company information. For the F-16 analysis all technical information is available and will be used later for the validation of the trajectory model in Chapter 8. TU Delft colleague student Roel Eerkens performed his literature study within the NLR and worked on the ALOSS project [29].

In parallel TU Delft student Jan Vandamme investigated the influence of launch assist systems on launch vehicle performance. Vandamme performed a Multidisciplinary Design Optimization (MDO) for a large number of design parameters for a single stage to orbit rocket for different launch altitudes and velocities [108]. MDO uses optimization methods

to solve design problems incorporating a number of different disciplines or subsystems. The use of MDO allows designers to incorporate all relevant disciplines of an engineering problem simultaneously (MDO will be discussed in Chapter 2). The payload to initial mass ratio is optimized in this study for two types of liquid propellants mixtures: kerosene - liquid oxygen and liquid hydrogen - liquid oxygen.

One of main conclusions is that the payload ratio always increases for an increasing launch altitude (maximum 40 km) as it does for an increasing launch velocity (maximum 2,000 m·s⁻¹). The payload ratios rise from 3.1% and 2.1% for the no assist case to a maximum of 19% and 15.1% for the hydrolox and kerolox launchers respectively. The launch velocity has a larger impact on the performance of the launcher than the launch altitude. Low assist flights and flights with a 0° initial flight path angle prefer high-lift trajectories. For a complete overview of all conclusions of Vandamme's study is referred to [108].

Vandamme developed a tool in the Tudat framework and used pieces of code from Frank Engelen, who developed an ascent simulator for unguided rockets [31]. Tudat (TU Delft Astrodynamics Toolbox) is a C++ library that provides functionality to perform astrodynamics simulations [100]. Tudat is developed within the Astrodynamics & Space missions chair at TU Delft's faculty of Aerospace Engineering. It is set up with particular focus on modularity and robustness of code. The library contains several environmental models, reference frames and numerical integrators. In addition there are user developed applications that are available for other users.

1.2 Introduction to Air Launch

A good point to start the discussion about air launch is an attempt to answer the question: why to investigate air launch? The launch of a rocket from an aircraft or other reusable platform provides a reduction in the required ΔV to achieve orbital altitude and velocity. Besides the initial altitude and velocity of the launch vehicle there are more benefits. The benefits of air launch that are explained in this section originate, unless stated otherwise, from [27], [89] and [93]. There are different methods to launch the rockets from the carrier aircraft, these methods are discussed in detail in [103].

First, the initial flight of a conventional ground launched vehicle takes place in the most dense layers of the atmosphere, this causes inefficiencies related to drag loss. A significant portion of the vehicle's propellant is already consumed before it reaches the launch altitude for an air launched vehicle. The effect of drag on the vehicle diminishes as the atmosphere thins during the ascent. At about 10 km altitude, the density of the atmosphere is only 25% of the density at sea level. Beginning the flight at that altitude will drastically reduce the drag loss. In addition, air launch will limit the gravity loss because the time that an air launched vehicle needs for the ascent will be shorter than for a ground launched vehicle. Also the shorter flight time of an air launched vehicle results in a reduction in steering losses.

From literature it can be concluded that air launch provides a reduction in ΔV to orbit of ~ 300 - 950 m·s⁻¹ for subsonic launch conditions [93]. For the launch altitude it can be concluded the higher the better [93]. The optimal release flight path angle is around 30° but has for subsonic release velocities a range of almost $\pm 15^\circ$ [93]. There is no need for a wing for close to optimum release flight path angles, however, for small release flight path

angles a wing can reduce the required ΔV with $\sim 100\text{-}200\text{ m}\cdot\text{s}^{-1}$ compared to a wingless launch vehicle [93]. A wing might also be required for the pitch up since aerodynamic control surfaces are more effective than thrust vectoring control (TVC) [30]. According to [117] is air launch more beneficial for small launch vehicles because for these vehicles drag loss is more significant.

Besides the reduction in losses also a more efficient nozzle design can be utilized for an air launched vehicle because of the lower ambient pressure at launch altitude. Every rocket engine or motor³ is designed for a certain altitude, the so-called design altitude, for this altitude the ambient pressure equals the exit pressure of the nozzle and ideal expansion will occur (see Figure 1.2) [120]. The first stage nozzle design of any ground launched vehicle is typically a compromise due to the range of altitudes it will experience during ascent. The nozzle design of the first stage for an air launched vehicle needs less compromise, since it operates over a smaller range of pressures. In literature it is claimed that only more efficient nozzle expansion can reduce the required amount of ΔV to orbit with $105\text{ to }180\text{ m}\cdot\text{s}^{-1}$ [26, 84].

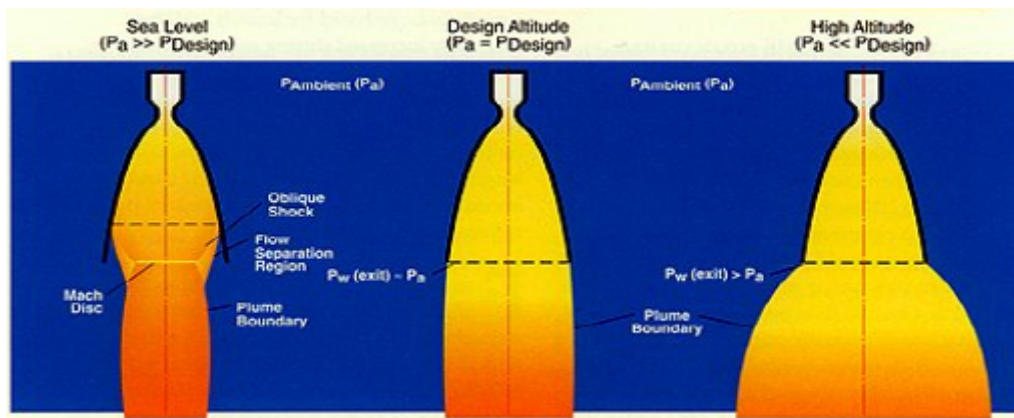


Figure 1.2: Comparison of nozzle expansion behavior [78].

Air launch also reduces the aerodynamic loads on the launch vehicle [50]. As the launcher accelerates it passes through a point at which the maximum dynamic pressure occurs. The dynamic pressure depends on the atmospheric density and velocity of the vehicle. As the density is reduced the loads on the rocket are lessened and the structural design can be simplified. This results in a lower structural mass of the launch vehicle. This advantage is diminished if the air launch is executed at low altitude with high velocity. The last performance advantage of air launch is a reduction in acoustic loads compared with ground launch [57]. Acoustic reflections from the ground can damage the launch vehicle and often requires additional structural reinforcements for the launch vehicle.

In addition to performance benefits air launch has operational benefits. First of all, an air launched vehicle does not require a fixed launch site. Therefore, a wide range of orbital inclinations can be entered due to the mobility of the launch platform. This operational benefit is actually also a performance benefit because the flexibility of launch latitude and azimuth removes the need of expensive, in terms of ΔV , dog-leg maneuvers [114]. Another

³According to [98] the word "motor" is as common to solid rockets as is the word "engine" to liquid rockets.

operational advantage of air launch is that it does not require complex launch facilities. Finally, air launch is not restricted to the extremely demanding weather conditions that are imposed to a ground launch because it can fly to another location or can be launched above the weather.

There are no fundamental disadvantages to air launch. A major problem with air launch is the problem of certification. The ignition of a rocket engine in the proximity of a manned aircraft is the main reason for flight clearance authorities to be reluctant to certify air launched vehicles. A problem with the certification was one of the primary reasons for the cancellation of AirLaunch LLC's QuickReach launch vehicle [90]. The president of SpaceWorks Inc. (involved in the GOLauncher concept) expressed that certification issues are the major threat for the program [17, 25]. Of course, the gross take-off weight (GTOW) and the geometry of an air launched vehicle are restricted by the limitations of the carrier aircraft. Therefore, the growth potential for air launched vehicles is also limited. The final disadvantage is the risky separation of the launch vehicle from the carrier aircraft.

A high performance aircraft (HPA) is considered as carrier aircraft for the 10 kg payload class and a large transport aircraft or airliner for the 2,000 kg payload class. For the HPA the F-16 is selected as carrier aircraft. The overall tank dimensions and mass characteristics of the 370 gallon external fuel tank (see Figure 1.3) of the F-16 are used as limits for 10 kg payload class launch vehicles. The limitations of each of the two aircraft categories and therefore, the constraints for the air launched vehicle are shown in Table 1.1. The limitations for the 2,000 kg payload class launch vehicles are based on average values for proposed carrier aircraft in other air launch studies [103].



Figure 1.3: F-16 External 370 gallon fuel tank [106]

The above mentioned performance and operational benefits imply a potential cost advantage for air launch [6, 19]. First because the claimed performance gain allows a lower GTOW, thus cost, for the launch vehicle when it is air launched. Second, the concepts of operations (CONOPS) of an air launched vehicle does only require limited ground and launch facilities, this will provide another cost advantage [19]. On the other hand, the only operational air launched vehicle, Pegasus XL, is one of the most expensive launch vehicles in terms of €/kg payload. From a preliminary cost survey performed during the literature study followed that air launch is not necessary more expensive than ground

launch. The payload mass to orbit is more important than the launch method (ground or air launch) [103].

1.3 Research Question and Objectives

Based on the outcomes of the literature study it can be concluded that air launch can provide performance benefits to ground launch in terms of the required amount of ΔV and the GTOW [103]. However, those claims are rarely supported by simulation results. Also the potential cost advantages indicated in [103] will be investigated. MDO is proposed as the tool for this research. It is deemed to be the most suitable approach to make a comparison between optimized air launched and ground launched vehicles for various launch conditions based on the research plan and literature study [103, 104] and the work from Vandamme [108, 109]. The software tool developed by Engelen [31] and modified by Vandamme within the Tudat framework is used as a starting point.

For this thesis work the following research question is investigated:

What is the performance gain in terms of cost, gross take-off weight and the amount of ΔV required to orbit for an optimized expendable air launched vehicle in comparison to an optimized expendable ground launched vehicle for different launch parameters (release altitude, velocity and flight path angle), payload classes and the presence of a wing?

The two payload classes that will be evaluated are 10 kg and 2,000 kg to LEO (a circular orbit at 780 km altitude). The vehicle will be launched from the equator in eastward direction. The launch location and target orbit are identical to the ones used in the ALOSS study. The primary objective of this thesis will be to find out if air launch can provide a cost advantage compared with ground launch by using current technology and existing carrier aircraft (that require none or limited modification) in the near term time frame (1-3 years). Additional research objectives will be:

1. Investigate the reduction in GTOW of air launch.
2. Investigate the ΔV advantages of air launch.
3. Investigate the relative importance of the three different launch parameters (release altitude, velocity and flight path angle).
4. Investigate the suitability of air launch for two different payload classes (10 kg and 2,000 kg).
5. Investigate the effects of a wing on the design, trajectory, cost and GTOW of an air launched vehicle.
6. Investigate the sensitivity of the solution to changes of the launch vehicle parameters.

The combinations of launch parameters that will be investigated are given in Table 1.1. As an application of the tool a case for the NLR will be examined. The payload mass will be maximized for a 500 km circular polar orbit from the Andøya Rocket Range (ARR)

in Norway for a launch vehicle that is subjected to ALOSS constraints. A comparison in cost per flight, GTOW and the required amount of ΔV to orbit between air launched and ground launched vehicles will also be made for this case.

Aircraft	F-16	Transport aircraft	Airliner
Air launch method	Captive on bottom	Internally carried	Captive on top
Payload to LEO [kg]	10	2,000	2,000
Release velocities [$\text{m}\cdot\text{s}^{-1}$]	[200, 250, 400]	[0, 150, 200, 250]	[200]
Release altitude [km]	[10.0, 15.0]	10.0	[7.5, 10.0]
Flight path angle [$^{\circ}$]	[0, 25, 50, 75, 90]	[0, 15, 50, 90]	[0, 15]
Wing	No	No	Yes
Max. GTOW [ton]	1.45	105	140
Dimensions [m]	5.5 x 0.67 x 0.67	33.8 x 3.5 x 3.5	33.8 x 3.5 x 3.5

Table 1.1: Release conditions that are investigated in this thesis research.

1.4 Outline Thesis Research and Report

In this section the outline for this thesis research and report will be discussed. This starts with an introduction to MDO and an overview of the tool architecture in Chapter 2. In Chapter 3 the dynamic system for the ascent of a launch vehicle is discussed.

In this thesis research models will be identified for all disciplines of launch vehicle design. These models will be individually verified and validated. This is done first for the environmental models in Chapter 4. Next the propulsion model is described and validated in Chapter 5. The launch vehicle geometry and the mass model will be addressed in Chapter 6. In Chapter 7 the aerodynamic model for launch vehicles and the implementation of the Missile Datcom software are discussed. Chapter 8 deals with a description of the launch vehicle's trajectory. Finally, the cost model is discussed and validated in Chapter 9.

The tool as a whole will be validated during the MDA and MDO validation in Chapter 10. Now the tool is validated results can be generated for the cases described above. These results will be presented in Chapter 11. The next step is to investigate the sensitivity of the results to known and unknown errors in the individual models. The results of the sensitivity analysis are given in Chapter 12. If time was not a constraint the next step would be to refine the models to which the solutions are the most sensitive and generate new and more accurate results. However, this step will not be executed in this research. The report is concluded with Chapter 13 that presents the most important conclusions and recommendations of the thesis research.

Multidisciplinary Design Optimization and Tool Architecture

The tool that will be used for this study is Multidisciplinary Design Optimization (MDO). MDO uses optimization methods to solve design problems incorporating a number of different disciplines or subsystems. The use of MDO allows designers to incorporate all relevant disciplines of an engineering problem simultaneously. MDO and Multidisciplinary Design Analysis (MDA) should be distinguished. MDA refers to a process where multiple discipline analyses are brought to a consistent state. Loosely stated: an MDO optimizes certain design variables that are used in an MDA.

This chapter starts with the introduction of the general optimization problem. In the next section MDO including the aspects of MDO for launch vehicle design are discussed. This is followed by a discussion about optimization algorithms. Next the objective function and constraint handling method are discussed. In the final section of this chapter the architecture of the tool that is used for this study is explained.

2.1 General Optimization Problem

Up to a certain point engineering design is all about optimization, an engineer chooses values for design parameters to improve some objective. However, these design parameters are restricted by constraints and might influence each other. In this section a brief mathematical introduction to optimization is given, all the formulas and terminology used follow from [110].

The general optimization problem is about finding a set of n -independent variables, $\mathbf{x} = (x_1, x_2, \dots, x_N)^T$, that will minimize¹ the outcome of a function that is dependent on those variables, $f(\mathbf{x})$. The problem is constrained by equality constraints, $\mathbf{h}(\mathbf{x})$, and inequality constraints, $\mathbf{g}(\mathbf{x})$. The mathematical formulation for this problem is:

$$\min f(\mathbf{x}) \tag{2.1}$$

¹In case of maximizing $f(\mathbf{x})$, the objective function can be changed to $\min f(-\mathbf{x})$.

Subject to:

$$\mathbf{h}(\mathbf{x}) = 0 \text{ for } i = 1, 2, \dots, j \quad (2.2)$$

$$\mathbf{g}(\mathbf{x}) \geq 0 \text{ for } i = j + 1, \dots, n \quad (2.3)$$

$$x_i^L \leq x_i \leq x_i^U \text{ for } i = 1, 2, \dots, n \quad (2.4)$$

where j is the number of equality constraints and $n - j$ the number of inequality constraints. Equation 2.4 restricts the values of the variables to a lower and upper bound. The number of equality constraints may not exceed the number of variables, however, the number of inequality constraints is not limited. In case that the constraints are not linear the problem is called a non-linear optimization problem.

2.2 Multidisciplinary Design Optimization

In the last decades MDO has grown in popularity. MDO is already incorporated in many engineering fields such as maritime, automotive and especially aerospace engineering. The use of MDO allows designers to incorporate all relevant disciplines of an engineering problem simultaneously. The main motivation for using MDO is that the performance of a multidisciplinary system is not only driven by the performance of the individual disciplines but also by their interactions. However, including more disciplines simultaneously increases the complexity of the problem and therefore the computation time required to find an optimum.

2.2.1 Introduction to Multidisciplinary Design Optimization

In addition to the description of the general optimization problem in Section 2.1, some extra variable and function types have to be defined [5]:

- The design variables, \mathbf{z} . The design variables are the variables that will be changed during the optimization process to find an optimal design.
- The coupling variables, \mathbf{y} . These variables are used to link the different disciplines.
- Coupling functions, $c(x, y, z)$. These functions compute the coupling variables between the disciplines.
- Residual functions, $\mathbf{R}(x, y, z)$. The residual functions quantify the satisfaction of the individual state equations. Ideally, a residual function is zero.

There should be noted that the in Section 2.1 defined state variables, \mathbf{x} , will not directly be optimized. The state variables depend on the design variables.

If the discipline boundaries are ignored, an MDO problem can be seen as a standard constrained nonlinear programming problem as is described in Section 2.1 [62]. The aim is to find values for the design variables, that do not violate the constraints, that will minimize the objective function. The choice of the objective function, the constraints, and

the design variables in a given system are solely chosen by the designer. Each discipline is modeled using a so-called discipline analysis [62]. This discipline analysis often involves a computer program that receives some input values (design variables and other parameters) and calculates some outputs. One of the major challenges of MDO is how to manage the interactions between the different disciplines. The different discipline analyzes are often mutually interdependent: one analysis requires the outputs of other analyzes as input [62]. In addition, the objective and constraint functions depend in general on both the design variables and the analysis outputs from the different disciplines.

If this interdependence is taken into account this results into a more accurate representation of the behavior of the system. An MDO architecture can be defined as: *"a consistent, formal setting for managing this interdependence in the design process"* [62].

2.2.2 Multidisciplinary Design Optimization for Launch Vehicle Design

After the general description of MDO it is now time to introduce MDO for launch vehicles. In a lot of studies MDO is applied to the design of (air) launch vehicles. For a survey of all MDO studies about launch vehicle design is referred to [5]. Figure 2.1 shows the classical disciplines for launch vehicle design.

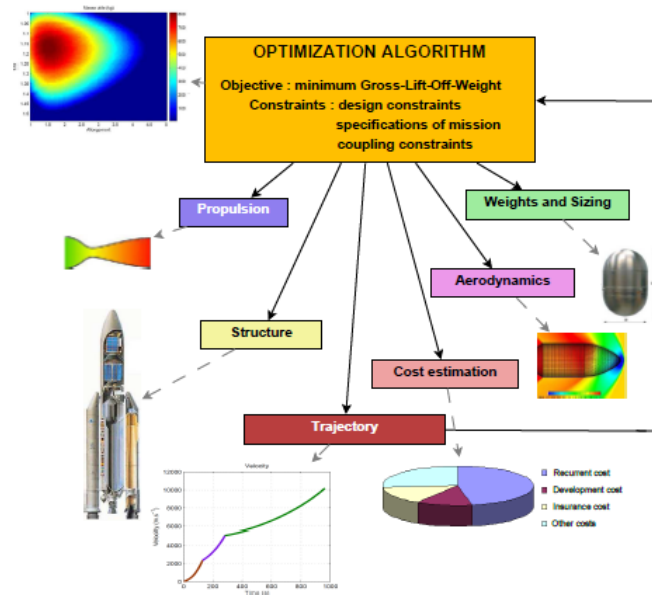


Figure 2.1: Classical decomposition of the different disciplines in launch vehicle design [5].

In the literature study two main types of MDO architectures were discussed: monolithic architectures and distributed architectures [103]. A monolithic architecture uses only one global optimizer for the entire MDO problem. Distributed architectures decompose the optimization problem to multiple problems that optimize the design for the individual disciplines. According to [5] monolithic MDO architectures are most used for launch vehicle design MDO. Monolithic architectures are less complicated than distributed architectures, however, they are less suitable for large scale problems. On the other hand, there are studies that show that monolithic architectures can provide good solutions for

large scale problems in launch vehicle design [5, 7]. Therefore it is decided to use the most common class of monolithic architectures: the Multi Discipline Feasible (MDF) method class. The MDF method solves a coupled system of disciplines by a iterative procedure and is considered to converge once the coupling variables generated by each discipline analysis have remained constant within a specified tolerance over a number of successive iterations [62]. This means that feasibility with respect to the constraints is enforced at each optimization iteration.

2.3 Optimization Algorithms

The optimizing problem that will be evaluated in this study clearly is non-linear. Therefore, an optimization algorithm is necessary. In the following section the two main categories of optimization algorithms are discussed: the gradient-based algorithms and heuristic algorithms.

Gradient-based algorithms are the classical optimization algorithms. This type of algorithms need information about the gradient and sometimes also the Hessian of the objective function and constraints [86]. Most of the gradient algorithms are iterative methods. In general the solution will converge close to a minimum. However, this will be a local minimum. A local minimum is only a global minimum if the objective function is convex. A function is convex if the graph of the function lies below the line segment joining any two points of the graph [110]. For this problem the objective function is not convex. A gradient-based optimizer also needs an initial guess that acts as a starting point from which it can start the search to the local optimum in its vicinity. A good initial guess is necessary because otherwise the solution will 'march' towards the (wrong) local minimum [77]. Gradient-based algorithms have problems to handle discrete design variables (for instance, a discrete design variable will be the number of stages) because these functions are indifferentiable. One of the most powerful gradient-based methods to solve constrained differentiable problems is Sequential Quadratic Programming (SQP) [5]. Several gradient-based (and local) optimization methods, for example Newton's Method and the Steepest Descent, are discussed in [109].

Heuristic algorithms are fundamentally different from gradient methods. The main principle behind heuristic algorithms is that the search is performed in a stochastic manner as opposed to a deterministic manner for gradient-based algorithms. A gradient method is a local method while a heuristic method is a global optimization technique. In addition, heuristic algorithms allow working with non-differentiable functions and constraints whereas gradient-based algorithms require differentiability and smoothness in the objective function and constraints [5]. Moreover, heuristic algorithms do not need an initial guess for the solution because they directly aim at the solution. A downside of heuristic algorithms is that a lot of iterations are required and that the convergence might be unclear [77].

In the next paragraphs three types of heuristic algorithms that are available in PaGMO and that will be evaluated in this study are briefly discussed. For a more detailed description of these different algorithms is referred to [109].

The most popular type of heuristic algorithms is the class of genetic algorithms. A genetic algorithm uses an evolutionary approach. Essentially, genetic algorithms use evolutionary

processes from genetics to optimize a function. An initial population of possible solutions to a problem is chosen. Each solution has a particular fitness that reflects the quality of that particular gene. The values for all design variables are converted to chromosomes (a binary notation). These genes are recombined via a crossover mechanism which results in future generations of populations. The genes with the highest fitness survive to later generations. A subset of the genetic algorithms are the differential evolution algorithms that uses real numbers instead of chromosomes. The use of real numbers introduces a different approach for the crossover mechanism.

The origin of Particle Swarm Optimization (PSO) also follows from nature and it is based on the behavior of flocks of birds or schools of fish. In a PSO, candidate solutions (the so-called particles) will move through the search space by following those particles that have the lowest cost at any iteration in the optimization [86]. Each particle keeps track of the best solution that it has achieved during the process. Simultaneously, the best value of any neighbors to a particle is also tracked. The PSO will move in a direction towards the particle's best solution and the neighbors best solution.

In the literature study it is concluded that heuristic algorithms are preferred to deterministic algorithms [103]. The two main reasons for that are that heuristic algorithms can find a global minimum and that heuristic algorithms can handle non-differentiable functions. The question remains which heuristic algorithm to choose. This decision is not trivial because according to the “no free lunch” theorem there is no optimization method that outperforms all others in the totality of the problems [119]. A comparison between different heuristic optimization algorithms for launch vehicle design published in literature does not provide the conclusive answer which heuristic algorithm performs best for launch vehicle design and trajectory optimization [16, 85].

The development of a heuristic optimization algorithm takes a lot of time. Therefore, an existing optimization algorithm will be used. A very good option for this can be the Parallel Global Multiobjective Optimizer (PaGMO). PaGMO is a C++ platform that contains a number of optimization algorithms and is developed by ESA [83]. A large advantage of using PaGMO is that it is already validated [108] and that it can easily be used in conjunction with Tudat. In Vandamme's tool a differential evolution algorithm from PaGMO was selected for the optimization. It is decided to adopt this algorithm and the settings of this algorithm for this study as well. However, because of the “no free lunch” theorem it is decided to test different heuristic algorithms during the sensitivity analysis in Chapter 12 in order to investigate the sensitivity of the achieved objective value, computation time and robustness to the use of different heuristic algorithms.

2.4 Objective Function and Constraint Handling

Most algorithms in PaGMO can only handle one objective [83]. Therefore, in this study a single objective is evaluated. The primary goal is to minimize the launch vehicle's cost, however, the launch vehicle should first reach the target orbit. The constraint handling in this study is simple: as soon as a constraint is violated the simulation of the ascent is cancelled and a value is assigned to the objective function.

In case that the launch vehicle is not valid, for instance, can not provide enough ΔV or is too large, a function value of 10^7 is assigned. As soon as a valid launch vehicle violates a trajectory constraint the following objective function, F , is used:

$$F = -H$$

In which H is the altitude in meters at the moment of abort. Over the generations the individuals will reach higher altitudes and eventually find a path for which no trajectory constraints are violated, a so-called admissible trajectory [110]. In this case the objective function is constructed as:

$$F = -\frac{1^{10}}{|a - a_{target}| + 1^6 \cdot |e - e_{target}|} \quad (2.5)$$

For which a and e are respectively the semi-major axis and the eccentricity. The goal for individuals that follow an admissible trajectory is to fly a trajectory that brings them close to the target orbit. In case that the differences between the target and simulated semi-major axis and eccentricity are small enough ($\Delta a=10,000$ m, $\Delta e=0.005$), the objective value is evaluated by:

$$F = -\frac{1^{15}}{\text{cost per launch}} \quad (2.6)$$

Where the cost per launch are defined in fiscal year (FY) 2013 euros. These individuals will be optimized for cost.

2.5 Tool Architecture

Early in this report the architecture of the simulation tool is introduced. The flowchart of the simulation tool can be found in Figure 2.2. A detailed description of this figure will result in a very long section. Therefore, only the top level architecture of the tool is discussed. For details about the different code blocks is referred to the corresponding chapters in which the individual disciplines are discussed.

The input to the tool is basically the initial state of the launch vehicle. The optimization algorithm generates the initial values for the design variables and these values are passed on to the vehicle construction code block. The values for the design variables will evolve over the generations and converge to an optimal solution. First the propulsion and the geometry and mass characteristics of the individual stages are calculated. The thermodynamic properties are obtained from an external database. Next the geometry and mass of the remaining vehicle components are determined and the vehicle is assembled. Next the validity of the vehicle is checked. In case that the vehicle is not valid the simulation is aborted and a high value to the objective function is assigned. For a valid vehicle the cost per flight are calculated by the cost code block.

Now it is time to start the simulation of the launch vehicle's ascent. First, a body information code block is constructed. This code block contains all vehicle information but also the state of the vehicle. After an update of the state the body information code block transforms the state vector to different reference frames. Before that can be done first the aerodynamic coefficients have to be determined. The body information code block communicates with the Missile Datcom database and selects the appropriate launch vehicle configuration. This code block also communicates with the environmental

code block in order to obtain the environmental conditions. From the body information code block the thrust, gravitational and aerodynamic forces are constructed and these force vectors are passed on to the equations of motion. Next the state propagator uses the calculated accelerations from the equations of motion. Now the state is integrated and after that there is checked for constraint violations. In case that a constraint is violated the simulation of the launch vehicle's ascent is terminated and a value to the objective function is assigned that depends on the altitude at the moment of abort. If the vehicle follows an admissible trajectory the state is updated and passed on to the body information code block and the next time step can be started. For every time step it is checked if an event is scheduled (stage burn-out or fairing separation) and if this is the case the body information code block is accordingly updated. The simulation is stopped when the action time of the launch vehicle is elapsed (burn-out of the last stage) or if the launch vehicle reaches stop conditions (target semi-major axis and eccentricity). The trajectory is determined by a series of pitch variables that are design variables. The history of the parameters is stored in a separate file and the data is post-processed in MATLAB.

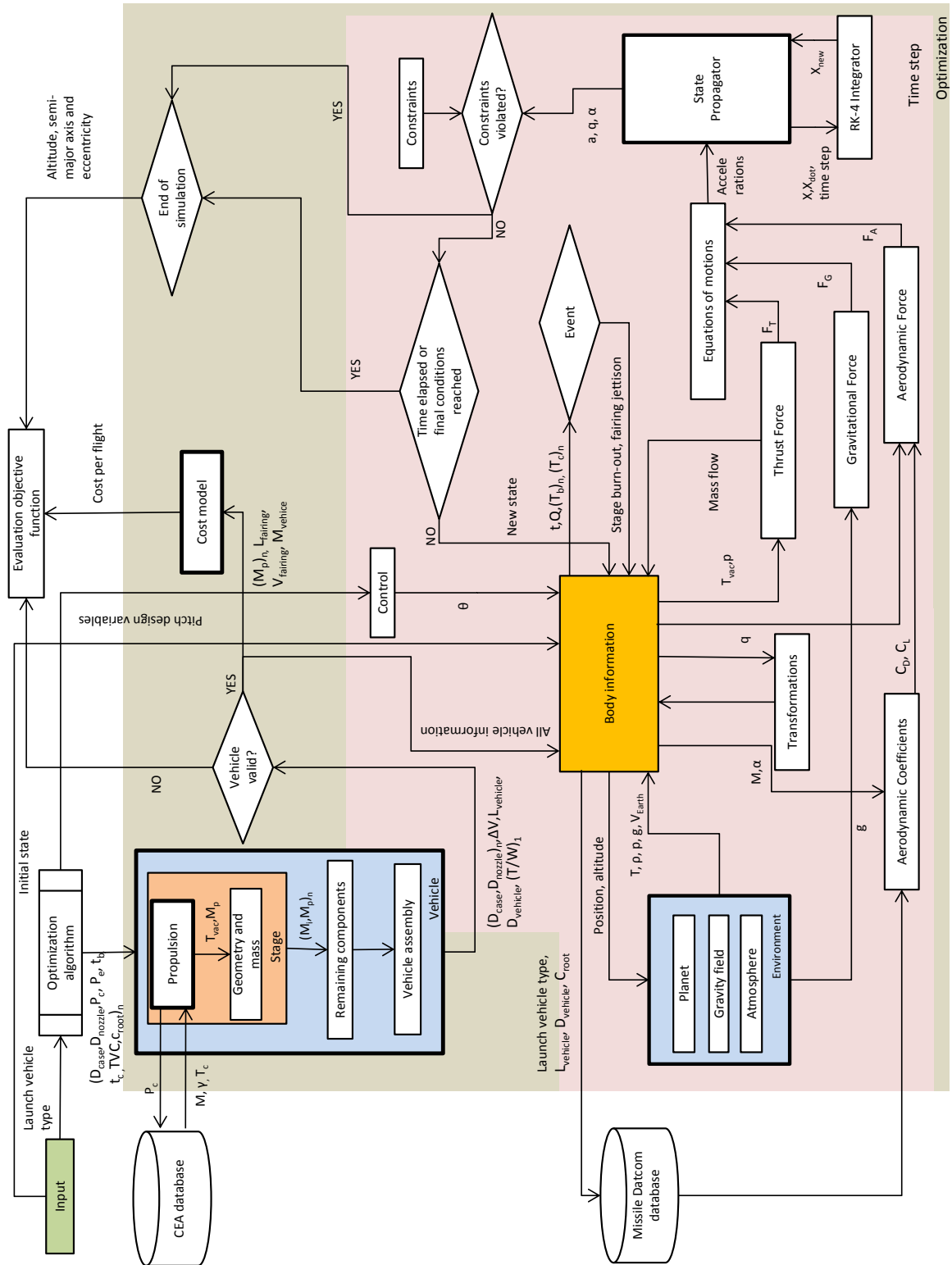


Figure 2.2: Top level overview of the MDO tool used for this thesis research.

Flight Mechanics

Before the different disciplines for the MDO will be addressed the dynamic system for the ascent of a launch vehicle is discussed. In several theses [82, 108] and textbooks [21, 69] this dynamic system is already discussed in detail. In this chapter only a short recap will be given. In addition, on several points throughout the chapter the use of Tudat is discussed to provide the reader insight which elements of Tudat are used for this tool.

In the first section of this chapter the state variables will be discussed. Next reference frames are explained and the final section of this chapter deals with the equations of motion of launch vehicles.

3.1 State Variables

The state variables express the position and the velocity of a rigid body that is moving around another one. In the tool three different types of state variables are used and those three will be briefly discussed below. For the transformation between the different types of state variables the relations that are present in Tudat are used. These relations are verified by transforming a state in Cartesian elements to spherical elements and that state is then transformed to orbital elements. The state in orbital elements is transformed back to spherical elements and finally back to Cartesian elements. The state is identical to the original state, hence, it can be concluded these relations in Tudat are valid.

3.1.1 Cartesian Components

The first type of state variables follows from a basic mathematical coordinates system: the Cartesian coordinate system. The use of Cartesian components provide neither a direct nor a clear insight in the physical problem of the launch vehicle's ascent trajectory. On the other hand, Cartesian components are very useful in the computation and integration of the equations of motion. The reason for this is that Cartesian coordinates avoid singularities (for example, when the flight path angle is $\pm 90^\circ$). The Cartesian components are:

- Position: x , y and z
- Velocity: \dot{x} , \dot{y} and \dot{z}

3.1.2 Spherical Components

The use of spherical components provides more insight in the ascent trajectory of a launch vehicle. Spherical components are always defined in a rotating reference frame as:

- Position:
 - Distance r
 - Longitude τ ($-180^\circ \leq \tau < 180^\circ$)
 - Latitude δ (from $-90^\circ \leq \delta < 90^\circ$)
- Velocity:
 - Ground speed V_G
 - Flight path angle γ (from $-90^\circ \leq \gamma < 90^\circ$)
 - Heading χ ($-180^\circ \leq \chi < 180^\circ$)

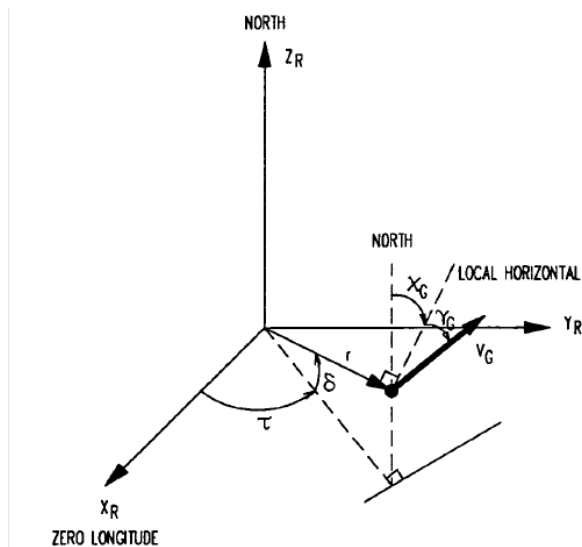


Figure 3.1: Spherical coordinates [69].

The distance, r , is the distance from the center of the planet to the launch vehicle. The longitude can be measured positively to the east. The latitude is measured along the meridian from the equator and is positive north. The velocity V_G is the modulus of the velocity vector. The flight path angle, γ , is the angle between the velocity vector and the local horizontal plane. The heading angle, χ , is the projection of the velocity vector in the local horizontal plane with respect to the local north. In the case that χ is 90° the heading will be east.

3.1.3 Orbital Elements

Orbital elements are the third way to describe the state. Orbital elements are useful when describing the motion of a body's orbit around a planet with respect to an inertial reference frame (see Section 3.2). The six orbital elements are defined as [113]:

- e : the eccentricity ($0 \leq e < 1$)
- a : the semi major axis ($a > R_e$)
- i : the inclination ($0^\circ \leq i < 180^\circ$)
- ω : argument of pericenter ($0^\circ \leq \omega < 360^\circ$)
- Ω : the longitude of the ascending node ($0^\circ \leq \Omega < 360^\circ$)
- θ : mean anomaly ($0^\circ \leq M < 360^\circ$)

The eccentricity defines the shape of the elliptical orbit, describing how much the orbit is elongated compared to a circular orbit. The semi major axis is the size of the orbit and is defined as the sum of the pericenter and apocenter distances (see Figure 3.2) divided by two. The following two elements define the orientation of the orbital plane. The inclination is the vertical tilt of the elliptical orbit with respect to the reference plane (Earth's equatorial plane), measured at the ascending node, where the orbit passes upwards through the reference plane. The longitude of the ascending node defines the location of the ascending node with respect to the reference frame's vernal point. The argument of perigee defines the location of the pericenter with respect to Earth's surface. The true anomaly defines the position of the satellite in the orbit with respect to the location of the pericenter. The orbital elements are shown in Figure 3.2.

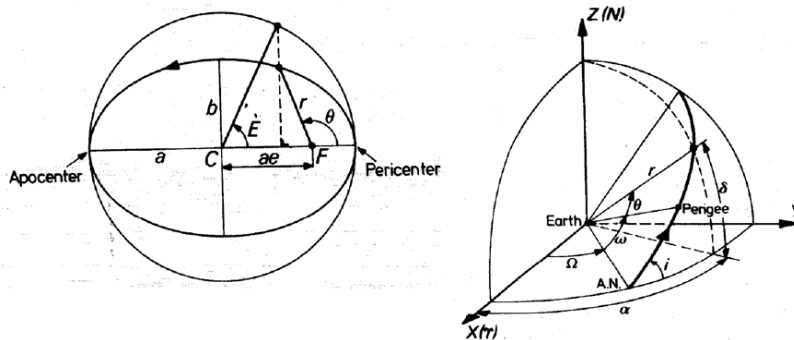


Figure 3.2: Orbital elements [21].

3.2 Reference Frames

In this section the use of different reference frames will be discussed. On first glance, one may think why would you use more than one reference frame? The reason is that some reference frames make the derivation and description of the equations of motion easier. Another reason for using multiple reference frames is that certain definitions of vectors are more sensible in a certain reference frame, while they are not in others. An example

of a reference frame is given in Figure 3.3. The different reference frames applicable to the ascent of a launch vehicle are described in detail in [69, 72] and have already been discussed in the work of Engelen [31] and Vandamme [108, 109].

A special frame is an inertial reference frame, an inertial reference frame is a reference frame with respect to which a particle remains at rest or in uniform rectilinear motion if no resultant force acts upon that particle [113]. The (pseudo) inertial geocentric reference frame (see Figure 3.3) is a pseudo inertial reference frame that can only be used as an inertial one as long as the influence of Earth's movement around the Sun is very small.

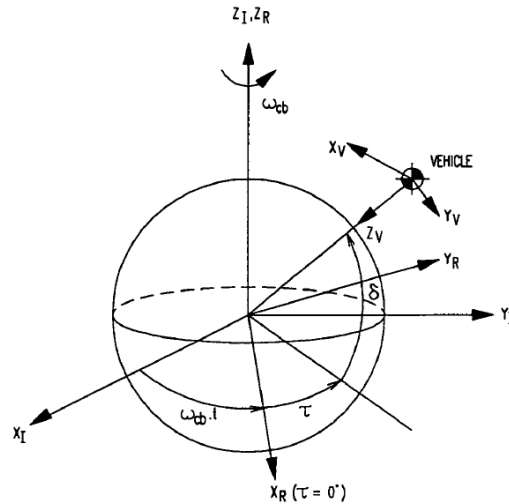


Figure 3.3: Relation between the inertial and rotating geocentric frame (I and R) and the vertical frame (V) [69].

In the tool the following reference frames (see Figure 3.3) are used: (pseudo) inertial geocentric reference frame, rotating geocentric frame, vertical reference frame, body reference frame and aerodynamic reference frame. The body reference frame and aerodynamic reference frame are discussed respectively in Chapter 5 and 7. For most of these reference frames the coordinates are defined in Cartesian as well as spherical coordinates.

Eventually all vectors have to be defined in the same reference frame. Therefore, the vectors should be transformed by transformation matrices in vectors for the correct reference frame. The attitude of a vehicle relative to any inertial reference frame can be described by three successive rotations through three Euler angles. An example of the angles involved in a transformation is given in Figure 3.4.

For the use of Euler angles and the transformation matrices between different reference frames is again referred to [69] and [72]. It should be noted that the transformation matrices between the reference frames have already been incorporated in the Tudat environment. In the tool all forces are transformed from their reference frame to the inertial geocentric reference frame in which the integration will take place. For this study the references frame transformation matrices are verified by step-wise transforming of a vector in an inertial geocentric reference frame to an aerodynamic frame and back again to an inertial geocentric reference frame. At the end of the coordinate transformations the vector is again identical to the input vector and based on this it can be concluded that transformation matrices in Tudat are correct.

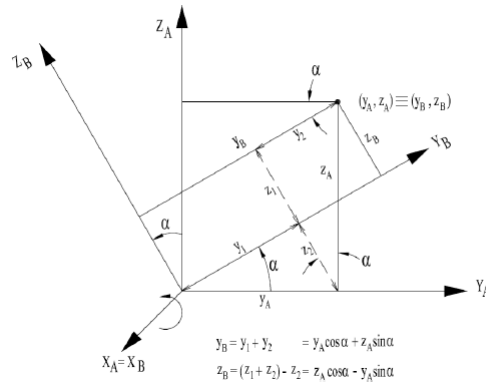


Figure 3.4: Rotation from reference frame A to reference frame B [70].

3.3 Equations of Motion for a Launch Vehicle

The equations of motion are based on the three laws of Newton. Newton's first two laws are only valid in an inertial reference frame and by using Newton's law relativistic effects are neglected. The three laws are defined as [113]:

- Newton's 1st law: Every particle continues in its state of rest or uniform motion in a straight line relative to an inertial reference frame, unless it is compelled to change that state by forces acting upon it.
- Newton's 2nd law: The time rate of change of linear momentum of a particle relative to an inertial reference frame is proportional to the resultant of all forces acting upon that particle and is collinear with and in the direction of the resultant force.
- Newton's 3rd law: If two particles exert forces on each other, these forces are equal in magnitude and opposite in direction (action = reaction).

In a three dimensional space the motion of a rigid body can be described by a combination of translational and rotational equations. The rigid body has 6 degrees of freedom (DoF), for trajectory simulation the main interest is in the motion of the vehicle's center of mass. Neglecting the rotational equation of motions will reduce the problem to 3 DoF. For this study the vehicle is assumed to be a point mass because rotational dynamics would require precise information about the vehicle's configuration. In addition, it would require detailed surface information as well as the mass distribution of the vehicle throughout time. This will increase the number of variables that have to be optimized tremendously and shifts away the focus from the main objective of this study: the comparison between air launch and ground launch. This introduces the assumption that the control system can generate the required moments to change the attitude of the vehicle. A derivation of the equations of motion for a mass-varying body can be found in [21] or [109].

The equations of motions for a launch vehicle in a rotational geocentric reference frame or an Earth-centered, Earth-fixed reference frame (see Figure 3.5) are defined in spherical coordinates as [5]:

$$\dot{r} = V \cdot \sin(\gamma) \quad (3.1)$$

$$\dot{V} = \frac{T \cdot \cos(\theta - \gamma) - D}{m} - g \cdot \sin(\gamma) + \omega_E \cdot r \cdot \cos(\delta) (\sin(\gamma) \cos(\delta) - \sin(\delta) \cos(\gamma) \cos(\chi)) \quad (3.2)$$

$$\dot{\gamma} = \frac{[L + T \cdot \sin(\theta - \gamma)] \cos(\mu)}{m \cdot V} + \left(\frac{V}{r} - \frac{g}{V} \right) \cos(\gamma) + 2\omega_E \cdot \sin(\chi) \cos(\delta) \quad (3.3)$$

$$+ \frac{\omega_E^2 \cdot r \cdot \cos(\delta) (\cos(\gamma) \cos(\delta) + \sin(\gamma) \sin(\delta) \cos(\chi))}{V}$$

$$\dot{\tau} = \frac{V \cdot \cos(\gamma) \sin(\chi)}{r \cdot \cos(\delta)} \quad (3.4)$$

$$\dot{\delta} = \frac{V \cdot \cos(\gamma) \cos(\chi)}{r} \quad (3.5)$$

$$\dot{\chi} = \frac{[L + T \cdot \sin(\theta - \gamma)] \sin(\mu)}{m \cdot V \cdot \cos(\gamma)} + \frac{V \cdot \cos(\gamma) \sin(\chi) \tan(\delta)}{r} \quad (3.6)$$

$$+ 2\omega_E (\sin(\delta) - \cos(\chi) \cos(\delta) \tan(\gamma)) + \frac{\omega_E^2 \cdot r \cdot \sin(\delta) \cos(\delta) \sin(\chi)}{V \cdot \cos(\gamma)}$$

$$\dot{m} = -q \quad (3.7)$$

Variables that were not earlier defined are: the bank angle, μ , the pitch angle, θ , the angular velocity of the Earth, ω_E and the mass flow rate, q . The four forces in the equations are the thrust force, T , the drag force, D , the lift force, L , and the gravitational attraction, g .

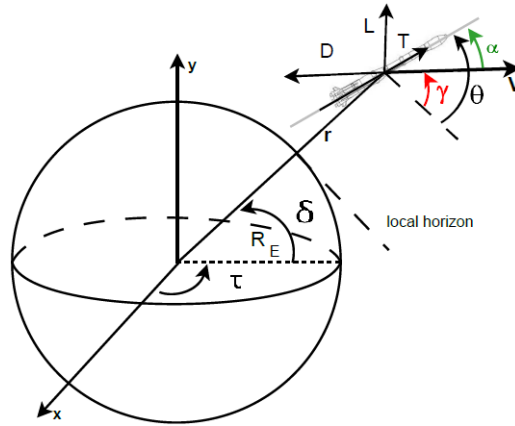


Figure 3.5: Earth-centered, Earth-fixed reference frame (adapted from [5]).

During his thesis Frank Engelen developed an ascent trajectory simulator in the Tudat framework [31]. This trajectory simulator was modified and used again by Vandamme [108]. At an earlier point in this study it was decided to use this trajectory simulator and adapt it for multistage launch vehicles. This updated simulator is verified and validated in Chapter 8.

Environment

The performance of the launch vehicle will be impacted by its environment. Therefore, it is important to understand and model the environment of the launch vehicle. In this chapter the gravitational and atmospheric environment are discussed. Due to the fact that the main objective of this study will be a comparison between ground and air launch, the environmental models are not deemed to be the most important models. For the same reason the effect of wind on the launch vehicle is not investigated in this study. The environmental models that are used in Vandamme's tool are also used for this study. For a more detailed overview of different environmental models is referred to [70] and [109].

4.1 Gravitational Model

The external force caused by gravity is one of the main forces that acts on the launch vehicle. Gravity is the natural phenomenon by which physical bodies are attracted to each other with a force proportional to their masses [113]. The force, \mathbf{F}_G , between two point masses (or homogeneous spheres), M_A and M_B , can be described by Newton's law of universal gravitation:

$$\mathbf{F}_G = -G \frac{M_A \cdot M_B}{r_{AB}^3} \mathbf{r}_{AB} \quad (4.1)$$

With G the universal gravitational constant and \mathbf{r}_{AB} the distance between the two objects. In the case of attraction between a launch vehicle and the Earth, the mass of the launch vehicle is negligible and Equation 4.1 can be written as:

$$\mathbf{F}_G = -G \frac{M_E}{r^3} \mathbf{r} \quad (4.2)$$

This model is called the central gravity model. In other MDO studies for launch vehicles the central gravity model is used [5, 15]. In reality, the Earth is neither homogeneous nor a perfect sphere. A more detailed model takes in account the flattening of the Earth and uses a so-called harmonic expansion model to find a more accurate expression of the

gravity force on the launch vehicle. The even harmonics describe the oblateness of the Earth, which are symmetric about Earth's equatorial radius. The odd harmonics are antisymmetric about Earth's equatorial radius and are the so-called 'pear-shape' terms (for a detailed description see [70]). The difference between the central gravity model and this more complex model is less than $5 \mu\text{g}$ [44]. So, in the case of a total gravity loss of $1,000 \text{ m}\cdot\text{s}^{-1}$, the difference in gravity loss between the two models will be less than $0.005 \text{ m}\cdot\text{s}^{-1}$. In Section 8.4 the trajectory model of the tool is validated and in the case that the most dominant effect, the J_2 -effect, is included, the difference in gravity loss compared with the central gravity model is $0.003 \text{ m}\cdot\text{s}^{-1}$. This difference is considered insignificant, therefore, the central gravity model will be used.

4.2 Atmospheric Model

During its journey to orbit the launch velocity will cross different layers of the atmosphere that all have different characteristics. The most relevant characteristics for the simulation of a launch vehicle are the atmospheric pressure, density and temperature. The values of these characteristics do not only depend on altitude but also on the location on Earth, day of the year and the local weather conditions. Therefore, the atmosphere is a difficult environment to model. The most straightforward method to describe the atmosphere is assuming the exponential atmosphere (for the equations see [70]). The exponential atmosphere is used in an MDO study for launch vehicles [5].

Besides the exponential atmosphere, there are two types of models: a standard atmosphere and a reference atmosphere [70]. The standard atmosphere is a hypothetical vertical distribution of atmospheric properties, which is roughly a representation of the yearly average conditions at mid-latitudes (between 23° and 66° latitude North and South). On the other hand, a reference atmosphere includes latitudinal, seasonal, geomagnetic, and solar effects. For the comparison between air and ground launch the atmospheric conditions should be identical, so, a standard atmosphere will be used.

Vandamme tool used the US Standard Atmosphere 1976 [20] and this model is already implemented in Tudat. Therefore, this model will also be used for this study. This model is used in another MDO study for launch vehicles [15]. The US Standard Atmosphere 1976 represents atmospheric parameters up to $1,000 \text{ km}$ altitude at a latitude of 45° North. All formulas below follow from [20].

The US 1976 uses two different altitudes: the geometric altitude [m], Z , and the geopotential altitude [m'], H . The geopotential altitude is an adjustment for the geometric height using the variation of gravity with elevation. In the US 1976 the lower atmosphere (below 86 km geometrical altitude) is divided into eight layers. The molecular temperature of the atmosphere, T_M , is given by:

$$T_M = T_{M,b} + L_{M,b} \cdot (H - H_b) \quad (4.3)$$

Where $T_{M,b}$ is the molecular temperature of layer b at the lowest boundary of layer b . The molecular temperature gradient for layer b is given by $L_{M,b}$ and $(H - H_b)$ indicates the difference in geopotential height between the current altitude and the starting altitude of layer b . In all eight layers the temperature changes linearly. The reference heights, H_b ,

Subscript b	H_b [km]	$L_{M,b}$ [K·km ⁻¹]	P_b [N·m ⁻²]
0	0	-6.5	101,325
1	11	0	22,632
2	20	+1	5,475
3	32	+2.8	868
4	47	0	111
5	51	-2.8	79
6	71	-2.0	4
7	84.85	-6.5	4

Table 4.1: Reference heights and temperature gradients for the different layers of the US Standard Atmosphere 1976 (adapted from [20]).

and the molecular temperature gradients, $L_{M,b}$, for the different layers are given in Table 4.1.

For higher altitudes Equation 4.3 does not hold anymore. The layer between 86 and 91 km is an isothermal layer at 180.87 K. The temperature of the next layer (between 91 and 110 km altitude) is calculated according to the following formula:

$$T = T_8 - 76.32 \cdot \left(1 - \left(\frac{Z - Z_8}{-19.94}\right)^2\right)^{0.5} \quad (4.4)$$

Where T_8 is 263.19 K and Z_8 is 91 km. The temperature for the next layer (from 110 to 120 km altitude) can be described with:

$$T = T_9 + 12 \cdot (Z - Z_9) \quad (4.5)$$

With T_9 240 K and Z_9 110 km. For the last layer of the atmosphere (120 km up to 1,000 km altitude) holds:

$$T = T_\infty - (T_\infty - T_{10}) \cdot \exp(-\lambda\xi) \quad (4.6)$$

$$\lambda = 12 / (T_\infty - T_{10}) \quad (4.7)$$

$$\xi = \frac{(Z - Z_{10}) \cdot (r_0 + Z_{10})}{(r_0 + Z)} \quad (4.8)$$

with T_∞ as the exoatmospheric reference temperature (1000 K), Z_{10} as 120 km, T_{10} as 360 K and r_0 as 6356.76 km.

Until this point only the temperature is discussed. Now an expression for the pressure will be given. For altitudes below 86 km altitude the pressure can be calculated by:

$$P = P_b \left(\frac{T_{M,b}}{T_{M,b} + L_{M,b}(H - H_b)} \right)^{\left(\frac{g_0 \cdot M_0}{R \cdot L_{M,b}} \right)} \quad (4.9)$$

Or for the isothermal layers below 86 km:

$$P = P_b \cdot \left(\frac{-g_0 \cdot M \cdot (H - H_b)}{R \cdot T_{M,b}} \right) \quad (4.10)$$

The values for P_b can be found in Table 4.1. With R_A the universal gas constant and M the molecular weight of the atmosphere. M is constant until 80 km altitude and shows a drop of 0.04% between 80 and 86 km altitude [20]. This drop is considered insignificant. For altitudes above 86 km altitude the pressure will be computed as a function of the geometric altitude and the kinetic temperature T :

$$P = \sum P_i = \sum n_i \cdot k \cdot T = \frac{\sum n_i \cdot R \cdot T}{N_A} \quad (4.11)$$

Where N_A is Avogadro's constant, k the Boltzmann constant and $\sum n_i$ the sum of all densities of the individual gas species in the atmosphere above 86 km altitude (see [20] for actual values of $\sum n_i$). The last atmospheric parameter that is required is the atmospheric density, ρ , and this parameter will be found by assuming the perfect gas law. For a thorough explanation of the perfect gas law is referred to [103]. So, under the assumption that the atmosphere is a perfect gas:

$$\rho = \frac{P \cdot M}{R_A \cdot T} \quad (4.12)$$

The tabulated US Standard Atmosphere 1976 model that is available in Tudat works only until 120 km. This is not a problem because from the trajectory validation case in Section 8.4 follows that at 120 km altitude the dynamic pressure is less than 2 Pa. Vandamme validated this atmospheric model during his thesis work, therefore, it is deemed unnecessary to repeat this [108].

Propulsion

In this chapter will be discussed how the propulsion of the launch vehicle is modeled. In the literature study it is concluded that air launch is the most promising for solid propelled rockets, therefore, this chapter is limited to the description of solid rocket propulsion [103]. Most of the design parameters that will be used for this study are related to the propulsion system. From these design parameters the thrust force is calculated and passed on to the trajectory module. The parameters from the propulsion system are also used to determine the mass characteristics of the launch vehicle as will be described in Chapter 6.

This chapter starts with an explanation of the thrust model. In the next section the solid rocket motor model is discussed. This is followed by a section about the validation of this model and in the final section of this chapter the constraints related to propulsion are discussed.

5.1 Thrust Model

In this section the most important equations for the thrust model are given. For a more detailed description and derivation of the equations is referred to [120]. The thrust that is provided by an ideal rocket motor in the atmosphere, T , is given by [120]:

$$T = \dot{m} \cdot U_e + A_e \cdot (p_e - p_a) \quad (5.1)$$

With \dot{m} the mass flow that mostly depends on the generation of gaseous propellants, U_e the true velocity of the exhaust gases, A_e the nozzle exit area and p_e the exit pressure at the nozzle and p_a the ambient pressure. The first term $\dot{m} \cdot U_e$ is also called momentum thrust and the second term $A_e \cdot (p_e - p_a)$ is also referred to as pressure thrust.

In vacuum the ambient pressure is zero and therefore, the equation for vacuum thrust, T_{vac} , is given by:

$$T_{vac} = \dot{m} \cdot U_e + A_e \cdot p_e \quad (5.2)$$

Throughout this chapter vacuum thrust is discussed but the atmospheric effects on the thrust are not neglected. During the simulation the product of the ambient pressure and

exit area is subtracted from the calculated vacuum thrust. Next the equivalent exhaust velocity in vacuum, U_{eqvac} , is introduced:

$$U_{eqvac} = U_e + \frac{A_e \cdot p_e}{\dot{m}} \quad (5.3)$$

And the vacuum specific impulse, I_{spvac} , is obtained by:

$$I_{spvac} = \frac{U_{eqvac}}{g_0} \quad (5.4)$$

With g_0 the gravitational acceleration on Earth's surface. Note that g_0 is always constant even on other celestial bodies.

In this section also the most fundamental equation in rocket motion is introduced: Tsiolkovsky's¹ equation or the rocket equation. This equation states that in vacuum gravity-free space the change in velocity, ΔV , that is delivered by the vehicle's propulsion system only depends on the equivalent exhaust velocity, U_{eqvac} , and the mass ratio, Λ , between initial mass, M_0 and burn-out mass, M_e , of the rocket. Tsiolkovsky's equation is derived in [2] and given by:

$$\Delta V = U_{eqvac} \cdot \ln \left(\frac{M_0}{M_e} \right) = U_{eqvac} \cdot \ln(\Lambda) = g_0 \cdot I_{spvac} \cdot \ln(\Lambda) \quad (5.5)$$

So, the amount of ΔV is independent of the manner in which the propellant mass is expelled as a function of time. However, one should keep in mind that for a launch vehicle the thrust delivered by the propulsion system should be higher than the launch vehicle's weight (at least at take-off).

Normally the thrust of launch vehicle is defined in a propulsion or thrust reference frame which is a body reference frame rotated with the elevation angle of the thrust force, ε_T , and the azimuth angle of the thrust force, ψ_T (see Figure 5.1). However, for this study it will be assumed that both angles are zero thus the propulsion frame is identical to the body frame.

¹After Konstantin Tsiolkovsky (1857-1935), a Russian and Soviet rocket scientist and pioneer of the astronautic theory.

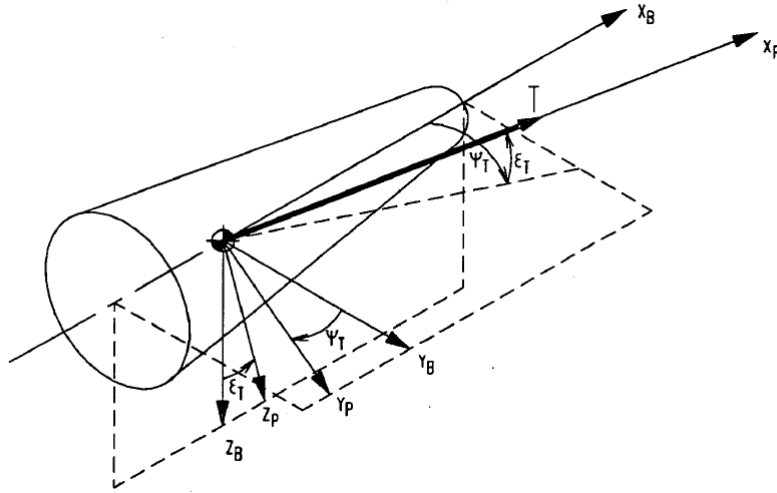


Figure 5.1: Relation between the propulsion frame (index P) and the body frame (index B). All angles are indicated in positive direction [69].

5.2 Modeling Solid Rocket Propulsion

A detailed description of solid rocket motors (SRM) is given in the literature study [103] and only the most important conclusions will be described in this report.

First of all, modeling a SRM is not as straightforward as modeling a liquid rocket engine. In the literature study an approach was developed to model the performance of a SRM. The aim of the modeling would be to select a certain set of design variables that will determine all propulsion characteristics that are required for the other MDO disciplines. This will be a thrust versus time curve (or a constant thrust) to the trajectory module and the mass and geometry for the motor to the vehicle module.

It is chosen to model the performance of the SRM but not to perform a grain analysis. During the literature study it was concluded that the chamber pressure of a SRM is not constant over time [103]. However, for this study it will be assumed that the chamber pressure (thus thrust) is constant. During the sensitivity analysis in Chapter 12 the influence of regressive thrust profiles on the optimized vehicle and trajectory will be examined. However, there are several SRMs for which the chamber pressure and thrust are more or less constant, two examples are shown in Figure 5.2.

The model used for the solid rocket motors uses the ideal rocket theory. The ideal rocket theory was described in detail in the literature study [103]. In Section 5.2.1 the design variables for every stage and the corresponding equations that determine the performance of the SRM are discussed.

5.2.1 Modeling of Solid Rocket Motor

During the literature study the following method to determine the propulsion characteristics of a SRM was developed. This method is loosely based on the models of SRMs in [49] and [50] and uses equations from [120]. The five design variables for the SRM are

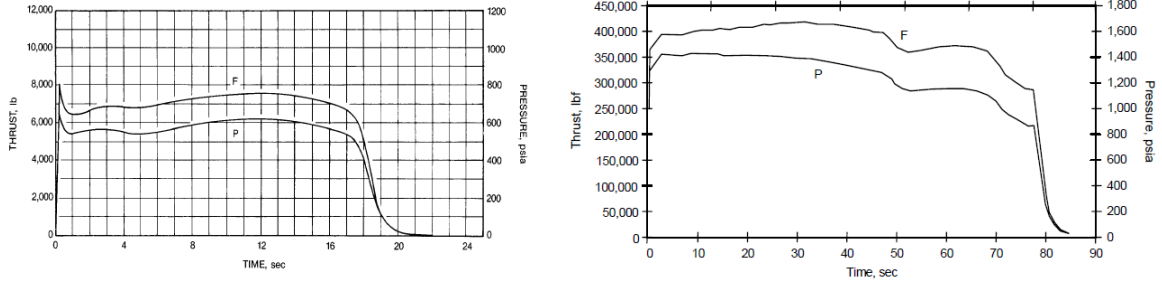


Figure 5.2: Thrust and pressure over burn time for the Star 26 and CASTOR 120 SRM [4].

given in Table 5.1. The propellant type is also an input variable to the tool but as will be described in Section 5.2.2 for this study only one propellant type is discussed. The tool can easily be adapted for others propellants by adding the thermodynamic characteristics of these propellants.

Symbol	Description
p_c	Pressure in the combustion chamber
p_e	Exit pressure in the nozzle
t_b	Burn time
D_{case}	Diameter of the motor casing
D_{exit}	Diameter of the nozzle exit

Table 5.1: Design variables for the SRM.

Thermodynamic data, that is generated by an external program, is implemented in tabulated form (see Section 5.2.2). The chamber temperature, T_c , the ratio of specific heats, γ , and the mean molecular mass of the combustion gases, M , are calculated by this program for different chamber pressures. From these thermodynamic characteristics the Vandekerckhove function, Γ , and the specific gas constant, R , can be determined:

$$\Gamma = \sqrt{\gamma} \left(\frac{2}{\gamma + 1} \right)^{\left(\frac{\gamma + 1}{2(\gamma - 1)} \right)} \quad (5.6)$$

$$R = \frac{R_A}{M} \quad (5.7)$$

The next step is to calculate the area expansion ratio of the motor, ε , by using the pressure ratio:

$$\varepsilon = \frac{A_e}{A_t} = \frac{\Gamma}{\sqrt{\frac{2 \cdot \gamma}{\gamma - 1} \cdot \left(\frac{p_e}{p_c} \right)^{\left(\frac{2}{\gamma} \right)} \left(1 - \left(\frac{p_e}{p_c} \right)^{\left(\frac{\gamma - 1}{\gamma} \right)} \right)}} \quad (5.8)$$

The throat area can be calculated from the exit diameter and the nozzle expansion ratio:

$$A_t = \frac{A_e}{\varepsilon} = \frac{\pi \left(\frac{D_{exit}}{2} \right)^2}{\varepsilon} \quad (5.9)$$

The following step is to determine the mass flow, \dot{m} :

$$\dot{m} = \frac{p_c \cdot A_t \cdot \Gamma}{\sqrt{R \cdot T_c}} \quad (5.10)$$

Now the characteristic velocity, c^* , which depends on the propellant properties and design of the combustion chamber and the "characteristic thrust coefficient", C_F° , that follows from the nozzle design can be calculated:

$$c^* = \frac{1}{\Gamma} \sqrt{R \cdot T_c} \quad (5.11)$$

$$C_F^\circ = \Gamma \sqrt{\frac{2\gamma}{\gamma-1} \left(1 - \left(\frac{p_e}{p_c} \right)^{\frac{\gamma-1}{\gamma}} \right)} \quad (5.12)$$

The true exhaust velocity, U_e , is given by:

$$U_e = c^* \cdot C_F^\circ \quad (5.13)$$

Also the pressure thrust has to be added to obtain the ideal vacuum thrust, $T_{vac_{id}}$:

$$T_{vac_{id}} = \dot{m} \cdot U_e + A_e \cdot p_e \quad (5.14)$$

For real SRMs the ideal rocket theory does not hold and a correction factor, ξ , has to be introduced:

$$T_{vac} = \xi \cdot (\dot{m} \cdot U_e + A_e \cdot p_e) \quad (5.15)$$

In theory the correction factor only has to be applied for the momentum thrust. However, the correction factor will be calculated based on regression data (see Section 5.3). Therefore, it does not matter if the correction factor is applied on the total ideal vacuum thrust or only on the ideal momentum thrust. In the latter case the correction factor would be higher. For the value of the correction factor, ξ , is referred to Section 5.3.

The propellant mass, M_p , is given by:

$$M_p = (\dot{m} \cdot t_b) (1 + SF) \quad (5.16)$$

In which, SF is the sliver fraction². The sliver fraction is also an user input and is for this study fixed at a typical value of 3% [98]. The effects of varying values for the sliver fraction are examined during the sensitivity analysis in Chapter 12. The length of the nozzle and the motor case are calculated in Section 6.1.

²The percentage of unburned propellant that results from the grain geometry.

5.2.2 Solid Rocket Propellants

In the literature study it was concluded that a composite hydroxyl terminated polybutadiene (HTPB) propellant is the most common propellant for SRMs [120]. In addition HTPB has superior properties to other propellant types and other composite propellants [120]. Composite propellants consist of a separate fuel and oxidizer that are usually blended together in some initially liquid plastic or rubbery binder material. In most cases an organic salt, for example, ammonium perchlorate (AP), is used as oxidizer. A survey of propellants with different concentrations of fuel, binder and oxidizer is given in the literature study. It should be noted that it is assumed that the propellant only consists of the above mentioned three constituents. In reality, small fractions of catalyst and curing agents are present [98].

The free available tool NASA Glenn Equilibrium Program (CEA) is used to analyze and compare the performance of these different propellants [42, 64]. CEA calculates complex chemical equilibrium product concentrations from any set of reactants and determines thermodynamic and transport properties for the product mixture. CEA assumes one dimensional forms of the continuity, momentum and energy equations, zero velocity at the combustion chamber inlet, complete and adiabatic combustion, isentropic expansion in the nozzle, homogeneous mixing, ideal-gas law and zero temperature and velocity lags between condensed and gaseous species [42].

For a range of different chamber pressures (30 to 100 bar) and different propellant compositions the differences between the computed values of the characteristic velocity, c^* , were compared. The difference in the minimum and maximum values for c^* was found to be less than 1% [103]. Therefore, it was concluded that the performance difference between the different propellants is marginal. So, for this study only one propellant is chosen and for arbitrary reasons the HTPB 1912 propellant is selected. This propellant consists of 19% aluminum, 12% HTBP and 69% AP. HTBP 1912 propellant is used in the P-80, Z-23 and Z-9 SRMs for the Vega launch vehicle [23].

With CEA the thermodynamic characteristics of HTPB 1912 are calculated for different chamber pressures. The thermodynamic characteristics are the chamber temperature, T_c , the ratio of specific heats, γ , and the mean molecular mass of the combustion gases, M . Based on a survey of available SRMs a minimum chamber pressure of 30 bar and maximum chamber pressure of 100 bar will be used as boundaries. These thermodynamic characteristics will be implemented in the tool in tabulated form. A summary of the thermodynamic properties for HTBP 1912 for different chamber pressures and an overview of the input parameters for CEA can be found in Appendix C.

5.3 Validation Propulsion Model

After the propulsion model is defined it has to be validated. *"Model validation is the process of determining the degree to which a model is an accurate representation of the real world from the perspective of the intended model purpose"* [81]. For this thesis research a database with 32 solid rocket stages is created. The data for all these stages can be found in Appendix D. The stages are divided into three categories: large solid rocket motors ($T_{vac} > 200$ kN), small solid rocket motors with TVC ($T_{vac} < 200$ kN) and small solid rocket motors without TVC ($T_{vac} < 200$ kN). The validation for all 32 motors is deemed a

too large work package for this thesis, therefore, from the database only 14 motors from the three categories are validated. This will be done for their geometry and inert mass properties in Chapter 6 and in this section for the vacuum thrust, Isp and propellant mass. It should be noted that in the model described in Section 5.2.1 a constant vacuum thrust over time is assumed. In reality this is not true for all motors that are evaluated and from this some differences between the model and reality can already be explained.

One has to keep in mind that the thrust calculated by the model described in the previous section still assumes the ideal rocket theory. In the literature study a detailed overview of all the different correction factors that have to be applied on the vacuum thrust were discussed [103]. From the evaluation of the 14 motors the average vacuum thrust error predicted by the model is found to be +6.37%. Hence the ideal vacuum thrust that is calculated by the model in Section 5.2.1 is reduced by 6.37%, so, a single correction factor to the ideal vacuum thrust of 0.9363 is applied. For this study and conceptual design this approach is valid. However, in reality the losses are different in every motor and depend, for example, on the percentage of aluminum in the propellant (losses due to the presence of a condensed phase) or the divergence half angle of the nozzle (geometrical losses due to the radial component of the exhaust momentum) [98].

For statistical analysis both the absolute or squared error can be used to assess the accuracy of the estimation. For this study the different statistical measures proposed by Castellini are used [15]. The statistical measures that will be used are simple but provide very transparent information about the accuracy of the models. For the validation three statistical measures are introduced that will also be used in the next chapters for the validation of the other disciplines. The first one is the mean error, μ , which provides a measure about how well the model can predict the vacuum thrust force. The mean error is mathematically defined as:

$$\mu = \frac{100\%}{n} \cdot \sum_{i=1}^n \frac{(y_i - \bar{y}_i)}{y_i} \quad (5.17)$$

Where y_i is the actual value of the vacuum thrust and \bar{y}_i is the estimated value of the vacuum thrust by the model. The sum of all errors is divided by the number of motors evaluated, n , and multiplied by 100%. The absolute mean error, E , is almost identical to the mean error and is mathematically defined as:

$$E = \frac{100\%}{n} \cdot \sum_{i=1}^n \frac{|y_i - \bar{y}_i|}{y_i} \quad (5.18)$$

The final statistical measure is the standard deviation of the error, σ :

$$\sigma = 100\% \cdot \sqrt{\frac{\sum_{i=1}^n \left(\mu - \left(\frac{y_i - \bar{y}_i}{y_i} \right) \right)^2}{n - 1}} \quad (5.19)$$

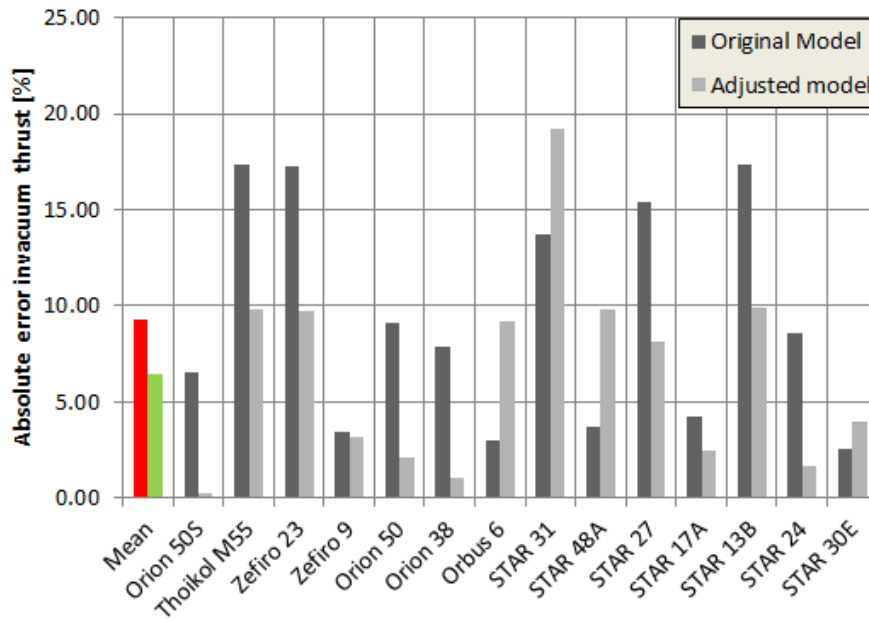


Figure 5.3: Absolute error [%] in calculated vacuum thrust compared with the actual vacuum thrust.

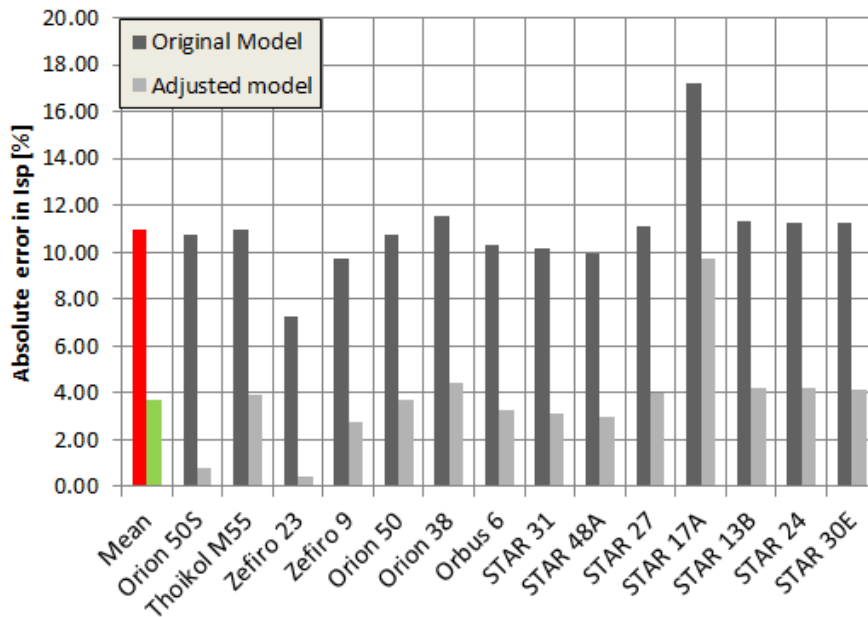


Figure 5.4: Absolute error [%] in calculated vacuum Isp compared with the actual vacuum Isp.

In Figure 5.3 the absolute error for the calculated vacuum thrust for the 14 motors is shown. Detailed validation data for the individual motors can be found in Appendix E. From this figure it can be concluded that the correction factor reduces the absolute error for most motors. After the correction the absolute errors for all motors except for the

STAR 31 are below 10%. No explanation is found for the underestimation with more than 19% of the vacuum thrust of the STAR 31 motor. It should be noted that most motors use other propellants than HTBP1912, therefore, it can be concluded that the effect of another (solid) propellant on the vacuum thrust force is limited because the absolute error remains below 7%.

In Figure 5.4 the absolute error for the calculated vacuum Isp for the 14 motors is shown. The correction factor in vacuum thrust also reduces the relative and absolute error in vacuum Isp to less than 4%.

The absolute error in the estimation of the propellant mass can be found in Figure 5.5. A typical sliver fraction of 3% [98] is used and this results in the lowest mean error of +0.06%, the absolute mean error is 6.83%.

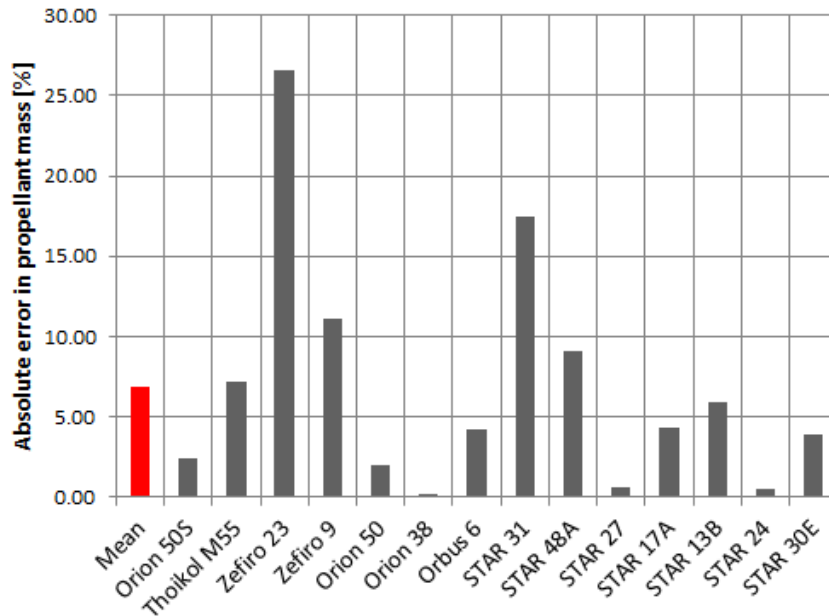


Figure 5.5: Absolute error [%] in calculated propellant mass compared with the actual propellant mass.

In Table 5.2 the statistical figures for the estimation of the most relevant parameters for the propulsion model are summarized. These statistical figures will be used as input parameters for the sensitivity analysis in Chapter 12. In general it can be concluded that all errors margins are acceptable because the absolute errors are smaller than 7% and all standard deviations remain below 11%. However, the results from the sensitivity analysis will determine if these errors are indeed acceptable.

Description	E [%]	μ [%]	σ [%]
Ideal vacuum thrust	9.28	+6.37	9.10
Vacuum thrust with correction factor	6.46	-0.41	8.52
Ideal vacuum Isp	11.0	+11.0	2.10
Vacuum Isp with correction factor	3.68	+3.68	2.14
Propellant mass	6.83	+0.06	10.2

Table 5.2: Statistical figures of the error in the estimation of the most relevant parameters for the propulsion model.

5.4 Propulsion Constraints

The modeling of the propulsion system introduces constraints that have to be included. In general the diameter of the nozzle exit, D_{exit} , is smaller than the diameter of the motor casing, D_{case} . For some motors, for instance, Pegasus' first stage the Orion 50S, the diameter of the nozzle exit is slightly larger than the diameter of the casing [4]. In order to avoid unrealistic configurations the diameter of the nozzle exit is constrained at 1.15 times the diameter of the motor casing for the first stage. For the other stages the nozzle exit diameter is not allowed to exceed the diameter of the motor casing.

In the case that a nozzle is over-expanded shock waves will occur at the nozzle exit. If the pressure ratio between the exit pressure, p_e , and the ambient pressure, p_a , is not high enough these shock waves may propagate upstream and cause flow separation [120]. It is hard to predict for which pressure ratio flow separation really starts to occur because this depends on the surface roughness of the nozzle wall, the detailed shape of the nozzle and the viscosity of the exhaust gases [120]. For conical nozzles the empirical determined conservative Summerfield criterion can be used. This criterion states that pressure ratio $\frac{p_e}{p_a}$ may never drop below 0.35-0.45. As will be discussed in Chapter 6 a bell-shaped nozzle is used for this study. At low altitudes bell-shaped nozzles are likely to experience flow separation [120]. Therefore, it is decided that the pressure ratio is not allowed to drop below 0.40. For the motors of the upper stages the minimum exit pressure is constrained at 0.05 bar, which is the minimum exit pressure that is found in literature for SRMs that operate in close to vacuum conditions [4].

Launch Vehicle Modeling

In the previous chapters several MDO disciplines are already discussed, now, the modeling of the launch vehicle itself will be discussed. In order to achieve the required orbital velocity multistage launch vehicles are required. Stages are dropped-off after extinction, in order to reduce the remaining mass that has to be accelerated. For a detailed description, other advantages of multistage launch vehicles and a calculation example is referred to the literature study [103].

The first section of this chapter discusses the geometry models of the launch vehicle. Next the mass models of all the elements of the launch vehicle will be discussed and validated. In the final section of this chapter constraints for the launch vehicle are given.

6.1 Geometry Models

The launch vehicle's geometry has an influence on the launch vehicle's aerodynamic characteristics. Furthermore, geometry limitations play a role in air launch. Therefore, it is important to define the geometry of the launch vehicle. In this section the geometry of the individual stages, the launch vehicle, the fairing and the aerodynamic lifting surfaces are described. The length of the individual stages is validated in Section 6.1.1. In Vandamme original tool a single stage liquid rocket was modeled and Vandamme's geometry model cannot be used for this work. Therefore, a new geometry model has to be developed.

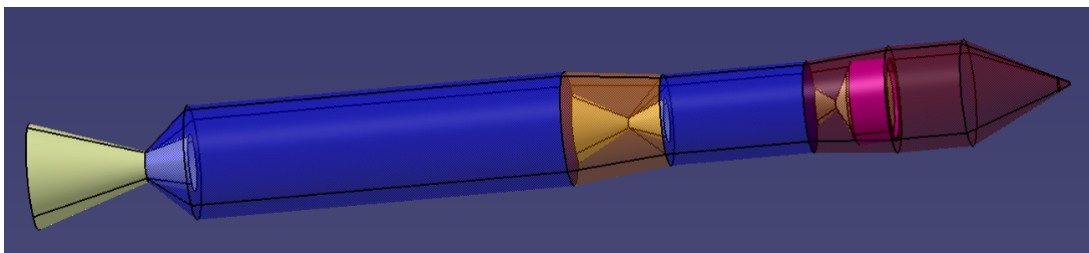


Figure 6.1: Impression of the launch vehicle model.

6.1.1 Stage

The discussion from Section 5.2 is continued here. First the length of the motor casing will be calculated. For the calculation of the length of the casing a constant value for the fill factor, FF , is assumed. Also the fill factor is one of the variables that will be investigated during the sensitivity analysis. The fill factor or volumetric loading fraction is a percentage of the total volume occupied by the grain. The fill factor is an user input and in this study it has a constant value of 95% [98]. Under the assumption that the wall and insulation of the motor case will be 1% of the diameter of the motor case, the length of the motor case is calculated with:

$$L_{case} = \frac{M_p}{\rho_p \cdot \pi \left(\frac{0.99 \cdot D_{case}}{2} \right)^2 \cdot FF} \quad (6.1)$$

Where ρ_p is the density of the propellant and has a value of $1,850 \text{ kg}\cdot\text{m}^{-3}$ [15]. It should be noted that for this study only cylindrical motor cases are evaluated while in reality there are also spherical motor cases. Next the length of the nozzle convergent and divergent can be calculated. In the model a conical nozzle is assumed. The geometry for the nozzle convergent and divergent is given in Figure 6.2.

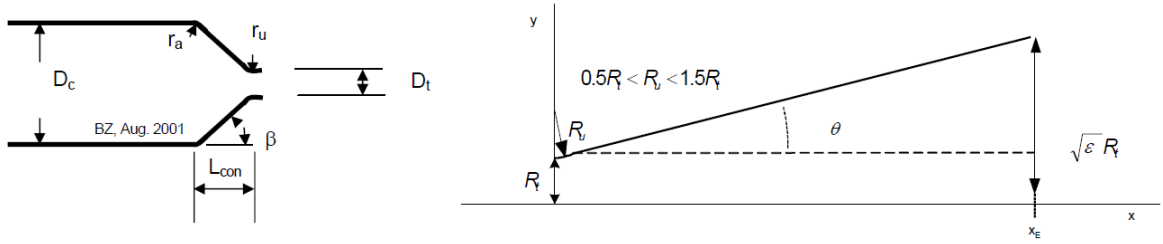


Figure 6.2: Schematic of the nozzle convergent (left) and nozzle divergent (right) for a conical nozzle [120].

From Figure 6.2 the following formulas for the lengths of the nozzle convergent, L_{con} , and nozzle divergent, L_{div} , can be derived:

$$L_{con} = \frac{D_{case} - D_t}{2 \cdot \sin(\beta)} \quad (6.2)$$

$$L_{div} = R_u \cdot \sin(\theta) + \frac{R_e - R_t - (R_u - R_u \cdot \cos(\theta))}{\tan(\theta)} \quad (6.3)$$

With R_u the longitudinal radius of the throat. Typical values for the nozzle convergent half angle, β , are $30\text{-}60^\circ$ [49] and for the nozzle divergent half angle, θ , $12\text{-}18^\circ$ [98] or $15\text{-}24^\circ$ [49]. For this study β and θ will be taken constant at 30° and 15° respectively.

In this study only the length of the individual rocket stages is validated (14 stage with lengths varying between 0.64 m and 8.4 m). Using the statistical figures introduced in Section 5.3 a mean error of over 40% is found (see also Figure 6.3 or the details in Appendix F). This error is deemed unacceptable and therefore a correction is applied. First a partially submerged nozzle is introduced. For a submerged nozzle a significant

part of the nozzle structure is submerged in the motor case, this will reduce the length of the nozzle convergent section (see Figure 6.4). For this study it will be assumed that the opening of the nozzle convergent will be 50% of the motor case diameter.

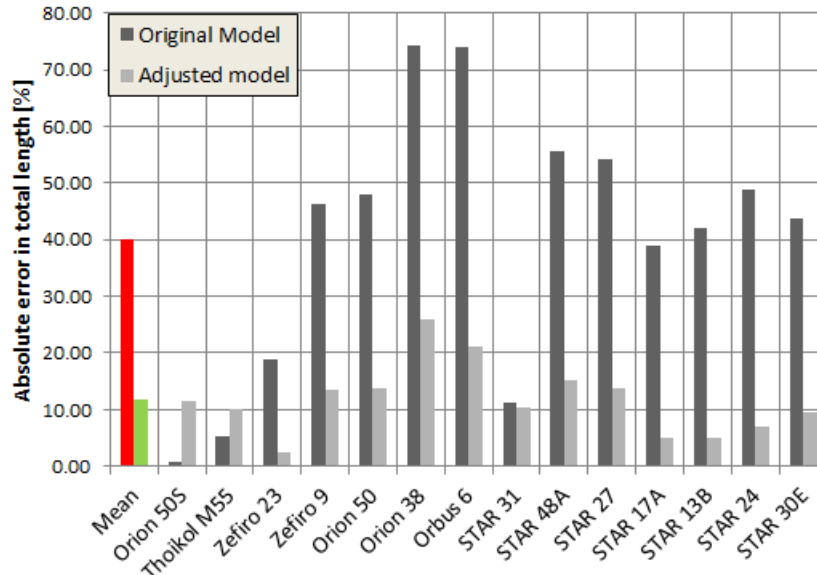


Figure 6.3: Absolute mean error [%] in calculated length of the stage compared with the actual length.

In addition the conical nozzle is changed to a bell-shaped nozzle, which is shorter [98]. It is common to give the length of a bell-shaped nozzle as a fraction of the length of conical nozzle with a 15° convergent half angle [98]. A 80% bell nozzle is used, so, the calculated length of the nozzle divergent can simply be corrected with a factor 0.8 [98].

These two changes result in a reduction of the mean error to 7.15%. From Figure 6.3 it can be concluded that the stages that have the largest error before the correction are corrected the most. For instance, for the Orbus 6 stage the adjustment of the model reduces the error from more than 70% to less than 20%. If it is attempted to reduce the mean error to zero, this will result in a higher value for the absolute mean error.

A summary of the statistical figures can be found in Table 6.1. Based on Table 6.1 it can be concluded that the errors after the adjustment of the model can be considered acceptable. However, the definitive answer will follow from the sensitivity analysis.

Description	E [%]	μ [%]	σ [%]
Total length original	40.1	+40.1	23.2
Total length adjusted	11.7	+7.15	11.5

Table 6.1: Statistical figures of the error in the estimation of the stage's length.

6.1.2 Launch Vehicle

For this study launch vehicle stages are considered that have only one motor and burn sequentially. The reason for this is that almost all solid propelled launch vehicles have

this configuration [33, 47].

The lengths of the motor case, L_{case} , the nozzle convergent part, L_{con} , and the nozzle divergent part, L_{div} , have already been calculated in the previous section. Between the start of the nozzle of the next stage and the top of the motor case of the previous stage a constant distance of 0.10 meter is assumed. There is no data available to validate this assumption, however, the sensitivity to length of the launch vehicle will be investigated during sensitivity analysis. An overview of the geometry of a three stage rocket is given in Figure 6.4. The length of the interstage structure is given as L_{in} and the length of the payload fairing as $L_{fairing}$. These lengths are discussed in more detail in Section 6.2.2 and 6.1.3. From the configurations of Pegasus, Taurus and Vega follows that upper stage is encapsulated by the fairing [33, 47], therefore no interstage will be modeled between upper stage and the stage below. However, the user can easily update the model and include an interstage between upper stage and the stage below.

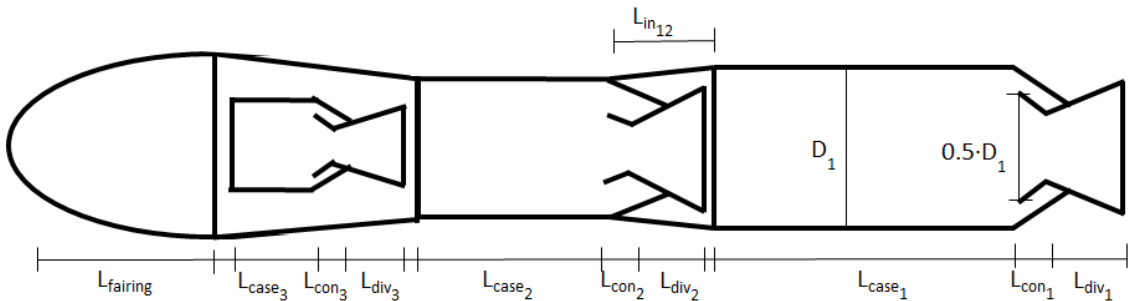


Figure 6.4: Geometry of a non-winged three stage launch vehicle (not to scale).

6.1.3 Fairing

The payload fairing is located on top of the rocket. In the literature study it is concluded that the available payload volume of the launch vehicle should be similar to the ones of existing launch vehicles [103]. The payload fairing consists of the three parts: the nose, the cylindrical section and a frustum that encapsulates the upper stage.

The top part of the fairing is an aerodynamic shaped ogive nose cone [73]. The profile of this shape is formed by a segment of a circle such that the body of the upper stage is tangent to the curve of the nose cone at its base. The base is on the radius of the circle. A geometric impression of a tangent ogive nose cone is given in Figure 6.5. Based on several fairing geometries in [47] it seems that the nose cone's length is almost equal to the diameter of the fairing (see also Figure 6.6b). This is also the assumption for the length of the conical part of the fairing.

There are no existing launch vehicles in the 10 kg payload class, therefore, a reasonable payload volume has to be assumed for this type of launcher. For this study it is assumed that in the payload fairing should be sufficient space for two 3U-CubeSats that will be deployed using the Poly Picosatellite Orbital Deployer (P-POD). The P-POD (see Figure 6.6a) is a standard deployment system that ensures that CubeSats are properly deployed. In general a 3U CubeSat has a mass of 3 kg and an empty P-POD a mass of 2.25 kg [55].

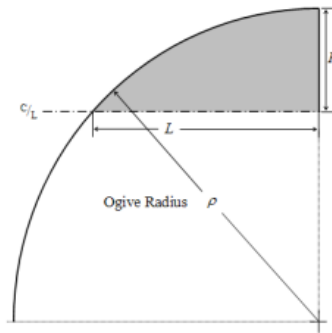


Figure 6.5: Geometry of a tangent ogive nose cone [73].

From [55] follows that the driving dimensions for a P-POD are 0.43 m, 0.14 m and 0.19 m. Therefore, the minimum dimensions of the payload fairing to fit the two P-PODs are $0.43 \times 0.28 \times 0.19$ m. The length of the fairing (without the nose cap) will be fixed at 0.43 m.

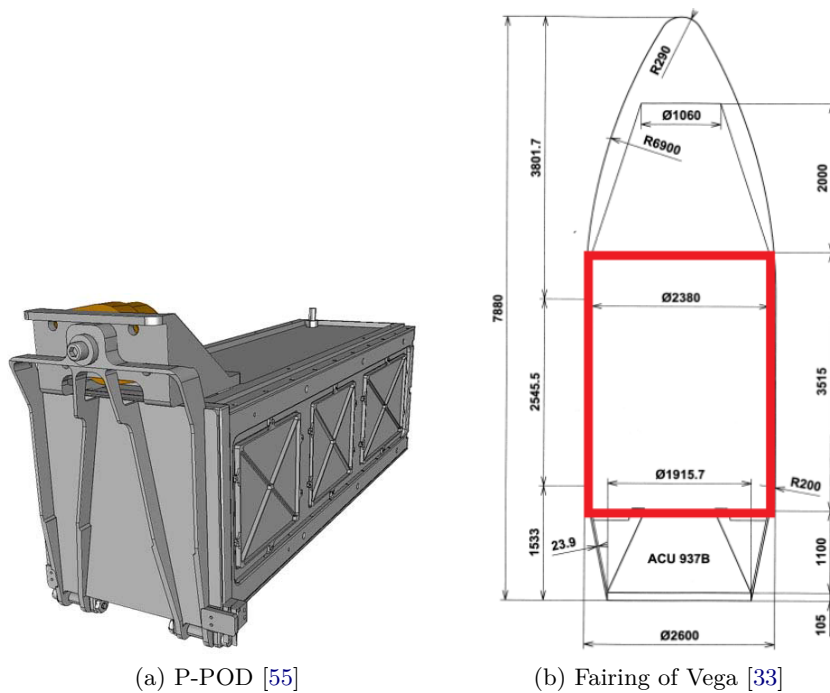


Figure 6.6: Impression of the P-POD and the fairing of VEGA.

For the 2,000 kg payload class the required payload volume should be the same as that for Vega. The dimensions of the payload fairing of Vega are shown in Figure 6.6b. The red rectangle resembles the volume that is taken in account because it is assumed that the available volume in the nose cap will match the volume of Vega's nose. So, the length of the fairing is fixed at 3.52 m and a minimum diameter of 2.60 m is required.

6.1.4 Aerodynamic Lifting Surfaces

Four design variables for the aerodynamic lifting surfaces were proposed in the literature study [103]. Because of limitations of the aerodynamic coefficient generator Missile Datcom (as will be explained in Chapter 7) a database had to be constructed. In order to avoid an extremely large database the number of design variables for the aerodynamic lifting surface is reduced to just one: the chord length at the wing root.

Based on Pegasus and the winged concepts in the NASA's HLS the other characteristics of the lifting surfaces are determined [6, 75]. The average taper ratio, $\lambda = \frac{c_{tip}}{c_{root}}$, of the different concepts is 0.16 and it will be assumed that the wing starts immediately at the top of the first stage. In addition the chord length ratio between the horizontal tail planes and the wing is fixed at 0.40. The taper ratio of the horizontal tail plane is also 0.16 and the trialling edge of the horizontal tail plane is located at the point where the motor case starts to converge (see Figure 6.7).

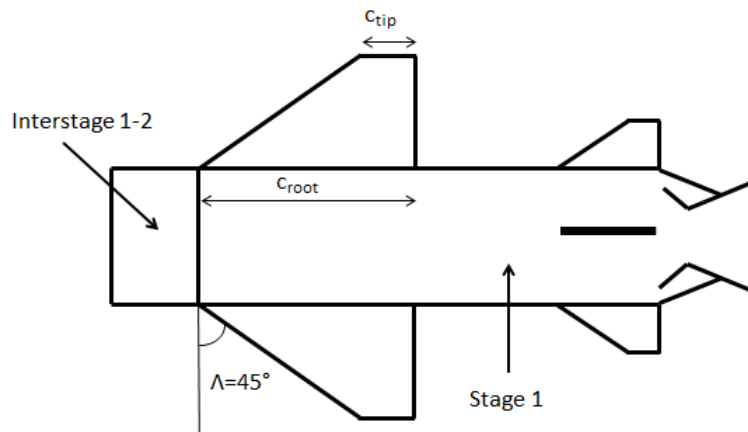


Figure 6.7: Geometry model winged launch vehicle (only the first stage is shown).

6.2 Mass Models

In the literature study different mass models were discussed [103]. The selected mass model is based on [15] but differs on several points. First of all, Castellini's mass model did not contain relations for the aerodynamic lifting surfaces. In addition, in Castellini's mass model the mass of the TVC system is calculated separately and in this model it is considered to be part of the nozzle mass. Also the Mass Estimation Relationship (MER) for the fairing is different because the data behind Castellini's relation was not present. The total mass breakdown of the launch vehicle for this study is given in Figure 6.8. In the subsections the mass models for each of the elements are separately validated. The model for the propellant mass is already described and validated in Chapter 5.

Normally validation for models is done for launch vehicles that are in the same class as the launch vehicles that are investigated. Unfortunately, for this study this approach can not completely be followed. First, because there are no launch vehicles in the 10 kg payload class it is impossible to use them for validation. Second, mass data for the individual components is extremely rare. Therefore, often data for launch vehicles that have a payload mass between the ones that are evaluated in this study are used for validation.

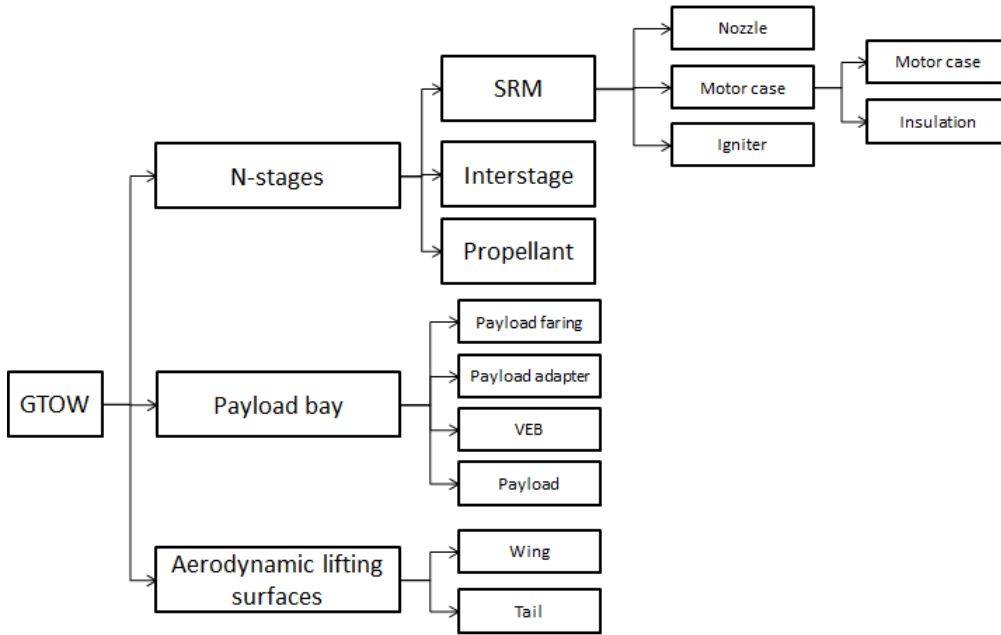


Figure 6.8: Mass breakdown structure of the launch vehicle.

6.2.1 Solid Rocket Motor

The mass model of the SRM consists of the nozzle, the motor case and the igniter.

6.2.1.1 Nozzle

The nozzle significantly contributes to the inert mass of the rocket stage. Based on the SRMs in the Solid Rocket Motor Database the nozzle mass is 14.9% to 41.6% (on average 23.9%) of the stage's total inert mass. According to [15] the best way to model the nozzle mass is as a function of the maximum vacuum thrust. Also in the relations for the nozzle mass in [120] the thrust force is the sizing variable (next to strength of the nozzle material). Because for this study the thrust is assumed to be constant the nozzle mass model will be based on the average thrust. This is already an explanation for some of the differences between the model and actual nozzle masses. The earlier mentioned database with 32 solid rocket stages is divided into three categories: large solid rocket motors ($T_{vac} > 200$ kN), small solid rocket motors with TVC ($T_{vac} < 200$ kN) and small solid rocket motors without TVC ($T_{vac} < 200$ kN). For each of these categories a MER is developed. The standard error of estimate (SEE) is a measure for the accuracy of the regression analysis. In mathematical form the SEE is given as:

$$SEE = \frac{100\%}{\frac{\sum_{i=1}^n y_i}{n}} \cdot \sqrt{\frac{\sum_{i=1}^n (y_i - \bar{y}_i)^2}{n - m}} \quad (6.4)$$

Where m is the number of reduced DoF, for example, for linear regression function $m=2$ and for a 2-degree polynomial regression function $m=3$. The results of the regression

analysis are shown in Figure 6.9, 6.10 and 6.11. Also the SEE and the 1 and 3 SEE lines are indicated in the figures to give an impression of the regression analysis's accuracy.

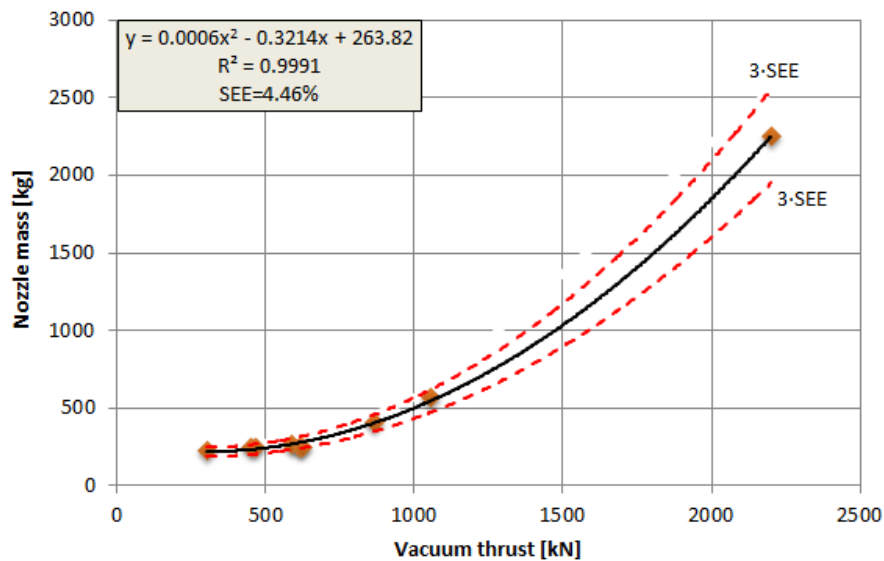


Figure 6.9: Correlation between nozzle mass and vacuum thrust for large SRMs ($T_{vac} > 200\text{kN}$).

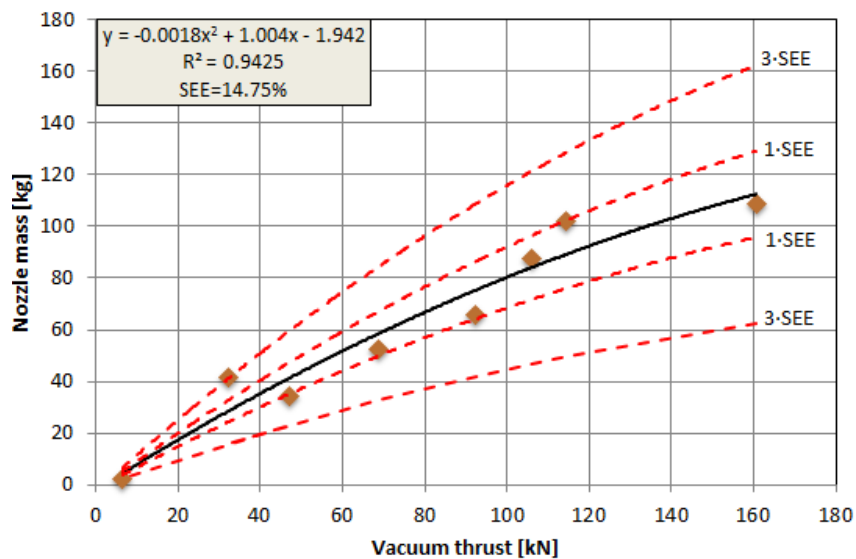


Figure 6.10: Correlation between nozzle mass and vacuum thrust for small SRMs with TVC ($T_{vac} < 200\text{kN}$).

These new MERs are validated for the 14 motors and the results can be found in Figure 6.12 and Table 6.2. From the regression analysis it follows that for the small motors (with or without TVC) the SEE is larger than for the large motors. This is also shown in Figure 6.12 where on average the absolute errors for the smaller motors are higher than for the larger motors.

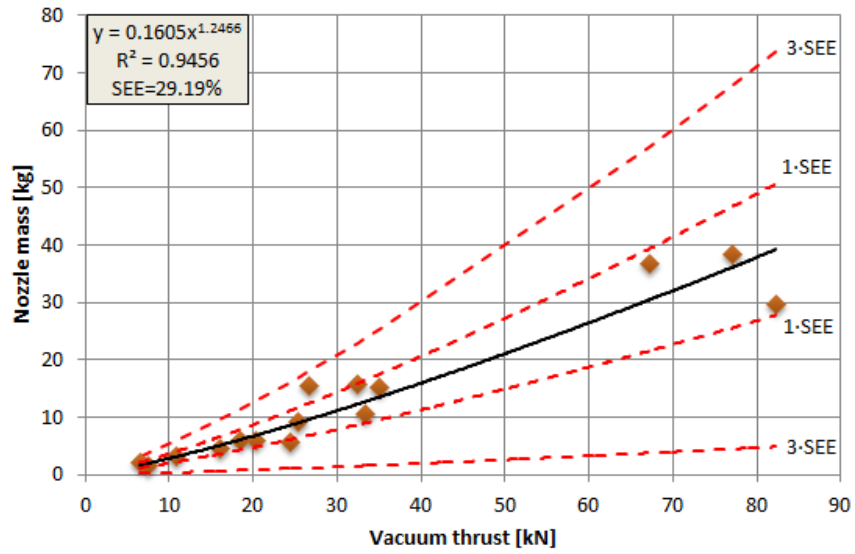


Figure 6.11: Correlation between nozzle mass and vacuum thrust for small SRMs without TVC ($T_{vac} < 200\text{kN}$).

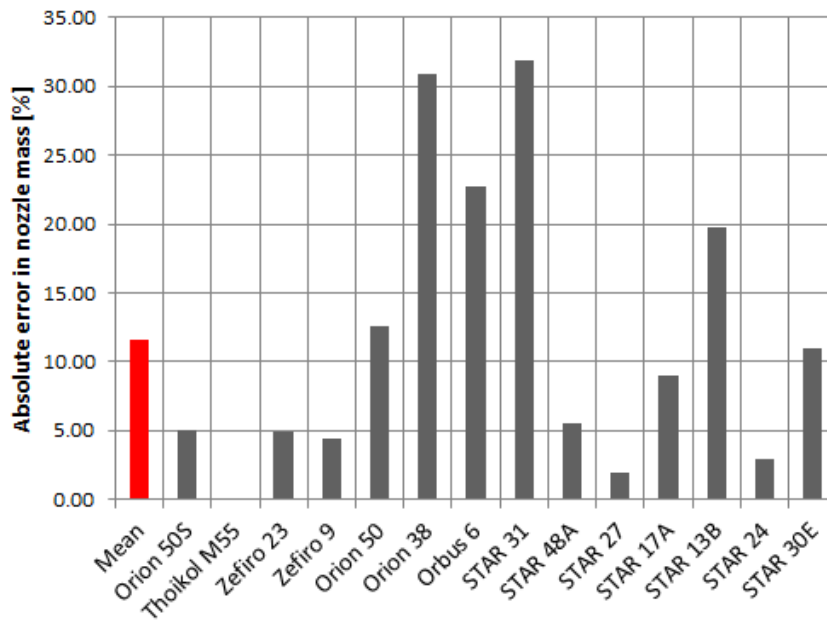


Figure 6.12: Absolute error [%] in calculated nozzle mass compared with actual nozzle mass.

Description	E [%]	μ [%]	σ [%]
Nozzle mass	11.6	+2.51	15.8

Table 6.2: Statistical figures of the error in the estimation of the nozzle mass.

6.2.1.2 Motor case

The mass of the motor case is modeled as two separate components: the mass of the motor case itself and the mass of the insulation layer.

Motor case The motor case can be estimated with the classical cylindrical pressure vessel relation. This introduces the assumption that the structural mass is entirely determined by the chamber pressure and that other loads can be handled by the internal pressure in the casing. Despite the fact that there are claims that the casing of SRMs can cope with these loads without extra reinforcements a safety factor, f_{safety} , of 1.5 is used [89]. This safety factor is composed of a safety factor for design burst pressure and a design safety factor [120].

The maximum stress in the motor case can be estimated with the membrane theory, which assumes that all loads are taken in tension and that there is no bending in the case wall [98]. Under the assumption of constant thickness the thickness of the motor case is given by [120]:

$$t = \frac{p_c \cdot D_{case}}{2 \cdot \sigma} \cdot f_{safety} \quad (6.5)$$

Where, σ , is the allowable material design stress. In this study the motor case is assumed to have a flat top, cylindrical body and frustum aft (see Figure 6.13).

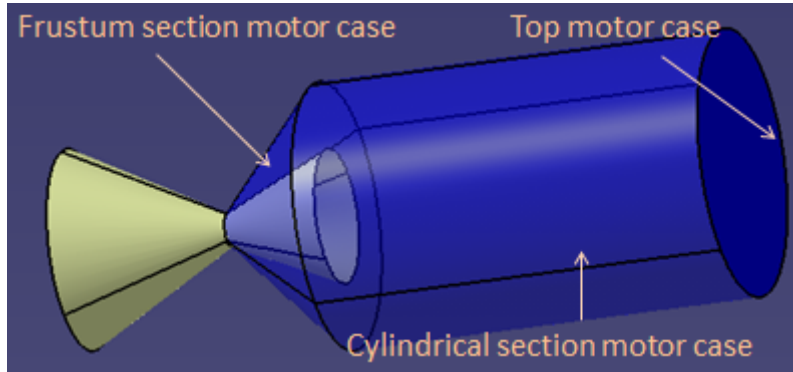


Figure 6.13: Geometry of the motor case.

The mass formulas for the three elements of the motor case are:

$$M_{case_{top}} = \rho \cdot \pi \cdot t \left(\frac{D_{case}}{2} \right)^2 \quad (6.6)$$

$$M_{case_{body}} = \rho \cdot \pi \cdot L_{case} \left(\left(\frac{D_{case}}{2} \right)^2 - \left(\frac{D_{case}}{2} - t \right)^2 \right) \quad (6.7)$$

$$M_{case_{frus}} = \frac{\rho \cdot \pi \cdot L_{frust}}{3} \left(\left(\left(\frac{D_{case}}{2} \right)^2 + \left(\frac{D_{case}}{2} \right) \cdot \left(\frac{D_{nozzle}}{4} \right) + \left(\frac{D_{nozzle}}{4} \right)^2 \right) - \right) \quad (6.8)$$

$$\left(\left(\frac{D_{case}}{2} - t \right)^2 + \left(\frac{D_{case}}{2} - t \right) \cdot \left(\frac{D_{nozzle}}{4} - t \right) + \left(\frac{D_{nozzle}}{4} - t \right)^2 \right)$$

Where, ρ , is the density of the material. Two possible materials that can be used for this casing are the Al-7075 alloy or a high strength Carbon Fiber Reinforced Plastic (CFRP) ($\rho=1,600 \text{ kg}\cdot\text{m}^{-3}$, $\sigma = 800 \text{ MPa}$) [15]. For this study all motors use CFRP as casing material. However, the actual material of the casing is used for the validation of the individual motors.

Insulation Because the thermal insulation mass has limited impact compared with the motor case mass an insulation layer with a constant thickness of 3 mm is assumed [15]. In addition, it is assumed that no insulation is required at the frustum because the hot gases have already entered the nozzle. In this study the insulation layer starts at 99% of diameter of the casing:

$$M_{insulation_{top}} = \rho_{in} \cdot \pi \cdot 0.003 \left(\frac{0.99 \cdot D_{case}}{2} \right)^2 \quad (6.9)$$

$$M_{insulation_{body}} = \rho_{in} \cdot \pi \cdot L_{case} \left(\left(\frac{0.99 \cdot D_{case}}{2} \right)^2 - \left(\frac{0.99 \cdot D_{case}}{2} - 0.003 \right)^2 \right) \quad (6.10)$$

As insulation material a simple rubber is used. The Ethylene-Propylene-Diene Copolymer (EPDM), $\rho_{in}=850 \text{ kg}\cdot\text{m}^{-3}$, is often used as insulation material for motor cases [23].

Validation Motor Case Mass Also the motor case mass is validated for the 14 SRMs. The results are shown in Figure 6.14 and the statistical figures are given in Table 6.3.

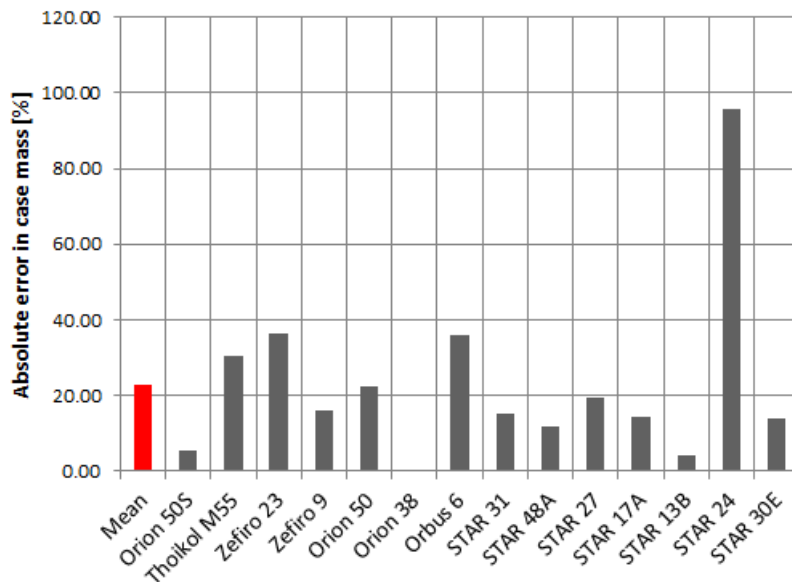


Figure 6.14: Absolute error [%] in calculated motor case mass compared with the actual motor case mass.

The estimated case mass of the STAR 24 motor is almost twice as high as the actual mass; all estimations for the other motors are within 40% of the actual case masses. It has to be noted that all STAR motors that are evaluated (except STAR 31) have a spherical case. One would expect an overprediction in the case mass for those motors, however, for all STAR motors except for the STAR 24 this is not the case.

It can be concluded that case mass is hard to model because the motor case mass is calculated based on the average chamber pressure. In reality the maximum chamber pressure of these motors is higher because the vacuum thrust is not constant over the burn time. The effect of a varying inert mass (thus also case mass) will be investigated during the sensitivity analysis in Chapter 12.

Description	E [%]	μ [%]	σ [%]
Motor case mass	22.9	+7.59	32.6

Table 6.3: Statistical figures of the error in the estimation of the motor case mass.

6.2.1.3 Igniter

For SRMs the igniter mass can be significant and it is modeled as a function of the available internal volume in the grain, V_{cavity} [15]. This is calculated by subtracting the volume of the propellant from the total volume of the motor case:

$$V_{cavity} = L_{case} \cdot \pi \left(\frac{0.99 \cdot D_{case}}{2} \right)^2 - \frac{M_p}{\rho_p} \quad (6.11)$$

The mass model is based on regression from the solid rocket boosters of Ariane V and the three stages of Vega (SEE 13.2%) and is given by [15]:

$$M_{igniter} = 20.62 \cdot V_{cavity}^{0.7368} \quad (6.12)$$

The igniter mass is not individually validated because it is only ~1-4% of the total inert mass of the motor [15, 98].

6.2.2 Interstage

The interstage geometry is simplified to a frustum with the length of the nozzle of the next stage plus the fixed distance between the stages of 0.1 meters. For the estimation of the interstage mass two MERs based on regression is used. The interstage mass can be determined for lower stages by [15, 88]:

$$M_{int} = k_{sm} \cdot 7.7165 \cdot S_{int} \left(D_{int}^{3.3208} \right)^{0.4856} \quad (6.13)$$

Where k_{sm} is 1.0 for classical Al-alloys based structures and 0.7 for advanced composite based structures. For upper stages a slightly different regression formula can be used [15] [88]:

$$M_{int} = k_{sm} \cdot 5.5234 \cdot S_{int} \left(D_{int}^{3.3208} \right)^{0.5210} \quad (6.14)$$

It is hard to find interstage masses for launch vehicles because the interstage mass is often distributed over two stages, however, the models are validated using the interstage masses of Ariane IV, Ariane V, Vega and Atlas.

For detailed information is referred to Appendix F. For this study only aluminum based structures are evaluated, however, during the validation the actual materials of the interstages are used and during the sensitivity analysis the effect of a composite structure is investigated too. The summary for the statistical figures of the error in the estimation of the interstage mass is given in Table 6.4. The mean error is not large, however, the absolute mean error and the standard deviation of the error are considered high. From this it can be concluded that it is hard to predict the interstage mass based on regression.

Description	E [%]	μ [%]	σ [%]
Interstage mass	29.6	-6.00	33.2

Table 6.4: Statistical figures of the error in the estimation of the interstage mass.

6.2.3 Payload bay

In this model the payload bay of the launch vehicle contains the fairing, payload adapter, vehicle equipment bay (VEB) and the payload itself.

6.2.3.1 Fairing

The mass model for the fairing is based on the wetted area¹ of the fairing: $12.2 \text{ kg}\cdot\text{m}^{-2}$ [6]. For the calculations of the fairing's mass the fairing's geometry is assumed to consist of three elements: a conical nose, a cylindrical fairing and the fairing frustum (see Figure 6.15).

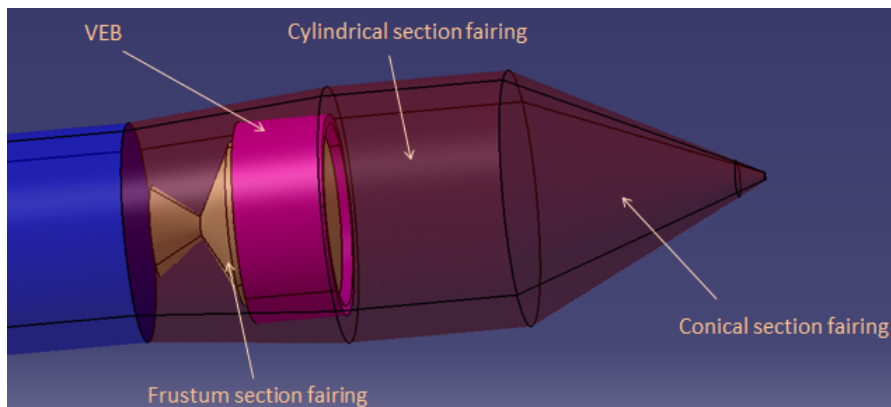


Figure 6.15: Simplified geometry of the fairing for the mass calculations.

The fairing mass is validated for Vega, Taurus, Pegasus, Minotaur, Kosmos and PSLV. The details are given in Appendix F. The statistical figures of the validation for the fairing mass can be found in Table 6.5. From these statistical figures it can be concluded that

¹The wetted area is the area which is in contact with the external airflow.

the simplification of the fairing's geometry and the use of the wetted area for the mass estimation is acceptable. The fairing mass is one of the parameters that is investigated in the sensitivity analysis in Chapter 12.

Description	E [%]	μ [%]	σ [%]
Fairing mass	14.5	-0.27	17.5

Table 6.5: Statistical figures of the error in the estimation of the fairing mass.

6.2.3.2 Payload adapter

For the payload adapter the following equation based on regression (SEE 38.2%) is used [15]:

$$M_{adapter} = 0.004775 \cdot M_{payload}^{1.0132} \quad (6.15)$$

With $M_{payload}$ the supported payload mass. The payload adapter mass will not be validated individually because its mass is almost negligible in comparison with the fairing mass. For Vega the payload adapter mass is less than 2% of the fairing mass [15].

6.2.3.3 Vehicle Equipment Bay

A MER for the VEB is given by [121]:

$$M_{int} = 0.404 \cdot M_{dry}^{0.6814} \quad (6.16)$$

This formula is based on regression (SEE 34%) and contains a lot of old launch vehicles for which the mass of the VEB is higher than for modern launch vehicles [122]. Some old launch vehicles are removed from the data set and the VEB masses of Ariane 44L and Vega are added. More details can be found in Appendix F.

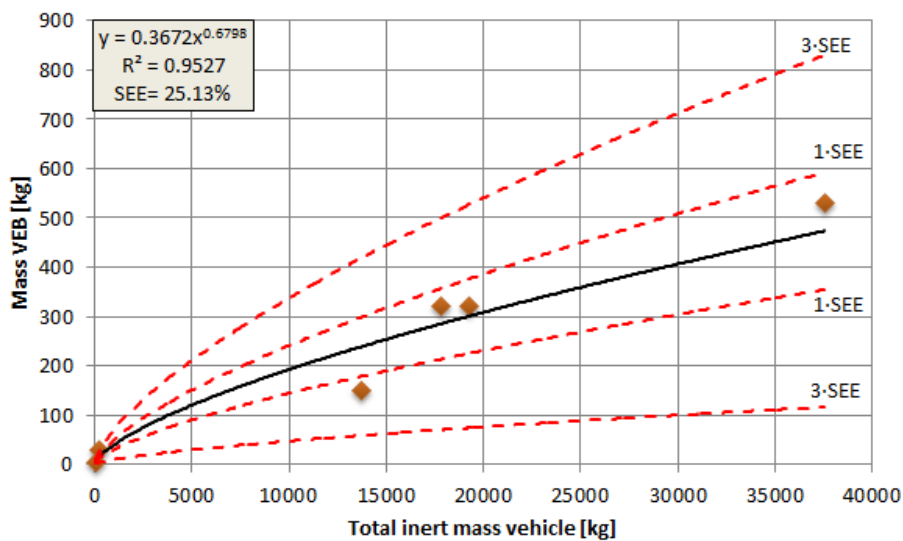


Figure 6.16: Correlation between the mass of the VEB and the total inert vehicle mass.

The SEE is reduced to 25% and the data and the statistical figures for the validation of the VEB are given in Table 6.6. Despite the fact that the SEE is decreased compared with original relation from [121] there remains a large absolute mean error and large standard deviation. Therefore, it is decided to investigate the sensitivity of the solution to a varying VEB mass during the sensitivity analysis.

Description	E [%]	μ [%]	σ [%]
VEB mass	30.9	+6.66	40.9

Table 6.6: Statistical figures of the error in the estimation of the VEB mass.

6.2.3.4 Payload

The payload depends on the launch vehicle type. A payload of 10 kg and of 2,000 kg will be evaluated in this study.

6.2.4 Aerodynamic Lifting Surfaces

The tool has to be able to cope with the effects of a wing and therefore, also be able to estimate the mass of the wing. An extensive list of MERs for wings and tails can be found in the work of Rohrschneider [88]. However, most of these relations are based on reusable launch vehicles (RLVs) where the lifting surfaces are sized for the reentry. Detailed modeling of the wing and tail is beyond the scope of this thesis research for which the evaluation of winged vehicles is only a sub objective. Therefore, the wing/tail mass will be solely based on the surface area of the wing or tail: $24.4 \text{ kg}\cdot\text{m}^{-2}$ [6]. The wing structure of Pegasus XL has a mass of 285 kg [47] and with this model the wing mass is estimated at 307 kg. In the sensitivity analysis the effect of a deviation in wing mass of 20% will be investigated.

6.2.5 Correction Total Inert Mass

In previous sections all individual components were validated. Now it is time to validate the total inert mass of the individual stages. The inert mass of the stage is calculated as the sum of the nozzle, igniter, motor case and insulation mass. On average the total inert mass of the stages was 16.6% lower than the real mass. Therefore, 16.60% is added to the inert mass of each stage. From Figure 6.17 and Table 6.7 it can be concluded that after the introduction of the correction factor the mean error (relative and absolute) is reduced at the expense of a small increase in the standard deviation of the error. The statistical measures given in Table 6.7 will be used as input parameter for the sensitivity analysis in Chapter 12.

Description	E [%]	μ [%]	σ [%]
Total inert mass original	17.2	-16.6	11.9
Total inert mass updated	12.4	-2.76	13.8

Table 6.7: Statistical figures of the error in the estimation of the total inert mass.

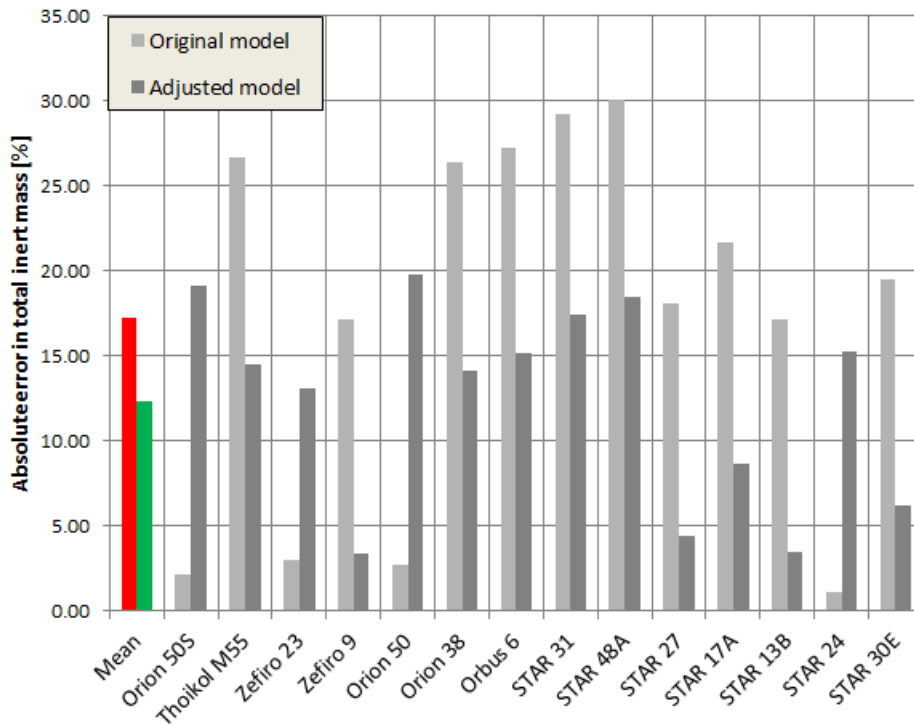


Figure 6.17: Absolute error [%] in calculated total inert mass compared with the actual total inert mass.

6.3 Launch Vehicle Constraints

Also the launch vehicle configuration introduces several constraints to the design of the launch vehicle. These constraints will be discussed below.

The first constraint deals with the total length of the launch vehicle, L_{tot} . The limitations of the carrier aircraft introduce a maximum length of the launch vehicle (values can be found in Table 1.1). In addition the GTOW of the launch vehicle is also restricted to the values given in Table 1.1. The same holds for the diameter of the launch vehicle, however, the design variables can not have values above the limit value. Hence the launch vehicle's diameter will not be modeled as an active constraint.

In order to ascend the initial thrust to weight ratio, $\left(\frac{T}{W}\right)_{init}$, of the launch vehicle should be larger than 1.0. Actually this is only a strict requirement for a ground launch, however, to avoid unrealistic configurations the $\left(\frac{T}{W}\right)_{init}$ has to be larger than 1.15 for both ground and air launched vehicles.

In order to avoid unrealistic vehicle configurations that will never reach orbit and consume precious computation time a constraint for the vehicle's amount of ΔV is introduced. For ground launch a minimum ΔV of $9,000 \text{ m}\cdot\text{s}^{-1}$ is required and for air launch $8,200 \text{ m}\cdot\text{s}^{-1}$ [45].

Aerodynamics

A launch vehicle encounters the atmosphere during its journey to orbit. The aerodynamics involved during that portion of the flight have a large influence on the launch vehicle's ascent. In the literature study external software tools were evaluated and Missile Datcom was selected [103]. This decision was based on the availability of the tool and because Frank Engelen developed a routine to implement Missile Datcom in the Tudat framework [31].

In the first section of this chapter the aerodynamic model is explained. This is followed by a discussion about Missile Datcom. In this section also the limitations and the way Missile Datcom is implemented in the tool are discussed. The final section of this chapter attempts to validate the aerodynamic model.

7.1 Aerodynamic Model

The lift force, L , drag force, D , and side force, S , are given by:

$$D = \frac{1}{2} C_D \cdot \rho \cdot V^2 \cdot S_{ref} \quad (7.1)$$

$$S = \frac{1}{2} C_S \cdot \rho \cdot V^2 \cdot S_{ref} \quad (7.2)$$

$$L = \frac{1}{2} C_L \cdot \rho \cdot V^2 \cdot S_{ref} \quad (7.3)$$

With C_L , C_D and C_S respectively, the lift, drag and side force coefficient and S_{ref} the aerodynamic reference surface. It is common for missiles and launch vehicles to take the frontal cross-sectional area of the body as the aerodynamic reference surface [37, 65]. It should be noted that during all simulations the side slip angle is set to zero. This in combination with the absence of wind makes the side force irrelevant for the simulations. However, in the tool the side force coefficient is calculated and can easily be implemented

for future applications. The same holds for the bank angle that is currently set to zero in the tool but in reality depends on the roll angle, side slip angle and angle of attack [72]. The aerodynamic forces are defined in an aerodynamic reference frame as is shown in Figure 7.1. In the definition used for the aerodynamic reference frame in the tool and Figure 7.1 the drag (x-direction), side (y-direction) and lift (z-direction) force are negative in the positive directions in the frame. Throughout this report the drag and lift force are always indicated positive, this means that they are negative in Figure 7.1.

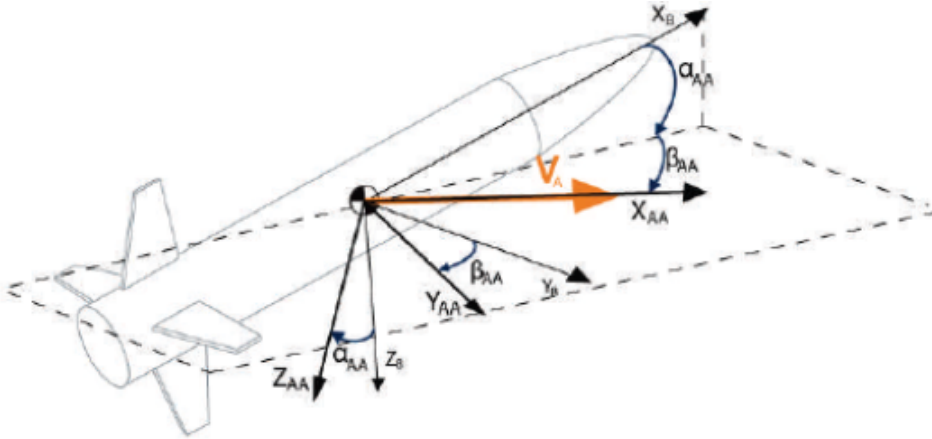


Figure 7.1: Aerodynamic reference frame (angles are indicated positive) [31].

In Chapter 3 it is already explained that a 3 DoF simulation will be executed, therefore, no information about pitching moment coefficients is required. Hence the lift and drag coefficients are the only relevant aerodynamic coefficients for this study. For a description of the wing is referred to Section 6.1.4.

Only the aerodynamic coefficients for the initial launch vehicle configuration are calculated. After the first staging event the coefficients from the initial launch vehicle will be used to calculate the aerodynamic forces for the rest of the launch vehicle.

7.2 Missile Datcom

The U.S. Air Force Missile Datcom is a semi-empirical aerodynamic prediction code that calculates aerodynamic forces, moments, and stability derivatives as a function of angle of attack and Mach number for a variety of axisymmetric and non axisymmetric missile configurations [12]. Also it allows the user to add fin configurations that can resemble wings. Missile Datcom source code is subjected to International Traffic in Arms Regulations (ITAR) and, therefore, not available to non-U.S. persons. However, the 1999 version (revision 3) of the software is distributed as a supplement to the book "Design Methodologies for Space Transportation Systems" [43]. Missile Datcom is widespread and used for the prediction of aerodynamic coefficients for launch vehicles within the TU Delft [31, 82, 108] and in the rest of the academic world [15, 85, 87, 93]. The different geometries and flight conditions that can be handled by Missile Datcom are shown in Figure 7.2. An old version of Missile Datcom (1986) was also used for the prediction of the aerodynamic characteristics of Pegasus [67].

PARAMETER	SYMBOL	PRIORITY 1	PRIORITY 2	SOURCE
ANGLE OF ATTACK, DEG.	α	$-20 \leq \alpha \leq 30$	$-180 \leq \alpha \leq 180$	AEROMECHANICS
ANGLE OF YAW, DEG.	β	$-20 \leq \beta \leq 20$	$-180 \leq \beta \leq 180$	SURVEY AND
AERODYNAMIC ROLL, DEG.	ϕ	$0 \leq \phi \leq 45$	$0 \leq \phi \leq 180$	WORLD'S
MACH NUMBER	M	$0 \leq M \leq 6$	$0 \leq M \leq 10$	MISSILE
BODY FINENESS RATIO	$(l/d)_B$	$5 \leq (l/d)_B \leq 20$	$1 \leq (l/d)_B \leq 30$	SYSTEMS
NOSE FINENESS RATIO	$(l/d)_N$	$.5 \leq (l/d)_N \leq 5$	$0 \leq (l/d)_N \leq 7$	
FIN EXPOSED SPAN TO DIAMETER	b/d	$1 \leq b/d \leq 6$	$0 \leq b/d \leq 10$	↓
FIN ASPECT RATIO	AR	$0.6 \leq AR \leq 4$	$0.1 \leq AR \leq 10$	
FIN PLANFORM		TRIANGULAR TRAPEZOIDAL	ALL	
WING/TAIL ORIENTATION		IN-LINE	ALL	
CONTROL METHOD		ALL MOVEABLE FIN	ALL	
REYNOLDS NUMBER/FT	R_N	$3 \times 10^5 \leq R_N \leq 2 \times 10^7$	$10^3 \leq R_N \leq 3 \times 10^7$	MACH-ALTITUDE
FIN DEFLECTION/INCIDENCE, DEG.	δ	$0 \leq \delta \leq 30$	$0 \leq \delta \leq 60$	BOUNDARY
ROLL RATE, RAD/SEC.	p	$0 \leq p \leq 1$	$0 \leq p \leq 6$	MISSILE SYSTEM
PITCH RATE, RAD/SEC.	q	$0 \leq q \leq 1.5$	$0 \leq q \leq 3$	ANALYSIS
YAW RATE, RAD/SEC.	r	$0 \leq r \leq 1.5$	$0 \leq r \leq 3$	↓
FIN DEFLECTION RATE, RAD/SEC.	$\dot{\delta}$	$0 \leq \dot{\delta} \leq 10$	$0 \leq \dot{\delta} \leq 28$	

Figure 7.2: The different geometry and flights conditions that can be evaluated by Missile Datcom [111].

An overview of the different methods used by Missile Datcom to predict the aerodynamic characteristics of missiles thus launch vehicles is given in Figure 7.3.

Parameter	Subsonic/Transonic (M<1.2)	Supersonic (M>1.2)
Potential Normal Force	Option 1: Nose-cylinder: MBB charts, MBB TN-WE-2-9769 and Boattail: NSWC charts, NSWC-TR-81-156 and Flare: Army charts AMCP 706-280, or Option 2: Slender Body Theory	Option 1 and Option 2: Second Order Shock Expansion, NSWC-TR-81-156, or Van Dyke Hybrid theory, NSWC-TR-81-156, or Modified Newtonian theory, NASA-TND-176
Viscous Normal Force	Jorgensen viscous crossflow, NASA-TR-R-474 and AEDC-TR-75-124	Jorgensen viscous crossflow, NASA-TR-R-474 and AEDC-TR-75-124
Potential Pitching Moment	Option 1: Nose-cylinder: MBB charts, MBB TN-WE-2-9769 and Boattail: NSWC charts, NSWC-TR-81-156 and Flare: Army charts AMCP 706-280, or Option 2: Slender Body Theory	Option 1 and Option 2: Second Order Shock Expansion, NSWC-TR-81-156, or Van Dyke Hybrid theory, NSWC-TR-81-156, or Modified Newtonian theory, NASA-TND-176
Viscous Pitching Moment	Jorgensen viscous crossflow, NASA-TR-R-474 and AEDC-TR-75-124	Jorgensen viscous crossflow, NASA-TR-R-474 and AEDC-TR-75-124
Skin Friction Drag	Turbulent: Van Driest II, MDAC West Handbook Laminar: Blasius, Hoerner Fluid Dynamic Drag Roughness: USAF Datcom section 4.1.5.1	Turbulent: Van Driest II, MDAC West Handbook Laminar: Blasius, Hoerner Fluid Dynamic Drag Roughness: USAF Datcom section 4.1.5.1
Pressure/Wave Drag	M<Mcrit: USAF Datcom section 4.2.3.1 M>Mcrit: Transonic area rule, AIAA-90-0280	Second Order Shock Expansion, NSWC-TR-81-156, or Van Dyke Hybrid theory, NSWC-TR-81-156, or Modified Newtonian theory, NASA-TND-176
Base Drag	Cylinder: NSWC charts, NSWC-TR-92/509 Boattail: NASA method, NASA-TR-R-100 Flare: NSWC charts, NSWC-TR-81-358	Cylinder: NSWC charts, NSWC-TR-92/509 Boattail: NASA method, NASA-TR-R-100 Flare: NSWC charts, NSWC-TR-81-156
Protuberance Drag	M<0.6: Hoerner Fluid Dynamic Drag M>0.6: cubic fairing, AIAA-94-0027	M<5.0 Modified Newtonian theory wit, AIAA-94-0027 M>5.0: Modified Newtonian theory
Axial force at angle of attack	Allen and Perkins Crossflow, NASA TR-1048	Second Order Shock Expansion, NSWC-TR-81-156 Assumed zero for Van Dyke Hybrid and Modified Newtonian theory
Dynamic derivatives	LMSC code, LMSC-D646354 and D646354A Slender Body Theory, AIAA 97-2280	LMSC code, LMSC-D646354 and D646354A Slender Body Theory, AIAA 97-2280
Magnus derivatives	SPIN 73 code, FRL-TR-4588	SPIN 73 code, FRL-TR-4588
Plume effects	not calculated	Chapman Korst model, AIAA 90-0618

Figure 7.3: Overview of methods used for axisymmetric body-alone aerodynamics by Missile Datcom [111].

7.2.1 Limitations Missile Datcom

Despite the fact that Missile Datcom is often used it has some severe limitations. First, the software is not able to accurately predict asymmetric vehicles. Next, the 1999 version of the code is only valid until an angle attack of 30° and for higher angles of attack it switches to an empirically derived (less accurate) method. Finally, the 1999 version has problems with the prediction of the axial force coefficient in the transonic regime, as was already noted by [31] and [82]. This last problem is solved for later versions of the software, unfortunately, these versions are considered ITAR.

Another problem was observed during the familiarization phase with Missile Datcom. If the real geometry from Vega is used high values for the drag coefficient were obtained (see Figure 7.4). If this is compared with a launch vehicle with a uniform diameter that has the same nose shape and length as Vega large differences are observed.

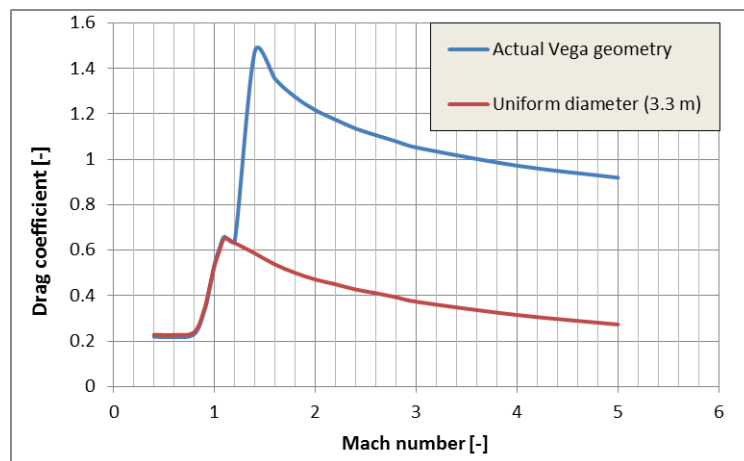


Figure 7.4: Predicted drag coefficient at various Mach numbers by Missile Datcom at $\alpha=0^\circ$ for Vega's actual shape and for a vehicle with an uniform diameter.

In the final report about Missile Datcom is stated that the method used to predict the wave drag at supersonic Mach numbers has the tendency to overestimate the wave drag [111]. The fact that the geometry is estimated as a series of conical frustums results in higher predicted axial forces [111]. This phenomena is also observed in [63]. Therefore, for this study only uniform cross-sectional bodies are observed.

7.2.2 Implementation of Missile Datcom in the Tool

One has to keep in mind that Missile Datcom is a FORTRAN program that has its origin in the 1970s. The user manual describes in detail how to set-up a case file or how to interpret the output files [12]. The first step is setting up a case file, which has to be named "for005.dat". A single missile or launch vehicle can be simulated up to 20 difference angles of attack combined with up to 20 different Mach numbers (see the input values used for this study in Table 7.1). Hence a single case consists of a maximum of 400 different coefficient sets.

For each Mach number a Reynolds number (or altitude) is assigned. The shape of the missile or launch vehicle is described based on definitions of different elements, for exam-

ple, the nose, body or fins. After the input file is defined, the Missile Datcom program is executed manually. One of the output files (for004.dat) that contains the bulk of generated information can be processed by the Missile Datcom Database Code Block developed by Frank Engelen [31]. This code block processes the Missile Datcom files: first all coefficients are stored in a look-up table as a function of Mach number and angle of attack. Because a coefficient depends on only two variables bi-linear interpolation can be used to estimate the value of the coefficient for every Mach number and angle of attack. If the value of the Mach number is beyond the boundaries of the database the limit value is chosen.

Mach numbers [-]					Angles of attack [deg]				
0.30	0.60	0.80	0.90	0.95	-30.0	-20.0	-15.0	-10.0	-8.00
1.00	1.05	1.10	1.20	1.30	-6.00	-4.00	-2.00	-1.00	0
1.40	1.60	1.80	2.00	2.50	1.00	2.00	3.00	4.00	6.00
3.00	3.50	4.00	4.50	5.00	8.00	10.0	15.0	20.0	30.0

Table 7.1: Mach numbers and angles of attack evaluated in Missile Datcom for this study.

Missile Datcom can be implemented directly in the tool, however, this results in a high computational load as is observed in [15] and [108]. Vandamme constructed a database of several launch vehicle configurations. The difference in obtained objective value between the integrated Missile Datcom (more precise) and the Missile Datcom database was less than 0.01% [108]. That difference is considered negligible, therefore, a database is constructed for this study as well.

Actually, three databases will be constructed: one for the small launch vehicles (payload mass 10 kg), one for the large launch vehicles (payload mass 2,000 kg) and one for the winged large launch vehicles (also payload mass 2,000 kg). The two variables for each of the launch vehicle configurations are the length and diameter. For winged launch vehicles also the chord length at the wing root is used to find the proper configuration. An overview for all launcher configurations available in the three databases is given in Appendix G.

7.3 Validation Aerodynamic Model

The validation of the aerodynamic model for real launch vehicles is hard because very limited data is available and the detailed geometry of the launch vehicle is not always known. In this section an attempt is made to validate Missile Datcom for body alone launch vehicles and winged launch vehicles.

7.3.1 Body Alone Launch Vehicles

The validation for the body alone case will be based on literature because a study is available that compares the outcomes of Missile Datcom and Aeroprediction (another tool that is evaluated in the literature study) with wind tunnel data [95]. For a body alone configuration the predicted values for the normal, C_N , and axial force coefficient, C_A , are compared with wind tunnel data at Mach 2.0.

The normal and axial coefficient are related to the lift and drag coefficients. The lift force is defined as the force perpendicular to the velocity vector and the drag force parallel to the velocity vector. The normal force is perpendicular to the center line of the launch vehicle (or chord line in case of an airfoil) and the axial force is defined parallel to the center line. The lift and normal force and drag and axial force are identical when the velocity vector is parallel to the center line of the launch vehicle (angle of attack is zero).

The results of this comparison are shown in Figure 7.5. From this figure it can be concluded that Missile Datcom is able to predict the normal force coefficient but has more problems with axial force coefficient, however, the prediction follows the trend of the wind tunnel data. According to [95] the axial force coefficient is the most difficult to predict.

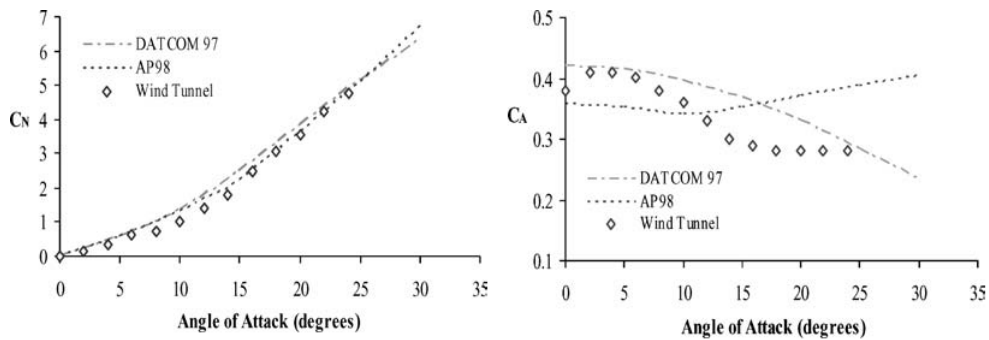


Figure 7.5: Wind tunnel results versus Missile Datcom and Aeroprediction 98 predictions for a body alone configuration for Mach 2.0 [95].

The aerodynamic coefficients for the ALOSS vehicle used by the NLR are also available for this study [105]. For details of the ALOSS vehicle is referred to Appendix B. Figure 7.6 shows the predicted zero lift drag coefficients for ALOSS by the NLR and by Missile Datcom.

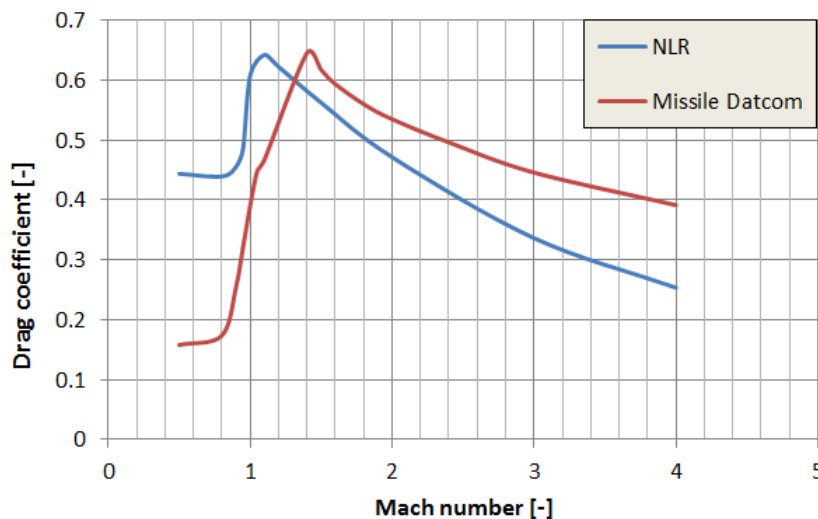


Figure 7.6: Predicted drag coefficient at various Mach numbers by the NLR and Missile Datcom at $\alpha=0^\circ$ for the ALOSS launch vehicle.

Despite the fact that there are differences in the predicted drag coefficients the same trends for supersonic velocities are observed. The values for the drag coefficient start to differ for hypersonic velocities. Possible explanation would be the different nose shapes, the relatively blunt nose that is used for this thesis work results in high drag forces in the hypersonic regime [37]. Unfortunately the in-house developed tool from the NLR that generates the aerodynamic coefficients is considered confidential and, therefore, no insight can be given in the methods used to calculate the drag coefficients.

7.3.2 Pegasus

In Figure 7.7 the estimated values for the aerodynamic coefficients by Missile Datcom are compared with real wind tunnel data from [66]. The geometry of Pegasus' wing and tail is estimated based on [67] and [75]. In general the results from Missile Datcom and wind tunnel data show good correspondence.

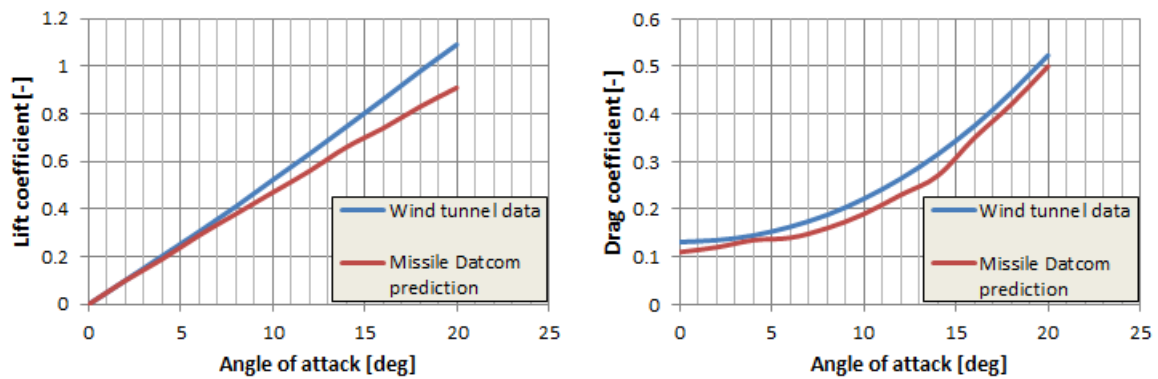


Figure 7.7: Wind tunnel results versus Missile Datcom predictions for Pegasus for Mach 2.0 (reference area is the wing area of Pegasus). Wind tunnel data from [66].

7.3.3 Conclusion

The previous two subsections show that it is very hard to validate the aerodynamic model based on limited data. Based on the preceding subsections no values can be assigned to the accuracy of Missile Datcom. In literature it is claimed that Missile Datcom has errors of $\pm 20\%$ for the axial and normal force coefficients [11, 95]. Also [15] reports mean errors of 20% for Missile Datcom for Ariane V and Vega. Therefore, a mean error, μ , of 0.0%, an absolute mean error, E , of 40.0% and a standard deviation of the error, σ , of 20.0% are used for this study.

Trajectory

In this chapter the trajectory of the launch vehicle will be discussed. For this study the launch vehicle will follow a direct ascent (DA) trajectory to orbit [114]. For a DA trajectory the burn-out conditions of the final stage are identical to the injection conditions of the desired orbit. An alternative trajectory would be a Hohmann Transfer Ascent (HTA) where the satellite is first launched into a parking orbit of approximately 200 km altitude before the satellite is injection into the final orbit. HTA minimizes the required energy to reach the final orbit [114]. The total weight delivered to a 400 km circular orbit can increase from ~58 kg to ~68 kg when the trajectory is changed from DA to HTA for a subsonic air launched vehicle with a GTOW of 3.2 ton [13]. However, the fact that this study only evaluates SRMs, that are not re-ignitable, makes the application of a HTA extremely hard. Moreover, for the ALOSS project also a direct ascent trajectory is used. For the comparison between air and ground launch a launch from the equator in eastward direction to a 780 km circular orbit will be evaluated, which matches with the target orbit of ALOSS.

The first section of this chapter discusses trajectory optimization with heuristic algorithms. This is followed by a section about the velocity losses that the launch vehicle encounters during its journey to orbit. Next numerical integration will be discussed. This is followed by the validation of the trajectory model. In this section also the optimal step size for the numerical integrator is determined. The final section of this chapter discusses the trajectory constraints.

8.1 Trajectory Optimization with Heuristic Algorithms

Heuristic optimization algorithms simply guess values for the control variables and over the generations the control variables will converge to a value close to the optimal control function. According to [8] the use of heuristic optimization algorithms is not competitive with gradient methods in the field of trajectory optimization. However, earlier it is decided that for this study a heuristic optimization algorithm will be used in a monolithic architecture. For a thorough discussion about the different trajectory optimization methods is referred to [8] or [103]. During the validation of the tool it will be shown that a

heuristic algorithm is able to optimize trajectories.

For this study a parametric control law is used that is determined by defining discretization points all along the trajectory. A number of pitch angles is selected for each stage and the interval is divided over the burn time of the stage. These points are optimized in order to satisfy the optimality conditions of the problem. The control law is defined by linear interpolation between the discretization points. In order to reduce the computation time, it is common to use piece-wise linear functions to interpolate the control law [5]. Another method is proposed by Pagano and Vandamme implemented it in his tool [82, 108]. This method expresses the pitch function as a polynomial, for example, a fourth-degree polynomial:

$$\theta(t) = a_0 + a_1t + a_2t^2 + a_3t^3 + a_4t^4 \quad (8.1)$$

In the literature study it was concluded that for a conventional launch vehicle the use of polynomial function is the preferred option because it requires less design variables and produces a smoother curve. In the case of an air launched vehicle a pull-up maneuver is difficult to model with a polynomial. Based on this and the fact that parametric control laws more frequently appear in literature there is a preference for using a parametric control law [1, 5, 56].

For the first stage a total of four discretization points (excluding the initial pitch angle which is equal to the initial flight path angle) are selected and for the other stages three discretization points. An extra discretization point for the first stage is chosen because launch vehicles change their attitude mostly during the initial phases of the flight [101]. Therefore, the discretization points are located at 5%, 20%, 60% and the end of the burn time of the first stage. For the other stages the discretization points are chosen for the start, 50% of the burn time and the end of the burn time. In Figure 8.1 the optimized parametric control law for the MDA validation of Taurus is shown.

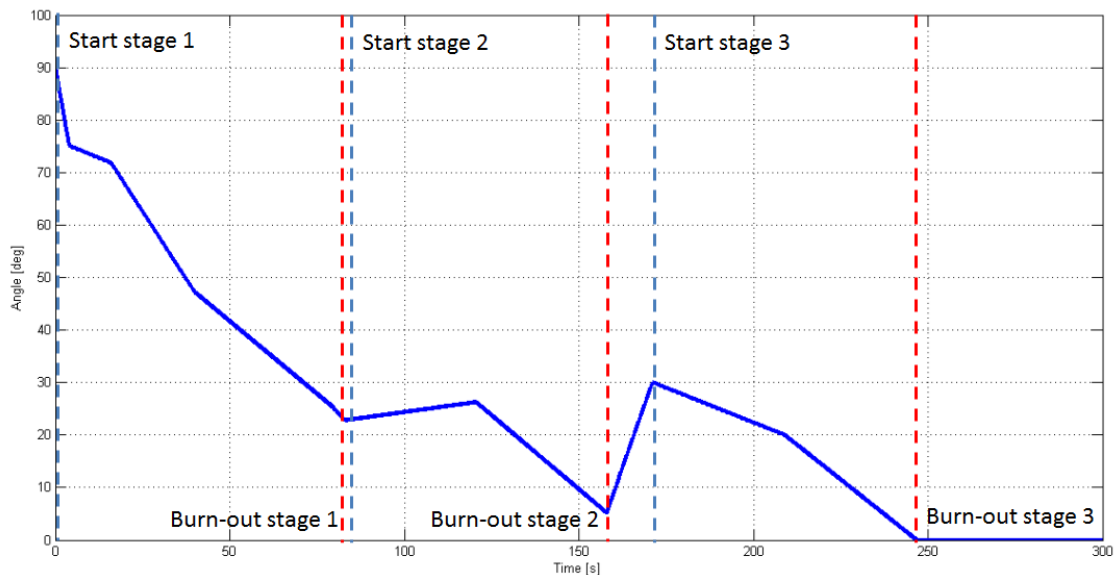


Figure 8.1: The parametric control law for the pitch angle for the MDA validation of Taurus for the first three stages.

8.2 Velocity Losses

During its way to orbit the launch vehicle experiences velocity losses and this increases the required amount of ΔV that has to be provided by the launch vehicle. For a thorough description of the characteristics of these losses is referred to [29] and [109]. For this study the drag loss, ΔV_{drag} , the gravity loss, $\Delta V_{gravity}$ and the steering loss, $\Delta V_{steering}$, are examined. The drag loss is defined by and calculated in the tool as:

$$\Delta V_{drag} = \int_0^{t_e} \frac{D}{m} \cdot dt = \int_0^{t_e} \frac{C_D \cdot \rho \cdot V^2 \cdot S_{ref}}{2 \cdot m} \cdot dt \quad (8.2)$$

From Equation 8.2 follows that in order to decrease the drag loss the velocity has to be low for the denser layers of the atmosphere. Drag loss is more significant for smaller launch vehicles because for these launch vehicles the ratio surface area versus mass is higher than for large launch vehicles [117]. Typical values for drag loss are in the range of 40 to 156 $\text{m}\cdot\text{s}^{-1}$ for large ground launched vehicles [45].

Next to drag loss the vehicle is also exposed to gravity loss and this loss is calculated in the simulation tool with:

$$\Delta V_{gravity} = \int_0^{t_e} g \cdot \sin(\gamma) \cdot dt \quad (8.3)$$

The flight path angle, γ , has to most influence on the gravity loss because the gravitational acceleration, g , only varies between 9.81 $\text{m}\cdot\text{s}^{-2}$ (at sea level) and 7.96 $\text{m}\cdot\text{s}^{-2}$ (at 700 km altitude). Shallower flight path angles and shorter burn times lead to a lower gravity loss. For a trajectory to a parking orbit (~ 200 km) the gravity loss for ground launched vehicles is typical between 1,150 and 1,576 $\text{m}\cdot\text{s}^{-1}$ [45]. For direct ascent to sun-synchronous orbits or geostationary transfer orbits values for the gravity loss between 2,000 and 2,400 $\text{m}\cdot\text{s}^{-1}$ are found [60].

Steering the launch vehicle during its way to orbit is causing a steering loss. The steering loss arises because the thrust vector is not always parallel to the velocity vector [92]. Values for the steering loss for ground launched vehicles are in the wide range of 38 to 358 $\text{m}\cdot\text{s}^{-1}$ [45]. The steering loss is defined as:

$$\Delta V_{steering} = \int_0^{t_e} \frac{T}{m} \cdot (1 - \cos(\alpha)) dt \quad (8.4)$$

8.3 Numerical Integration

Numerical integration is required for determining the launch vehicle's trajectory. In this section numerical integration will be briefly discussed. In general numerical integration is always a trade-off between accuracy and computation time. The smaller the step size of the integration the higher the accuracy and the longer the computation time. In the literature study it is decided to selected a numerical integrator that is already available

in Tudat. At this moment only single step, constant step size numerical integrators are available in Tudat [100]. For convenience it is decided to adapt the Runge-Kutta 4 that is used by Vandamme. The optimal step size for this integrator is investigated in Section 8.4.

The main characteristic of a single step method is that it makes no use of the function values calculated in earlier steps to predict the value of the function at the next step. The discussion in this section is based on [76]. So, every integration step is completely independent of one another. Suppose a general differential equation:

$$\dot{\mathbf{y}} = \mathbf{f}(t, \mathbf{y}) \quad (8.5)$$

The integration of this differential equation is required. The initial value is given by: $\mathbf{y}_0 = \mathbf{y}(t_0)$. A numerical integrator approximates the value for \mathbf{y} at a later time: $t_0 + h$, where h is the step size. This can be done by using an increment function, Φ , that approximates the slope of \mathbf{y} between (\mathbf{y}_0, t_0) and $(\mathbf{y}(t_0 + h), t_0 + h)$. For a time t the value for the function at time $t + h$ is given by:

$$\mathbf{y}(t + h) \approx \mathbf{y}(t) + h \cdot \Phi = \eta(t + h) \quad (8.6)$$

Where $\eta(t + h)$ is the approximate solution. The Runge-Kutta 4 method estimates the increment function based on four slopes between t and $t + h$:

$$\Phi_{RK4} = \frac{1}{6} (k_1 + 2 \cdot k_2 + 2 \cdot k_3 + k_4) \quad (8.7)$$

Where the four slopes are defined as:

$$\mathbf{k}_1 = \mathbf{f}(t, \mathbf{y}(t)) \quad (8.8)$$

$$\mathbf{k}_2 = \mathbf{f}\left(t + \frac{h}{2}, \mathbf{y} + \mathbf{k}_1 \cdot \frac{h}{2}\right) \quad (8.9)$$

$$\mathbf{k}_3 = \mathbf{f}\left(t + \frac{h}{2}, \mathbf{y} + \mathbf{k}_2 \cdot \frac{h}{2}\right) \quad (8.10)$$

$$\mathbf{k}_4 = \mathbf{f}(t + h, \mathbf{y} + \mathbf{k}_3 \cdot h) \quad (8.11)$$

In graphical form the four slopes are visualized in Figure 8.2. The local truncation error¹ of Runge-Kutta 4 is given by:

$$e_{RK4} = |y(t + h) - \eta(t + h)| \leq \text{const} \cdot h^5 \quad (8.12)$$

Hence the error is in the order of h^5 .

¹The truncation error is the error made by truncating an infinite sum and approximating it by a finite sum.

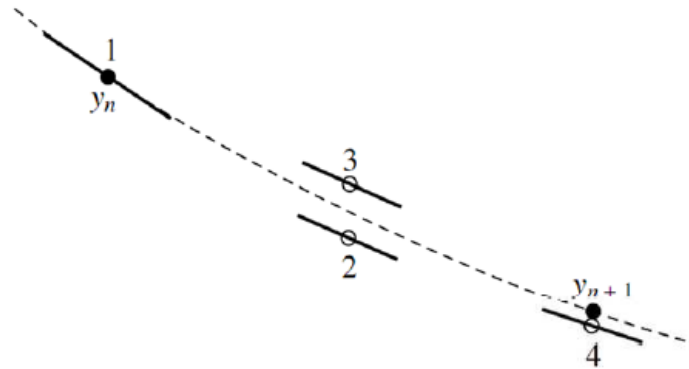


Figure 8.2: Visualization of the four slopes used for the Runge-Kutta 4 integrator [76].

8.4 Validation Trajectory Model

During the development of the ascent simulator by Frank Engelen, the simulator was validated by simulating the flight of the single stage sounding rocket DAVE. The outcomes of this simulation were compared with actual flight data from DAVE. The flight data showed similar trends as the simulated flight and Engelen was able to explain the differences between the measurement data and simulation data [31]. After this the tool is heavily modified by Vandamme and once again for this work. Therefore, it is deemed necessary to validate the trajectory model again. As is described in Section 8.1 a parametric control law for the pitch angle is used to guide the launch vehicle. In literature very limited data is available for the pitch angle history of launch vehicles during the ascent to orbit. Therefore, the data from the ALOSS project that is provided by the NLR is used [105]. Of course this is not actual flight data but NLR's simulations are executed by an in house developed simulator [106]. This section is concluded by an examination of the accuracy of the simulation results for various step sizes.

Unfortunately the parametric control law and coasting times for the obtained data set are different than the ones used in [106]. The ALOSS launch vehicle is launched from the equator in eastward direction with an initial velocity of $236 \text{ m}\cdot\text{s}^{-1}$ at 15 km altitude. The release flight path angle is 50° and the vehicle has an initial angle of attack of 0° . For the trajectory model validation only the trajectory is validated hence the values for the propulsion, geometry and mass characteristics of the ALOSS vehicle are used [106]. The properties of the ALOSS vehicle can be found in Appendix B.

It should be noted that the NLR did not include the influence of the ambient pressure on the thrust. In the tool the product of the ambient pressure and exit area is subtracted from the vacuum thrust, however, for this validation case this is not done. In order to be able to validate the trajectory model the atmosphere and vehicle properties have to be identical. Therefore, the exact thrust and mass history for ALOSS will be used and is hard coded in the tool as can be shown in Figure 8.3.

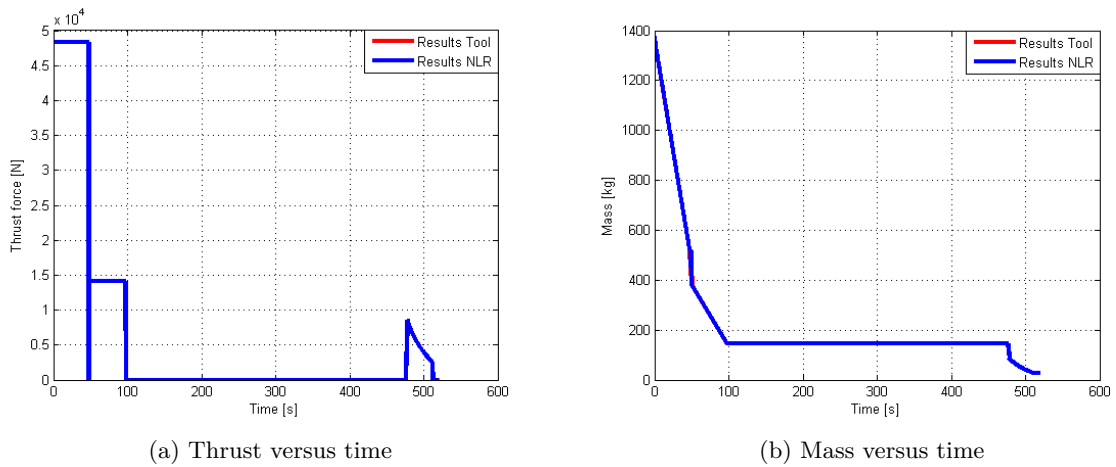


Figure 8.3: Comparison of the thrust and mass versus time of the tool and NLR's tool for the ALOSS F-16 case.

There is a difference between the atmospheric models that are used both studies. Therefore, it is decided that the height versus density relation from the atmospheric model that is used by the NLR is implemented in the tool for this validation step. The NLR did not take in account the lift force. By the tool used for this work a maximum value of 2,300 N is predicted for the lift force. This is also an explanation for the difference in angle of attack (thus flight path angle) during the initial phase of the flight. The drag force and angle of attack are shown in Figure 8.4. The drag force that is predicted is slightly higher than for the NLR. This also results in a higher predicted drag loss of $166.2 \text{ m}\cdot\text{s}^{-1}$ compared to the $147.7 \text{ m}\cdot\text{s}^{-1}$ from the NLR.

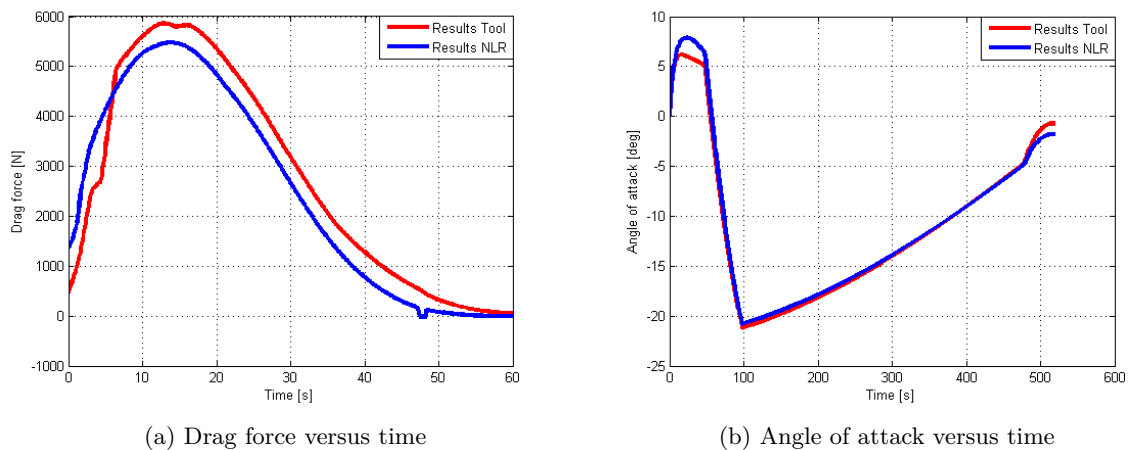


Figure 8.4: Comparison of the drag force and angle of attack of the tool and NLR's tool for the ALOSS F-16 case.

The altitude and velocity of the two tools are given in Figure 8.5. The outcomes are very similar except for a small difference in final altitude of 3.2 km. This is caused by a slightly

shallower flight path angle predicted by the tool as can be seen in Figure 8.6.

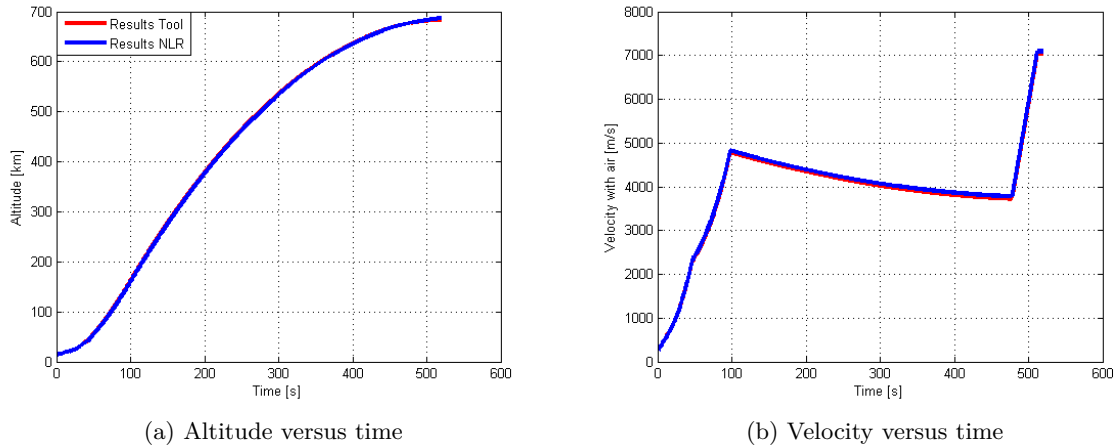


Figure 8.5: Comparison of the altitude and velocity versus time of the tool and NLR's tool for the ALOSS F-16 case.

In Figure 8.6 it is shown that the parametric pitch control law that is used is identical for the two tools. For the flight path angle both tools show good correspondence as well. The difference in predicted flight path angle between the two tools that starts to develop during the burn of the third stage can not be explained. Some hypotheses are that there are small deviations from zero for yaw, roll and side slip angles that influence the direction of the thrust force or a difference in the accuracy of the numerical integration.

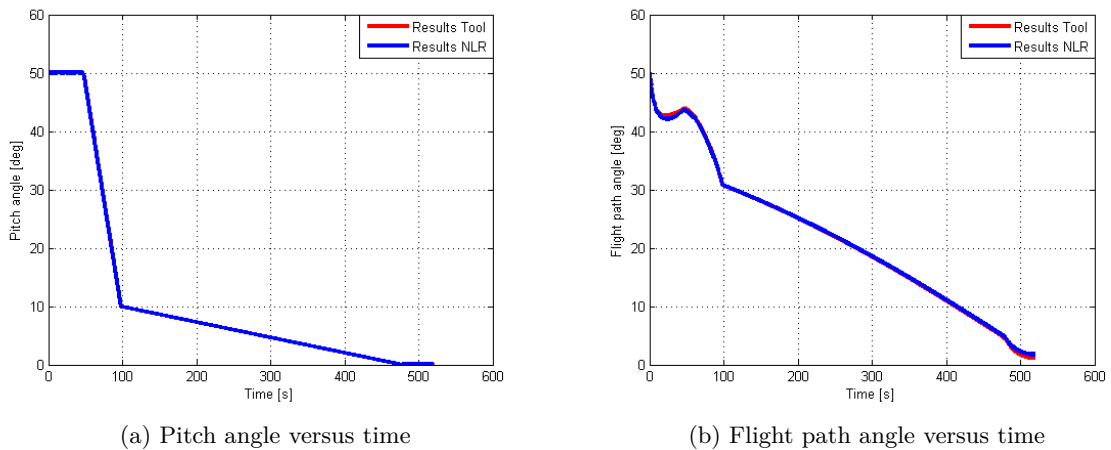


Figure 8.6: Comparison of the pitch and flight path angle of the tool and NLR's tool for the ALOSS F-16 case.

In [106] the gravity loss for ALOSS was given, however, this loss was calculated by simply subtracting the velocity and the drag loss from the delivered ΔV and therefore, did not calculate the gravity loss according to Equation 8.3 [105]. The gravity loss predicted by the tool is $1,727 \text{ m}\cdot\text{s}^{-1}$. A steering loss of $97.95 \text{ m}\cdot\text{s}^{-1}$ is found.

Based on the validation performed above it can be concluded that the tool is able predict the trajectory of the launch vehicle with good accuracy.

Step size selection In this subsection the step size for the Runge-Kutta 4 integrator is determined. The goal is to identify a step size that provides the highest accuracy for a reasonable computation time. The smaller the step size the longer the computation time. The approach will be to integrate the trajectory of the ALOSS F-16 case for a very small step size (0.005 s) and the final altitude will be assumed as the approximate reality. Next the same integration will be executed for larger step sizes as is down in Table 8.1.

Step size [s]	Final altitude [m]	Absolute error [m]	Relative error [%]
0.0050	678,093	-	-
0.010	678,291	198	0.0292
0.020	679,088	995	0.147
0.050	681,883	3,790	0.559
0.10	683,976	5,883	0.868
0.20	686,482	8,389	1.24
0.50	696,421	18,328	2.70
1.0	402,984	275,109	40.6

Table 8.1: Final altitude of the ALOSS F-16 case for different step sizes for the Runge-Kutta 4 integrator.

A relative error of 1% is deemed acceptable, therefore, a step size of 0.1 s will be used in this study.

8.5 Trajectory Constraints

In the previous chapters constraints for propulsion and launch vehicle design were implemented, now it is time to introduce the trajectory constraints. The values of the constraints that are discussed below are user inputs. Values for actual launch vehicles are taken in order to only evaluate realistic trajectories.

The first constraint is the maximum dynamic pressure, q_{max} . Some values that are obtained from literature for q_{max} : Pegasus 57.5 kPa [80], Ariane V 57.0 kPa [15] and PSLV-C19 90 kPa [54]. It is decided to take the maximum value found in literature thus q_{max} will be constrained in the tool at 90.0 kPa.

The constraint for a maximum value for the axial acceleration, a_x , of the launch vehicle is already implemented in Vandamme's tool. The axial acceleration of a launch vehicle can be given by [82]:

$$a_x = \frac{T(t) - D(t)}{m \cdot g_0} \quad (8.13)$$

The maximum acceleration will be constrained to 100 m·s⁻² which is in correspondence with the maximum acceleration considered in the ALOSS study [106]. It should be noted

that this value is almost twice as high as the maximum acceleration for large launch vehicles [82].

An important trajectory constraint is the maximum bending load. However, the calculation of the bending moment requires a lot of information about the vehicle that is not available. As a first indicator the so-called $q \cdot \alpha$ limit can be used, which is the product of the dynamic pressure and the total angle of attack (see [82] for more details). However, because the slide slip angle is set to zero for all simulations the total angle of attack is equal to the normal angle of attack. In [6] a bending load limit of 5,000 lbf · deg or 4,170 Pa · rad is used. This value corresponds with the bending load limit of the PSLV C-19 launcher of 4,000 Pa · rad [54]. Hence the bending load limit will be constraint at 4,170 Pa · rad. For winged launch vehicles the $q \cdot \alpha$ limit is deducted from flight data for Pegasus. At the moment of q_{max} Pegasus has an approximate angle of attack of 12° [67], this leads to a $q \cdot \alpha$ of ~18,000 Pa · rad. This value will be used as constraint for horizontal launched vehicles. It should be noted that the bending moment for slender launch vehicles is a problem, however, this is not taken in account by the $q \cdot \alpha$ limit.

The interaction between the atmosphere and launch vehicle does not only produce aerodynamic forces but also heat flux, \dot{Q} , due to convection and radiation. As long as the fairing is attached there will be no constraint for the heat flux. However, after fairing jettison the heat flux may not exceed 1,135 W · m⁻² [79]. The maximum heat flux can be found in the stagnation point and can be (approximated) using the free-stream enthalpy convective model [35]:

$$\dot{Q} = \frac{1}{2} \cdot \rho \cdot V^3 \quad (8.14)$$

This free-stream enthalpy convective model is also used in the MDO study for conceptual launch vehicle design by Balesdent [5]. For this study more complicated models, for example, the Detra-Kamp-Riddel formulation or Fay-Riddel formula for respectively the supersonic and hypersonic regime, are considered unnecessary. This is because when the fairing is separated the launch vehicle experiences free-stream conditions [35].

The last trajectory constraint is the maximum angle of attack, α_{max} , this constraint is only introduced because Missile Datcom can only cope with angles of attack smaller than 30°. This constraint is already present in the current tool from Vandamme.

In Chapter 3 it is stated that for this study it will be assumed that the control system is able change the attitude of the launch vehicle. Therefore, a limitation to the maximum pitch rate, $\dot{\theta}_{max}$, can be assigned. A typical value for the $\dot{\theta}_{max}$ is 5 ° · s⁻¹ [14]. However, the maximum pitch rate will not be modeled as an active constraint because there are other constraints that indirectly constrain the pitch rate such as the $q \cdot \alpha$ limit and α_{max} . Additional trajectory constraints that can be included but at this conceptual phase do not add value are for example, constraints regarding the impact locations of the burned-out stages or a constraint for the minimum distance to the carrier aircraft.

Chapter 9

Cost

During the first years of the space age attaining maximum performance and minimum weight dominated the criteria for launch vehicle design. In the following years a "design-to-cost" philosophy was adopted in which a predetermined budget was available for the design, production and operations of the launch vehicle [51]. Nowadays national prestige and military power are much less important in the launch vehicle industry and businesses in this industry are more and more becoming to act as a regular commercial business. Therefore, the philosophy of "design-for-cost" or "Cost-Engineering", which attempts to define a launch vehicle concept that results in minimum development, production and operations cost, is nowadays adapted in the launch vehicle industry [51].

The last discipline of the MDO that will be discussed is the modeling of cost for the development, design and operations of a launch vehicle. In the literature study different cost estimation methods were discussed [103]. Parametric cost estimation is deemed the best method because it can be easily implemented in an MDO process. A parametric cost estimation is basically a combination of mathematical relationships that are deducted from historical data. These mathematical relationships, also called cost estimation relationships (CERs), relate cost to physical, technical and performance parameters that are correlated with program cost [99].

In the first section of this chapter a top level overview of the cost model is given. The three following sections deal with the models for the development, production and operations cost. In the final section of this chapter the cost model is validated.

9.1 Cost Model

In the literature study it was concluded that TransCost was the most promising model [103]. However, during familiarization with TransCost it was noticed that TransCost has the tendency to overestimate the cost for solid rocket stages. In [15] it was also observed that the CERs in TransCost are not able to accurately predict the cost of small solid rocket stages. Fortunately, an adapted TransCost model developed by Martino was found that was better capable in predicting the cost of small solid rocket stages [61]. The data behind the CERs from [61] is not as transparent as the data for TransCost but originates

from ESA and therefore, has to be based on the Ariane V booster and the stages for the Vega launch vehicle. The production cost for small solid rocket stages (propellant mass < 10,000 kg) is still overestimated by Martino's model. Therefore, it is decided to develop a CER based on data gathered by [107] and data found in literature [94].

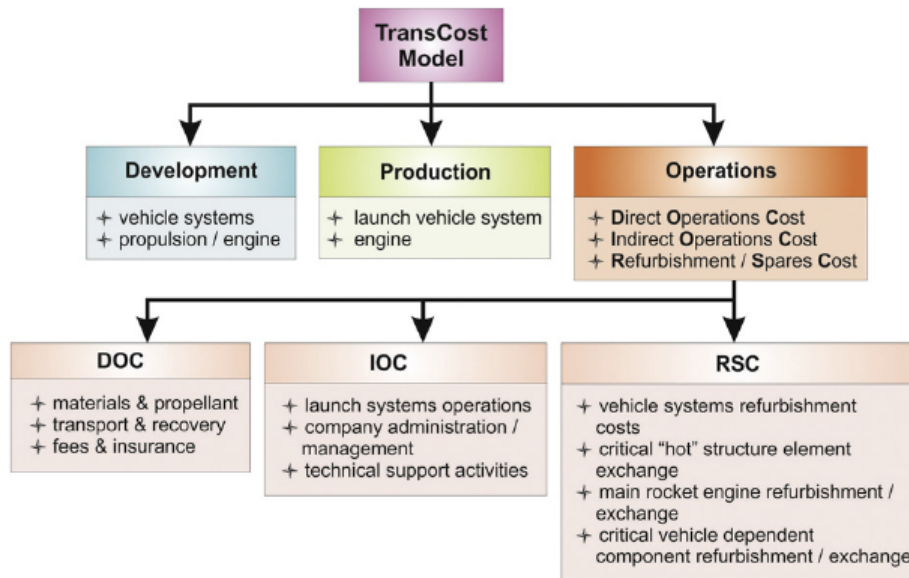


Figure 9.1: TransCost Model breakdown [99].

For the sake of brevity not all three cost models are discussed in detail. The outcomes of the validation for all three cost models can be found in Section 9.5. In Figure 9.1 a breakdown for the TransCost model can be found. TransCost estimates the cost for the development, production and operations for multistage expendable and reusable launch vehicles. Every category consists of a series of CERs that depend on input values like launch vehicle mass, complexity and expected launch rate. For this work TransCost version 6.2 was used. This is an old version, however, the differences with more recent versions are not too large [99, 107]. For details about the work of Martino is referred to his dissertation [61].

In Figure 9.2 the breakdown for the final cost model is shown. It shows large similarities with the TransCost breakdown in Figure 9.1. The largest difference between the models is the addition of a CER for the fairing (inherited from Martino's model) and a correction factor and additional cost for air launch. It might be a good moment to recall that the goal of this thesis research is to make a comparison between the cost for ground and air launch for equal performance. The original TransCost model accommodates a large number of correction factors for elements that are not directly related to the cost of the launch vehicle itself. For example, a correction factor for the productivity of the work force in the country where the vehicle is developed or a correction factor for the experience of the team. It is decided to limit the amount of correction factors to a minimum to keep overview and moreover to avoid that these factors accidentally influence the outcome of the cost estimation. The values used for the large number of correction factors are generally based on [52] and [61]. Because there is only very little cost data available the

correction factors can not be validated. Therefore, the sensitivity of the cost per launch to varying correction factors is investigated during the sensitivity analysis in Chapter 12. In the original TransCost model cost are defined in Man-Years (MYr) and this is used because the projects evaluated originate from different time periods, currencies and inflation rates [52]. However, in this work all cost are presented in FY2012 million euros.

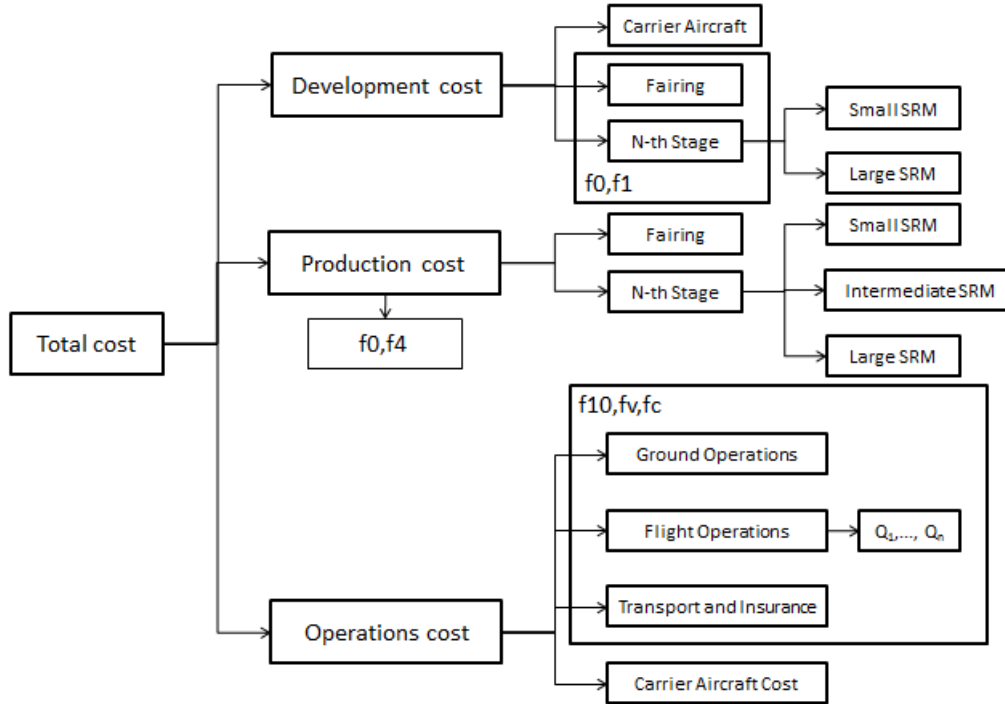


Figure 9.2: Breakdown of the final cost model.

9.2 Development Cost

The development cost of each stage is determined by a single CER. A different CER is used for small (propellant mass < 40,000 kg) and for large stages (propellant mass > 40,000 kg). The development cost, DC , of the individual stages are summed together and multiplied with an additional integration factor that depends on the number of stages and the launch vehicle configuration. In addition, the development cost of the fairing are calculated in a separated CER. The development cost of the fairing also contain the development cost of the VEB [61]. The following CERs are used to calculate the development cost for the fairing and the solid rocket stages [61]:

$$DC_{fairing} = (0.83 \cdot length_{fairing} + 33) \quad (9.1)$$

$$DC_{small\ SRM} = f_{TVC} \cdot 16.8 \cdot \left(\frac{M_p}{1000}\right)^{0.32} \quad (9.2)$$

$$DC_{large\ SRM} = 16.3 \cdot \left(\frac{M_p}{10}\right)^{0.54} - 1220 \quad (9.3)$$

Where $length_{fairing}$ is the total fairing length in meters and M_p the propellant mass in kilos. The correction factor for TVC, f_{TVC} , is 1.15 for a stage with TVC and 1.0 for a stage without TVC. For all stages the following two correction factors are applied: the system engineering factor (f_0) and the development standard factor (f_1). The system engineering factor corrects for the development of the interfaces between the stages and the overall system development cost. In the original TransCost model and Martino's work this factor is considered constant as respectively 1.1 [52] and 1.5 [61]. For this study it is decided to make this factor dependent on the number of stages and the launch vehicle configuration. The correction factors for different number of stages and launch vehicle configurations are given in Table 9.1.

Number of stages	Ground launch	Air launch
2	1.2	1.3
3	1.3	1.4
4	1.4	1.5

Table 9.1: Development system engineering correction factor, f_0 , for different launch vehicle configurations.

The development standard factor takes into account the kind of project, from minor variations of existing projects, which will require a limited effort, to a new concept approach, with new techniques and new technologies. Based on [61] the development standard factor for the three different kind of vehicles is given in Table 9.2.

Type of project	Correction factor
Winged air launched vehicle	1.0
Air launched vehicle	0.9
Ground launched vehicle	0.8

Table 9.2: Development standard factor, f_1 , for different project types [61].

Also the development cost for the carrier aircraft, $DC_{aircraft}$, have to be taken in account. These cost are not development cost in the strict definition of the word but they will be regarded as development cost because these cost will be amortized over the lifetime of the program. The development cost for the carrier aircraft include the cost for the acquisition of the aircraft, the cost for modification and the cost for development and testing of the carrier aircraft. These cost for a Boeing 747-400F are given in Table 9.3 and are based on the outcomes of NASA's HLS [6].

Description	Cost in FY €M
Aircraft acquisition cost	23.1
Aircraft modification cost	47.7
Aircraft development and testing	111
Total	182

Table 9.3: Estimated cost for the acquisition, modification and testing of a Boeing 747-400F to a carrier aircraft [6].

For the 10 kg payload class an F-16 is used. This fighter aircraft does not have to be purchased and the cost of developing the hardware and certifying the launch vehicle to be launched from under an F-16 is estimated at ~1.5 million euros [105]. At this moment it is impossible to verify how sound this number is, therefore, the influence of the cost for development and testing of the carrier aircraft on the cost per flight is investigated in the sensitivity analysis.

The total development cost will be amortized over all the flights of the launch vehicle. In the introduction a total of 120 launches, l , is taken as baseline for this study. Hence the amortized development cost per flight are given by:

$$DC_{flight} = \frac{f_0 \cdot f_1 \cdot \left(\sum_{i=1}^N DC_{SRM_i} + DC_{fairing} \right) + DC_{aircraft}}{l} \quad (9.4)$$

9.3 Production Cost

The model for the production cost, PC , is similar to the one for the development cost. There are different CERs for small, intermediate and large solid rocket stages and again there is a separate CER for the fairing. The CERs that are used hold for the first unit that is produced, the so-called the theoretical first unit (TFU). Another important factor is the learning factor, p , which represents the cost reductions due to series production.

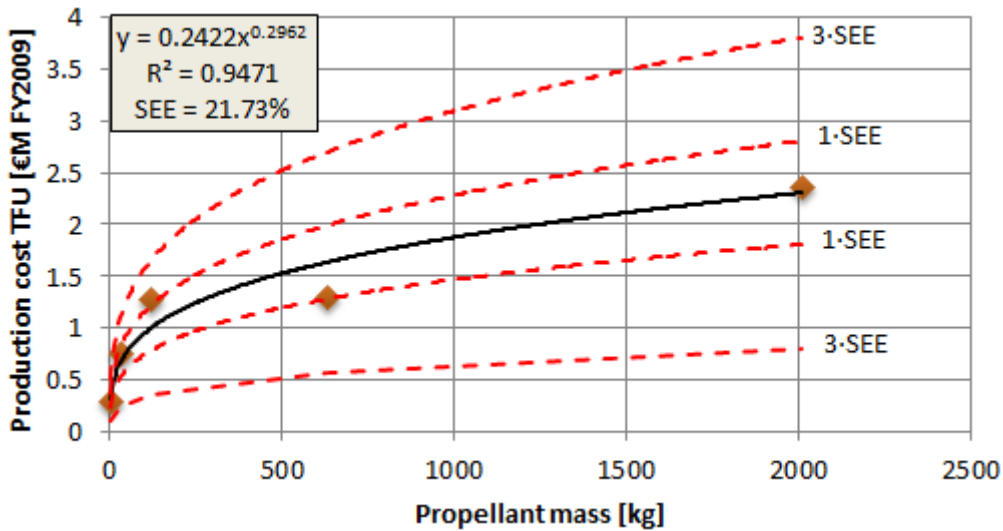


Figure 9.3: Correlation between propellant mass and TFU production cost for small SRMs.

Martino’s model still overestimates the production cost of solid rocket stages with a propellant mass smaller than 10,000 kg, therefore, it is decided to develop a CER. Michel van Pelt from ESA provided valuable data and in combination with cost data for additional motors from [94] a CER based on regression is developed (see Figure 9.3). More details about the data behind this CER can be found in Appendix H.

If the developed CER for small SRMs is combined with the CERs from Martino's model, the following CERs are used [61] :

$$PC_{fairing} = (0.83 \cdot volume_{fairing})^{0.63} \quad (9.5)$$

$$PC_{small\ SRM} = 0.2422 \cdot M_p^{0.2962} \quad (9.6)$$

$$PC_{intermediate\ SRM} = 3.12 + 0.068 \left(\frac{M_p}{1000} \right) \quad (9.7)$$

$$PC_{large\ SRM} = 2.3 \cdot \left(\frac{M_p}{11 - 5 \cdot \frac{M_p - 40,000}{200,000}} \right)^{0.399} - 38.25 \quad (9.8)$$

For details about the calculation of the volume of the fairing (unit is m^3), $volume_{fairing}$, is referred to Appendix H. The propellant mass, M_p , is again in kilos. It should be noted that the propellant cost have already been included in the CERs above [52, 61]. In Figure 9.4 the three different CERs are plotted on a logarithmic scale. In order to avoid "jumps" there is switched from the CER for small to the one for intermediate solid rocket stages at 13,000 kg. The dotted lines in Figure 9.4 show extrapolation of the original data set.

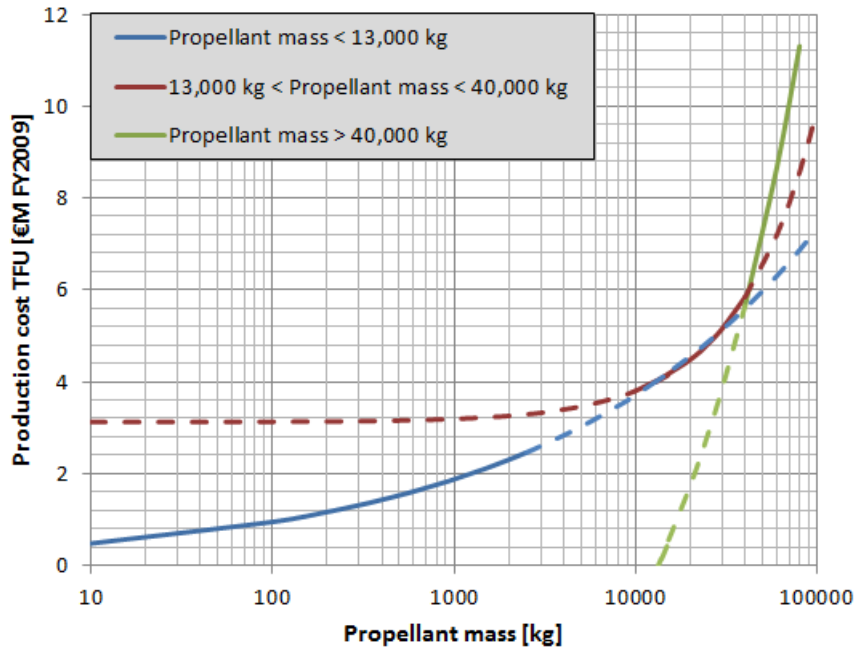


Figure 9.4: Production cost TFU as function of propellant mass using the three different CERs.

Also two correction factors will be taken in account for the production cost. The first one is the system engineering factor for production, f_0 , that considers the production of the interfaces between the stages and the overall system development cost. For the

production the integration effort is much smaller than for the development [61]. Contrary to the systems engineering correction factor for development for this correction factor a constant value of 1.05 is used [52, 61]. The second correction factor is the cost reduction for series production factor, f_4 , which is the fundamental factor which takes into account the cost reduction due to series production. The correction factor, f_4 , can be calculated for a specific launch vehicle from the batch with [52]:

$$f_4 = n^{\frac{\ln(p)}{\ln(2)}} \quad (9.9)$$

So, for a learning factor, p , of 0.9 the production of the 120th launch vehicle would only cost 48.3% of the TFU. More interesting is the average cost reduction factor for the batch of launch vehicles. This can be determined by [52]:

$$f_4 = \frac{1}{N} \sum_{i=1}^N i^{\frac{\ln(p)}{\ln(2)}} \quad (9.10)$$

For example the average cost reduction factor for a batch of 120 launch vehicles with a learning factor of 0.9 is 0.566. Common values for the learning factor are between 0.75 and 0.95 and these values depend on the annual production rate and the dry mass of the vehicle [52]. For launch vehicles with a 10 kg payload a learning factor of 0.8 is used and for the launch vehicles with 2,000 kg payload a learning factor of 0.9. This results in an average cost reduction factor of 0.566 for large launch vehicles and 0.309 for small launch vehicles.

Hence the average production cost per launch vehicle are given by:

$$PC_{flight} = \frac{f_0 \cdot f_4 \cdot \sum_{i=1}^N (PC_{SRM_i} + PC_{fairing})}{l} \quad (9.11)$$

9.4 Operations Cost

Assessment of launch vehicle's operations cost, CO , is much more difficult than modeling development and production cost, because of the complex relationship between a large number of criteria and a limited database [52]. Indirect operations cost are negligible for expendable launch vehicles and therefore, only the direct operations cost are modeled [61]. The first element of the operations cost are the ground operations cost. These cost entail management and support of the engineering site, assembly integration and checkout of the launcher (not of the payload) and launch preparation such as erection (in case of horizontal processing). The following CER is used to estimate the ground operations cost [52]:

$$CO_{ground} = 8.0 \cdot M_{GTOW} \cdot L^{-0.90} \cdot N^{0.70} \quad (9.12)$$

Where, M_{GTOW} is the GTOW of the launch vehicle (in tons), L the annual launch rate and N the number of stages.

The second element of the operations cost are the flight operations cost. The flight operations entail the mission plans, evaluation and management, launch and flight operations

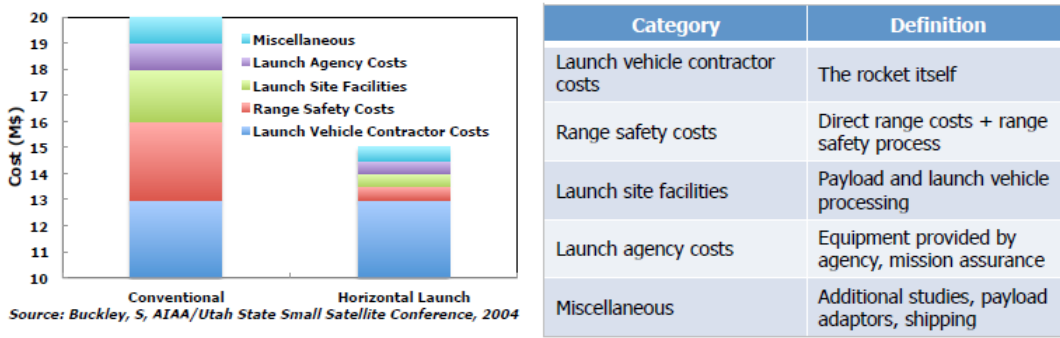


Figure 9.5: Comparison between several cost for conventional and horizontal launch [19].

itself, tracking and data relay operations. The flight operations cost can be estimated by [52]:

$$CO_{flight} = 20 \cdot \sum_{i=1}^N Q_i \cdot L^{-0.65} \quad (9.13)$$

With Q_i as the complexity of the i^{th} stage. For solid rocket stages a complexity of 0.15 is used [52]. For a winged launch vehicle a value of 0.40 is taken for the complexity of the first stage.

The cost for transport and insurance of the launch vehicle are assumed to be 10% of the ground and flight operations cost [61].

$$CO_{Transport\ Insurance} = \frac{CO_{ground} + CO_{flight}}{0.90} \quad (9.14)$$

In addition three different correction factors will be applied. The launch vehicle type factor, f_v , considers the kind of propellant of the launcher and the type of launch vehicle. For this study the launch vehicle type factor is 0.3 for solid launch vehicles and 0.5 for winged solid launch vehicles [61]. Next the processing type factor, f_c , that considers the different cost for launchers processed horizontally or vertically has to be considered. For horizontal processed launch vehicles 0.5 is used and for vertical processed launch vehicles 0.7 [61]. For all launch vehicle types, except for the ground launched 2,000 kg payload class launch vehicle, horizontal processing is assumed.

The final correction factor is the air launch cost correction factor (f_{10}). From data of [19] (see also Figure 9.5) it can be concluded that operations cost for the flight and ground operations for horizontal launch are ~30% of the cost for vertical launch. This is considered extremely optimistic and, therefore, the air launch cost correction factor is assumed to be 0.50.

The final element of the operations cost that has to be taken in account are the cost of the carrier aircraft, $CO_{aircraft}$, itself. The annual cost for necessary maintenance, insurance and registration for Orbital's Stargazer aircraft are estimated at 3.5 million euro [19]. If these cost are extrapolated based on the empty masses of both aircraft an annual fixed cost of 5.5 million euro is found for a Boeing 747-400F [48]. The operations cost for the aircraft during the missions are considered insignificant compared to the annual fixed cost.

For the 10 kg payload launch vehicle the F-16 is not purchased and the operations cost for a typical mission are estimated at ~10-50k euro [105].

The total operations cost per flight are given by:

$$CO = f_v \cdot f_c \cdot f_{10} (CO_{ground} + CO_{flight} + CO_{Transport Insurance}) + CO_{aircraft} \quad (9.15)$$

9.5 Validation Cost Model

In this section the cost model described in the previous sections is validated with real advertised prices for launch vehicles. Also the results from the TransCost model and the model of Martino are given. In order to avoid a long section only the main results are presented. For all assumptions and literature used for the individual launch vehicles is referred to Appendix H. Some warnings about the advertised prices. First, the advertised prices originate from different fiscal years. All prices are corrected to FY€2013 using the numbers for the cost history of MYr for the US and European aerospace industry (updated cost per man year from TransCost 8.1 obtained from [61]).

Second, it is not always clear if additional services like payload integration and telemetry and tracking support are included in the advertised prices. Third, there are different prices for different customers, for example, the price for a Pegasus XL launch vehicle varies with more than 40% for different customers [10]. Where possible the advertised price for a (single) full commercial launch is taken.

In Figure 9.6 the advertised cost per launch are compared with the estimated cost of the three models. Immediately becomes clear that TransCost overestimates the cost. Martino's model and the final model show good correspondence and are slightly above the advertised cost.

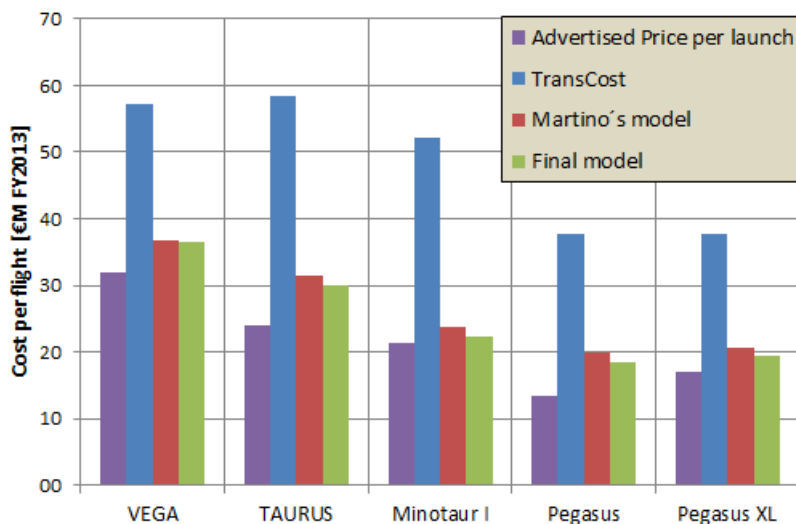


Figure 9.6: The advertised cost per flight, and the estimated cost by TransCost, Martino's model and the final model.

The differences between Martino's model and the final model become more clear in Figure

9.7 and Table 9.4. It can be concluded that the error in the estimated launch vehicle cost for all launch vehicles is lower for the final model than for Martino's model. The mean error of the final model is 6% lower than Martino's mean error and the standard deviation of the error is identical. It can be concluded that the final model is able to predict the cost per launch with a reasonable accuracy.

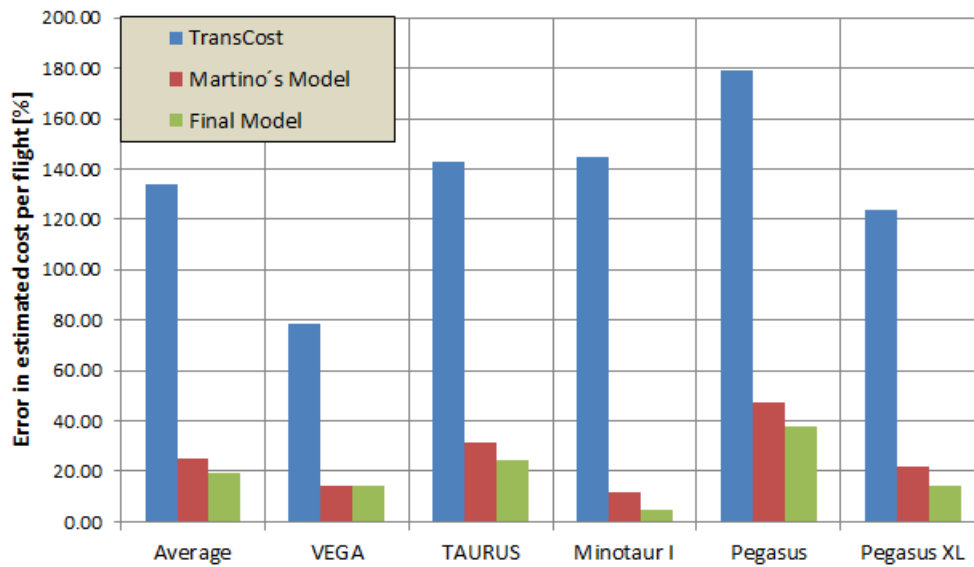


Figure 9.7: Error in estimated cost per flight for TransCost, Martino's model and the final model.

Description	E [%]	μ [%]	σ [%]
TransCost	133	+133	31.1
Martino's model	25.3	+25.3	14.3
Final model	19.1	+19.1	14.3

Table 9.4: Statistical figures of the error in the estimation of the launch cost for the three different cost models.

The outcomes of the cost estimation depend on a lot of variables for which it is impossible to validate their values. Therefore, a special effort in the sensitivity analysis is made for the effects of changing input parameters for the cost model.

Verification and Validation

The verification and validation of the tool are major challenges for this study. Verification is the proof of compliance with the original requirements [41]. In generally for MDO studies the validation is more critical [15]. Earlier a definition for model validation is given, the validation of the tool itself, entails the proof that the tool accomplishes the intended purpose [41]. So, in other words: is this tool capable of performing an MDO for expendable ground and air launched vehicles?

In previous chapters the individual disciplines of launch vehicle design were validated against real solid rocket stages and launch vehicles. Now it is time to validate the tool as a whole against two launch vehicles: Taurus and Pegasus XL. Again it should be noted that these launch vehicles are not in the classes of vehicles that will be examined during this study. However, there are no launch vehicles in the 10 kg payload class and Vega has a liquid propelled upper stage and this can currently not be modeled by the tool. Before the tool is validated against Taurus and Pegasus XL, the ALOSS vehicle is validated.

10.1 Validation ALOSS Launch Vehicle

For the MDA validation the values of ALOSS are used as input parameters for the design variables for the models that are used in this study. A description of the ALOSS launch vehicle is given in Appendix B. Identical values are used as for the ALOSS study for: the safety factor (1.75), the motor case material (titanium), the interstage material (composite), the density of the propellant ($1,800 \text{ kg}\cdot\text{m}^{-3}$) and the density of the insulation material ($1,900 \text{ kg}\cdot\text{m}^{-3}$). The results and differences with the actual ALOSS configuration can be found in Table 10.1.

Despite the fact that the thrust levels for ALOSS are modeled for average thrust and in this study as vacuum thrust the models show good correspondence. The values for the other propulsion characteristic, the specific impulse, are also similar. For the first two stages the propellant mass shows good correspondence too. The higher propellant mass for the third stage can be explained by the fact that the maximum value of the thrust is taken to calculate the propellant mass while for ALOSS a regressive thrust (thus mass

flow) is modeled for the third stage. The length of first stage shows good correspondence, however, the length of the second stage differs with 14.3%.

Larger differences between the models can be found for the inert masses. In general the masses for the motor case (including insulation) show better correspondence than the nozzle masses. The nozzle mass differs because an additional mass for the TVC system is assigned by the NLR while in the model used for this work the TVC mass is already included in the nozzle mass (see Section 6.2). In the ALOSS report it is stated that different methods for estimating the TVC system mass lead to a large difference in predicted TVC system mass, therefore, a detailed design is necessary in order to get a good estimate [106]. The correction factor for the inert mass applied in the model used for this work corrects the deviations of inert mass between the models within 20%. The effect of changes in inert mass will be investigated in the sensitivity analysis in Chapter 12.

	Component	ALOSS	Model	Difference [%]
Stage 1	Vacuum thrust [kN]	48.3	52.33	+8.35
	Isp [s]	284.0	285.2	+0.42
	Motor length [m]	2.59	2.527	-2.42
	Mass propellant [kg]	862.8	895.8	+3.82
	Mass case [kg]	48.5	52.30	-3.69
	Mass nozzle [kg]	45.9	45.63	-33.7
	Mass TVC [kg]	22.9		
	Total inert mass [kg]	123.1	115.8	-5.95
Stage 2	Vacuum thrust [kN]	14.1	13.88	-1.53
	Isp [s]	294.0	297.1	+1.05
	Motor length [m]	1.13	1.291	+14.2
	Mass propellant [kg]	244.8	237.7	-2.89
	Mass case [kg]	26.3	20.43	-22.3
	Mass nozzle [kg]	13.5	11.65	-42.3
	Mass TVC [kg]	6.7		
	Total inert mass [kg]	46.5	38.00	-18.3
Stage 3	Vacuum thrust [kN]	8.6	7.770	-10.5
	Isp [s]	294.0	297.1	+1.05
	Motor length [m]	0.84	1.056	+25.7
	Mass propellant [kg]	60.7	92.00	+51.6
	Mass case [kg]	4.9	7.070	+12.2
	Mass nozzle [kg]	3.5	5.682	+9.26
	Mass TVC [kg]	1.7		
	Total inert mass [kg]	11.5	12.49	+8.59

Table 10.1: Characteristics of the stages for MDA validation for the ALOSS launch vehicle.

The mass properties for the entire ALOSS vehicle and the results of the MDA validation are given in Table 10.2. The difference in GTOW is 5.20%, however, the differences for the individual stages are higher. Above the difference between the individual stages are already addressed, therefore, only the additional components of the launch vehicle are discussed. It should be noted that the fairing of the ALOSS launch vehicle is not

jettisoned. In the models used for this study there is no interstage between the second and third stage because the third stage is entirely encapsulated by the fairing. At a late moment in this study it is concluded that there has to be an interstage that carries the third stage. This is not taken in account in this study and it is recommended to implement this interstage for future work. The effect of adding this interstage, which is basically an addition of inert mass to the second stage is investigated in the sensitivity analysis. There is relative large difference in VEB mass and the payload adapter is not modeled by NLR.

Component	Mass ALOSS [kg]	Mass MDA [kg]	Differences [%]
Start mass stage 1	1379.5	1451	+5.20
Propellant mass stage 1	862.8	895.8	+3.82
Dry mass stage 1	123.1	115.8	-5.95
Interstage 1/2	5.0	5.284	+5.7
Start mass stage 2	388.5	434.4	+11.8
Propellant mass stage 2	244.8	237.7	-2.89
Dry mass stage 2	46.5	38.00	-18.3
Interstage 2/3	5.0	-	-
Start mass stage 3	87.2	158.7	+82.0
Propellant mass stage 3	60.7	92.00	+51.6
Dry mass stage 3	11.5	12.49	+8.61
Fairing	5.0	29.91	+498
Avionics/VEB	5.0	13.78	+176
Payload adapter	-	0.50	-
Payload	10.0	10.0	-

Table 10.2: Mass properties for MDA validation for the ALOSS launch vehicle (all data from [106]).

Based on the MDA performed above it can be concluded that both models differ on several points. However, the differences for the key parameters (propulsion characteristics, propellant mass and inert mass of the stages) are deemed acceptable. One final remark: the NLR compared the results of the ALOSS motors with actual motors and based on this the NLR concluded that the inert masses for the ALOSS motors are significantly higher (no numbers available) than the inert masses of the actual motors [106].

10.2 Multidisciplinary Design Analysis Validation

For the MDA validation values from existing launch vehicles are assigned to the design variables and it is checked if the MDA results in a design similar to the existing launch vehicle. It is actually validated how the individual disciplines perform when they are coupled.

10.2.1 Multidisciplinary Design Analysis Validation Taurus

The data from Taurus originates from [47], [79] and [112] and the input parameters for the MDA can be found in Appendix I. Table 10.3 summarizes the most important vehicle characteristics for the output of the MDA.

Parameter	Actual	MDA	Error [%]
Propulsion properties [kN]			
Vacuum thrust stage 1	1,766	1,659	-6.08
Vacuum Isp stage 1	280.0	280.5	+0.54
Vacuum thrust stage 2	454.4	455.0	+0.13
Vacuum Isp stage 2	285.0	289.6	+1.60
Vacuum thrust stage 3	113.8	117.0	+2.84
Vacuum Isp stage 3	290.2	300.9	+3.70
Vacuum thrust stage 4	32.20	32.56	+1.01
Vacuum Isp stage 4	287.0	299.7	+4.41
Mass properties [kg]			
Inert mass stage 1	4,211	3,959	-5.98
Propellant mass stage 1	48,809	49,358	+1.12
Inert mass stage 2	1,088	735	-32.5
Propellant mass stage 2	12,154	12,374	+1.81
Inert mass stage 3	345	238	-31.0
Propellant mass stage 3	3,025	3,086	+2.01
Inert mass stage 4	203	67.3	-66.8
Propellant mass stage 4	782	772	-1.23
Fairing mass	400	524	+31.0
Total inert mass	7,386	6,728	-8.91
Payload mass	1,050	1,050	-
GTOW	72,156	72,292	+0.13
Geometry properties [m]			
Length stage 1	10.7	11.0	+2.80
Length stage 2	7.60	9.22	+21.4
Length stage 3	2.65	3.03	+14.3
Length stage 4	2.08	1.67	-19.7
Total length	29.0	30.7	+5.64
Cost [€M FY2012]			
Cost per flight	24.0	30.1	+25.4

Table 10.3: Summary of the MDA vehicle output parameters for Taurus compared with the actual values for Taurus.

It can be concluded that the results from the MDA for the three propulsion parameters (vacuum thrust, vacuum Isp and propellant mass) are very similar to the actual values of the propulsion parameters. This is different for the inert masses of the individual stages. The reason for this is that all stages are modeled with a motor case that consists of a composite material. In reality the motor cases of stage 2, 3 and 4 of Taurus are made from aluminum and if their inert mass is calculated with an aluminum motor case the

following masses would be obtained: 1,246 kg (+14.5%), 413 kg (+19.7%) and 105 kg (-48.3%). For stage 2 and 3 the differences are now acceptable, however, the inert mass of stage 4 is still low compared with the real value. According to [4] the inert mass of the Orion 38 is 122 kg, so this means that for Taurus the rest of the inert mass of stage 4 (81 kg) would be interstage mass or more likely the mass of the connection between the stage and the fairing. This also explains the difference between the actual fairing mass and the fairing mass calculated in the MDA. The difference in obtained value for the GTOW of the MDA and the actual value can be considered negligible. It should be noted that the inert masses of the stages include the interstage masses.

Parameter	Actual	MDA	Error [%]
Time: 83.00 s Stage 2 Ignition / Stage 1 Separation			
Altitude [km]	42.50	43.70	+2.82
Velocity [m·s ⁻¹]	2,202	2,146	-2.54
Time: 161.1 s Stage 2 Burn-out			
Altitude [km]	153.9	135.9	-11.7
Velocity [m·s ⁻¹]	4,639	4,725	+1.85
Time: 171.1 s Stage 3 Ignition			
Altitude [km]	165.0	148.6	-9.94
Velocity [m·s ⁻¹]	4,514	4,699	+4.10
Fairing Separation			
Time [s]	179.2	144.7	-19.6
Altitude [km]	175.0	111.4	-36.3
Velocity [m·s ⁻¹]	4,598	3,976	-13.5
Time: 254.2 s Stage 3 Burnout			
Altitude [km]	291.0	266.5	-8.42
Velocity [m·s ⁻¹]	6,552	6,829	4.23
Time: 750.4 s Stage 4 Ignition			
Altitude [km]	689.0	692.4	+0.49
Velocity [m·s ⁻¹]	6,014	6,315	+5.00
Time: 823.6 s Stage 4 Burnout / Orbit Injection			
Altitude [km]	691.0	705.0	+2.03
Velocity [m·s ⁻¹]	7,511	7,627	+1.54
Additional parameters			
Semi-major axis [km]	691.0	782.6	+13.2
Eccentricity [-]	~0.000	0.023	-
Maximum dynamic pressure [kPa]	-	89.9	-
Drag loss [m·s ⁻¹]	-	175.1	-
Gravity loss [m·s ⁻¹]	-	1,499	-
Steering loss [m·s ⁻¹]	-	42.88	-

Table 10.4: Summary of the MDA trajectory parameters for Taurus compared with the actual values for Taurus.

The lengths of the individual stages (including the interstage lengths) show some errors, however, these errors are considered acceptable. The MDA overpredicts the cost per flight

for the launch vehicle and this is in correspondence with the conclusions in Chapter 9. Also for the other disciplines holds that the errors correspond with the mean errors found in the previous chapters.

Now the trajectory of Taurus (payload mass 1,050 kg) is validated for a launch from the Vandenberg Launch Site to a 691 km altitude circular orbit sun-synchronous orbit. The burn-out altitudes and velocities of Taurus's stages are obtained from [79]. It should be noted that the burn times stated in [79] are slightly longer than the ones modeled in the MDA. These burn times include the ignition delay time and the ignition rise time. However, the model used in this study assumes instantaneous thrust. In the MDA the coasting times are made slightly longer in order to keep the ignition of the stages at the same points in time.

From PaGMO a differential evolution algorithm is selected to optimize the pitch control law. The results and differences between the outcome of the MDA and Taurus' trajectory are shown in Table 10.4. From this table it can be concluded that the launch vehicle generated by the MDA performs slightly better than Taurus. Despite the fact the launch vehicle's trajectory was aimed for a 691 km circular orbit it reached a higher orbit. The reasons for this are the lower inert mass of the upper stages and an earlier fairing jettison than for Taurus. The maximum dynamic pressure of the MDA vehicle occurs after 47.2 seconds and has approximately the value of the constraint, unfortunately, the q_{max} for Taurus is not known. However, the burn-out conditions of the first stage of the MDA and Taurus are very comparable, hence, the dynamic pressure profile for Taurus is probably not very different. Also for the trajectory it can be concluded that the MDA and the actual trajectory show good correspondence. Some figures of the most important parameters for this MDA can be found in Appendix I.

10.2.2 Multidisciplinary Design Analysis Validation Pegasus XL

After the MDA validation of Taurus it is time to do a MDA validation for the only existing expendable air launched vehicle: Pegasus XL. The data for Pegasus is obtained from multiple sources [47, 71, 79, 112] and the input parameters can be found in Appendix I. The most important vehicle characteristics for the MDA are shown in in Table 10.5.

In general the same phenomena are observed for Pegasus XL as for Taurus. First the results of the MDA for the propulsion characteristics show good correspondence with those of Pegasus XL. Second, the inert masses calculated during the MDA are lower than for Pegasus XL. The MDA assumes a composite as material for the motor casing while Pegasus XL's stages have aluminum motor casings. The differences in motor case mass are larger for Pegasus XL than for Taurus. Also the calculated length and cost per launch show the same behavior as for the MDA of Taurus: the lengths of most stages are larger and the estimated cost per launch are higher than the advertised cost for the actual launch vehicle.

Now it is time to compare the trajectory of the MDA with Pegasus XL's trajectory. The burn-out altitudes and velocities for Pegasus XL's stages originate from [71]. The most important trajectory parameters from the MDA and Pegasus XL are given in Table 10.5. The Pegasus launch vehicle is dropped and uses its wing and control surfaces to pull up. This causes a problem for the MDA since a wing is modeled but not the control surfaces. Aerodynamic control surfaces are more effective than the thrust force for changing the

launch vehicle's attitude [30]. The slower pull up explains the lower burn-out altitude of the first stage of the MDA. This is also an explanation for the significant higher maximum dynamic pressure that is experienced for the MDA.

For the rest of the flight the MDA validation vehicle can use its lower inert mass to "catch-up" with the trajectory of Pegasus XL. In the end both vehicles reach almost identical orbits. From the MDA validation for Pegasus XL it can be concluded that despite the fact that the pitch up maneuver is not as efficient as for Pegasus XL the tool is able to simulate a pitch up maneuver and to predict the trajectory of winged launch vehicles. Some figures of the most important trajectory parameters for this MDA can be found in Appendix I.

Parameter	Actual	MDA	Error [%]
Propulsion properties [kN]			
Vacuum thrust stage 1	626.3	626.9	+0.10
Vacuum Isp stage 1	292.8	294.4	+0.54
Vacuum thrust stage 2	160.6	169.3	+5.43
Vacuum Isp stage 2	290.7	298.3	+2.61
Vacuum thrust stage 3	32.2	32.56	+ 1.01
Vacuum Isp stage 3	290.2	300.9	+3.70
Mass properties [kg]			
Inert mass stage 1	2,886	1,340	-50.9
Propellant mass stage 1	15,014	15,451	+2.91
Inert mass stage 2	416	382	-8.13
Propellant mass stage 2	3,925	4,155	+5.85
Inert mass stage 3	203	75.7	-62.7
Propellant mass stage 3	770	772	+0.31
Fairing mass	194	181	-6.53
Total inert mass	3,992	2,348	-41.17
Payload mass	227	227	-
GTOW	23,701	22,727	-4.11
Geometry properties [m]			
Length stage 1	10.3	11.1	+8.14
Length stage 2	3.11	3.49	+12.2
Length stage 3	1.34	1.70	+26.9
Total length	17.4	18.9	+8.54
Cost [€M FY2012]			
Cost per flight	16.9	19.3	+14.2

Table 10.5: Summary of the MDA vehicle output parameters for Pegasus XL compared with the actual values for Pegasus XL.

Parameter	Actual	MDA	Error [%]
Time: 71.00 s Stage 1 Burn-out			
Altitude [km]	59.63	44.31	-25.7
Velocity [m·s ⁻¹]	2,415	2,513	+4.06
Time: 90.30 s Stage 2 Ignition			
Altitude [km]	87.51	67.87	-22.4
Velocity [m·s ⁻¹]	2,380	2,415	+1.47
Fairing Separation			
Time [s]	107	124.2	+16.1
Altitude [km]	110.0	111.4	+1.30
Velocity [m·s ⁻¹]	2,765	3,446	+24.6
Time: 161.0 s Stage 2 Burnout			
Altitude [km]	208.3	178.8	-14.2
Velocity [m·s ⁻¹]	5,469	5,618	2.72
Time: 589.0 s Stage 3 Ignition			
Altitude [km]	739.0	727.4	-1.57
Velocity [m·s ⁻¹]	4,564	4,712	+3.24
Time: 655.0 s Stage 3 Burnout / Orbit Injection			
Altitude [km]	741.0	735.5	-0.74
Velocity [m·s ⁻¹]	7,487	7,492	+0.07
Additional parameters			
Semi-major axis [km]	741.0	737.6	-0.46
Eccentricity [-]	~0.000	0.0085	-
Maximum dynamic pressure [kPa]	57.5	75.0	+30.4
Drag loss [m·s ⁻¹]	-	326.8	-
Gravity loss [m·s ⁻¹]	-	1,526	-
Steering loss [m·s ⁻¹]	-	247.5	-

Table 10.6: Summary of the MDA trajectory parameters for Pegasus XL compared with the actual values for Pegasus XL.

10.3 Multidisciplinary Design Optimization Validation

In this final validation step it will be checked if in the case that requirements for an existing launch vehicle are given the optimizer is able to find a similar or even better design (in terms of cost). The objective functions described in Section 2.4 are used for this MDO validation. It should be noted that during the MDO validation the launch vehicle is optimized for cost while for the design of Taurus and Pegasus XL also other factors, for instance, reliability, are taken in account. It is more interesting to compare the results of the MDO with the results of the MDA than with the actual values of the launch vehicle because the MDA and MDO uses the same models.

10.3.1 Multidisciplinary Design Optimization Validation Taurus

For the MDO validation of Taurus a payload of 1,050 kg is launched from Vandenberg Launch Site to a 691 km altitude circular orbit sun-synchronous orbit by a four stage

launch vehicle. This MDO validation is immediately a test for the optimizer because 36 variables have to be optimized. A differential evolution algorithm is chosen to perform this task. According to [5] the initial population size should be 2 to 4 times the number of design variables. Hence a population of 100 individuals is chosen and this initial population will evolve over 3,000 generations.

The characteristics of the best individual after 3,000 generations are shown in Table 10.7. More details of the best individual are given in Appendix I. The MDO has a GTOW comparable to the MDA and Taurus. Despite the fact that the advertised price for Taurus is still 21.6% lower than the cost per launch for this optimized launch vehicle the cost per launch compared with the outcome of the MDA is almost 1 million euros lower.

Parameter	Actual	MDA	MDO	Difference MDA and MDO [%]
Propulsion properties [kN]				
Vacuum thrust stage 1	1,766	1,659	1,180	-28.87
Vacuum Isp stage 1	280.0	280.5	284.3	+1.35
Vacuum thrust stage 2	454.4	455.0	606 .0	+33.2
Vacuum Isp stage 2	285.0	289.6	299.0	+3.25
Vacuum thrust stage 3	113.8	117.0	140.4	+20.0
Vacuum Isp stage 3	290.2	300.9	305.8	+1.63
Vacuum thrust stage 4	32.20	32.56	62.81	+92.9
Vacuum Isp stage 4	287.0	299.7	306.5	+2.27
Mass properties [kg]				
Inert mass stage 1	4,211	3,959	2,339	-40.9
Propellant mass stage 1	48,809	49,358	40,216	-18.5
Inert mass stage 2	1,088	735	1,232	+67.6
Propellant mass stage 2	12,154	12,374	22,026	+78.0
Inert mass stage 3	345	238	255	+7.14
Propellant mass stage 3	3,025	3,086	3,622	+17.4
Inert mass stage 4	203	67.3	148	+120
Propellant mass stage 4	782	772	1,750	+126
Fairing mass	400	524	582	+11.1
Total inert mass	7,386	6,728	5,724	-14.9
Payload mass	1,050	1,050	1,050	-
GTOW	72,156	72,292	73,338	+1.45
Geometry properties [m]				
Length stage 1	10.7	11.0	20.7	88.2
Length stage 2	7.60	9.22	10.3	11.7
Length stage 3	2.65	3.03	3.72	22.8
Length stage 4	2.08	1.67	2.41	44.3
Total length	29.0	30.7	42.9	39.7
Cost [€M FY2012]				
Cost per flight	24.0	30.1	29.2	-2.99

Table 10.7: Summary of the MDO vehicle output parameters for Taurus compared with the MDA vehicle output parameters.

Parameter	Actual	MDA	MDO	Difference MDA and MDO [%]
Stage 2 Ignition / Stage 1 Separation				
Time [s]	83.00	83.00	100.9	+21.6
Altitude [km]	42.50	43.70	30.58	-30.0
Velocity [m·s ⁻¹]	2,202	2,146	1,099	-48.8
Time: 161.1 s Stage 2 Burn-out				
Time [s]	161.1	161.1	204.3	+26.8
Altitude [km]	153.9	135.9	128.2	-5.67
Velocity [m·s ⁻¹]	4,639	4,725	4,077	-13.7
Time: 171.1 s Stage 3 Ignition				
Time [s]	171.1	171.1	208.3	+21.7
Altitude [km]	165.0	148.6	134.9	-9.22
Velocity [m·s ⁻¹]	4,514	4,699	4,061	-13.6
Fairing Separation				
Time [s]	179.2	144.7	193.7	+33.9
Altitude [km]	175.0	111.4	111.6	+0.18
Velocity [m·s ⁻¹]	4,598	3,976	3,483	-12.40
Time: 254.2 s Stage 3 Burnout				
Time [s]	254.2	254.2	283.4	+11.5
Altitude [km]	291.0	266.5	269.3	+1.05
Velocity [m·s ⁻¹]	6,552	6,829	5,837	-14.5
Time: 750.4 s Stage 4 Ignition				
Time [s]	750.4	750.4	736.4	-1.87
Altitude [km]	689.0	692.4	679.8	-1.82
Velocity [m·s ⁻¹]	6,014	6,315	5,211	-17.5
Stage 4 Burnout / Orbit Injection				
Time [s]	823.6	823.6	817.6	-0.73
Altitude [km]	691.0	705.0	679.9	-3.56
Velocity [m·s ⁻¹]	7,511	7,627	7,597	-0.39
Additional parameters				
Semi-major axis [km]	691.0	782.6	679.3	-13.2
Eccentricity [-]	~0.000	0.023	0.0042	-81.7
Maximum dynamic pressure [kPa]	-	89.9	75.0	-16.6
Drag loss [m·s ⁻¹]	-	175.1	166.3	-5.03
Gravity loss [m·s ⁻¹]	-	1,499	1,785	+19.1
Steering loss [m·s ⁻¹]	-	42.88	126.0	+194

Table 10.8: Summary of the MDO trajectory parameters for Taurus compared with the MDA trajectory parameters.

The vacuum thrust for the MDO's upper stages are higher than those for Taurus and the MDA. On the other hand, the vacuum thrust of the first stage is significantly lower than for Taurus and the MDA. Also the vacuum Isp for the MDO's upper stages are higher than for Taurus and the MDA and this shows that the optimizer "understands" that mass for upper stages is more critical than mass for lower stages [2]. The propellant mass of the MDO's first stage is lower than for Taurus and the MDA but for all other stages it is

higher. The lower inert mass that is observed for the MDA is also present in this MDO.

An interesting point is that the propellant mass of the MDO is higher than of the MDA. Based on that one would expect that the cost per launch for the MDO would be higher than for the MDA. Surprisingly, the opposite is true and this is caused by the different CERs that are used for the production cost. The CER for the production cost for intermediate SRMs ($13,000 \text{ kg} < \text{propellant mass} < 40,000 \text{ kg}$) is less vulnerable to an increase in propellant mass than the CER for large SRMs (payload mass $> 40,000 \text{ kg}$). Therefore, the propellant mass of the MDO's first stage is lower and the propellant mass of the second stage is significantly higher than for the MDA and Taurus. Another interesting point is that the exit pressure of the first stage is optimized such that it almost equals the minimum exit pressure before flow separation starts (see Appendix I). The same holds for the maximum ratio between the nozzle diameter exit and the motor case diameter.

The best individual from the MDO is longer and has a smaller diameter than the MDA and Taurus (see Appendix I). It can be concluded that this more slender launch vehicle attempts to minimize the drag loss. However, this slender launch vehicle has only $8.9 \text{ m}\cdot\text{s}^{-1}$ less drag loss than the MDA.

The trajectory of the MDO is compared with the trajectories of Taurus and the MDA in Table 10.8. The trajectory is different because the MDO's first stage has a lower vacuum thrust and despite the longer burn time it is not able to reach the burn-out altitude and velocity of the MDA's first stage. This also is an explanation for the limited difference in drag loss between the MDA and MDO. The higher vacuum Isp and propellant masses of the MDO's upper stages lead to a better performance than for Taurus' upper stages and eventually the two vehicles reach approximately the same orbit. A preliminary conclusion that can be drawn is that the optimizer prefers higher propellant masses for the upper stages because the SRM is more efficient at higher altitudes. Some figures for the MDO's trajectory are shown in Appendix I.

10.3.2 Multidisciplinary Design Optimization Validation Pegasus XL

The final validation for the tool is the MDO validation for Pegasus XL. The MDO is performed for an identical orbit and payload mass as is described in Section 10.2.2. A differential algorithm is selected that has to optimize 26 design variables. An initial population of 80 individuals is evolved over 3,000 generations. The characteristics of the best individual after 3,000 generations are shown in Table 10.9. The optimizer is able to optimize this problem for cost because the cost per flight for the MDO is more than 1.3 million euros lower than for the MDA. In addition, the GTOW of the MDO is significantly lower than for the MDA and Pegasus XL. The vacuum thrust and the inert mass are lower for the first two stages. Also the earlier explained effect of a composite motor casing on the inert mass is important. Therefore, the propellant masses of the first two stages of the MDO are lower than for the MDA and Pegasus XL. The same phenomenon for the vacuum Isp is observed as for Taurus' MDO: the upper stages have a higher vacuum Isp. The launch vehicle is significantly smaller than Pegasus XL, however, the diameter of the MDO is slightly larger, more details can be found in Appendix I.

Parameter	Actual	MDA	MDO	Difference MDO and MDA [%]
Propulsion properties [kN]				
Vacuum thrust stage 1	626.3	626.9	448.2	-28.5
Vacuum Isp stage 1	292.8	294.4	288.3	-2.07
Vacuum thrust stage 2	160.6	169.3	109.4	-35.4
Vacuum Isp stage 2	290.7	298.3	297.0	-0.44
Vacuum thrust stage 3	32.2	32.56	32.77	+0.64
Vacuum Isp stage 3	290.2	300.9	308.2	+2.43
Mass properties [kg]				
Inert mass stage 1	2,886	1,340	1,025	-23.5
Propellant mass stage 1	15,014	15,451	11,544	-25.3
Inert mass stage 2	416	382	200	-47.6
Propellant mass stage 2	3,925	4,155	2,339	-43.7
Inert mass stage 3	203	75.7	79.4	+4.89
Propellant mass stage 3	770	772	821	+6.35
Fairing mass	194	181	191	+5.52
Total inert mass	3,992	2,348	1,775	-24.4
Payload mass	227	227	227	-
GTOW	23,701	22,727	16,479	-27.5
Geometry properties [m]				
Length stage 1	10.3	11.1	6.61	-40.5
Length stage 2	3.11	3.49	3.10	-11.2
Length stage 3	1.34	1.70	2.06	+21.2
Total length	17.4	18.9	14.6	-22.8
Cost [€M FY2012]				
Cost per flight	16.9	19.3	18.0	-6.74

Table 10.9: Summary of the MDO vehicle output parameters for Pegasus XL compared with the MDA vehicle output parameters.

The burn-out altitudes and velocities for the MDO, the MDA and Pegasus XL are given in Table 10.10. The pull-up maneuver for the MDO is more efficient than for the MDA and this is probably caused by its lower GTOW. This more efficient pull-up also explains the lower maximum dynamic pressure of the MDO compared with the q_{max} of Pegasus XL and the MDA. The coasting time between the first two stages of the MDO is 10 seconds shorter than for Pegasus XL and the burn time of the MDO's second stage is shorter too. This is followed by a longer coasting period between the second and third stage for the MDO. The final orbit of the MDO shows good correspondence with the MDA and Pegasus XL's final orbit. Some figures for the MDO's trajectory can be found in Appendix I.

The MDO validation for Pegasus XL again shows that the tool has the capability to optimize launch vehicles and their trajectories for cost. The MDO for Pegasus XL shows a higher cost reduction compared with the MDA than is the case for Taurus.

Parameter	Actual	MDA	MDO	Difference MDA and MDO [%]
Burn-out stage 1				
Time [s]	71.00	71.00	70.8	-0.28
Altitude [km]	59.63	44.31	61.47	+38.7
Velocity [m·s ⁻¹]	2,415	2,513	2,859	+13.8
Stage 2 Ignition				
Time [s]	90.30	90.30	78.8	-12.7
Altitude [km]	87.51	67.87	75.21	+10.8
Velocity [m·s ⁻¹]	2,380	2,415	2,815	+16.6
Fairing Separation				
Time [s]	107	124.4	98.7	-20.7
Altitude [km]	110.0	111.4	108.7	-2.42
Velocity [m·s ⁻¹]	2,765	3,446	3,202	-7.08
Stage 2 Burnout				
Time [s]	161.0	161.0	139.2	-13.5
Altitude [km]	208.3	178.8	198.0	+10.7
Velocity [m·s ⁻¹]	5,469	5,618	5,124	-8.79
Stage 3 Ignition				
Time [s]	589.0	589.0	606.8	+3.02
Altitude [km]	739.0	727.4	734.9	+1.03
Velocity [m·s ⁻¹]	4,564	4,712	4,141	-12.1
Stage 3 Burnout / Orbit Injection				
Time [s]	655.0	655.0	680.1	+3.83
Altitude [km]	741.0	735.5	724.2	-1.54
Velocity [m·s ⁻¹]	7,487	7,492	7,484	-0.11
Additional parameters				
Semi-major axis [km]	741.0	737.6	735.8	-0.24
Eccentricity [-]	~0.000	0.0085	0.0025	-70.7
Maximum dynamic pressure [kPa]	57.5	75.0	47.3	-36.9
Drag loss [m·s ⁻¹]	-	326.8	311.1	-4.80
Gravity loss [m·s ⁻¹]	-	1,526	1,670	+9.44
Steering loss [m·s ⁻¹]	-	247.5	119.2	-51.8

Table 10.10: Summary of the MDO trajectory parameters for Pegasus XL compared with the MDA trajectory parameters.

Chapter 11

Results

In the preceding chapters the various disciplines of the tool are discussed and after the validation of the tool itself in the previous chapter, it is time to use the tool to investigate the performance benefits of air launch.

In the first section of this chapter the 10 kg payload class is discussed. Next the results for the wingless and winged 2,000 kg payload class are described. The final section of the chapter deals with an application for the tool, the launch of microsattellites from the Andøya Rocket Range in Norway.

11.1 10 kg Payload Class

In this section the results for the 10 kg payload class will be discussed. Throughout this section the results from the simulations will be compared with the actual ALOSS case. The vehicle characteristics of the ALOSS launch vehicle can be found in Appendix B. The ALOSS launch vehicle is for this work considered as the reference case. This three stage vehicle is launched at $250 \text{ m}\cdot\text{s}^{-1}$ under a flight path angle 50° from 15 km altitude. The ALOSS launch vehicle is used to validate the trajectory model of this tool in Section 8.4. In the following subsections the launch vehicle will be optimized for different release conditions and number of stages. As is described in Chapter 2 a differential algorithm will be used for the optimization. For the optimization performed in this section the differential algorithm is set with a weight and crossover probability of both 0.9. In Section 12.5 the effect of different settings of the algorithm is investigated. A population of 70 individuals is evolved over 10,000 generations. The objective function and the constraint handling have been discussed in Section 2.4.

11.1.1 Optimized ALOSS Launch Vehicle

As already stated by the NLR itself the ALOSS launch vehicle follows a sub-optimized trajectory [106]. In addition, this tool uses different models to calculate the performance, geometry and masses of the stages than are used by the NLR (see Section 10.1). Therefore, it is decided that first an air launched vehicle for the same release conditions as ALOSS

and subjected to the same constraints (geometry, mass and maximum acceleration) is optimized.

After 10,000 generations 67 of the 70 individuals are valid vehicles that follow an admissible trajectory. The search space of the design variables for the launch vehicle are given in Appendix J. A scatter plot for the GTOW and the cost per flight for all 67 valid vehicles is shown in Figure 11.1. This figure makes clear that all valid individuals outperform the original ALOSS vehicle in terms of GTOW and cost per flight. In addition a trend is observed that a lower GTOW results in a lower cost per flight. This is expected since the cost model is based on the propellant mass and the propellant makes up over 80% of the vehicle's GTOW. The GTOW of the valid individuals varies with 22.0% (between 931 kg and 1,194 kg) and the cost per flight with 9.56% (between €1.889 million and €2.089 million).

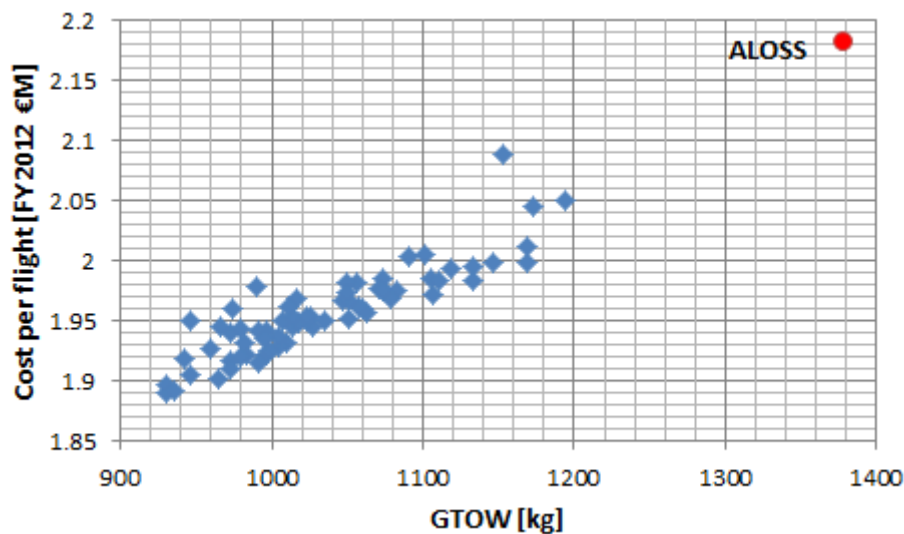


Figure 11.1: GTOW versus cost per flight for all valid optimized vehicles for the ALOSS case.

Another observation is that the values for the design variables are spread over the entire search space. This is shown for the burn time in Figure 11.2 for which the search space of stage 1 is between 40 and 70 seconds, for stage 2 between 30 and 70 seconds and for stage 3 between 30 and 50 seconds. This search space is based on the burn times of the SRMs in the Solid Rocket Motor Database in Appendix D.

From Figure 11.2 also follows that the thrust forces for all stages of ALOSS are higher than for the optimized launch vehicles. It should be noted that the values for the thrust forces for ALOSS represents the average thrust force. The burn times for ALOSS are shorter than for the optimized vehicles (there are two exceptions for the second stage). It can also be observed that the vacuum thrust of the optimized third stages only varies with 27.7% (from 2,001 N to 2,769 N) while the vacuum thrust of the first and second stage varies with respectively 33.9% (from 25,235 N to 38,181 N) and 52.4% (from 4,542 N to 9,551 N). An explanation for this could be that the range of thrust forces for the third stage that do not violate the constraint for the maximum acceleration but still provide sufficient ΔV within the search space of the burn time is limited.

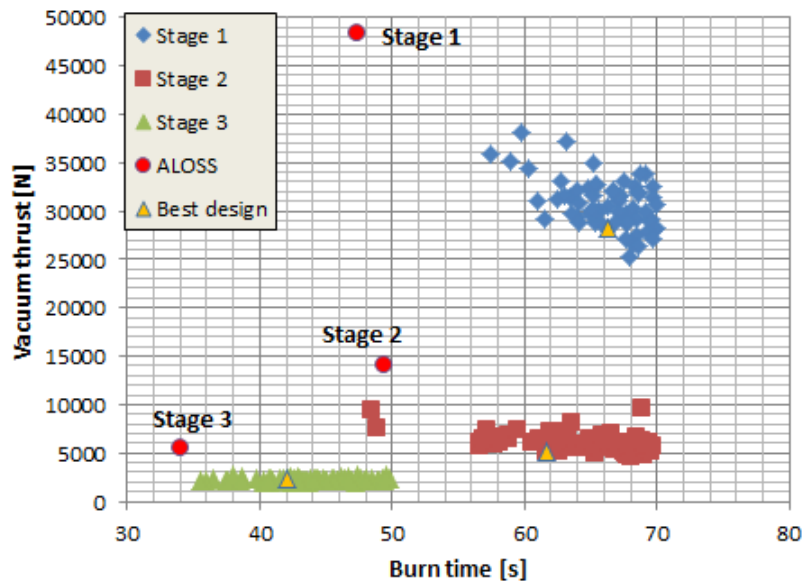


Figure 11.2: Burn time versus vacuum thrust for all valid optimized vehicles for the ALOSS case.

In Figure 11.3 the inert masses and the propellant masses for each stage are shown on a logarithmic scale. In this figure it can be observed that the propellant mass ratio, $\frac{M_p}{M_p + M_i}$, for all optimized vehicles and all stages is higher than for ALOSS. This is caused by the different models that are used to calculate the inert mass (for more details see Section 10.1).

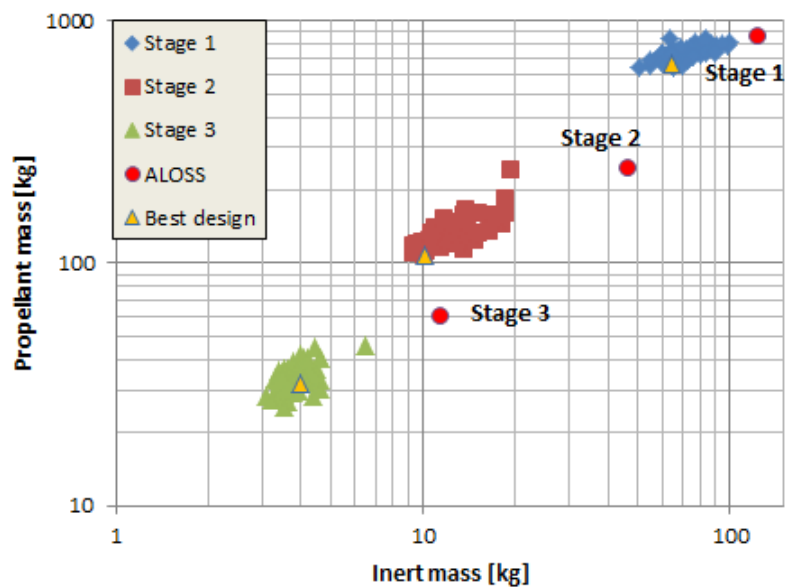


Figure 11.3: Inert mass versus propellant mass for all valid optimized vehicles for the ALOSS case.

It is time to compare the trajectory of the optimized vehicles with the trajectory of the

original ALOSS vehicle. It should be noted that the pitch control law used for ALOSS presented in Section 8.4 is slightly different from the pitch control law used in [106] and so, the final orbit. In order to attain a circular orbit of 780 km the pitch control law from [106] has to be used. In addition to the trajectory for the cheapest and lightest design two other noticeable trajectories will be shown: the vehicle with the lowest gravity and lowest drag loss. The most important vehicle characteristics are shown in Table 11.1, all values for the design variables and additional figures can be found in Appendix J.

Parameter	Unit	ALOSS	Cost and GTOW	Gravity loss	Drag loss
Cost per flight	€M	2.182	1.890	2.051	2.003
GTOW	kg	1,380	930.6	1,194	1,091
Vehicle length	m	5.5	5.422	5.437	5.410
Vehicle diameter	m	0.66	0.5605	0.6467	0.5729
Gravity loss	$\text{m}\cdot\text{s}^{-1}$	1,920	1,673	1,583	1,773
Drag loss	$\text{m}\cdot\text{s}^{-1}$	165.8	176.4	171.6	142.9
ΔV	$\text{m}\cdot\text{s}^{-1}$	8,793	8,633	8,559	8,754

Table 11.1: Summary of the most important characteristics for the optimized ALOSS case.

As is already shown in Figure 11.1 the cheapest design is also the design with the lowest GTOW. The cost reduction with respect to ALOSS is 13.4% and the GTOW can be reduced by 32.6%. For the three optimized individuals the length and diameter of the launch vehicle are almost the same. The maximum differences in length and diameter for the 67 individuals are respectively 6.56% (from 5.136 m to 5.497 m) and 18.2% (from 0.5482 m to 0.6705 m). These small deviations are caused by the geometry constraints that are imposed to this problem. Based on the above, it can be concluded that the constraint for the length is the limiting constraint. The ΔV provided by the optimized launch vehicles are for the best case $234 \text{ m}\cdot\text{s}^{-1}$ (2.66%) lower than for ALOSS. The steering loss is the largest for the vehicle with the lowest drag loss since it attains a large absolute angle of attack in comparison with the other vehicles.

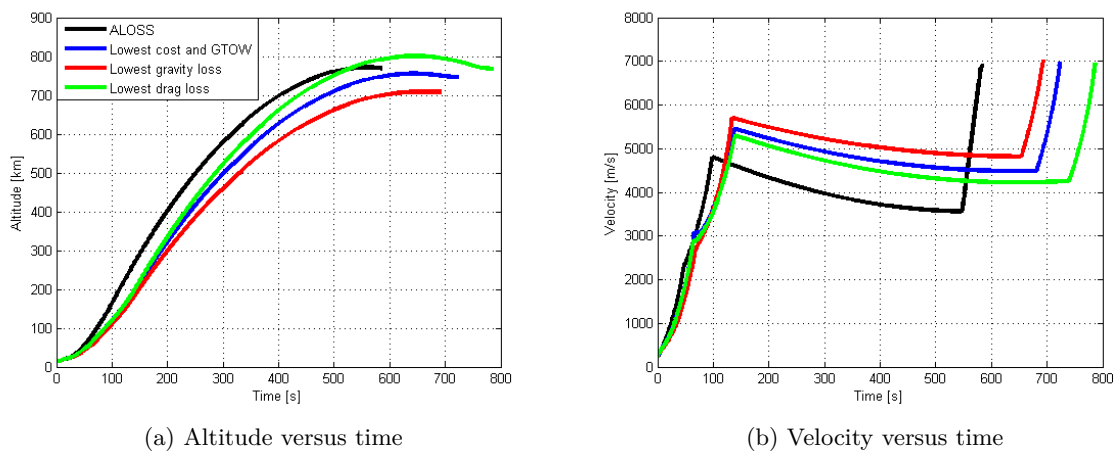


Figure 11.4: Altitude and velocity versus time for the several ALOSS cases.

In Figure 11.4 the altitude and the velocity over time for the four cases are shown. The simulation is stopped when the vehicle reaches the right orbit, therefore, the action time for the different vehicles is different. From Figure 11.4 it can be concluded that all vehicles reach more or less the same orbit and have the same velocity. The difference in final altitude is caused by the tolerances of 10 km in semi-major axis and 0.01 in eccentricity.

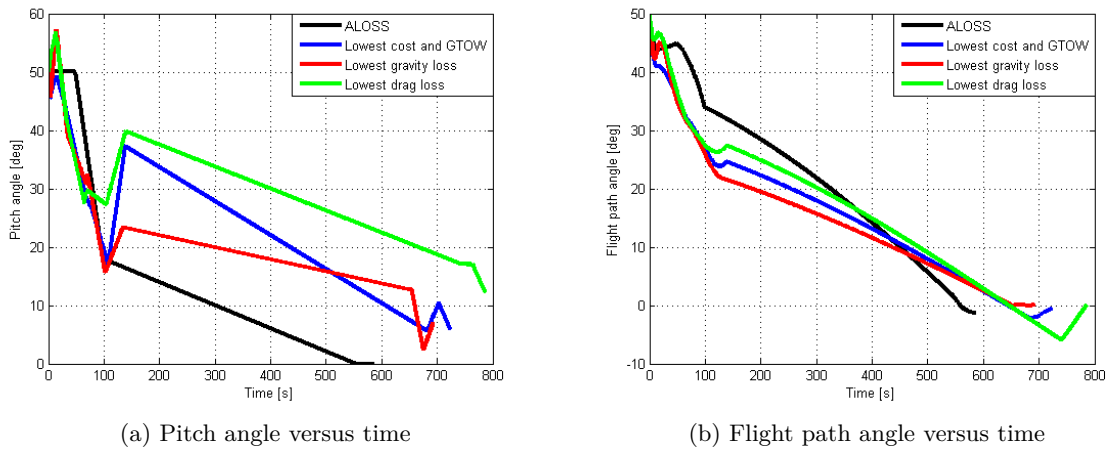


Figure 11.5: Pitch angle and flight path angle for several ALOSS cases.

In Figure 11.5 the pitch and flight path angle over time for the vehicles are given. The flight path angle for ALOSS remains the highest for the largest part of the flight and therefore it has the highest gravity loss despite its shorter total action time.

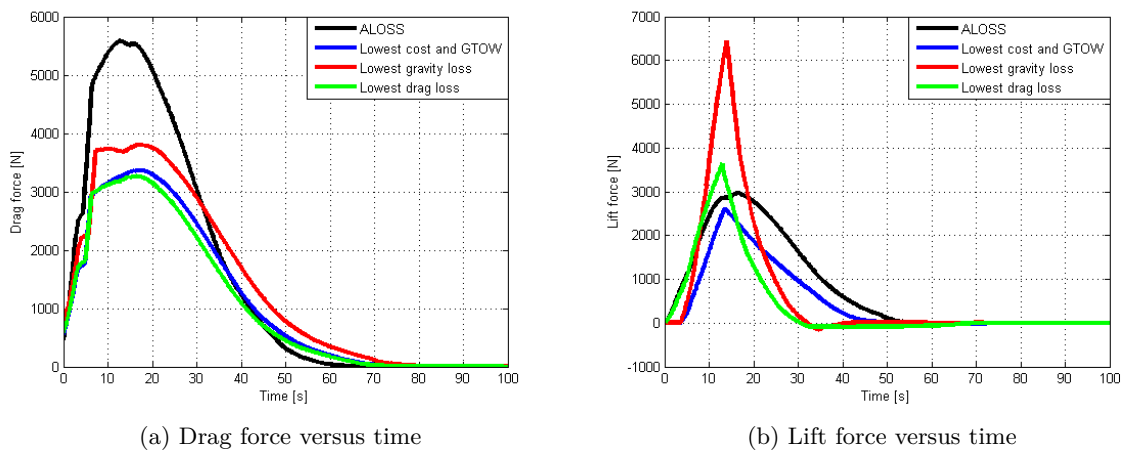


Figure 11.6: Drag and lift force for several ALOSS cases.

In Figure 11.6 the drag and lift force for the various vehicles can be found. ALOSS has the largest drag force, however, its drag loss is not higher than for the other cases. This is caused by the higher mass of the original ALOSS vehicle. Another interesting effect is that the lift force for the vehicle with the lowest gravity loss is larger than the drag force

between 10.0 s and 16.9 s. This high lift force is caused by the 15° angle of attack that is attained by that vehicle.

11.1.2 Ground launch and Release Flight Path Angle

In this section the optimized vehicles for ground launch and for different release flight path angles will be presented. The release altitude and velocity remain constant at 15.0 km and $250 \text{ m}\cdot\text{s}^{-1}$. The most important characteristics for each of the optimized vehicles is presented in Table 11.2 and the details can be found in Appendix J. For the 50° release flight path angle the best individual in terms of cost and GTOW from Section 11.1.1 is used.

The numbers in this table show that air launch can provide a cost reduction of 28.1% and a reduction in GTOW of 70.1% compared to ground launch. Another interesting observation is that the cost per flight and GTOW for the different release flight path angles only varies with respectively 6.03% and 18.1% (only 2.60% and 9.19% if horizontal launch is not taken in account). The flat optimum for the release flight path angle is also observed in [93].

For drag loss one expects that the largest release path angle results in the lowest drag loss because the launch vehicle will initially follow an almost vertical trajectory, this will be at the expense of an increase in gravity loss. This is in correspondence with the data in Table 11.2, except for a higher gravity loss for the 0° case compared to the 25° case and a lower drag loss for the 75° case than for the 90° . This can be explained by the different trajectories that the vehicles follow. The fact that the optimized vehicle for 75° has a slightly lower GTOW but not has a lower price per flight than the optimized vehicle for 50° can be explained because the cost models are based on the propellant mass.

The ΔV advantage of air launch compared with ground launch is in the best case $1,225 \text{ m}\cdot\text{s}^{-1}$ (or 12.4%). This number is higher than the reported number of $\sim 500\text{-}950 \text{ m}\cdot\text{s}^{-1}$ in ΔV advantage of air launch for comparable release conditions for a Minotaur I launch vehicle [93]. However, in [93] the Minotaur LV is evaluated in its original configuration hence the expansion ratio of the engines is not changed. Also the higher GTOW of Minotaur (36,200 kg) reduces the importance of drag loss. Therefore, it can be concluded that these numbers are in correspondence with each other.

Parameter	Unit	50°	Ground launch	0°	25°	75°	90°
Cost per flight	€M	1.890	2.628	2.011	1.930	1.902	1.940
GTOW	kg	930.6	3,087	1,128	1,017	923.8	976.8
Vehicle length	m	5.422	6.745	5.469	5.440	5.395	5.482
Vehicle diameter	m	0.5605	0.9126	0.6571	0.6102	0.6172	0.5801
Gravity loss	$\text{m}\cdot\text{s}^{-1}$	1,673	2,215	1,589	1,586	1,875	1,820
Drag loss	$\text{m}\cdot\text{s}^{-1}$	176.4	558.5	460.9	346.7	125.2	147.6
ΔV	$\text{m}\cdot\text{s}^{-1}$	8,633	9,858	8,851	8,687	8,718	8,716

Table 11.2: Summary of the most important characteristics for the optimized ground launched vehicle and the optimized vehicles for various release flight path angles.

It has to be noted that the constraint for the bending load for the horizontal launch case had to be relieved to $10,000 \text{ Pa}\cdot\text{rad}$ instead of $4,170 \text{ Pa}\cdot\text{rad}$ because for the original

constraint the launch vehicle was not able find an admissible trajectory (see also Figure J.8 in Appendix J). This problem is also identified in [87] and [89].

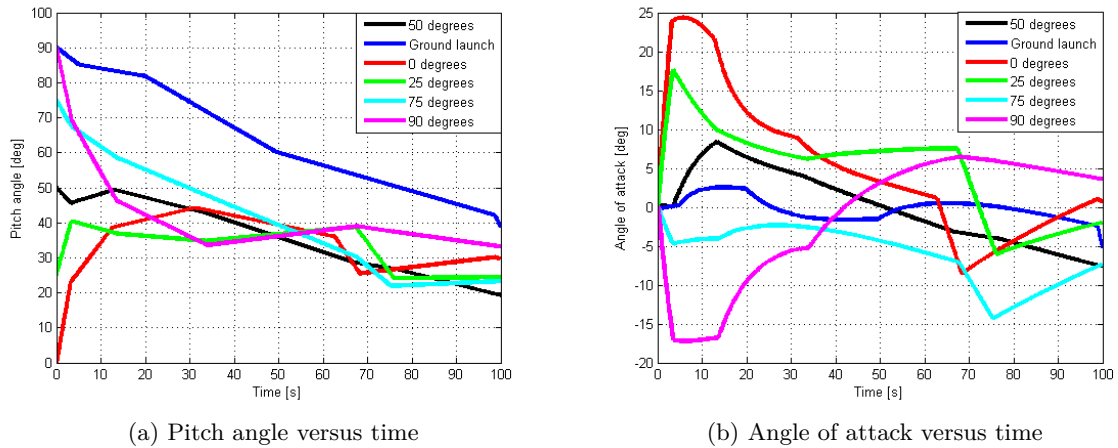


Figure 11.7: Pitch angle and angle of attack for the first 100 seconds for the optimized ground launched vehicle and optimized air launched vehicles for various release flight path angles.

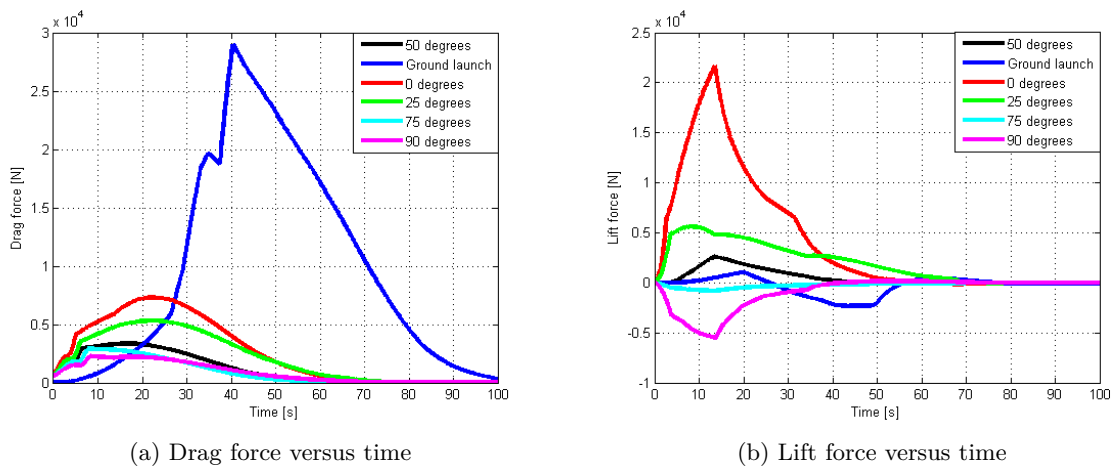


Figure 11.8: Drag and lift force for the optimized ground launched vehicle and optimized vehicles for various release flight path angles.

The optimized ground launched vehicle is a stubby design with a slenderness (length diameter ratio) of 7.4 while the air launched vehicles have a slenderness between 8.4 and 9.7. This low slenderness is also an explanation for the high drag loss. The reason why the optimizer comes up with this final design lies in the trade-off between a lower inert mass (thus a higher ΔV) and a lower drag loss. Suppose that the only variable that is changed is the slenderness of the first stage, therefore, the stage's diameter is decreased. If the stage's diameter is decreased significantly the exit diameter has to be decreased as well. This causes a reduction in the expansion ratio, in order to maintain the same thrust

level the chamber pressure has to be increased (higher case mass). In any case, in order to carry the amount of propellant the length of motor case has to be increased. Another effect would be that the longer motor case requires more insulation. Therefore, it is the question whether the effect of a lower drag loss is not diminished by a reduction in ΔV because of a higher inert mass.

In Figure 11.7 the pitch angle and angle of attack for the optimized vehicles are shown for the first 100 seconds of the flight. In case that the vehicle is launched horizontally, under a flight path angle of 25° and even under 50° the vehicle pitches up first. This results in a high angle of attack hence high lift and drag forces as can be seen in Figure 11.8. The angle of attack for the ground launched vehicle remains within $\pm 5^\circ$ for the first 45 seconds of the flight, so, the optimized ground launched vehicle follows a gravity turn in order to reduce the drag losses.

11.1.3 Release Altitude and Velocity

Previously the release flight path angle is investigated and in this subsection different release altitudes and velocities will be addressed. The release flight path angle remains constant at 50° . The most important characteristics of the optimized vehicles can be found in Table 11.3.

Parameter	Unit	15 km	10 km	15 km	15 km
		250 m·s ⁻¹	250 m·s ⁻¹	200 m·s ⁻¹	400 m·s ⁻¹
Cost per flight	€M	1.890	2.080	1.973	1.813
GTOW	kg	930.6	1,225	1,064	807.3
Vehicle length	m	5.422	5.478	5.438	5.388
Vehicle diameter	m	0.5605	0.6649	0.5947	0.5156
Gravity loss	m·s ⁻¹	1,673	1,805	1,645	1,724
Drag loss	m·s ⁻¹	176.4	372.3	191.7	164.5
ΔV	m·s ⁻¹	8,633	8,904	8,686	8,482

Table 11.3: Summary of the most important characteristics for the optimized air launched vehicles for various release altitudes and velocities.

Table 11.3 shows that reducing the release altitude has a large effect on the optimized design. This is of course caused by the larger influence of the atmosphere at lower altitudes. First of all, the drag loss for the optimized vehicle for 10 km release altitude is more than twice as high as for the vehicle that is optimized for 15 km release altitude. This is despite the fact that the GTOW of the optimized vehicle for 10 km release altitude is 24.0% higher. The amount of additional ΔV (270 m·s⁻¹ or 3.04%) that has to be provided by the optimized launch vehicle for 10 km results in a higher GTOW (+31.6%) and cost per flight (+9.13%).

Moreover, Figure 11.9 shows a larger pressure loss for the first stage compared to the cases with a release altitude of 15 km. The initial thrust of the first stage is for the 10 km release altitude 91.5% of the maximum thrust and for the 15 km release altitude cases between 95.0 and 98.0%.

A reduction of the release velocity with 50 m·s⁻¹ has much less an influence on the vehicle's design than reducing the release altitude from 15 km to 10 km. In Figure 11.9 it can

be seen that the optimized vehicles with a release velocity of $250 \text{ m}\cdot\text{s}^{-1}$ and $200 \text{ m}\cdot\text{s}^{-1}$ approximately follow the same trajectory. Therefore, their losses are comparable and the only difference in the amount of ΔV provided by these vehicles originates from the initial difference in release velocity. The same holds for increasing the release velocity: the reduction in the amount of ΔV to reach orbit is equal to the difference in release velocity. Due to the logarithm nature of the rocket equation a small difference in the amount of ΔV required results in a significant change in GTOW.

The conclusions above are not in correspondence with the conclusions in [93] which claim that the launch parameter that has the most influence on the reduction in ΔV from air launch is the launch velocity. However, again it has to be noted that in [93] the Minotaur LV is evaluated in its original configuration, therefore, the expansion ratio of the engines is not changed. Also the higher GTOW of Minotaur (36,200 kg) reduces the importance of drag loss. Reducing the launch altitude has a large effect on the expansion ratio and results in a higher drag loss.

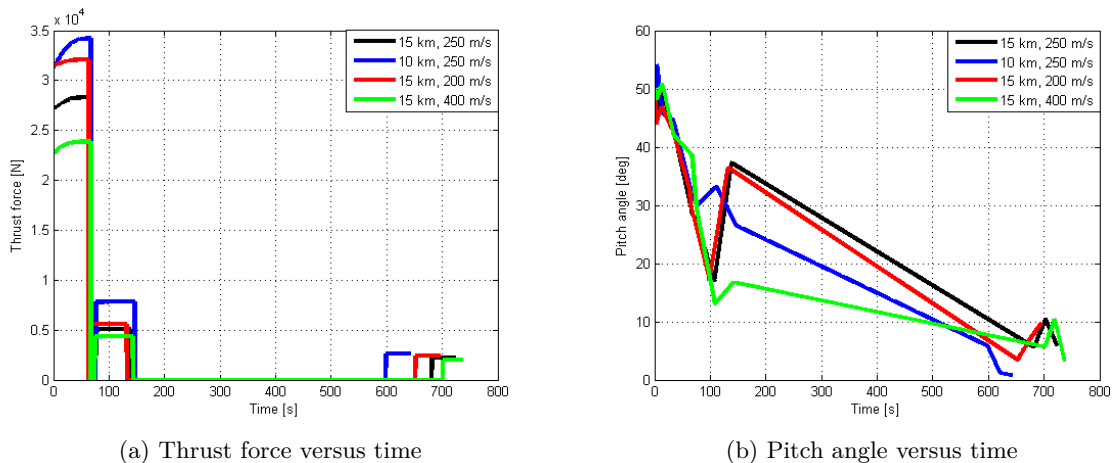


Figure 11.9: Thrust force and pitch angle versus time for the optimized air launched vehicles for different release altitudes and velocities.

11.1.4 Number of stages

The simulation tool in its current form is able to optimize two, three and four stage launch vehicles. Solid single-stage-to-orbit (SSTO) vehicles are considered unrealistic especially in the case that the burn time is restricted and constant thrust is modeled. In the previous sections only three stage vehicles are evaluated and therefore, two and four stage vehicles will be discussed in this section. The release conditions remain identical to the release conditions for ALOSS.

First two stage vehicles are addressed. The settings and constraints remain identical to the settings for the three stage vehicle. However, the optimizer could not generate a vehicle that provides sufficient ΔV that followed an admissible trajectory. The reason for this is that the limited search space for the burn time results in high accelerations. Therefore, it is decided to extend the search space for the burn time to 100 seconds for every stage. Even then none of the vehicles reach the target orbit. Figure 11.10 shows

the final orbit characteristics of the valid vehicles. None of the vehicles reaches the target orbit within the tolerance for the semi-major axis and eccentricity.

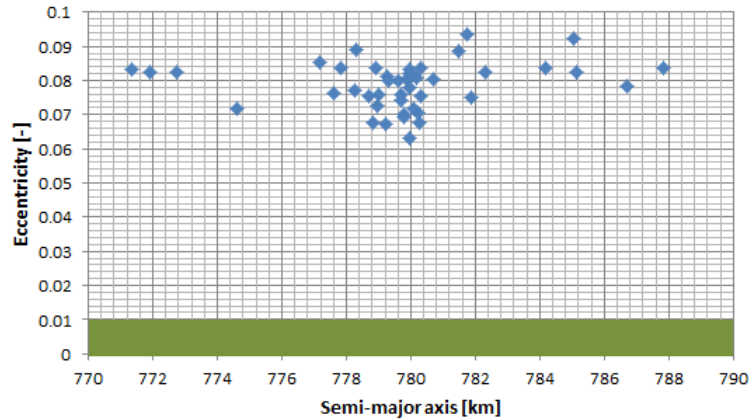


Figure 11.10: Final value for the semi-major axis and eccentricity for all optimized two stage vehicles (green area indicates the tolerances for orbit).

Within the same constraints and search space as for the three stage vehicle the optimizer is also not able to find a four stage vehicle that follows an admissible trajectory. This is caused by geometry constraint for the length of 5.50 meters. It is decided to slightly relax this constraint to 6.50 meters, however, the launch vehicle exceeds now the dimensions of the F-16 370 gallon external fuel tank. Several valid vehicles are found that follow an admissible trajectory and reach the right target orbit. The characteristics of the individual with the lowest cost per flight (and GTOW) is presented in Table 11.4. From this table follows that the GTOW between the three and four stage vehicle is almost identical. The same holds for the total velocity loss and provided amount of ΔV . However, the cost per flight is for the three stage vehicle 17.7% lower than for the four stage vehicle.

Parameter	Unit	Three stage vehicle	Four stage vehicle
Cost per flight	€M	1.890	2.296
GTOW	kg	930.6	965.0
Vehicle length	m	5.422	6.164
Vehicle diameter	m	0.5605	0.6210
Gravity loss	$\text{m}\cdot\text{s}^{-1}$	1,673	1,617
Drag loss	$\text{m}\cdot\text{s}^{-1}$	176.4	230.0
ΔV	$\text{m}\cdot\text{s}^{-1}$	8,633	8,637

Table 11.4: Summary of the most important characteristics for the optimized three and four stage air launched vehicles.

The flight path angle for the optimized three and four stage vehicles show also good correspondence (see Figure 11.11). The main difference is that the optimized four stage vehicle pitches down earlier during the first 50 seconds of the flight (see Figure 11.11) and this results in a higher drag and lower gravity loss.

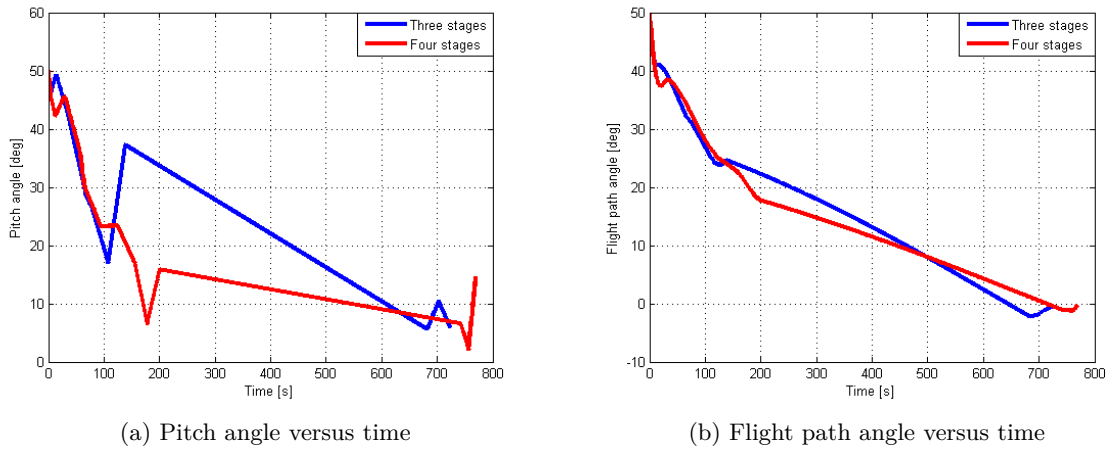


Figure 11.11: Pitch angle and flight path angle for the three and four stage optimized air launched vehicle.

11.2 2,000 kg Payload Class

After the 10 kg payload class it is now time to discuss the 2,000 kg payload class. The settings for the differential algorithm, the population size and the number of generations evaluated are identical to the ones of the 10 kg payload class. First ground launch, vertical air launch and horizontal air launch will be compared. Next the effects of a different release altitude and release velocity are examined. In the final part of this section winged vehicles will be evaluated. For the sake of brevity the effect of a two or four stage launch vehicle is not investigated for the 2,000 kg payload class.

11.2.1 Ground launch, Horizontal and Vertical Launch

The evaluation of the 2,000 kg payload class starts with a comparison between ground launch, vertical air launch and horizontal air launch. Also the launch under a small release flight path angle of 15° will be evaluated.

During the literature study it was concluded that for the 2,000 kg payload class two air launch methods can be used [103]. The first one is a vertical drop from the cargo bay of a large transport aircraft (the launch vehicle is internally carried). The second option is to launch the vehicle horizontally from under or on top of an airliner. For a throughout description and the advantages and disadvantages of both methods is referred to the literature study [103]. The geometry constraints for both methods are identical with 33.8 m for the vehicle's length and a maximum diameter of 3.3 m. The maximum value for the GTOW is 105 tons for internally carried vehicles and 140 tons for other vehicles. For an explanation how these constraints are determined is again referred to the literature study [103].

Table 11.5 shows the most important characteristics for the optimized vehicles. On first glance a launch under a small release flight path angle is the most promising: lowest cost per flight, lowest GTOW and least ΔV required. The optimized launch vehicle for

a launch at 10 km altitude, with a release velocity of $200 \text{ m}\cdot\text{s}^{-1}$ under a release flight path angle of 15° reduces the cost per flight with 25.5% and the GTOW with 36.3%. Moreover, the ΔV required is reduced with $792 \text{ m}\cdot\text{s}^{-1}$ (8.50%) compared to ground launch. It has to be noted that for an internally carried launch vehicle the carrier aircraft does not necessary requires permanent modifications [91]. Therefore, a purchase of this aircraft might not be required. This will lead to a reduction in the cost per flight and a more throughout analysis about this is given in Section 12.1.2.2.

Parameter	Unit	Ground launch	10 km	10 km	10 km
			$0 \text{ m}\cdot\text{s}^{-1}$	$200 \text{ m}\cdot\text{s}^{-1}$	$200 \text{ m}\cdot\text{s}^{-1}$
			90°	0°	15°
Cost per flight	€M	26.66	20.76	22.01	19.87
GTOW	kg	144,148	95,023	108,820	91,878
Vehicle length	m	35.41	32.21	29.65	29.00
Vehicle diameter	m	2.466	2.149	3.353	2.639
Gravity loss	$\text{m}\cdot\text{s}^{-1}$	2,147	1,576	1,613	1,370
Drag loss	$\text{m}\cdot\text{s}^{-1}$	124.4	82.72	459.1	302.7
ΔV	$\text{m}\cdot\text{s}^{-1}$	9,327	8,703	9,025	8,534

Table 11.5: Summary of the most important characteristics for the optimized vehicles for ground launch and horizontal and vertical air launch for the 2,000 kg payload case.

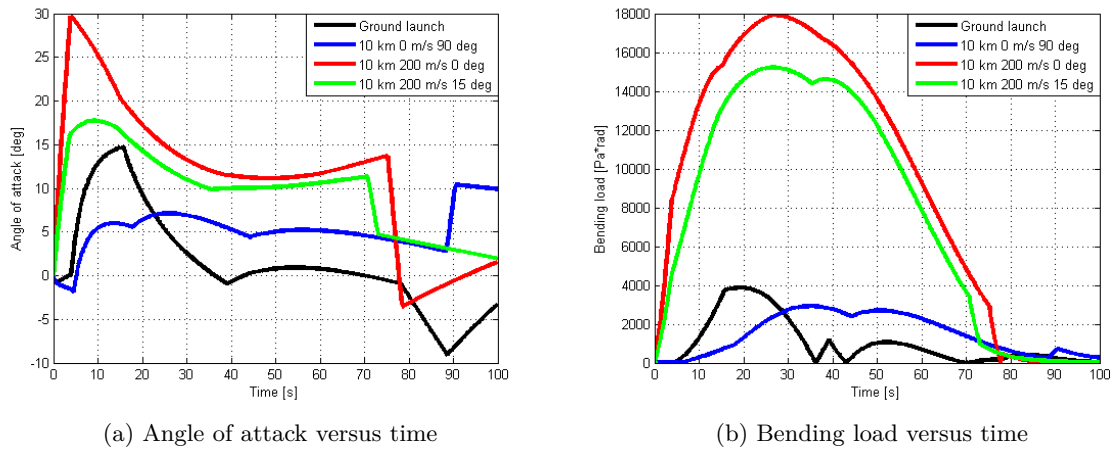


Figure 11.12: Angle of attack and bending load versus time for the optimized vehicles or ground launch and horizontal and vertical air launch for the 2,000 kg payload case.

The large differences between the optimized air launched vehicle for horizontal launch and the launch under a small flight path angle are interesting. These differences can be explained by the inability of the horizontally launched vehicle to pitch up which results in a high angle of attack (see Figure 11.12). This also leads to a very high steering loss of $244.5 \text{ m}\cdot\text{s}^{-1}$ for the horizontally launched vehicle. From Figure 11.12 also high bending

loads that approaches the limit value are observed for horizontal launch.. This $q \cdot \alpha$ limit is relaxed to 18,000 Pa· rad, which is in correspondence with the $q \cdot \alpha$ limit of Pegasus. Since the differences in maximum $q \cdot \alpha$ are large between the different optimized vehicles it is proposed to model the bending load more carefully in future studies and to apply a correction factor on the inert mass of the vehicles that experience a large bending moment. The ground launched vehicle shows an initial angle of attack but when it approaches the segment of the flight where the highest dynamic pressure occurs (30 to 60 seconds) the angle of attack is almost zero.

All values for the design variables, details about the vehicles and additional figures can be found in Appendix J. It is interesting to see that for all optimized air launched vehicles the nozzle exit diameter is larger than the motor case diameter while this is not the case for the optimized ground launched vehicle. A wider nozzle exit diameter than case diameter results in more efficient nozzle expansion and is also a characteristic of the Orion 50S SRM which is used as Pegasus' first stage [4].

11.2.2 Release Altitude and Velocity

Step two for the 2,000 kg payload class is to investigate the effect of a different release altitude and velocity. Therefore, the release flight path angle remains constant at 15° . The most important characteristics for the optimized vehicles can be found in Table 11.6. From this table it can be concluded that the effect of reducing the release velocity with $50 \text{ m}\cdot\text{s}^{-1}$ does not have a much larger effect on the required ΔV than the initial difference in release velocity. Reducing the launch altitude does have a larger effect on the ΔV required than a reduction in release velocity. These results are in correspondence with the results for varying release altitude and velocity for the 10 kg payload class.

In order to be able to compare both payload classes also an optimization for ALOSS release conditions for the 2,000 kg case is performed. The performance advantages for ALOSS release conditions compared to ground launch are 31.3% for the cost per flight, 47.8% for GTOW and $797 \text{ m}\cdot\text{s}^{-1}$ (8.65%) in required ΔV . The advantage in cost per flight for the two different payload classes are very comparable 28.1% and 29.8%. The smaller advantage for the 2,000 kg payload class compared to the 10 kg payload for the GTOW and ΔV are a result of the reduced importance of drag loss for heavier vehicles.

Parameter	Unit	10 km	10 km	7.5 km	15 km
		$200 \text{ m}\cdot\text{s}^{-1}$	$150 \text{ m}\cdot\text{s}^{-1}$	$200 \text{ m}\cdot\text{s}^{-1}$	$250 \text{ m}\cdot\text{s}^{-1}$
		15°	15°	15°	50°
Cost per flight	€M	19.87	20.35	20.56	18.30
GTOW	kg	91,878	95,938	97,236	75,182
Vehicle length	m	29.00	29.38	29.78	31.23
Vehicle diameter	m	2.639	2.698	2.678	2.035
Gravity loss	$\text{m}\cdot\text{s}^{-1}$	1,370	1,359	1,521	1,624
Drag loss	$\text{m}\cdot\text{s}^{-1}$	302.7	304.8	312.4	41.17
ΔV	$\text{m}\cdot\text{s}^{-1}$	8,534	8,600	8,641	8,530

Table 11.6: Summary of the most important characteristics for different release altitudes and velocities for the 2,000 kg payload class..

11.2.3 Winged Launch Vehicles

In this final section of the 2,000 kg payload class the effects of a wing will be examined. As explained in Section 6.1 the wing is modeled with one variable: the mean chord length. Table 11.7 shows the most important characteristics of the optimized winged vehicles. Also the most important characteristics for the wingless launch vehicles with identical release conditions (release altitude 10 km and release velocity $200 \text{ m}\cdot\text{s}^{-1}$) are shown in this table.

Parameter	Unit	0°		15°	
		Wingless	Winged	Wingless	Winged
Cost per flight	€M	22.01	21.43	19.87	20.79
GTOV	kg	108,820	87,206	91,878	83,173
Vehicle length	m	29.65	30.21	29.00	30.67
Vehicle diameter	m	3.353	2.281	2.639	2.121
Gravity loss	$\text{m}\cdot\text{s}^{-1}$	1,613	1,609	1,370	1,483
Drag loss	$\text{m}\cdot\text{s}^{-1}$	459.1	271.0	302.7	234.9
ΔV	$\text{m}\cdot\text{s}^{-1}$	9,025	8,609	8,534	8,550

Table 11.7: Summary of the most important characteristics for optimized winged air launched vehicles for various release flight path angles.

For the horizontal launch a wing provides a reduction in the cost per flight (2.65%), GTOV (19.9%) and ΔV (4.60%) required. For a release flight path angle of 15° the winged vehicle only provides a GTOV advantages (9.47%). As is stated in Chapter 9 the values in the cost model for the development standard factor, f_1 , the vehicle type, f_v , and the complexity of the first stage, Q_1 , are higher for winged vehicles because they are deemed more complex. This explains the higher cost per flight for a winged vehicle even with a lower GTOV.

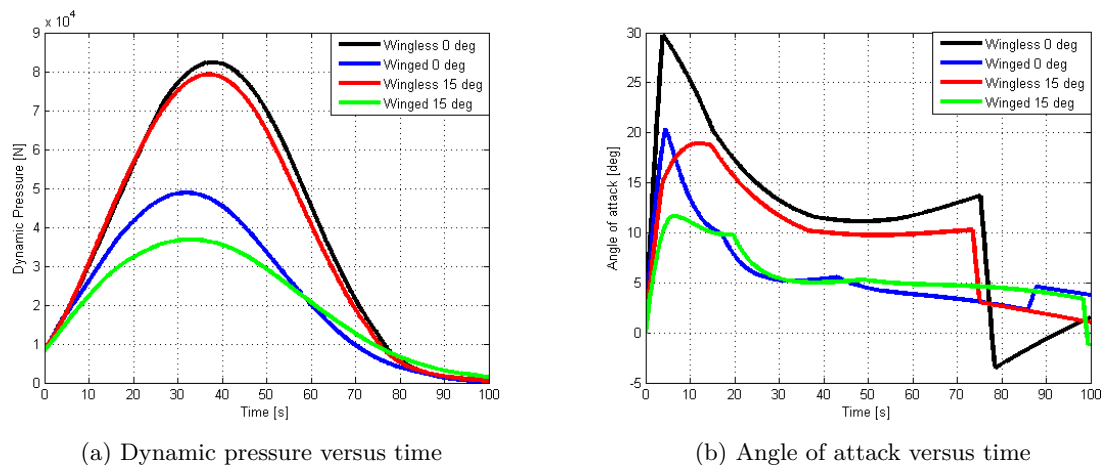


Figure 11.13: Dynamic pressure and angle of attack versus time for the optimized winged air launched vehicles for the 2,000 kg payload class.

The dynamic pressure and angle of attack for the optimized vehicles are shown in Figure

11.13. The wingless vehicles cannot generate sufficient lift to pitch up and therefore remain longer in the dense regions of the atmosphere. Therefore, a higher dynamic pressure for these vehicles is observed. Moreover, the optimized wingless vehicles initially attain a very high angle of attack in order to pitch up. This also explains the longer total action time of the wingless vehicles compared to the winged vehicles.

Figure 11.14 shows the drag and lift force for the optimized vehicles. The presence of the wing results in an earlier maximum drag force. The difference in lift force between the winged and wingless vehicles is one first glance not too large, however, one has to keep in mind that the wingless vehicles attain a much higher angle of attack.

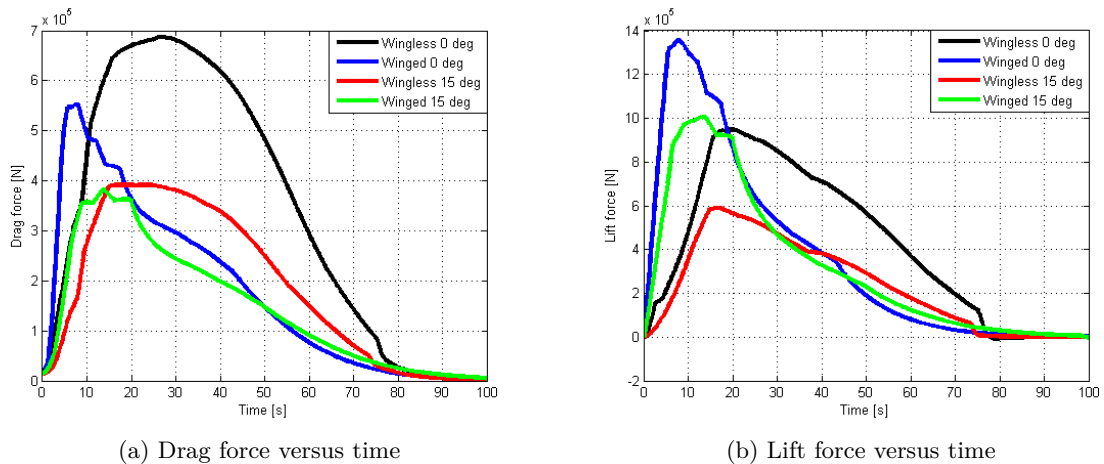


Figure 11.14: Drag and lift force versus time for the optimized winged air launched vehicles for the 2,000 kg payload class.

11.3 Application of the Tool: Launch from Andøya

In the final section of this chapter the tool is used for an actual application: the launch of a microsatellite from the Andøya Rocket Range (ARR). The ARR is a rocket launch site situated on the Andøya island in northern Norway (69.294°N 16.012°E). More than 1,200 sounding rockets of all known configurations have been launched from this launch site [3]. Recently, the ARR is proposed as the launch site for orbital (ground) launch vehicles. The Norwegian/Finnish Nammo Raufoss company and the Norwegian Defense Research Establishment (FFI) have started a study into the feasibility of ground launching microsatellites (1-10 kg) from the ARR using hybrid rocket engines from the currently under development North Star family of sounding rockets [22].

In September 2013 the Netherlands and Norway signed the Technical Arrangement on “Military Use of Space” [74]. The NLR as well as the FFI are involved in this arrangement. A small work package of this arrangement is allocated to a feasibility study to develop an orbital launch vehicle for microsatellites. Also air launch is considered as one of the options and for an initial feasibility study this tool can be used. Identical launch conditions and constraints are used as for the ALOSS case. The target orbit will be a 500 km circular polar orbit.

11.3.1 Maximize Payload Mass

For this application the objective of the optimizer is changed to maximize the payload mass, all other settings remain the same. The optimized vehicle can delivered a payload of 12.5 kg to a 500 km polar orbit for identical release conditions as ALOSS. The constraint for the vehicle's length is limiting the maximum payload mass. Also a ground launched vehicle is optimized for a 12.5 kg payload mass to a 500 km circular polar orbit.

The most important characteristics for the optimized air and ground launched vehicle are given in Table 11.8. The vehicles are heavier than for the launch from the equator in eastward direction because they do not have the rotational velocity of the Earth and because they have to put a larger payload in orbit.

The performance advantages of air launch to ground launch show good correspondence with the numbers in Section 11.1.2. Air launch can provide a reduction in cost per flight of 26.9% and in GTOW of 66.7%. The velocity losses are also comparable with those of a launch from the equator. The ΔV that is provided by the optimized air launched vehicle is higher for the launch from the equator ($180 \text{ m}\cdot\text{s}^{-1}$) while the ground launched vehicle shows a reduction in ΔV compared to a launch from the equator ($110 \text{ m}\cdot\text{s}^{-1}$). The reason for this is most likely that this vehicle follows a more optimal trajectory than the launch from the equator. The details for these optimized vehicles as well as figures that show their trajectories can be found in Appendix J.

Parameter	Unit	Air launched vehicle	Ground launched vehicle
Cost per flight	€M	1.999	2.730
GTOW	kg	1,107	3,325
Vehicle length	m	5.471	8.620
Vehicle diameter	m	0.6222	0.6711
Gravity loss	$\text{m}\cdot\text{s}^{-1}$	1,186	1,417
Drag loss	$\text{m}\cdot\text{s}^{-1}$	183.0	588.2
ΔV	$\text{m}\cdot\text{s}^{-1}$	8,813	9,748

Table 11.8: Summary of the most important characteristics for the optimized air and ground launched vehicle with a payload mass of 12.5 kg from a launch from ARR to a 500 km polar orbit.

11.3.2 Use of Existing Solid Rocket Motors

In this section it is also investigated which orbital altitude with which payload can be achieved from ARR for a polar orbit with commercial of-the-shelf (COTS) SRMs under the ALOSS constraints. Again identical launch conditions as for ALOSS are used. Based on Section 11.1.4 a three stage air launched vehicle would be the most advantageous in terms of cost and GTOW.

Unfortunately, no suitable existing SRM for the first stage complies with the diameter constraint of 0.673 m for the rocket. In addition the constraint for the maximum acceleration of $100 \text{ m}\cdot\text{s}^{-2}$ was impossible to maintain, however, it is tried to respect the constraints as much possible. For instance, the use of a STAR 17 motor for the third stage leads to accelerations above $350 \text{ m}\cdot\text{s}^{-2}$ and therefore, this motor was omitted. The mass and geometry of the additional components are calculated using the relations described in

Chapter 6. The selected SRMs results in a maximum acceleration for stage 2 of $121.3 \text{ m}\cdot\text{s}^{-2}$ and $109.6 \text{ m}\cdot\text{s}^{-2}$ for stage 3.

The highest orbit that could be achieved was a 250 km circular polar orbit for a payload mass of 10 kg. The vehicle characteristics for the vehicle that consists of the STAR 30E, STAR 27H and STAR 15G motors are given in Table 11.9. For the characteristics of the motors themselves is referred to Appendix D or J. If these motors had to be developed for this application the cost per flight amounts to €2.131 million. This price is higher than for the vehicle that is optimized for maximum payload to a 500 km orbit. It has to be noted that none of these three engines have TVC.

The thrust curves for the STAR 30E and the STAR 27H motor allow the assumption of constant thrust, however, for the STAR 15G motor regressive thrust and mass flow has to be modeled [4]. The STAR 30E is an apogee kick motor and is designed for (almost) vacuum conditions, therefore, it has a low exit pressure (0.0659 bar). Given the pressure at 15 km altitude of 0.120 bar this results in a pressure ratio $\frac{p_e}{p_a}$ of 0.549 which is still above the minimum acceptable pressure ratio (0.40), hence, no flow separation will occur.

Parameter	Unit	Air launched vehicle from COTS SRMs
Cost per flight	€M	2.131
GTOW	kg	1,197
Vehicle length	m	5.221
Vehicle diameter	m	0.763
Gravity loss	$\text{m}\cdot\text{s}^{-1}$	848.3
Drag loss	$\text{m}\cdot\text{s}^{-1}$	269.3
ΔV	$\text{m}\cdot\text{s}^{-1}$	8,654

Table 11.9: Vehicle characteristics for a launch vehicle consisting of COTS SRMs.

Sensitivity Analysis

After the three validation steps the sensitivity to changing variables will be examined with a sensitivity analysis. What will be the influence for varying parameters on the cost per flight, GTOW and payload mass? These parameters can either be design variables or the outputs from the models for the different disciplines. Two types of sensitivity analyses are proposed to be executed sequentially: the one-at-a-time approach and a Monte-Carlo analysis. These two types of sensitivity analyses were also used for the validation in the work of Castellini [15].

In the first two sections only the one-at-a-time approach and the Monte-Carlo analysis are discussed. In these sections mainly the influence of vehicle design parameters and cost parameters are discussed. This is followed by a study to the effects of a regressive burning grain. Next the effect of the implementation of a constraint with respect to the regression rate is addressed. In the final section of this chapter the effect of the use of different heuristic algorithms is studied.

12.1 One-at-a-time Approach

The one-at-a-time (OAT) approach is a common used and simple method where only one parameter is changed at a time and all the others kept constant. This process is repeated for all parameters. The parameter is changed by a percentage equal plus and minus the absolute mean error, E (worst-case scenario) [15]. The general goal of the one-at-a-time analysis is to identify to which parameters the design is the most sensitive. Due to its simplicity the one-at-a-time approach does not take into account the simultaneous variation of parameters. This means that the one-at-a-time approach can not detect the presence of interactions between different parameters.

This section is divided in a section about the 10 and the 2,000 kg payload class. These subsections again are broken down into different subsections. The vehicle design parameters, cost parameters, atmospheric parameters and the use of the different materials are separately discussed.

12.1.1 10 kg Payload Class

For the 10 kg payload class the vehicle design parameters, atmospheric parameters, the sensitivity to different materials and cost parameters are sequentially discussed in this section.

12.1.1.1 Vehicle Design Parameters

The optimized vehicle that is launched under similar conditions as ALOSS (see Section 11.1.1 for details) is taken as the baseline design and will be subjected to the OAT approach. All parameters will remain the same except for the trajectory parameters. These parameters are allowed to vary with $\pm 1^\circ$ from their nominal values in order to achieve the target orbit within the tolerances. In addition a small deviation (± 10 seconds) in the coasting time is allowed. The objective function for the tool is changed to maximize the payload mass for the given variations to the nominal values of the parameters. A population of 20 individuals is evolved over 300 generations using the same settings for the differential evaluation algorithm as in Chapter 11. During the OAT approach the launch vehicle is allowed to violate the constraints for the vehicle length and the maximum acceleration because the effects on the cost per flight, GTOW and payload mass are investigated.

Parameter	Variations		GTOW		Payload mass		
	[-]	[%]	[kg]	[%]	[kg]	[%]	$\delta_{pay}/\delta_{par}$
Vacuum thrust stage 1	1.83 kN	+6.46	+4.365	+0.469	+2.227	+22.3	+1.22 kg/kN
Vacuum thrust stage 2	0.326 kN	+6.46	+1.633	+0.175	+1.176	+11.8	+3.61 kg/kN
Vacuum thrust stage 3	0.145 kN	+6.46	+1.565	+0.168	+1.488	+14.9	+10.3 kg/kN
Isp stage 1	10.9 s	+3.68	+2.699	+0.290	+1.532	+15.3	+0.141 kg/s
Isp stage 2	11.1 s	+3.68	+1.273	+0.137	+1.008	+10.0	+0.091 kg/s
Isp stage 3	11.3 s	+3.68	+0.973	+0.105	+0.924	+9.25	+0.082 kg/s
Sliver fraction stage 1	13.3 kg	+40.0	+12.95	+1.39	-0.952	-9.53	-0.071 kg/kg
Sliver fraction stage 2	2.17 kg	+40.0	+1.628	+0.175	-0.608	-6.08	-0.280 kg/kg
Sliver fraction stage 3	0.643 kg	+40.0	+0.745	+0.080	-0.721	-7.22	-1.12 kg/kg
Fill fraction stage 1	0.045 [-]	+5.0	-2.184	-0.235	+0.440	+4.40	0.879 %/%
Fill fraction stage 2	0.045 [-]	+5.0	-0.216	-0.023	+0.300	+3.00	0.600 %/%
Fill fraction stage 3	0.045 [-]	+5.0	-0.275	-0.030	+0.155	+1.55	0.311 %/%
Inert mass stage 1	8.06 kg	+12.4	+7.506	+0.807	-0.952	-9.52	-0.118 kg/kg
Inert mass stage 2	1.26 kg	+12.4	+0.941	+0.101	-0.373	-3.74	-0.296 kg/kg
Inert mass stage 3	0.49 kg	+12.4	+0.136	+0.016	-0.505	-5.05	-1.02 kg/kg
Length stage 1	0.26 m	+11.7	+4.900	+0.527	-0.528	-5.28	-2.02 kg/m
Length stage 2	0.11 m	+11.7	+1.028	+0.110	-0.245	-2.45	-2.31 kg/m
Length stage 3	0.075 m	+11.7	+0.136	+0.015	-0.365	-3.65	-4.86 kg/m
Fairing mass	2.90 kg	+14.5	+3.021	+0.325	-0.345	-3.49	-0.108 kg/kg
VEB mass	2.67 kg	+30.9	+0.011	+0.001	-2.669	-26.7	-0.998 kg/kg
Drag coefficient	-	+40.0	-0.634	-0.068	-0.602	-6.02	-0.150 %/%
Lift coefficient	-	+40.0	-0.348	-0.037	+0.322	+3.22	+0.081 %/%

Table 12.1: Results of the OAT approach for the best air launched vehicle for $+E$.

The effects of the varying parameters on the GTOW and payload mass are shown in Table 12.1 (results for $+E$) and 12.2 (results for $-E$). Two types of sensitivities will be discussed in this section: the effect of the introduction of the error E and the sensitivity ($\delta_{pay}/\delta_{par}$) of the payload mass to the variations of the specific parameter. The effect of the introduction of the error E on the cost per flight, GTOW and payload mass is a measure for the severity of the errors in the model.

Suppose two different models for two different parameters: one model has an absolute mean error of 40% and other one only of 5%. On first glance one would try to update and refine the model that has an E of 40%. Suppose now that the nominal values for the parameters are varied with E . It could very well be that for the parameter that has an E of 40% the payload mass only changes with 10% while for the parameter that has an E of 5% the payload mass changes with 20%. Now the first priority will be updating and refining the model that has an E of 5%.

Parameter	Variations		GTOW		Payload mass		
	[-]	[%]	[kg]	[%]	[kg]	[%]	$\delta_{pay}/\delta_{par}$
Vacuum thrust stage 1	1.83 kN	-6.46	-7.137	-0.766	-4.835	-48.3	-2.64 kg/kN
Vacuum thrust stage 2	0.326 kN	-6.46	-2.439	-0.261	-1.931	-19.3	-5.92 kg/kN
Vacuum thrust stage 3	0.145 kN	-6.46	-1.390	-0.149	-1.320	-13.2	-9.11 kg/kN
Isp stage 1	10.9 s	-3.68	-2.340	-0.251	-1.185	-11.9	-0.109 kg/s
Isp stage 2	11.1 s	-3.68	-0.957	-0.103	-0.706	-7.06	-0.0638 kg/s
Isp stage 3	11.3 s	-3.68	-0.655	-0.070	-0.622	-6.22	-0.055 kg/s
Sliver fraction stage 1	13.3 kg	-40.0	-12.64	-1.36	+1.248	+12.5	+0.093 kg/kg
Sliver fraction stage 2	2.17 kg	-40.0	-1.327	-0.143	+0.895	+8.95	+0.412 kg/kg
Sliver fraction stage 3	0.643 kg	-40.0	+0.091	+0.001	+0.823	+8.23	+1.28 kg/kg
Fill fraction stage 1	0.045 [-]	-5.0	+2.345	0.252	-0.175	-1.75	-0.349 %/%
Fill fraction stage 2	0.045 [-]	-5.0	+0.449	0.048	-0.032	-0.32	-0.063 %/%
Fill fraction stage 3	0.045 [-]	-5.0	+0.079	0.009	0.00	0.00	0.00 %/%
Inert mass stage 1	8.06 kg	-12.4	-7.256	-0.780	+1.202	+12.0	+0.149 kg/kg
Inert mass stage 2	1.26 kg	-12.4	-0.667	-0.072	+0.635	+6.35	+0.502 kg/kg
Inert mass stage 3	0.49 kg	-12.4	-0.052	-0.006	+0.540	+5.40	+1.10 kg/kg
Length stage 1	0.26 m	-11.7	-2.853	-0.307	+0.625	+6.25	+2.40 kg/m
Length stage 2	0.11 m	-11.7	-2.356	-0.253	+0.398	+3.98	+3.76 kg/m
Length stage 3	0.075 m	-11.7	-1.404	-0.151	+0.686	+6.85	+9.12 kg/m
Fairing mass	2.90 kg	-14.5	-2.684	-0.288	+0.472	+4.72	+0.146 kg/kg
VEB mass	2.67 kg	-30.9	+0.031	+0.003	+2.657	+26.6	+0.994 kg/kg
Drag coefficient	-	-40.0	+0.846	+0.092	+0.795	+7.94	+0.199 %/%
Lift coefficient	-	-40.0	-0.253	-0.027	-0.239	-2.39	-0.0598 %/%

Table 12.2: Results of the OAT approach for the best air launched vehicle for $-E$.

It should be noted that the effects of introducing E depend of the type of vehicle. For instance, a variation in mass for the VEB of 2.0 kg has a larger effect on a payload of 10.0 kg than a variation of 15.0 kg on a payload of 2,000 kg. For a payload of 10.0 kg changes in the payload mass below 1.0 kg (10.0%) are deemed small.

The results of the OAT for the effects on the cost per flight are so small that these results

are omitted from Table 12.1 and 12.2. Except for the variation of the cost per flight with E that has an effect of ± 0.361 €M on the cost per flight there are no parameters that have a larger influence on the cost per flight than 0.0057 €M (0.30%). A variation in the cost per flight does not have an influence on the GTOW and payload mass, therefore, this parameter is not presented in the tables.

The introduction of E for the propulsion parameters results in a change in payload mass of more than 10% (except for the Isp of stage 2 and 3). By far the largest effect on the payload mass (-48.3%) occurs for a deviation from the nominal value of the vacuum thrust of the first stage with $-E$. The error introduced for the sliver and fill fraction has less influence on the payload mass than the propulsion characteristics. Also the errors for the inert mass models have a smaller effect on the payload mass than the errors for the propulsion parameters. The absolute mean error in the length does not have a large influence on the payload mass as well (maximum +6.85% for $-E$ for stage 3). The same holds for the fairing mass (+4.72% for $-E$) and the aerodynamic coefficients (+7.94% for $-E$ for the drag coefficient). The effect of the absolute error in the VEB mass has an effect of 26.5% on the payload mass.

Based on the effects that the absolute mean error, E , has on the payload mass it can be concluded that the models for the propulsion characteristics and for the VEB mass are the first ones that require a refinement.

The sensitivity for the vacuum thrust is the largest for the third stage with a ratio of 1.0 to 10.0 for $+E$ (an increase of the thrust with 1.0 kN results in an increase in payload mass with 10 kg). For $-E$ a higher sensitivity to the vacuum thrust for the first and second stage is observed than for $+E$. This can be explained by the fact that a change in vacuum thrust also influences the nozzle mass (see Figure 6.10). Therefore, the deviation of the GTOW is also larger than the difference in payload mass. For the sensitivity to the vacuum Isp holds that the payload mass is the most sensitive to variations for the stage with the lowest Isp and in this case this is the first stage.

A change in the sliver fraction introduces a change in the total propellant mass. As expected the sensitivity of the payload mass for changes in the sliver fraction is the highest for the third stage because an increase of 1.0 kg in inert mass (and that is sliver at the end) reduces the payload mass with 1 kg. However, the values in Table 12.1 and 12.2 are slightly different. The reason for this is that the propellant mass determines the size of the motor case, therefore, increasing the sliver fraction also increases the mass of the motor case. Therefore, the effect on the payload mass by changing the propellant mass with 1.0 kg is larger than 1.0 kg for the third stage. The sensitivity of the payload mass to variations for inert mass shows the same behavior as for the sliver fraction. The third stage is the most sensitive to a change in inert mass. Moreover, the influence that the inert mass has on the VEB's mass is also introducing a sensitivity larger than 1.0 to 1.0 for the third stage.

The influence of the stage's length on the GTOW and the payload mass is introduced in the relation used to determine the motor case's mass as well as the interstage mass (the interstage length depends on the nozzle length of the next stage). A shorter stage leads to a lower inert mass of the stage thus higher payload. The higher sensitivity to a variation in length for the third stage is again a result of its higher sensitivity to mass. The sensitivity of the payload mass to changes in the fairing mass are very limited (6.8-9.2 to 1), this is because the fairing is jettisoned at an early stage. The sensitivity of the

payload mass to a change in the mass of the VEB is approximately 1.0 to 1.0 since the VEB is located in the upper stage and will not be jettisoned.

Based on literature the drag and lift coefficient have an absolute mean error of 40%. However, the sensitivity of the GTOW and payload mass to these parameters is limited: drag coefficient 5.0-6.7 to 1.0 and lift coefficient 12-16 to 1.0. A positive deviation of the lift coefficient increases the payload mass for this case because this vehicle follows a trajectory with a positive angle of attack during the largest part of the atmospheric flight, however, there are also trajectories where an increase in lift coefficient leads to a lower payload mass.

From Table 12.1 and 12.2 it can be concluded that the payload mass is the most sensitive to changes in the upper stage's mass, sliver fraction, VEB's mass and propulsion characteristics. The payload mass shows limited sensitivity to the length of the stages, the fairing mass and the aerodynamic coefficients.

12.1.1.2 Atmospheric Parameters

Also the sensitivity of the payload mass to changes in the atmospheric parameters (pressure, density and temperature) is investigated. For a variation of these parameters with 10% the payload mass only changes with more than 0.01 kg (0.1%) for the density. A 10% change in density leads to a variation in payload mass of ± 0.11 kg (1.1%).

12.1.1.3 Sensitivity to Different Materials

In this final part of the OAT approach also the sensitivity of the payload mass and GTOW to different materials for the motor case is examined. Again the sensitivity of the cost per flight is so small (maximum deviation less than 0.05%) that it is omitted from Table 12.3. In the nominal case a composite motor case with a $\frac{\rho}{\sigma}$ of $2.0 \text{ kg}\cdot\text{m}^{-3}\cdot\text{MPa}^{-1}$ is used. Here two additional materials for motor cases are considered: an aluminum motor case and a titanium motor case.

From the numbers in Table 12.3 it follows that changing the material for the motor case has a large effect on the payload mass and also on the inert mass of the vehicle. Also the influence of changing the interstage from an aluminum structure to a composite structure is investigated. A composite structure would lead to a reduction in GTOW of 0.78 kg, however, the increase in payload mass would be negligible.

Parameter	$\frac{\rho}{\sigma}$	GTOW		Payload mass	
		[kg]	[%]	[kg]	[%]
	$[\text{kg}\cdot\text{m}^{-3}\cdot\text{MPa}^{-1}]$				
Aluminum	5.4 [15]	27.94	3.00	-6.624	-66.2
Titanium	3.7 [98]	11.42	1.23	-2.673	-26.7

Table 12.3: Results for OAT approach for different materials for the motor case.

12.1.1.4 Cost Parameters

Earlier the sensitivity of the cost per flight to changes in the vehicle design is calculated and now the sensitivity of the cost model itself will be addressed. This is again done

with first an OAT approach and later with a Monte Carlo analysis. As baseline the best individual for the ALOSS case and the optimized ground launched vehicle are taken. The ground launched vehicle is taken in account for this analysis to investigate potential differences in the sensitivity to varying cost parameters between air and ground launch. Details about these vehicles can be found in Chapter 11 and Appendix J.

In this OAT the sensitivity of the cost per flight to variations in twelve cost correction factors or cost parameters that are introduced in Chapter 9 is investigated.

Variations of some cost correction factors and parameters have a linear effect on the change in cost per flight. The parameters that have a linear effect on the change in cost per flight and the corresponding changes in cost per flight when a 10% deviation for these parameters is applied are given in Table 12.4. From this table it can be concluded that the sensitivity of the cost per flight to changes in these cost correction factors are smaller than the deviations of the parameters themselves. The most sensitivity cost correction factor is the system engineering factor for production, f_0 , for which a change of 10% results in a change in cost per flight of 6.66% or 6.51%. It should be noted that the sensitivity of the cost per flight to cost correction factors applied for the operations cost is larger for ground launched vehicles because the cost correction factor for air launch, f_{10} , is not applied to ground launched vehicles. The sensitivities to the cost per flight for the other parameters are more or less identical for ground and air launch.

Parameter	Nomenclature	Air launch		Ground launch	
		Change in cost per flight		Change in cost per flight	
		FY2012 €M	%	FY2012 €M	%
f_0	SE development factor	0.0396	2.10	0.0460	1.75
f_1	Development standard factor	0.0396	2.10	0.0460	1.75
$DC_{aircraft}$	Aircraft development cost	0.00450	0.238	-	-
f_0	SE production factor	0.1258	6.66	0.1711	6.51
f_v	Launch vehicle type	0.0138	0.730	0.0456	1.74
f_c	Processing type	0.0138	0.730	0.0456	1.74
Q_i	Complexity Stage	0.0021	0.111	0.0042	0.160
f_{10}	Correction factor air launch	0.0138	0.730	-	-
$CO_{aircraft}$	Cost carrier aircraft	0.00540	0.286	-	-

Table 12.4: Results sensitivity analysis of the OAT approach for the 10 kg payload class with a 10% deviation for the linear varying parameters in the cost model.

There are also three cost parameters for which variations for the value of the parameter does not result in a linear change in the cost per flight. The first one is the annual launch rate for which the deviations from the baseline of six launches per year are given in Table 12.5. It has to be noted that the total number of launches remains constant at 120 and, therefore, the annual launch rate only has effect on the flight and ground operations cost. From the numbers in Table 12.5 it becomes clear that the deviation in the launch rate is larger than the change in cost per flight. The change in cost per flight is higher for ground launched vehicles because the annual launch rate influences the operations cost and the operations cost for ground launch are not reduced by the cost reduction factor for air launch, f_{10} .

Annual launch rate		Air launch		Ground launch	
#	Deviation	Change in cost per flight		Change in cost per flight	
	[%]	[FY2012 €M]	[%]	[FY2012 €M]	[%]
2	-66.67	0.191	10.1	0.689	26.2
4	-33.33	0.0516	2.73	0.184	6.98
6	0.00	0.000	0.00	0	0.00
8	+33.33	-0.0276	-1.46	-0.0969	-3.69
10	+66.67	-0.0451	-2.39	-0.157	-5.99

Table 12.5: Results sensitivity analysis for a change in the annual launch rate for the 10 kg payload class.

After the annual launch rate the sensitivity of the cost per flight to variations in the total number of launches is examined. This sensitivity is shown for ground and air launch in Table 12.6. The total number of launches influences the development cost amortized per launch and the cost reduction for series production factor, f_4 . From Table 12.6 it becomes clear that the sensitivity of the cost per flight (in percentage) to a change in number of total launches is larger for air launch than for ground launch. This can be explained by the fact that also the modification and certification cost of the carrier aircraft have to be amortized for an air launched vehicle. For a total number of launches of 20 (also 40 in case of air launch) the relative change in cost per flight is higher than the relative change in the total number of launches.

Total number of launches		Air launch		Ground launch	
#	Deviation	Change in cost per flight		Change in cost per flight	
	[%]	[FY2012 €M]	[%]	[FY2012 €M]	[%]
20	-83.33	3.08	163.0	3.49	133
40	-66.67	1.37	72.7	1.59	60.5
60	-50.00	0.736	38.9	0.861	32.8
80	-33.33	0.386	20.4	0.456	17.3
100	-16.67	0.160	8.49	0.190	7.24
120	0.00	0.00	0.00	0.00	0.00
140	+16.67	-0.121	-6.42	-0.145	-5.52
160	+33.33	-0.217	-11.5	-0.260	-9.91

Table 12.6: Results sensitivity analysis for a change in the total number of launches for the 10 kg payload class.

In order to get a better insight into the influence of the total number of launches on the cost per flight a graph for the cost per flight versus the total number of launches is given in Figure 12.1.

The last cost parameter that will be evaluated is the learning factor, p . The learning factor together with the total number of units produced (number of launches) determines the cost reduction for series production factor, f_4 . The changes in cost per flight for varying values of the learning factor are shown in Table 12.7.

First of all, it can be concluded from Table 12.7 that the cost per flight is extremely sensitive to a change in learning factor, in the case that the learning factor is changed

from the baseline value of 0.80 to 0.95 (increase of 18.75%) the cost per flight changes with 2.48 €M (94.3%). In addition it can be observed that the sensitivity of the cost per flight is almost identical for air launch and ground launch.

Learning factor		Air launch		Ground launch	
[-]	Deviation	Change in cost per flight		Change in cost per flight	
	[%]	[FY2012 €M]	[%]	[FY2012 €M]	[%]
0.75	-6.25	-0.341	-18.0	-0.541	-20.6
0.80	0	0.00	0.0	0.000	0.0
0.85	+6.25	0.453	24.0	0.616	23.5
0.90	+12.5	1.048	55.5	1.43	54.3
0.95	+18.75	1.822	96.4	2.48	94.3

Table 12.7: Results sensitivity analysis for a change in the learning factor, p .

For the relation between the cost per flight and the learning factor a visual representation is given in Figure 12.1.

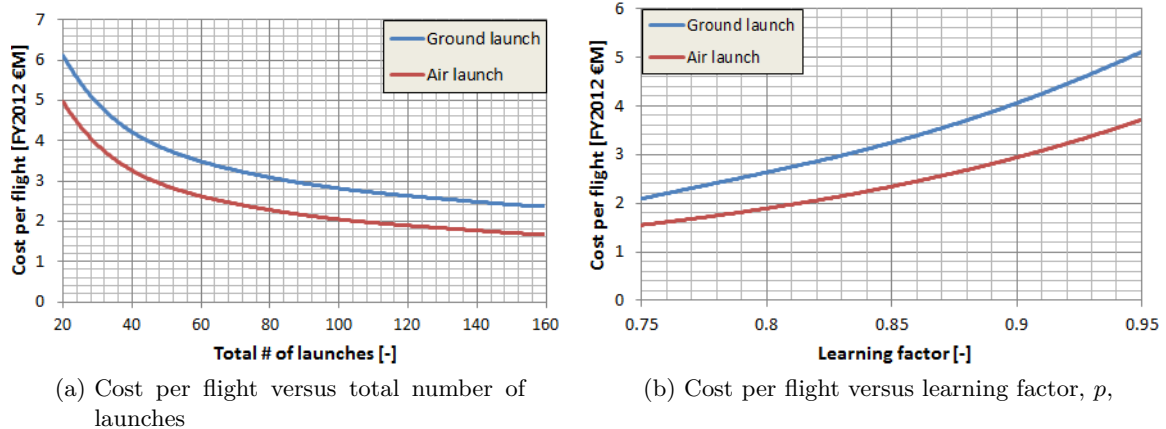


Figure 12.1: Cost per flight versus the total number of launches and learning factor, p , for the optimized air launched and optimized ground launched vehicle for the 10 kg payload class.

12.1.2 2,000 kg Payload Class

After the discussion of the 10 kg payload class the 2,000 payload class will be discussed. For the sake of brevity the OAT approach for the 2,000 kg payload class will be limited to the vehicle design parameters and cost parameters.

12.1.2.1 Vehicle Design Parameters

The optimized winged vehicle that is launched under a flight path angle of 15° (see Section 11.2.3 and Appendix J for details) is used for this OAT approach. The effects of the varying parameters on the GTOW and payload mass can be found in Table 12.8

(results for $+E$) and 12.9 (results for $-E$). In order to avoid repetition only the general trends and deviations from the 10 kg payload class are discussed. Again the sensitivity of the per flight (± 3.917 M€ per flight) is not presented in Table 12.8 and 12.9 since it has no influence on the GTOW and payload mass.

Parameter	Variations		GTOW		Payload mass		
	[-]	[%]	[kg]	[%]	[kg]	[%]	$\delta_{pay}/\delta_{par}$
Vacuum thrust stage 1	140	+6.46	+421.6	+0.507	+222.9	+11.1	+2.15 kg / kN
Vacuum thrust stage 2	28.5	+6.46	+310.8	+0.374	+289.2	+14.5	+10.2 kg / kN
Vacuum thrust stage 3	2.95	+6.46	+93.20	+0.112	+85.95	+4.30	+29.1 kg / kN
Isp stage 1	10.6	+3.68	+231.6	+0.278	+127.2	+6.36	+12.0 kg/s
Isp stage 2	11.0	+3.68	+169.1	+0.203	+157.7	+7.88	+14.4 kg/s
Isp stage 3	11.2	+3.68	+47.70	+0.0574	+51.75	+2.59	+4.60 kg/s
Sliver fraction stage 1	1,147	+40.0	+1067	+1.28	-108.4	-5.42	-0.0945 kg/kg
Sliver fraction stage 2	331.0	+40.0	+157.9	+0.190	-172.1	-8.60	-0.521 kg/kg
Sliver fraction stage 3	29.5	+40.0	-1.700	-0.002	-31.56	-1.58	-1.07 kg/kg
Fill fraction stage 1	0.045	+5.0	-95.10	-0.114	+15.67	+0.78	+0.157 %/%
Fill fraction stage 2	0.045	+5.0	-13.30	-0.016	+19.74	+0.99	+0.197 %/%
Fill fraction stage 3	0.045	+5.0	+1.900	+0.002	+9.490	+0.47	+0.095 %/%
Inert mass stage 1	439	+12.4	+384.5	+0.462	-39.36	-1.97	-0.0897 kg/kg
Inert mass stage 2	110	+12.4	+54.30	+0.0653	-53.99	-2.70	-0.492 kg/kg
Inert mass stage 3	16.0	+12.4	-1.100	-0.001	-16.13	-0.81	-1.01 kg/kg
Length stage 1	1.50	+11.7	+12.30	+0.0148	-30.86	-1.54	-20.5 kg/m
Length stage 2	0.792	+11.7	+65.50	+0.0788	-33.62	-1.68	-42.4 kg/m
Length stage 3	0.277	+11.7	+27.60	+0.0332	-12.05	-0.60	-43.5 kg/m
Wing mass	61.7	+40.0	-1.600	-0.002	-1.250	-0.06	-0.020 kg/kg
Fairing mass	81.9	+14.5	+61.20	+0.0736	-20.57	-1.03	-0.251 kg/kg
VEB mass	40.5	+30.9	-2.00	-0.002	-40.03	-2.00	-0.988 kg/kg
Drag coefficient	-	+40.0	-34.40	-0.0414	-31.02	-1.55	-0.039 %/%
Lift coefficient	-	+40.0	+51.70	+0.0622	+55.48	+2.77	+0.06935 %/%

Table 12.8: Results of the OAT approach for the best air launched vehicle for the 2,000 kg payload class for $+E$.

The relative changes of the GTOW and especially the payload mass due to the introduction of E are smaller than for the 10 kg payload case. The only parameters for which an introduction of E results in a deviation of the payload class with more than 10% are the vacuum thrust for the first and second stage. For the optimized vehicle the contribution of the second stage to the delivered ΔV is the largest, therefore, variations of parameters for the second stage and especially the performance variables results in large deviation of the payload mass.

The sensitivity $\delta_{pay}/\delta_{par}$ of the propulsion parameters is larger than for the 10 kg payload class but the relative importance between the stages remains the same. For parameters involving inert mass (inert mass, sliver fraction, fill fraction) the sensitivity is almost identical to the 10 kg payload case. The sensitivity of the payload mass to a change in length is larger because the 2,000 payload class vehicle is wider. The payload mass is

more sensitive to variations in the fairing mass than for the 10 kg payload class because the fairing is jettisoned at a later moment.

The sensitivity for the drag and lift coefficient is different than for the 10 kg payload class. The introduction of a wing, varying the wing mass has an almost negligible effect, results in sensitivity to the lift coefficient. For which a sensitivity of approximately 10 to 1 can be found.

Parameter	Variations		GTOW		Payload mass		
	[-]	[%]	[kg]	[%]	[kg]	[%]	$\delta_{pay}/\delta_{par}$
Vacuum thrust stage 1	140	-6.46	-424.2	-0.510	-238.4	-11.9	-2.30 kg/kN
Vacuum thrust stage 2	28.5	-6.46	-282.7	-0.340	-263.0	-13.1	-9.24 kg/kN
Vacuum thrust stage 3	2.95	-6.46	-92.90	-0.112	-84.97	-4.25	-28.8 kg/kN
Isp stage 1	10.6	-3.68	-224.4	-0.270	-123.5	-6.18	-11.6 kg/s
Isp stage 2	11.0	-3.68	-160.5	-0.193	-149.1	-7.45	-13.6 kg/s
Isp stage 3	11.2	-3.68	-55.90	-0.0672	-51.23	-2.56	-4.56 kg/s
Sliver fraction stage 1	1,147	-40.0	-1079	-1.297	+97.26	+4.86	+0.085 kg/kg
Sliver fraction stage 2	331	-40.0	-238.7	-0.287	+180.3	+9.02	+0.546 kg/kg
Sliver fraction stage 3	29.5	-40.0	+1.500	+0.002	+32.02	+1.60	+1.09 kg/kg
Fill fraction stage 1	0.045	-5.0	+97.10	+0.117	-14.66	-0.733	-0.147 %/%
Fill fraction stage 2	0.045	-5.0	+13.50	+0.016	-18.50	-0.925	-0.185 %/%
Fill fraction stage 3	0.045	-5.0	+0.2000	+0.002	-7.070	-0.353	-0.071 %/%
Inert mass stage 1	439	-12.4	-383.5	-0.461	+41.14	+2.06	+0.093 kg/kg
Inert mass stage 2	110	-12.4	-48.80	-0.0587	+58.15	+2.91	+0.529 kg/kg
Inert mass stage 3	16.0	-12.4	+1.000	+0.001	+16.64	+0.832	+1.04 kg/kg
Length stage 1	1.50	-11.7	-160.1	-0.192	+27.21	+1.36	+18.1 kg/m
Length stage 2	0.792	-11.7	-62.00	-0.0745	+37.55	+1.88	+47.4 kg/m
Length stage 3	0.277	-11.7	-18.80	-0.0226	+17.10	+0.855	+61.7 kg/m
Wing mass	61.7	-40.0	+4.60	+0.006	+4.650	+0.233	+0.075 kg/kg
Fairing mass	81.9	-14.5	-60.90	-0.0732	+21.450	+1.07	+0.262 kg/kg
VEB mass	40.5	-30.9	+2.10	+0.003	+39.74	+1.99	+0.981 kg/kg
Drag coefficient	-	-40.0	+31.00	+0.037	+29.67	+1.48	+0.0371 %/%
Lift coefficient	-	-40.0	-82.60	-0.099	-78.04	-3.90	-0.0976 %/%

Table 12.9: Results of the OAT approach for the best air launched vehicle for the 2,000 kg payload class for $-E$.

Based on Table 12.8 and 12.9 the errors in the models for the propulsion parameters have the largest influence on payload mass. The payload is the most sensitive to changes in the upper stage's mass, sliver fraction, VEB's mass and propulsion characteristics. This is correspondence with the outcomes of the sensitivity analysis of the 10 kg payload class.

12.1.2.2 Cost Parameters

For the 2,000 kg payload the sensitivity for the twelve cost parameters will be investigated for the best wingless air launched vehicle, the best winged air launched vehicle and the best ground launched vehicle.

Parameter	Nomenclature	Air launch wingless		Air launch winged		Ground launch	
		Δ in cost per flight		Δ in cost per flight		Δ in cost per flight	
		€M	%	€M	%	€M	%
f_0	SE development factor	0.2350	1.18	0.252	1.21	0.3279	1.23
f_1	Development factor	0.2350	1.18	0.252	1.21	0.3279	1.23
$DC_{aircraft}$	Aircraft development cost	0.1623	0.817	0.162	0.78	-	-
f_0	SE production factor	1.292	6.50	1.267	6.09	1.6813	6.31
f_v	Launch vehicle type	0.1674	0.843	0.268	1.29	0.6246	2.34
f_c	Processing type	0.1674	0.843	0.268	1.29	0.6246	2.34
Q_i	Complexity Stage	0.0021	0.0106	0.009	0.05	0.0059	0.0221
f_{10}	Correction factor air launch	0.1674	0.843	0.268	1.29	-	-
$CO_{aircraft}$	Cost carrier aircraft	0.09890	0.498	0.099	0.48	-	-

Table 12.10: Results sensitivity analysis of the OAT approach for the 2,000 kg payload class with a 10% deviation for the linear varying parameters in the cost model.

The cost parameters that have a linear effect on the cost per flight for the 2,000 kg payload class are given in Table 12.10. In general the same observations as for the 10 kg payload class hold. For instance, the sensitivity of the cost per flight to changes in these cost correction factors are smaller than the deviations of the parameters themselves and the sensitivity of the cost per flight is the largest for a variation in the SE development factor for production, f_0 . The differences for the winged and wingless air launched vehicles are the largest for the operations cost since the increased complexity for winged vehicles is taken in account in the launch vehicle type, f_v , and the complexity of the first stage, Q_1 . The influence of the carrier aircraft cost for development and operations is larger than for the 10 kg payload class since for that class the carrier aircraft will not be purchased.

Annual launch rate		Air launch wingless		Air launch winged		Ground launch	
#	Deviation	Change in cost per flight		Change in cost per flight		Change in cost per flight	
	[%]	[FY2012 €M]	[%]	[FY2012 €M]	[%]	[FY2012 €M]	[%]
2	-66.67	4.749	23.9	6.378	30.7	10.43	39.1
4	-33.33	1.220	6.14	1.6473	7.92	2.726	10.2
6	0.00	0.00	0.00	0.00	0.00	0.00	0.00
8	+33.33	-0.6237	-3.14	-0.8467	-4.07	-1.415	-5.31
10	+66.67	-1.004	-5.05	-1.3652	-6.57	-2.287	-8.58

Table 12.11: Results sensitivity analysis for a change in the annual launch rate for the 2,000 kg payload class.

In Table 12.11 the sensitivity of the cost per flight for different annual launch rates are given. The annual launch rate only has an influence on the ground and flight operations cost. The ground launched and winged air launched vehicle have a higher sensitivity to changes in the launch rate because the value for the launch vehicle type, f_v , that is a correction factor for the operations cost is higher than for the wingless air launched vehicle.

Total number of launches		Air launch wingless		Air launch winged		Ground launch	
#	Deviation	Δ in cost per flight		Δ in cost per flight		Δ in cost per flight	
	[%]	[FY2012 €M]	[%]	[FY2012 €M]	[%]	[FY2012 €M]	[%]
20	-83.33	25.20	127	25.98	125.0	22.86	85.8
40	-66.67	10.82	54.5	11.12	53.5	10.11	37.9
60	-50.00	5.661	28.5	5.806	27.9	5.380	20.2
80	-33.33	2.945	14.8	3.015	14.5	2.838	10.6
100	-16.67	1.201	6.04	1.228	5.91	1.165	4.37
120	0.00	0	0.00	0	0.00	0.000	0.00
140	+16.67	-0.9098	-4.58	-0.9285	-4.47	-0.9001	-3.38
160	+33.33	-1.621	-8.16	-1.653	-7.95	-1.612	-6.05

Table 12.12: Results sensitivity analysis for a change in the annual launch rate for the 2,000 kg payload class.

As can be seen in Table 12.12 the sensitivity of the cost per flight to a different number of total launches is large. This is in correspondence with the 10 kg payload class. An interesting phenomena for the 2,000 kg payload class is observed that when the total number of launches are reduced the cost advantage of air launch reduces. This is can be explained because the carrier aircraft development cost are 30-35% of the total development cost while for the 10 kg payload class these are only 10%. This is a result of the purchase of the aircraft for the 2,000 kg payload class that is not required for the 10 kg payload class. In Figure 12.2 the cost per flight versus the total number of launches is plotted.

Learning factor		Air launch wingless		Air launch winged		Ground launch	
#	Deviation	Change in cost per flight		Change in cost per flight		Change in cost per flight	
	[%]	[FY2012 €M]	[%]	[FY2012 €M]	[%]	[FY2012 €M]	[%]
0.80	-11.1	-5.866	-29.5	-5.753	-27.7	-7.634	-28.6
0.85	-5.56	-3.333	-16.8	-3.268	-15.7	-4.337	-16.3
0.90	0.00	0.00	0.0	0.000	0.0	0.000	0.0
0.95	+5.56	4.337	21.8	4.253	+20.5	5.644	21.2
0.99	+10.0	8.674	43.7	8.507	+40.9	11.29	42.3

Table 12.13: Results sensitivity analysis for a change in the learning factor, p , for the 2,000 kg payload class.

As for the 10 kg payload class the sensitivity of the cost per flight is the largest for the learning factor, p . The sensitivities can be found in Table 12.13. However, the relative sensitivity is smaller than for the 10 kg payload class. A visual representation of cost per flight versus the learning factor can be in Figure 12.13.

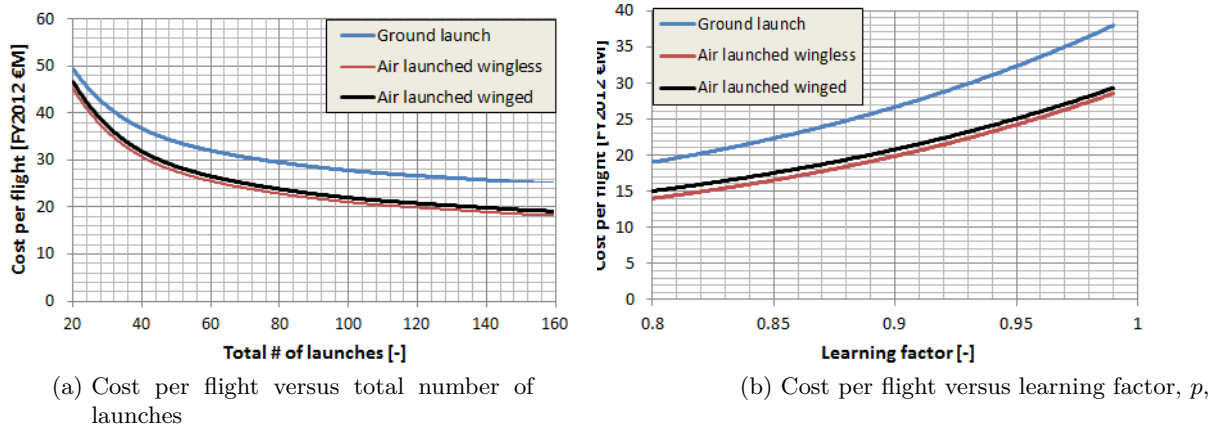


Figure 12.2: Cost per flight versus the total number of launches and learning factor, p , for the optimized wingless and winged air launched and optimized ground launched vehicle for the 2,000 kg payload class.

12.2 Monte-Carlo Analysis

The approach for the Monte-Carlo analysis is slightly different than for the OAT approach. In a Monte-Carlo analysis all the parameters are randomly varied at the same time. A Gaussian distribution with a mean error, μ , and standard deviation of the error, σ , is used to vary the parameters. This approach will lead to realistic variations of the nominal case because the uncertainties of the individual models are combined. A Monte-Carlo analysis allows full exploration of the parameters and accounts for interactions and nonlinear responses.

Also this section about the Monte-Carlo analysis is broken down in a part about the 10 kg payload class and the 2,000 kg payload class.

12.2.1 10 kg Payload Class

Below the Monte-Carlo analysis for the vehicle design parameters and the cost design parameters will be discussed for the 10 kg payload class.

12.2.1.1 Vehicle Design Parameters

The method used for the Monte-Carlo Analysis is identical to the OAT approach, only in this case all variables are varied simultaneously. The allowed deviations from the original values of the pitch parameters are relaxed to $\pm 5^\circ$. All parameters in Table 12.2 and the cost per flight will be taken in account in this analysis.

Normally a large number Monte-Carlo runs have to be executed in order to provide an accurate estimation for the bias and the 1σ ranges. However, it takes several minutes to

run each case, so, due to time restrictions only 150 runs are made. Out of the 150 runs for five combinations of parameters the final orbit was not achieved and for these case the payload mass was set to zero. The mean and the standard deviation of the Monte-Carlo distribution for 150 runs is given Table 12.14. A scatter plot of the values for the cost per flight, GTOW and payload mass including the 1σ and 2σ ranges are given in Figure 12.3.

Parameter	Cost per flight		GTOW		Payload mass	
	[FY2012 €M]	[%]	[kg]	[%]	[kg]	[%]
	1.889		930.6		10.00	
μ	2.249	+19.0	938.1	+0.803	10.88	+8.80
σ	0.1752	9.27	10.94	1.18	3.476	34.8
$\mu-\sigma$	2.074	+9.77	927.1	-0.372	7.404	-26.0
$\mu+\sigma$	2.425	+28.3	949.0	+1.98	14.36	+43.6

Table 12.14: Results for Monte-Carlo analysis for 150 runs for the design parameters.

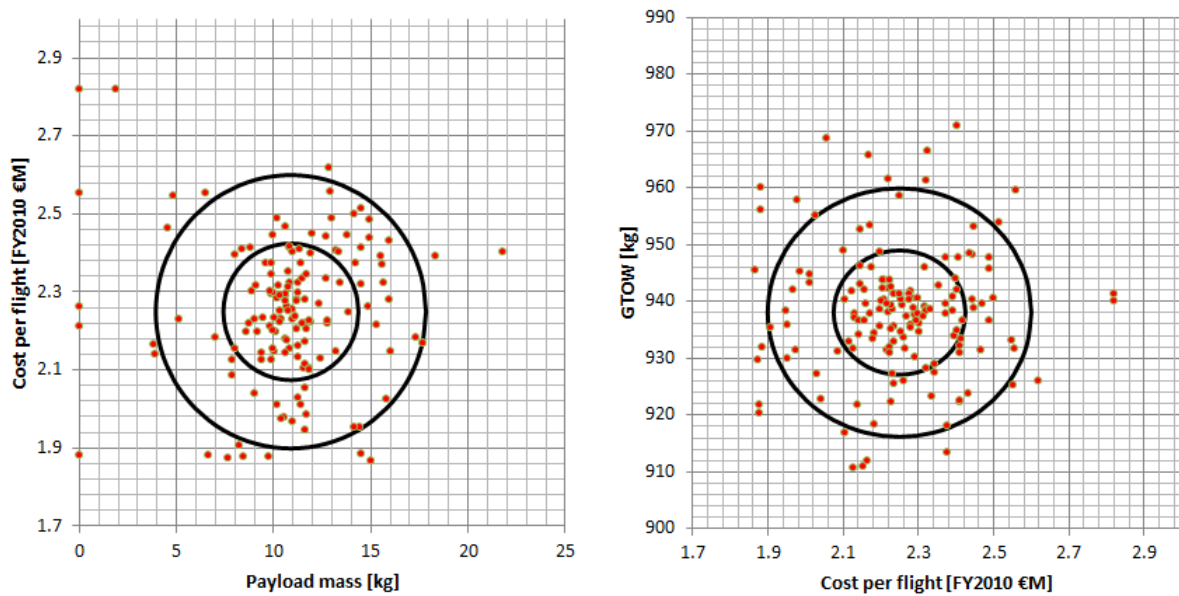


Figure 12.3: Scatter plot for the outcomes of the Monte-Carlo analysis for 150 runs for the cost per flight, payload mass and GTOW for the 10 kg payload class.

From Table 12.14 it can be concluded that the average payload mass is overestimated with 8.80% and that there is a large standard deviation. In Section 12.1 it is already concluded that there are several parameters that have a large influence on the payload mass even for variations within the errors that are present in the models. The small negative mean error for the vacuum thrust (-0.41%) is negated by the larger positive mean error for the vacuum Isp (+3.68%). Therefore, on average the propulsion characteristics are overestimated. Add to this the negative mean error for the total inert mass (-2.76%) which results in a higher performance thus higher payload mass. The large variation in the payload mass between the different runs can be explained by the large standard deviation

of the error in the VEB mass model (40.9%). Earlier it was concluded that variations of the VEB mass have a large influence on the payload mass for a payload mass of 10 kg.

The Monte-Carlo distribution shows a small overestimation of the GTOW (0.88%). The cost per flight are overestimated with 19.0% which shows an almost one to one relation with the positive mean error of 19.1% of the cost model. This can be explained because the propellant mass is only varied for uncertainties in the sliver fraction.

12.2.1.2 Cost Parameters

After the OAT analysis a Monte-Carlo analysis is performed to the varying cost parameters. Again the optimized air launched for ALOSS launch conditions and the optimized ground launched vehicle are considered as the baseline. The cost parameters are assumed to be normally distributed. All values for the cost parameters will be randomly varied simultaneously with standard deviations as a percentage of the nominal value (5%, 10%, 20%).

Parameter	Air launch		Ground launch	
	[FY2012 €M]	[%]	[FY2012 €M]	[%]
$\sigma=5\%$ for all parameters				
μ	1.890	+0.0106	2.628	+0.0076
σ	0.029	1.55	0.0325	1.24
$\mu-\sigma$	1.860	-1.53	2.596	-1.23
$\mu+\sigma$	1.919	+1.56	2.661	+1.24
$\sigma=10\%$ for all parameters				
μ	1.890	+0.0109	2.628	0.000
σ	0.058	3.08	0.0653	2.48
$\mu-\sigma$	1.831	-3.06	2.563	-2.48
$\mu+\sigma$	1.948	+3.09	2.693	+2.48
$\sigma=20\%$ for all parameters				
μ	1.890	0.0318	2.628	-0.0076
σ	0.118	6.22	0.132	5.01
$\mu-\sigma$	1.772	-6.19	2.496	-5.02
$\mu+\sigma$	2.007	+6.25	2.759	+5.00

Table 12.15: Results for Monte-Carlo analysis for the cost parameters that are different for air and ground launch for varying deviations for the mean.

Once again it has to be noted that this is a comparative study, therefore, only the cost parameters that differ from air and ground launch are taken in account. These parameters are all parameters evaluated in Section 12.1.1.4 minus the annual launch rate, the total number of launches, the learning factor, the complexity of the stages and the SE factor for production. Hence, the total number of launches and the learning factor remain constant during this analysis. A Monte-Carlo analysis for 100,000 random combinations is executed and the results can be found in Table 12.15.

From Table 12.15 it can be concluded that the σ of the cost per flight is smaller than the standard deviations that are applied to all parameters. Therefore, it can be concluded

that the uncertainties in the cost parameters that are different between air and ground launch do not have a large influence on the comparison in cost per flight between air and ground launch.

12.2.2 2,000 kg Payload Class

In this section the results of the Monte-Carlo analysis for the 2,000 kg payload mass will be discussed. First the Monte-Carlo analysis for the vehicle design parameters is addressed and this is followed by a discussion about the Monte-Carlo analysis for varying cost parameters.

12.2.2.1 Vehicle Design Parameters

The results of a Monte-Carlo analysis of 150 runs under identical conditions as in Section 12.2.1.1 are shown in Table 12.16.

Parameter	Cost per flight		GTOW		Payload mass	
	[FY2012 €M]	[%]	[kg]	[%]	[kg]	[%]
	20.79		83,173		2,000	
μ	24.22	+21.9	83,805	+0.760	2,097	+4.83
σ	1.926	9.69	669.5	0.805	187.6	9.38
$\mu-\sigma$	22.30	+12.2	83,136	-0.0446	1,909	-4.54
$\mu+\sigma$	26.15	+31.6	84,475	+1.57	2,284	+14.2

Table 12.16: Results for Monte-Carlo analysis for 150 runs for the design parameters for the 2,000 kg payload class.

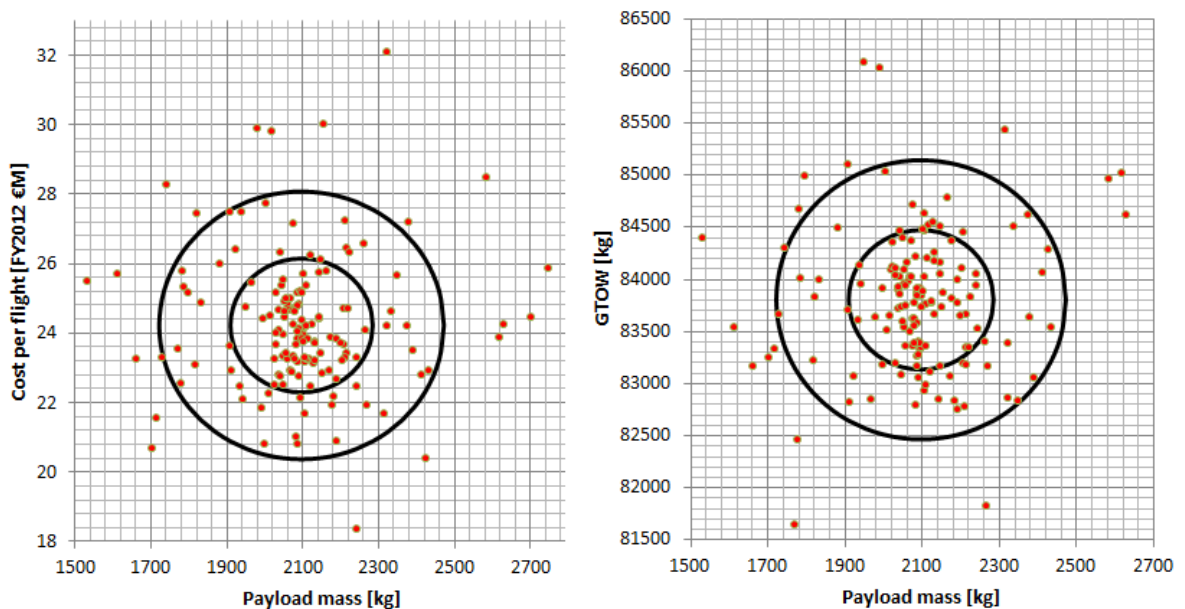


Figure 12.4: Scatter plot for the outcomes of the Monte-Carlo analysis for 150 runs for the cost per flight, payload mass and GTOW for the 2,000 kg payload class.

From this table it can be concluded that the payload mass is higher than the nominal case, however, the payload mass is less overestimated as for the 10 kg payload class and the standard deviation is also smaller. The deviation in the cost per flight is larger than the average error in the cost model, 19.1%.

The scatter plots for the Monte-Carlo analysis can be found in Figure 12.4. The observations above are in correspondence with the results of Section 12.2.1.1.

12.2.2.2 Cost Parameters

The cost parameters that differ between the three cases hence the ones that are evaluated during this Monte-Carlo analysis are all parameters evaluated in Section 12.1.1.4 minus the annual launch rate, the total number of launches, the learning factor and the SE factor for production. An identical approach as in Section 12.2.1.2 is followed. All values for the cost parameters will be randomly varied simultaneously with standard deviations as a percentage of the nominal value (5%, 10%, 20%). The results can be found in Table 12.17.

From Table 12.15 and in correspondence with the results of 10 kg payload class it can be concluded that the σ of the cost per flight is smaller than the standard deviations that are applied to all parameters. For the ground launched vehicle the σ is the largest. This is because more operations cost parameters are varied than for the 10 kg payload class and because the operations cost are the largest for the ground launched vehicle.

Parameter	Air launch wingless		Air launched winged		Ground launched	
	[FY2012 €M]	[%]	[FY2012 €M]	[%]	[FY2012 €M]	[%]
$\sigma=5\%$ for all parameters						
μ	19.87	+0.00151	20.79	+0.00866	26.66	+0.0116
σ	0.2407	1.21	0.3068	1.48	0.4993	1.87
$\mu-\sigma$	19.63	-1.21	20.49	-1.47	26.16	-1.86
$\mu+\sigma$	20.11	+1.21	21.10	+1.48	27.16	+1.88
$\sigma=10\%$ for all parameters						
μ	19.87	-0.00554	20.79	-0.00433	26.66	-0.00488
σ	0.4809	2.42	0.6179	2.97	0.9980	3.74
$\mu-\sigma$	19.38	-2.43	20.17	-2.98	25.65	-3.75
$\mu+\sigma$	20.35	+2.42	21.41	+2.97	27.65	+3.74
$\sigma=20\%$ for all parameters						
μ	19.86	-0.0101	20.79	-0.0101	26.654	-0.0124
σ	0.9742	4.90	1.2470	6.00	2.009	7.53
$\mu-\sigma$	18.89	-4.91	19.54	-6.01	24.65	-7.55
$\mu+\sigma$	20.84	+4.89	22.04	+5.99	28.66	+7.52

Table 12.17: Results for Monte-Carlo analysis for the cost parameters that are different for wingless air launched, winged air launched and ground launched vehicles for the 2,000 kg payload class for varying deviations for the mean.

12.3 Effects of a Regressive Burning Grain

In the literature study it is concluded that in general SRMs do not have a constant vacuum thrust over time. However, in this study constant vacuum thrust is assumed for each motor. This introduces the assumption of a neutral burning grain, which is valid for most motors in the SRM database in Appendix D. For a neutral burning grain the burning surface area thus thrust remains constant over the motor's burn time. In this section the effects for a regressive burning grain on the launch vehicle's performance are investigated. Progressive burning grains are rare for launch vehicles because for these grains the thrust thus the acceleration is increased towards the end of the burn time, therefore, high accelerations are imposed on the payload. In order to reduce the accelerations on the payload a regressive burning grain will be evaluated.

In the tool an extra design variable for each stage will be introduced. These extra design variables can attain values between 0.4 and 1.0 and represent the fraction of the initial vacuum thrust at burn-out. Over the burn time the thrust will be linearly decreased to the final value for the vacuum thrust. In reality the mass flow varies with the burning surface and regression rate (thus chamber pressure), however, to avoid a grain analysis the mass flow will be assumed to decrease linearly with the thrust. This means a reduction of 5% thrust results in a 5% lower mass flow. Again the optimized vehicle that is launched under similar conditions as ALOSS will be taken as the baseline.

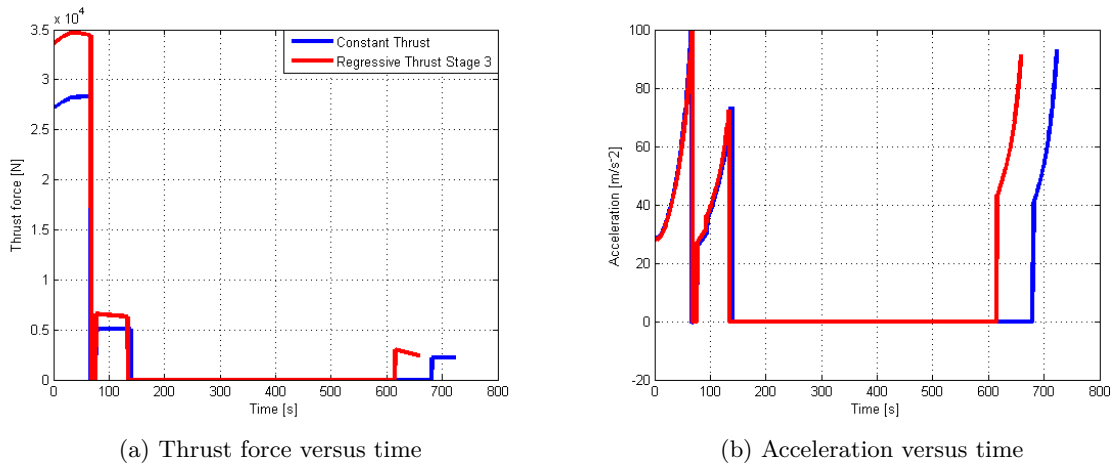


Figure 12.5: Thrust force and acceleration versus time for the optimized air launched vehicles with constant and regressive thrust.

Initially the fraction of the initial vacuum thrust at burn-out for all three stages was allowed to vary between 0.4 and 1.0. The best vehicle after the optimization for the same parameters as is done in Chapter 11 was very comparable with the final result of the ALOSS case (GTOW 972.1 kg). The three thrust variations parameters were respectively 0.995, 0.994, 0.982. Most likely this is caused by the fact that the nozzle mass is modeled as a function of the maximum vacuum thrust. Since the maximum thrust sizes the nozzle mass it is the most efficient to operate at this maximum thrust for the entire burn time. In addition due to geometry constraints the length of the nozzle can not always be increased, in order to achieve a higher initial thrust the chamber pressure has to be increased. This

also contributes to a higher inert mass of the stage.

In order to see the effect of a regressive burning grain on the GTOW and the cost per flight the search space for the thrust variation of the third stage is adapted to [0.2,0.8]. The third stage is selected because in general the upper stage is the most vulnerable to high accelerations and because the third stage is selected for regressive thrust for ALOSS as well. The optimized vehicle has a higher GTOW (1,170 kg) and cost per flight (2.034 €M) than the optimized vehicle with a constant thrust for the third stage. The fraction of the initial vacuum thrust at burn-out for the third stage is 0.7918. Details can be found in Appendix J. The thrust force and accelerations over time are shown in Figure 12.5. In these figures it is shown that a higher thrust for the first two stages is required to compensate for the higher GTOW.

Based on the above it can be concluded that for the models used in this tool a regressive burning grain does not enhance the performance of the launch vehicle in terms of GTOW and cost per flight.

12.4 Effect of the Implementation of a Constraint for the Web Thickness Case Diameter Ratio

During the literature study it was decided to not perform a complete analysis of the internal ballistics and the grain analysis because this was deemed to put too much emphasis on propulsion in this broad MDO study [103]. During this sensitivity analysis it will be checked if the approach for the performance model is valid.

The regression rate of the propellant, r , varies with the chamber pressure. An empirical expression that approximates the regression rate is given by De Viellie's law [120]:

$$r = a \cdot p_c^n \tag{12.1}$$

With n as the burning rate exponent and a as a rate coefficient that determines the unit for the regression rate, in this case $\text{mm}\cdot\text{s}^{-1}$. The input value for the chamber pressure, p_c , has to be in MPa. From Equation 12.1 follows that for a constant chamber pressure the regression rate is constant. For HTBP 1912 empirical values for a and n are not available. However, for TP-H-3340, which has a very similar chemical constitution as HTBP 1912 (see Appendix D), empirical values of 0.399 and 0.30 are found for respectively a and n [45]. It has to be noted that these relations are only valid for a pressure range between 2.75 and 5.00 MPa.

The most likely grain configuration for motors with a neutral burning grain (thus constant thrust) are star configurations and a rod and tube configuration [120]. An end-burner configuration also results in constant thrust, however, an end-burner configuration is considered unsuitable since the restrictive burning area results in a low mass flow thus thrust.

The propellant burns at any point perpendicular to the point at that surface as is shown in Figure 12.6, which shows the contour lines that representing the shape at different moments during the burn [120]. Therefore, it can be concluded that the burn time is determined by the thickness of the grain thus the diameter of the motor case. In the

propulsion model that is used for this study the diameter of the motor case and burn time are both design variables hence independent of each other.

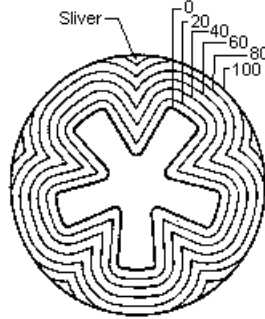


Figure 12.6: Evolution of burning area over time [120].

Another parameter that has to be defined is the web thickness, w :

$$w = \int_0^{t_b} r \cdot dt \quad (12.2)$$

From Equation 12.2 holds for a constant regression rate: $w = r \cdot t_b$. Since the propellant burns perpendicular to the surface the web thickness can never be larger than the radius of the motor case. In other words $2 \cdot w$ can never be larger than D_{case} . This limiting value is checked for all stages of the optimized vehicles of the 10 kg and 2,000 kg payload class. The disatisfactory outcome of this assessment was that the ratio $\frac{2 \cdot w}{D_{case}}$ varies between 1.0-2.1 for the optimized vehicles' stages for the 10 kg payload class. For the optimized vehicles' stages for the 2,000 kg payload class values between 0.40-1.25 for the ratio $\frac{2 \cdot w}{D_{case}}$ are found. For the third stage higher values for the ratio $\frac{2 \cdot w}{D_{case}}$ are found than for the first two stages. At this point it can be concluded that the motor configurations for the optimized vehicles presented in Chapter 11 for the 10 kg payload class are not completely realistic.

In order to see what the effect is of taking in account the regression rate the constraint that $\frac{2 \cdot w}{D_{case}} < 0.95$ is included and once again an air and ground launched vehicle for the 10 kg payload class are optimized. The air launched vehicle is released under ALOSS release conditions. The most important characteristics for the optimized vehicles including this constraint for $\frac{2 \cdot w}{D_{case}}$ are compared with the optimized vehicles without this constraint and the results are shown in Table 12.18. The detailed characteristics for the vehicles and some figures about the trajectory of the optimized vehicles can be found in Appendix J.

From Table 12.18 it can be observed that including the constraint for $\frac{2 \cdot w}{D_{case}}$ results in an increase in the cost per flight with 2.47% and the GTOW with 8.51% for the optimized air launched vehicle. The increase in cost per flight and GTOW for the optimized ground launched vehicle are respectively 2.34% and 9.00%.

Parameter	Unit	Air launched		Ground launch	
		Unconstrained	Constrained	Unconstrained	Constrained
Cost per flight	€M	1.890	1.937	2.628	2.691
GTOW	kg	930.6	1,017	3,087	3,393
Vehicle length	m	5.422	5.301	6.745	5.890
Vehicle diameter	m	0.5605	0.6696	0.9126	1.113
Gravity loss	m·s ⁻¹	1,673	1,496	2,215	2,086
Drag loss	m·s ⁻¹	176.4	233.4	558.5	790.7
ΔV	m·s ⁻¹	8,633	8,542	9,858	9,981

Table 12.18: Summary of the most important characteristics for the optimized vehicles with or without the $\frac{2 \cdot w}{D_{case}}$ constraint.

The implementation of the constraint for $\frac{2 \cdot w}{D_{case}}$ results in some differences in the vehicle design of the optimized vehicles, for instance, the diameters of the stages for the optimized launch vehicles increase (thus higher drag loss), the chamber pressures drop (thus lower regression rate), the burn times decrease (thus accelerations increases) and the length of the stage decrease which results in more flat designs than are found in the SRM Database in Appendix D.

Based on the statements above the results presented in Chapter 11 can still considered valid for comparative use. The validity of the results for the 10 kg payload class for absolute use is doubtful, however, a correction factor for the cost per flight and GTOW can be applied. For the 2,000 kg payload class the results are deemed to be valid for absolute use as well. For future work it is recommended to include a constraint for $\frac{2 \cdot w}{D_{case}}$.

12.5 Different Heuristic Optimization Algorithms

From Chapter 2 followed that according to the “no free lunch” theorem there is no optimization method that outperforms all others in the totality of the problems [119]. Therefore, the effect of the use of different heuristic algorithms on the fitness value will be investigated in this final section.

Besides the DE algorithm also a PSO and a simple GA from PaGMO are selected. The standard settings in PaGMO for these two algorithms will be used [83]. The algorithms have to optimize an air launched vehicle released under ALOSS conditions for a 2,000 kg payload mass. A initial population of 20 individuals will be evolved over 2,500 generations.

The average fitness value of the population and the best fitness value are given in Figure 12.7. From this figure it follows that the initial choice for DE was the right one since it outperforms the PSO (cost per flight 5.34% lower) and the GA (cost per flight 3.30% lower). For the GA early convergence is observed and this also results in a lower average fitness value of the population than for the DE. From Figure 12.7 becomes clear that the first individual that reaches the target orbit only is found after 1,120 generations while for the DE and GA this already occurs during the first 500 generations. It has to be noted that the DE performs also best with respect to the computational cost. Running the PSO or GA case took 3 to 4 times longer than the DE case.

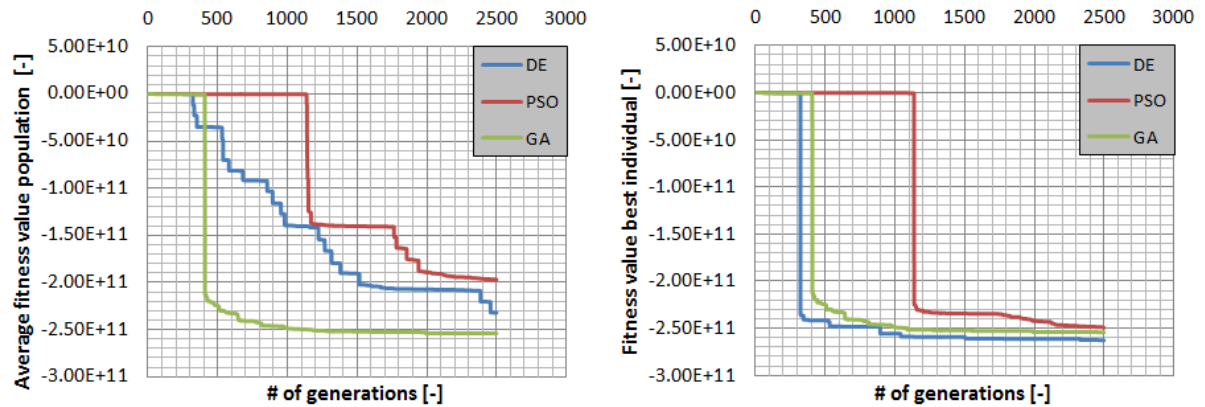


Figure 12.7: Evolution of the average and best fitness value for different heuristic algorithms over 2,500 generations.

Also the effect of different settings for the differential evolution algorithm will be investigated. Again the same case will be evaluated and the tabulated results for various sections for the weight and the crossover probability can be found in Table 12.19.

Crossover probability	0.70	0.80	0.90	0.99
Weight				
0.70	19.87	19.04	19.67	19.16
0.80	22.42	20.98	19.59	19.69
0.90	20.54	20.73	19.32	18.99
0.99	20.06	19.63	19.89	19.94

Table 12.19: Comparison of the cost per flight obtained for different weights and crossover probabilities of the DE.

From this table it can be concluded that the choice for different settings of the DE may lead to a lower cost per flight (-1.97%). It should be noted that the settings for which the weight is 0.99 have the tendency to converge quick and, therefore, result in a convergence at a local minimum and in long computation times.

Conclusions and Recommendations

During the entire era of space flight air launch is seen as a very promising concept. Despite its claimed advantages, air launch is up till now only a marginal success with the Pegasus launch vehicle from Orbital Sciences. Therefore, for this thesis research the following research question was investigated:

What is the performance gain in terms of cost, gross take-off weight and the amount of ΔV required to orbit for an optimized expendable air launched vehicle in comparison to an optimized expendable ground launched vehicle for different launch parameters (release altitude, velocity and flight path angle), payload classes and the presence of a wing?

In this final chapter the conclusions and recommendations of this thesis research are presented.

13.1 Conclusions

A Multidisciplinary Design Optimization (MDO) is deemed the most suitable approach for the comparison between air launch and ground launch. In earlier thesis work performed at the TU Delft an MDO tool in the Tudat framework is developed by Frank Engelen and Jan Vandamme. For the typical disciplines of launch vehicle design models are developed and validated.

The Multidisciplinary Design Analysis (MDA) and MDO validation tested the ability of the tool to model the design and the trajectory of launch vehicles. During the MDA validation it is shown that the tool is capable to do this for the design as well as for the trajectory. Also the errors between the models and the actual launch vehicles are in correspondence with the errors found for the individual disciplines. From the MDO validation it can be concluded that the optimized designs have realistic configurations and a lower cost than the designs for the MDA validation.

Launch vehicles in the 10 kg payload class are examined in conjunction with the NLR that conducted the Affordable Launch Opportunities for Small Satellites (ALOSS) study.

This study investigated if the use of an air launched platform for a dedicated launch for nano- and microsatellites (1-20 kg) can fulfill the market needs for a competitive price [106]. The ALOSS three stage launch vehicle has a GTOW of approximately 1.4 ton, a length of 5.50 meters and a diameter of 0.66 m and fits in the contours of the F-16 370 gallon external fuel tank. According to the model presented in Chapter 9 the cost per flight for ALOSS would be 2.18 €M based on a total of 120 launches. An F-16 is proposed as carrier aircraft and the vehicle is released at 15.0 km altitude with a velocity of approximately $250 \text{ m}\cdot\text{s}^{-1}$ under a flight path angle of 50° . The optimized air launched vehicle for a 10 kg payload subjected to the same constraints as ALOSS shows better performance than the original ALOSS vehicle in terms of the cost per flight (13.4%), the GTOW (32.6%) and the amount of ΔV required to orbit (2.66%). This difference mostly follows from the different models for vehicle design that are used.

Air launch can provide a reduction in the cost per flight in comparison with ground launch between 26.9 and 28.1% for ALOSS release conditions for vehicles in the 10 kg payload class. A launch at 10 km altitude, with a release velocity of $200 \text{ m}\cdot\text{s}^{-1}$ under a release flight path angle of 15° reduces the cost per flight with 25.5% for a wingless vehicle with a 2,000 kg payload. The optimized vehicle for the 2,000 kg payload class released for identical conditions as ALOSS results in a cost advantage of 31.3% compared to ground launch.

Air launching an optimized vehicle for a small payload mass reduces the GTOW between 63.5 and 70.1% compared to a conventional ground launch. An optimized vehicle for a payload of 2,000 kg payload can provide a reduction of 36.6% in GTOW for nominal release conditions. For ALOSS release conditions the GTOW reduction for air launch amounts to 47.8%.

The amount of ΔV required to orbit can be reduced by air launch with $935\text{-}1,225 \text{ m}\cdot\text{s}^{-1}$ (9.60-12.4%) for the 10 kg payload class. The ΔV advantage of air launch for the 2,000 kg payload class is between $302\text{ and }797 \text{ m}\cdot\text{s}^{-1}$ (3.24-8.55%). The smaller advantage for the 2,000 kg payload class compared to the 10 kg payload class for the GTOW and ΔV are a result of the reduced importance of drag loss for heavier vehicles. The values found for the ΔV advantages of air launch in this study are in correspondence with other claims in literature [93].

For a wingless launch vehicle horizontal launch is less advantageous than a launch under a positive release flight path angle. The difference in cost per flight is only 2.60% and for the GTOW 9.19% between the investigated positive release flight path angles for the 10 kg payload class. The flat optimum for the release flight path angle is also observed in [93]. Therefore, it can be concluded that the release flight path angle is not the most dominant launch parameter as long as it is positive. Decreasing the release altitude from 15.0 to 10.0 km increases the amount of ΔV ($270 \text{ m}\cdot\text{s}^{-1}$ or 3.04%) that has to be provided and results in a higher GTOW (+31.6%) and cost per flight (+9.13%). For the release conditions that are considered for this study small variations in the release velocity do not lead to an additional increase or reduction in velocity losses. Therefore, at 15 km altitude launching from supersonic release conditions will not provide an extra reduction in velocity losses. Similar trends are observed for the 2,000 kg payload class, however, the relative differences in the cost per flight, GTOW and the ΔV are smaller.

A three stage launch vehicle is deemed the most suitable for the 10 kg payload class. Since a two stage configuration is not able to reach the right target orbit within the given

constraints for the maximum acceleration and burn time. The optimizer was not able to construct a valid four stage launch vehicle within the ALOSS constraint for length. Even if the launch vehicle is allowed to be 6.50 meters a four stage configuration is more expensive than a three stage configuration (+17.7%) and has comparable values for the GTOW and the ΔV provided. The ALOSS constraint for the length is also for other cases the limiting constraint.

Winged vehicles provide a small cost advantage (2.45%) compared to wingless vehicles for horizontal launch as well as an advantage for the GTOW (19.9%) and the required amount of ΔV to orbit (4.60%). As soon as a winged launch vehicle will be released under a positive flight path angle the cost advantage and the ΔV advantage of the winged configuration will diminish quickly. Therefore, it can be concluded that for release under a positive flight path angle wingless vehicles are preferred. The bending loads of the optimized wingless vehicles are a factor 2 to 3 times larger than for the winged vehicles.

As an application of the tool the launch of a microsatellite from the Andøya Rocket Range is simulated. The vehicle that is optimized for payload mass can delivered a payload of 12.5 kg to a 500 km circular polar orbit within the ALOSS constraints. The differences between air and ground launch in cost per flight, GTOW and ΔV are comparable with a launch from the equator. The combination of the STAR 30E, STAR 27H and STAR 15G commercial of-the-shelf solid rocket motors can bring a payload of 10.0 kg to a 250 km circular polar orbit.

For the 10 kg payload class the introduction of the absolute error, E , for the different models causes the largest change in payload mass when E is introduced for the propulsion models and the mass model for the vehicle equipment bay (VEB). The payload mass is the most sensitive to changes in the inert mass and the sliver fraction of the upper stage, the propulsion characteristics and the mass of the VEB. The payload mass shows limited sensitivity to the length of the stages, the fairing mass, the aerodynamic coefficients and the atmospheric properties. The outcomes for the sensitivity analysis for the 2,000 kg payload class show identical trends, however, the relative changes in payload mass are lower than for the 10 kg payload class.

Changing the motor case material from a composite material to aluminum (-66.2%) or titanium (-26.7%) has a large effect on the payload mass for the 10 kg payload class. The cost per flight for air launch and ground launch for both payload classes is the most sensitive to variations in the total number of launches and the learning factor, p .

From the Monte-Carlo analysis follows an overprediction of the payload mass as well as the cost per flight for both payload classes. For the 10 kg payload class the large standard deviation ($\sigma=3.48\text{kg}$) for the payload mass for Monte-Carlo analysis can be explained by the large standard deviation of the error for the model of the VEB mass (40.9%).

It can be concluded that for the models used in this tool a regressive burning grain does not enhance the performance of the launch vehicle in terms of the cost per flight, the GTOW and the required amount of ΔV .

A constraint for the ratio between web thickness and case diameter is required in order to get realistic motor configurations. The introduction of this constraint results in an increase in the cost per flight between 2.34% and 2.47% and the GTOW between 8.51% and 9.00% for the optimized air and ground launched vehicle for the 10 kg payload case. For the 2,000 kg payload most unconstrained designs do not violate this constraint.

The choice for differential evolution as heuristic algorithm is deemed correct since it outperforms a particle swarm optimization algorithm (cost per flight 5.34% lower) and a genetic algorithm (cost per flight 3.30% lower). Slightly different settings for the differential evolution algorithm can improve the obtained solution even more (1.97%).

Based on this work it can not be explained why air launch up till now has only become a marginal success. This might be caused by other factors that were not investigated during this study, for instance, certification issues, politics or heritage.

13.2 Recommendations

In this section recommendations are given for the improvement of the different models that are used in this study. Also recommendations for additional features of the tool will be provided. Finally, also some recommendations for future research to air launch are given.

- From the sensitivity analysis followed that the models for the propulsion characteristics (vacuum thrust and Isp) and for the VEB mass are the first ones that have to be updated. Since the absolute error in these models results in the largest deviations for the payload mass.
- The cost per flight is the most sensitive to changes in the total number of launches and the learning factor. An extra effort can be done to evaluate, update and validate the values for these parameters.
- As indicated in Section 12.4 the implementation of a constraint for the ratio between the web thickness and case diameter is needed in order to obtain realistic motor configurations. Therefore, for future study this constraint has to be implemented in the tool.
- The assumption that there is no interstage required between the upper stage and the stage below since the upper stage is completely encapsulated by the fairing is not valid. For future work this interstage has to be included.
- The maximum vehicle's length is the sizing constraint for various cases, for example, for the four stage launch vehicle and the maximum payload mass from Andøya. Therefore, a more sophisticated geometry model for the launch vehicle is required.
- There is a difference between the inert mass and burn-out mass for a rocket stage because of ablative insulation layers. A short evaluation for ATK motors learns that the burn-out mass is typical between 3 and 10% lower than the total inert mass [4].
- Determining the bending moment requires a lot of information about the vehicle that is not available in the current tool. As a first indicator the so-called $q \cdot \alpha$ product is used. Large differences (a factor 3 to 4) in the maximum value of $q \cdot \alpha$ are observed for the optimized vehicles. For future work it is recommended to model the bending moment more accurately.
- There is no other publicly available software tool that is capable of predicting aerodynamic coefficients for launch vehicles with a higher accuracy than Missile Datcom

[103] and the sensitivity of the payload mass to variations in the aerodynamic coefficients is limited. Still it would be desirable to have a more accurate aerodynamic coefficient generator.

- At this moment the tool can only cope with stages that have only one motor and that are sequentially ignited. The implementation of multi-motor stages or booster stages might be interesting since some launch vehicles have such a configuration and especially in the case that also liquid rocket stages can be modeled (see below). Moreover, an axisymmetric rocket for which the stages are sequentially ignited is not always the best option in order to maximize the available volume and weight (attachment to multiple pylons) for launch vehicles that are launch from an HPA. Several studies propose the use of non-conventional configurations [59, 87]. It would be an useful addition to the tool if these configurations can be modeled and evaluated as well.
- Cost is highly correlated with risk. From the conclusions above it follows that air launch has cost advantages to ground launch, however, in this study the reliability of the launch vehicle is not examined. For future work it would be useful to evaluate the reliability of the launch vehicle, the carrier aircraft and the separation.
- The way that the solid rocket motor is currently modeled can also be applied to liquid and hybrid engines. The implementation of these types of engines requires additional thermodynamic data, other geometry and mass models and different cost models. The propulsion models and thermodynamic models for kerosine-liquid oxygen and liquid hydrogen-liquid oxygen are already available from the work of Vandamme [108]. However, these models require validation and have to be updated in order to be suitable for multistage launch vehicles. For his thesis research TU Delft colleague student Ruwan Ernst develops a design and optimization tool for liquid rocket engines [32]. Implementation of this tool is also considered for future work. The MDO architecture itself and the environmental and trajectory models do not require changes.
- Equipping the tool with a Graphical User Interface will enhance the usability of the tool.
- The tool can also be used for MDO for a launch from other celestial bodies (requires an update for the environmental models) or for suborbital space flight, for instance, space planes.
- From this study follows that air launch has cost and performance advantages and despite this air launch is only a marginal success. The certification of air launched vehicles is only briefly addressed in this work and [17] and [90] show that certification is an issue for air launched vehicles as well as for the modified carrier aircraft. For future study more emphasize on the certification aspect is desired.

Original Thesis Research Proposal

This Appendix contains the original thesis research proposal as was proposed at the end of the literature study [103]. The differences between the original research question and objective and those introduced in Chapter 1 are minimal.

A.1 Research Question and Objectives

The following research question is proposed:

What is the performance gain in terms of gross take-off weight and cost of an optimized air launched vehicle in comparison with an optimized conventional ground launched vehicle for different launch parameters (release altitude, velocity and flight path angle), payload classes and the presence of a wing?

The two payload classes that will be evaluated are 10 kg and 2,000 kg to low earth orbit (LEO). LEO is defined as a circular orbit at 200 km altitude.

The main objective of this thesis will be to find out if air launch can provide a cost advantage compared with ground launch by using current technology and existing carrier aircraft (that need limited modification). Additional research objectives will be:

- Investigate the reduction in GTOW of air launch.
- Investigate the ΔV advantages of air launch.
- Investigate the relative importance of the three different launch parameters (release altitude, velocity and flight path angle).
- Investigate the suitability of air launch for two different payload classes (10 kg and 2,000 kg).
- Investigate the effects of a wing on the design, trajectory, cost and GTOW of an air launched vehicles.

As can be read in the body of the literature report an MDO will be performed to make the comparison between ground and air launch. In order to achieve these objectives the combinations of different launch parameters given in Table 2.2 of the literature study will be evaluated. So, a total of 40 air launched cases and 2 ground launched cases will be evaluated for this study. Besides the development of the tool and fulfilling the main research objects it is planned to conduct a cost estimation of the SSTO liquid rockets from Vandamme's study (see section 10.4 of the literature study for more detail). In addition a meeting with people from the NLR that worked on the ALOSS project is scheduled [106]. In this meeting will be discussed if and how this thesis research can be useful for the NLR.

A.2 Preliminary Architecture Multidisciplinary Design Optimization

From the literature study follows that tool developed by Vandamme can not be used in its present form to answer the proposed research question [108]. A lot of modifications are required to make the tool suitable for answering the research question. An outline of the architecture of the MDO is given in Figure A.1. The environmental modules are the only modules that will remain in their current shape. For the trajectory model another control law is implemented and for the aerodynamic module new aerodynamic coefficients have to be implemented. All other modules will be created from scratch. In addition different design variables and constraints will be used for this study.

Below the different disciplines (from now on called modules) are discussed. For an overview of all design variables and constraints is referred to Table F.1 and F.3 of the literature study. The total number of design variables and constraints for various launch vehicle configurations is given in Table F.3 of the literature study.

A.2.1 Input

The input module deals with the input of the user. The following inputs are required:

- Payload mass
- Initial launch conditions (launch altitude, launch velocity and release flight path angle)
- Winged or wingless configuration
- Number of stages of the launch vehicle

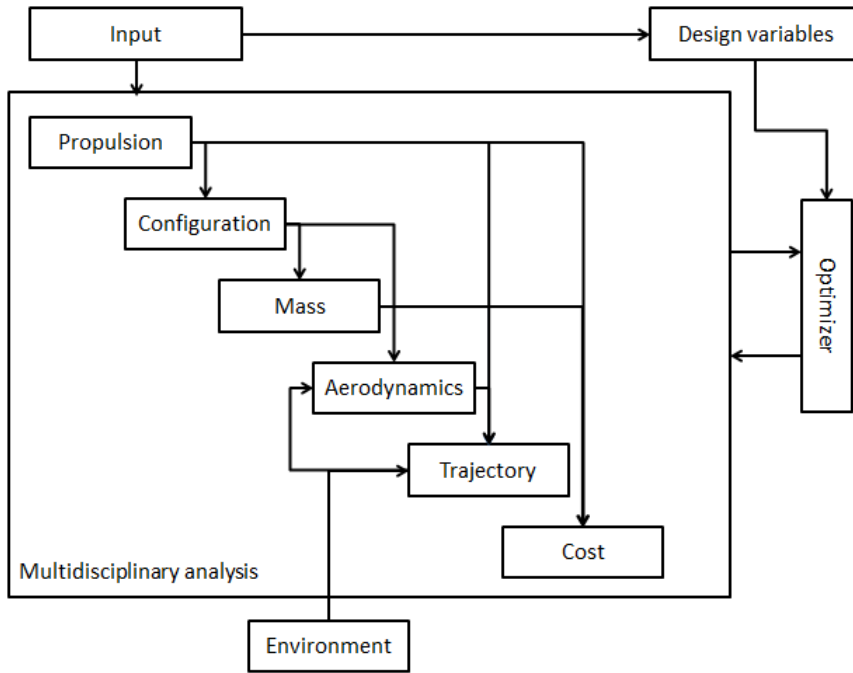


Figure A.1: Overview preliminary architecture MDO for the thesis research.

A.2.2 Optimizer

In Chapter 3 of the literature study it is concluded that it is too early to make a decision regarding which heuristic algorithm will be used for this study. This is because there is no optimization algorithm that outperforms all others in the totality of the problems [119]. A genetic algorithm (GE), differential evolution algorithm (DE) and particle swarm optimization algorithm (PSO) will be tested to select the best algorithm for this particular problem. It is proposed to use the Parallel Global Multiobjective Optimizer (PaGMO) that is developed by ESA. PaGMO is a C++ platform that contains a number of optimization algorithms.

A.2.3 Propulsion

The propulsion model is described in Section 6.3 of the literature study. Only one propellant, HTPB 1912, will be evaluated. The thermodynamic characteristics of the propellant will be calculated by CEA and will be implemented in tabulated form.

A.2.4 Configuration

The configuration module will calculate the dimensions of the motor casings, the nozzle lengths and the payload fairing. In the case that a wing is required it will create the wing.

A.2.5 Mass

In this module the weights of the stages, interstages and payload fairing are determined according to the mass model described in Section 7.3 of the literature study. A final decision on which models will be used for the individual mass components is made in the Development Phase (section A.4.2).

A.2.6 Aerodynamics

For the prediction of the aerodynamic coefficients the external software tool Missile DATCOM will be used. This tool will not be directly implemented in the MDO because the time to run Missile DATCOM will take some seconds for every call [15]. Therefore, the currently used approach in the tool of Vandamme will be used. In Missile DATCOM a database of aerodynamic coefficients for different launch vehicle is made and incorporated in the tool in tabulated form [108]. Linear interpolation between the data points will be used. From the previous work done in the faculty with Missile DATCOM a recommendation is made to include a dependency on the Reynolds number for the prediction of the aerodynamic coefficients [31, 108]. There will be investigated if this will be possible, however, this will not be a main goal.

A.2.7 Trajectory

The trajectory will be simulated by a 3 DoF trajectory earlier developed in the Tudat framework [31]. At this moment two methods for the trajectory control law are considered. The first method is the one used in the tool of Vandamme and estimates the pitch profile of the launch vehicle as a fourth-order polynomial [108]. In the alternative method the pitch profile of the launch vehicle is determined by selecting values for the pitch angle on three points for every stage. The pitch angle between these nodes is interpolated (linearly or by using a power law). A Runge-Kutta 4 integrator will be used for the integration of the trajectory, however, the step size is not determined yet. During the study different step sizes will be evaluated and the one that provides the highest accuracy for a reasonable computation time will be selected during the Testing Phase (section A.4.5).

A.2.8 Cost

In the cost module the cost for the development, production and operations for the launch vehicle will be calculated using the TransCost model. The model consists of a number of mathematical CERs that can easily be included in the tool. There should be noted that the cost for the acquisition, modification and operations of the carrier aircraft are not taken in account yet, however, NASA's Horizontal Launch Study provides some numbers for this [6].

A.2.9 Environment

The atmospheric and gravitational model used in Vandamme's tool will also be used for this study.

A.3 Assumptions and Limitations for this study

For this study the following assumptions are used:

- A safe separation between carrier aircraft and launch vehicle. Only the initial flight trajectory of the carrier aircraft will be taken in account as a constraint.
- The selected HPA aircraft can pass the transonic barrier with the launch vehicle external attached.
- It is assumed that total weight capacity of a HPA can be focused on one point.
- No launch vehicle configurations with boosters are examined. Most current solid propelled ground launched vehicles have only core stages.
- Only one engine per stage is evaluated. The effects of multiple engines per stage on the mass and geometry of the launch vehicle are difficult to model [15].
- There will be no possibility to include a small liquid propelled upper stage to improve the orbit injection accuracy.
- The control system can generate the required moments to change the attitude of the vehicle.
- A number of 120 launches over a period of 20 years is assumed [6, 15].
- The reliability of the launch vehicle will not be evaluated for this study.

A.4 Thesis Work Packages and Schedule

The thesis research should resemble the work of 42 ECTS (1,176 hours). This work load is equivalent to 30 full-time working weeks of 40 hours. The thesis research is planned to start in week 17 and to finish in week 50. A holiday break is planned from week 30 to 32. The work is scheduled for 28 weeks so, a 2 week margin is included. It is proposed to split the thesis research in nine different phases. The research phase for the different type of carrier aircraft will be executed sequentially. It should be noted that the first type of carrier aircraft, the HPA, is deemed the most important and the research for the other two types of carrier aircraft will only be done if time permits.

Beside the regular bi-weekly progress meetings three official reviews will be planned: the kick-off review, the mid term review and the green light review. Below the nine different phases are discussed and in figure A.2 a detailed schedule of the thesis research is given in the form of a Gantt chart.

A.4.1 Familiarization Phase (2.5 weeks)

In the initial phase of the thesis research the author will familiarize himself with the programming languages and software tools that will be used. The lectures of "IN4023 Programming in C++" course that are available on Collegerama will be used as an introduction the C++ programming language. The author will also familiarize himself with

Tudat and the PaGMO optimizers. Finally, familiarization with Missile DATCOM is also required. The author has already access to Missile DATCOM. At the end of this period also a kick-off review is planned. In this kick-off review the thesis proposal will be finalized.

A.4.2 Developing Phase (6 weeks)

The developing phase is the most longest phase of the thesis research. In this phase the new modules are developed and the existing models in Vandamme's tool will be updated. Also each model will separately be validated (see Chapter 11 of the literature study). The time allocated for developing or updating the individual models in Figure A.2 includes the validation. New modules have to be developed for propulsion, geometry, mass and cost. The environmental modules and trajectory module have to be evaluated and updated. The two proposed trajectory control laws are compared with the trajectories of existing launch vehicles. The aerodynamic module requires the generation of new aerodynamic coefficients by Missile DATCOM.

A.4.3 Tool Integration and Validation Phase (3.5 weeks)

In this phase the individual modules will be integrated to a single tool. After that the MDA and MDO validation against existing launch vehicles is performed sequentially. When required time is allocated to make a small updates in the individual modules.

A.4.4 Documentation Phase I (1 week)

In this first documentation phase the development of the tool will be documented. At the end of this period a mid-term review of the thesis research is scheduled. During this mid-term review there will be discussed if there are deviations from the agreed thesis proposal at the kick-off meeting and also some first results will be shared and discussed.

A.4.5 Research Phase I (5 weeks)

The research phase for the different type of carrier aircraft will be executed sequentially. In this phase a HPA is used as carrier aircraft. First the best step size for the numerical integrator and heuristic optimization algorithm are selected. The selection criteria for the step size numerical integrator are accuracy and computation time. For the optimization algorithm the selection criteria are the lowest objective value, computation time and robustness. Next the optimum number of stages for each of the configurations is selected. Now it is time to execute the simulations of the 14 cases for a HPA as described in Table 2.2 of the literature study and one simulation of a ground launched vehicle (payload mass 10 kg).

Next the sensitivity of the design to variations in the parameters is checked by a sensitivity analysis (see Chapter 11 of the literature study for more details). This will be done by a one-at-a-time approach and a Monte-Carlo analysis.

A.4.6 Documentation Phase II (1.5 weeks)

During this phase the comments from the mid-term review are incorporated and a draft thesis report will be developed that includes the results from Research Phase I.

A.4.7 Research Phase II (2.5 weeks)

In this second research phase the payload class of 2,000 kg will be evaluated for a large transport aircraft as carrier aircraft. In Research Phase I the heuristic optimization algorithm and best step size for the numerical integrator were already selected. For this second research phase only the optimum number of stages will be selected. Next the 14 cases as described in Table 2.2 of the literature study and one simulation of a ground launched vehicle (payload mass 2,000 kg) will be executed. Also a sensitivity analysis will be included. At the end of this phase a green light review will take place and an examination date will be planned.

A.4.8 Research Phase III (2.5 weeks)

For this final research phase first the optimum number of stages will be selected. This phase will investigate a winged air launched vehicle. The 12 cases as described in Table 2.2 of the literature study will be simulated and a sensitivity analysis will be conducted.

A.4.9 Documentation and Presentation Phase (3.5 weeks)

In this phase the thesis report is completed, the comments from the draft version are incorporated, the results of Research Phase II and III are included and the graduation is prepared. Most of the documentation is already done in the earlier phases of the study, however, still two weeks are required to finalize the report. In addition a draft conference paper, according to International Astronautical Federation (IAF) standards, will be written. Another 20 hours are required for a presentation of the final thesis and the preparations for graduation.

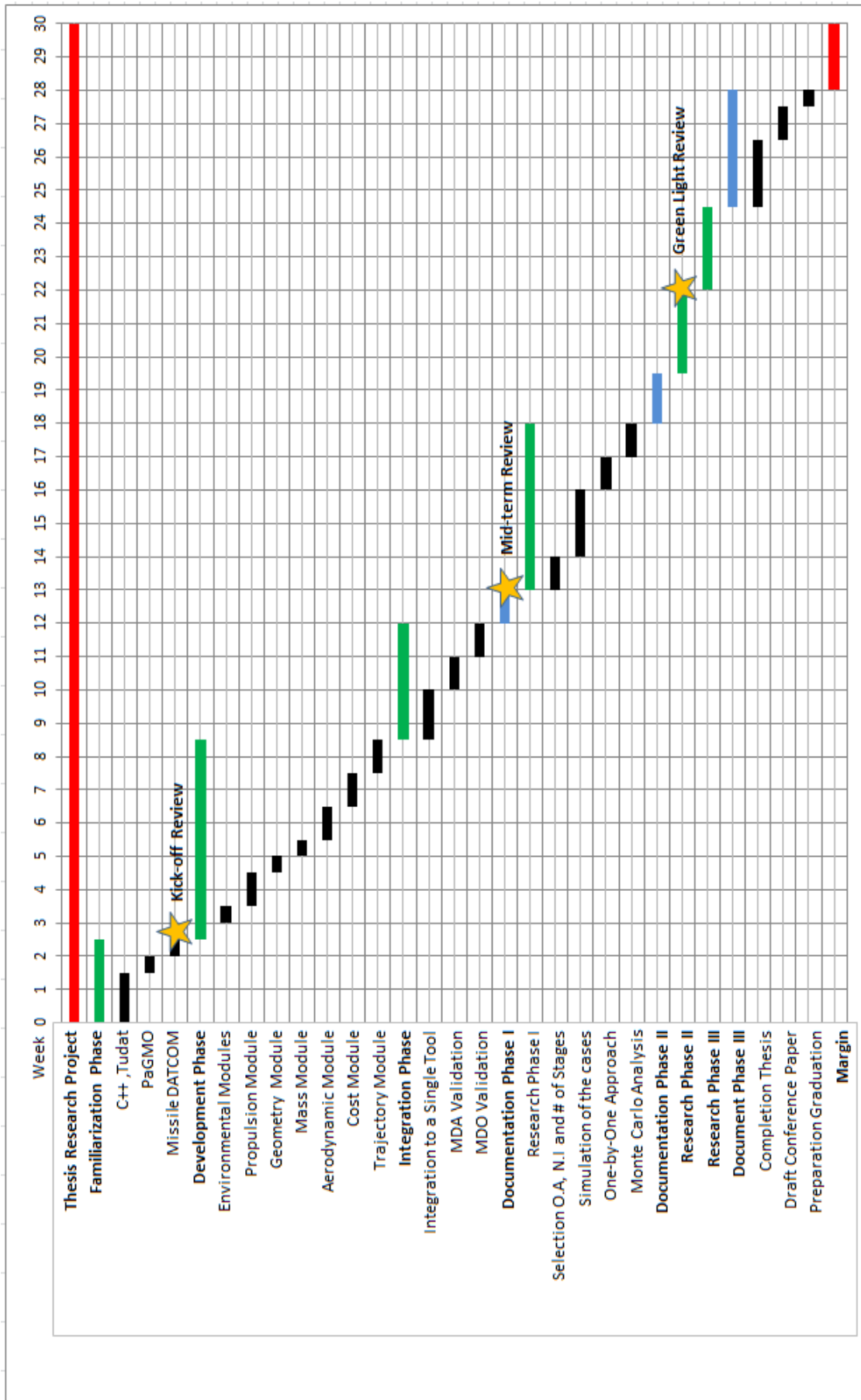


Figure A.2: Thesis schedule.

Appendix B

ALOSS Launch Vehicle Characteristics

In this Appendix the characteristics for the ALOSS launch vehicle are described. In addition, a MDA validation (only for the vehicle) for ALOSS is performed.

The NLR developed a preliminary design for a three stage launch vehicle that is launched from under pylon #4 or #6 of an F-16. The design has to fit within the contours of the F-16 370 gallon external fuel tank. Unfortunately, detailed characteristics of the size and weight of this tank are considered confidential by the Dutch MoD [105]. Therefore, an estimated length of 5.5 meters, a diameter of 0.66 meters and mass of 1,450 kg are used during this study. The launch vehicle is released at 15 km altitude with a release velocity of Mach 0.8 under a flight path angle of 50° . The characteristics of the three stages are given in Table B.1 and an impression of the vehicle can be found in Figure B.1.

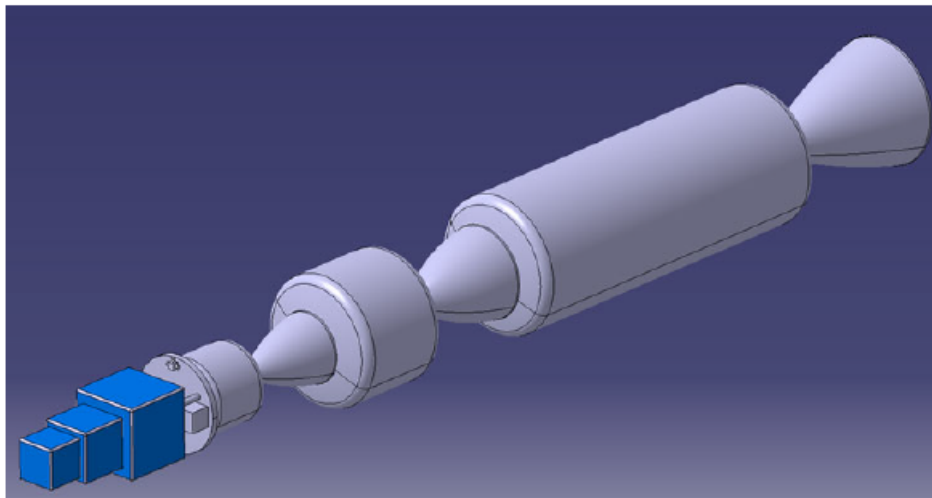


Figure B.1: Impression of the ALOSS launch vehicle [106]

Component	Stage 1	Stage 2	Stage 3
Chamber pressure [bar]	30.0	30.0	20.0
Exit pressure [bar]	0.120	0.05	0.05
Burn-time [s]	47.4	49.4	34.0
Case diameter [m]	0.660	0.630	0.380
Nozzle exit diameter [m]	0.606	0.440	0.340
Motor length [m]	2.59	1.13	0.84
Average thrust [kN]	48.3	14.1	8.6 ¹
Isp [s]	284.0	294.0	294.0
Mass propellant [kg]	862.8	244.8	60.7
Mass chamber [kg]	48.5	41.4	4.9
Mass nozzle [kg]	45.9	29.5	3.5
Mass insulation [kg]	5.8	12.2	1.4
Total inert mass [kg]	123.1	46.5	11.5
TVC [-]	Yes	Yes	Yes

Table B.1: Characteristics of the stages for ALOSS (all data from [106]).

Appendix C

Thermodynamic Properties of Solid Propellants

In this appendix the results from calculations with CEA [42, 64] for the thermodynamic properties of the HTPB 1912 propellant are published. HTPB is not standard included in the CEA database and therefore, the heat of combustion has to be defined by the user. The chemical formula for HTPB that is used is C 7.7075 H 10.65 O 0.223 N 0.063 and the heat of combustion for HTPB of $-58 \text{ kJ}\cdot\text{mol}^{-1}$ is used [15].

A combustion enthalpy and pressure problem was selected from CEA and an estimated value for the chamber temperature of 3,440 K was used. This estimate is based on the average chamber temperature of the SRMs described in [98]. An example input file is shown in Figure C.1.

```
problem
  hp  p,bar=30,31,32,33,34,35,  t,k=3440
react
  fuel=AL(cr) wt=19 t,k=298.15
  oxid=NH4ClO4(I) wt=69 t,k=298.15
  fuel=HTBP wt=12 t,k=298.15 h,kj/mol=-58 C 7.7075 H 10.65 O 0.223 N 0.063
end
```

Figure C.1: Input file CEA

For all chamber pressures between 30 bar and 100 bar the thermodynamic characteristics are calculated with an interval of 1 bar. The summary of the thermodynamic results of HTPB1912 for various chamber pressures is given in Table C.1. It should be noted that the results in Table C.1 show the thermodynamic equilibrium properties at the assigned pressures.

Chamber pressure	Temperature	Molar mass	Ratio of specific heats
[bar]	[K]	[g·mol ⁻¹]	[-]
30	3,480.67	29.399	1.1224
35	3,497.07	29.456	1.1230
40	3,511.13	29.506	1.1235
45	3,523.42	29.550	1.1240
50	3,534.31	29.588	1.1244
55	3,544.08	29.623	1.1248
60	3,552.93	29.655	1.1251
65	3,561.00	29.685	1.1254
70	3,568.42	29.712	1.1257
75	3,575.28	29.737	1.1259
80	3,581.65	29.760	1.1262
85	3,587.59	29.782	1.1264
90	3,593.16	29.803	1.1266
95	3,598.40	29.822	1.1268
100	3,603.33	29.841	1.1270

Table C.1: Thermodynamic properties of the HTBP1912 propellant for various chamber pressures.

Appendix D

Solid Rocket Stage Database

The solid rocket motor database used for this thesis work can be found in the table on the next page. This database contains 32 solid rocket stages that range from the extremely small STAR 12 GV to the large P-80 stage. The data for the individual rocket stages is obtained from publicly available literature sources mainly the production catalog from ATK [4] and the book of Sutton [98]. Data for the European motors comes from [15] and [34]. Not for all ATK motors values for the Isp are given, the missing ones are obtained from [53]. For the identification of the constituents for the different propellants also [118] is used.

Engine name	Thrust Average	Propellant Specific impulse	Chamber pressure Average	Propellant mass	Total inert mass
	[kN]	[s]	[bar]	[kg]	[kg]
P-80	2,200	280.1	95.0	88,000	7,300
Z-23	1,054	287.5	106.0	23,906	1,845
Thiokol M55	865.6	262.0	53.8	20,789	2,141
Orion 50S XLT	614.9	284.6	74.7	15,023	1,157
Orion 50S XLG	588.0	272.3	74.7	15,023	1,179
Orion 50 ST	454.4	285.0	58.6	12,157	1,016
Orion 50S XL	626.3	292.8	74.0	15,023	1,157
Orion 50S	465.1	292.3	56.1	12,163	1,016
Z-9	304.2	294.4	74.0	10,115	833
Orion 50 XL	160.6	290.7	68.3	3,924	395
Orion 50	114.6	290.2	55.8	3,025	345
Orbus 6	105.9	289.6	42.1	2,722	233
ORIOLE	92.5	288.5	65.1	976	198
STAR 48V	68.6	292.1	39.9	2,010	154
Orion 38	32.2	287.0	39.4	771	122
STAR 37GV	47.3	294.1	72.4	1,066	81.7
STAR 12GV	6.5	282.4	106.8	32.9	8.98
STAR 31	82.3	293.5	49.1	1,286	108
STAR 48A	77.2	283.4	37.4	2,430	144
STAR 48B	67.2	286.0	39.9	2,010	124
STAR 30E	35.1	290.4	37.0	631	42.5
STAR 26	33.4	271.0	39.6	231	38.8
STAR 30C/BP	32.5	291.8	38.1	591	41.1
STAR 30	26.6	293.0	35.4	51.5	37.7
STAR 27	25.4	287.9	38.8	334	27.5
STAR 20	24.5	286.5	45.1	273	27.6
STAR 24C	20.3	282.3	37.5	220	19.7
STAR 24	18.5	282.9	33.5	200	18.3
STAR 17A	16.0	286.7	46.2	112	13.4
STAR 17	10.9	286.2	55.4	70.1	9.43
STAR 13B	7.6	285.0	56.7	41.2	5.81
STAR 15G	6.5	281.8	61.0	79.6	14.0

Table D.1: Solid Rocket Stage Database (1/2).

Engine name	Nozzle mass	Case mass	Burn time	TVC	Propellant	Constituents propellant
	[kg]	[kg]	[s]	[-]	[-]	[-]
P-80	2,249	3,260	117	Yes	HTBP 1912	HTBP 12%, Al 19%, AP 69%
Z-23	572	900	71.0	Yes	HTBP 1912	HTBP 12%, Al 19%, AP 69%
Thiokol M55	402	1,656	52.6	Yes	TP-H1011	HTBP 14%, Al 16%, AP 70%
Orion 50S XLT	247	872	68.4	Yes	QDL-1	HTPB polymer, 19% Al
Orion 50S XLG	267	872	68.4	Yes	QDL-1	HTPB polymer, 19% Al
Orion 50 ST	247	753	75.0	Yes	QDL-1	HTPB polymer, 19% Al
Orion 50S XL	247	872	69.1	No	QDL-1	HTPB polymer, 19% Al
Orion 50S	247	753	75.3	No	QDL-1	HTPB polymer, 19% Al
Z-9	228	400	107	Yes	HTBP 1912	HTBP 12%, Al 19%, AP 69%
Orion 50 XL	109	250	69.7	Yes	QDL-1	HTPB polymer, 19% Al
Orion 50	10	214	75.6	Yes	QDL-1	HTPB polymer, 19% Al
Orbus 6	87.3	155	101	Yes	UTP-19360A	HTBP 14%, Al 18%, AP 68%
ORIOLE	65.8	97.1	30.0	Yes	SAA-144	Aluminized HTPB
STAR 48V	52.6	58.3	84.1	Yes	TP-H-3340	HTBP 11%, Al 18%, AP 71%
Orion 38	41.3	60.3	67.7	Yes	QDL-1	HTPB polymer, 19% Al
STAR 37GV	34.0	32.3	49.0	Yes	TP-H-3340	HTBP 11%, Al 18%, AP 71%
STAR 12GV	2.04	6.49	13.9	Yes	TP-H-3340A	HTBP 11%, Al 18%, AP 71%
STAR 31	29.7	41.73	45.0	No	TP-H-3340	HTBP 11%, Al 18%, AP 71%
STAR 48A	38.3	69.7	87.2	No	TP-H-3340	HTBP 11%, Al 18%, AP 71%
STAR 48B	36.8	58.3	84.1	No	TP-H-3340	HTBP 11%, Al 18%, AP 71%
STAR 30E	15.2	17.2	51.1	No	TP-H-3340	HTBP 11%, Al 18%, AP 71%
STAR 26	10.6	18.0	17.8	No	TP-H-3314	?
STAR 30C/BP	15.7	16.2	51.0	No	TP-H-3340	HTBP 11%, Al 18%, AP 71%
STAR 30	15.3	13.8	54.0	No	TP-H-3340	HTBP 11%, Al 18%, AP 71%
STAR 27	9.25	10.7	34.4	No	TP-H-3135	HTBP 12%, Al 16%, AP 72%
STAR 20	5.67	11.0	27.4	No	TP-H-3062	CTBP 14%, Al 16%, AP 70%
STAR 24C	5.94	6.40	28.0	No	TP-H-3062	CTBP 14%, Al 16%, AP 70%
STAR 24	5.94	5.90	29.6	No	TP-H-3062	CTBP 14%, Al 16%, AP 70%
STAR 17A	4.67	5.94	19.4	No	TP-H-3062	CTBP 14%, Al 16%, AP 70%
STAR 17	3.18	3.99	17.6	No	TP-H-3062	CTBP 14%, Al 16%, AP 70%
STAR 13B	1.68	2.54	14.8	No	TP-H-3062	CTBP 14%, Al 16%, AP 70%
STAR 15G	2.09	10.3	33.3	No	TP-H-3340	HTBP 11%, Al 18%, AP 71%

Table D.2: Solid Rocket Stage Database (2/2).

Appendix E

Propulsion Validation Data

In Table E.1 the validation data for the propulsion elements of SRM stages is given.

	Ideal				Corrected					
	Thrust	Error	Isp	Error	Thrust	Error	Isp	Error	Propellant	Error
	[kN]	[%]	[s]	[%]	[kN]	[%]	[s]	[%]	[kg]	[%]
Orion 50S	496.0	+6.53	321.4	+10.7	464.0	-0.25	294.5	0.77	12,456	+2.41
Thoikol M55	1,017	+17.3	290.7	+11.0	951.0	+9.85	272.2	3.89	19,293	-7.19
Zefiro 23	1,236	+17.2	308.3	+7.23	1,157	+9.75	288.7	0.41	30,257	+26.6
Zefiro 9	315.4	+3.44	323.0	+9.71	295.3	-3.15	302.4	2.72	11,237	+11.1
Orion 50	124.9	+9.07	321.4	+10.7	117.0	+2.13	300.9	3.69	3,086	+2.01
Orion 38	34.8	+7.90	320.0	+11.5	32.6	+1.03	299.7	4.42	772.5	+0.23
Orbus 6	78.5	-3.01	319.4	+10.3	73.5	-9.19	299.0	3.25	2,607	-4.21
STAR 31	71.0	-13.7	323.2	+10.1	66.5	-19.2	302.7	3.12	1,061	-17.5
STAR 48A	74.3	-3.67	311.6	+9.94	69.6	-9.80	291.7	2.94	2,210	-9.07
STAR 27	29.4	+15.4	319.8	+11.1	27.5	+8.09	299.4	4.01	331.7	-0.58
STAR 17A	16.7	+4.20	336.1	+17.2	15.6	-2.44	314.7	9.75	107.4	-4.34
STAR 13B	8.9	+17.3	317.2	+11.3	8.3	+9.87	297.0	4.23	43.67	+5.91
STAR 24	20.1	+8.55	314.8	+11.3	18.9	+1.64	294.7	4.18	198.8	-0.53
STAR 30E	36.0	+2.53	323.0	+11.2	33.7	-3.99	302.4	4.14	606.7	+3.91

Table E.1: Validation data for the propulsion elements of the SRM stages.

Appendix F

Launch Vehicle Validation Data

In Table F.1 the validation data for the fairing mass can be found. All actual fairing masses originate from [33] and [47].

Launch vehicle	Actual	Wetted area	Model	Error
	[kg]	[m ²]	[kg]	[%]
Vega	529	53.4	652	+23.2
Minotaur	194	15.1	184	-5.21
Taurus	360	24.2	296	-17.8
Pegasus	170	15.1	184	+8.30
PSLV	1,100	70.9	865	-21.3
KOSMOS	345	31.5	384	+11.2

Table F.1: Validation data for the fairing mass model.

The validation of the interstage mass is done for the interstages of Ariane IV [28], Ariane V [28], Vega [34] and Atlas [58]. The results can be found in Table F.2.

Launch vehicle	Stages	Material	Actual	D_{int}	S_{int}	Model	Error
			[kg]	m	[m ²]	[kg]	[%]
Ariane IV	1-2	Composite	480	3.8	35.5	515	+26.96%
	2-3	Aluminum	287	2.73	22.3	388	+35.34%
	2-3	Composite	226	2.73	22.3	272	+20.31
Vega	1-2	Aluminum	228	3.04	6.67	158	-30.63
	2-3	Aluminum	538	3.04	17.3	409	-23.90
	3-4	Aluminum	267	1.95	10.0	146	-45.25
Atlas IIA	1-2	Aluminum	545	3.05	38.2	706	+29.46
Atlas V 400	1-2	Aluminum	374	3.05	30.0	553	+47.98
Atlas V HLV	1-2	Aluminum	1,297	3.83	45.8	1,216	-6.23

Table F.2: Validation data for the interstage mass model.

For the validation of the VEB mass the MER based on regression analysis given in [121] was updated by the addition of VEB mass of Vega and Ariane 44L [33]. The other data is obtained from [122]. Note that the VEB mass for Vega is still overestimated by the new MER.

Launch vehicle	Actual	Model	Error
	[kg]	[kg]	[%]
Teamx MAV	4.6	7.1	+53.5
EADS MAV	29	15.9	-45.1
Ariane I	320	284.7	-11.0
VEGA	150	238.3	+58.8
Ariane 44L	530	472.8	-10.8
Ariane 2	320	300.8	-6.01

Table F.3: Validation data for the VEB mass model.

In Table F.4 the validation data for the total length of the stages is given. This data originates from the same sources as the data for the propulsion database in Appendix D.

Length	Actual	Original model	Error	Updated model	Error
	[m]	[m]	[%]	[m]	[%]
Orion 50S	8.86	8.93	+0.78	7.85	-11.4
Thoikol M55	7.49	7.88	+5.16	6.74	-10.0
Zefiro 23	8.39	9.98	+19.0	8.59	+2.37
Zefiro 9	4.12	6.02	+46.2	4.67	+13.4
Orion 50	2.67	3.95	+48.0	3.03	+13.8
Orion 38	1.35	2.35	+74.3	1.69	+25.9
Orbus 6	1.98	3.44	+73.9	2.40	+21.2
STAR 31	2.87	3.19	+11.1	2.57	-10.4
STAR 48A	2.03	3.16	+55.6	2.34	+15.3
STAR 27	1.24	1.91	+54.2	1.41	+13.7
STAR 17A	0.98	1.36	+39.0	1.03	+4.92
STAR 13B	0.64	0.91	+42.1	0.67	+4.90
STAR 24	1.03	1.53	+48.8	1.10	+6.98
STAR 30E	1.69	2.43	+43.7	1.85	+9.58

Table F.4: Validation data for the total length of the stages.

The validation data for mass of the solid rocket stages is given in Table F.5. For the actual nozzle, case and inert mass of the stages is referred to Appendix D.

Mass	Nozzle	Error	Case	Error	Inert (original)	Error	Inert (updated)	Error
	[kg]	[%]	[kg]	[%]	[kg]	[%]	[kg]	[%]
Orion 50S	235	-5.02	794.0	+5.45	1,038	+2.15	1,211	+19.1
Thoikol M55	403	+0.13	1,153.9	-30.3	1,570	-26.7	1,831	-14.5
Zefiro 23	544	-4.89	1,226.9	+36.3	1,789	-3.03	2,086	+13.1
Zefiro 9	218	-4.44	464.0	+16.0	691	-17.1	805	-3.35
Orion 50	89.2	-12.6	261.9	+22.3	355	+2.71	413	+19.8
Orion 38	28.5	-30.9	60.4	+0.13	90.2	-26.4	105	-14.2
Orbus 6	67.4	-22.7	98.9	-36.1	169	-27.2	197	-15.2
STAR 31	39.2	+31.9	35.4	-15.2	76.1	-29.2	88.8	-17.4
STAR 48A	36.2	-5.50	61.5	-11.7	100	-30.0	117	-18.4
STAR 27	9.07	-1.96	12.8	+19.5	22.5	-18.1	26.3	-4.47
STAR 17A	5.09	+9.01	5.10	-14.2	10.5	-21.7	12.2	-8.66
STAR 13B	2.01	+19.8	2.65	+4.26	4.81	-17.2	5.61	-3.46
STAR 24	6.12	+2.95	11.5	+95.8	18.1	-1.14	21.1	+15.3
STAR 30E	13.6	-11.0	19.6	+14.0	34.2	-19.5	39.9	-6.18

Table F.5: Validation data for the masses of the different SRM stage components.

Appendix G

Aerodynamic Launcher Configuration Database

In the three tables below the launch vehicle configuration databases for Missile Datcom are given. The lengths and diameters are chosen based on maximum dimensions of air launched vehicles for different configurations are given in Table 1.1. The chord length of the wing at the wing root is based on Pegasus and the designs from NASA's Horizontal Launch Study [6, 75].

Length [m]	3.0	3.5	4.0	4.5	5.5	6.0	6.5	7.0	8.0	9.0	10.0	12.0	14.0
Diameter [m]	0.3	0.3	0.3	0.3	0.3	0.3	0.4	0.5	0.5	0.6	0.6	0.7	0.7
	0.4	0.4	0.4	0.4	0.4	0.4	0.5	0.6	0.6	0.7	0.7	0.8	0.8
	0.5	0.5	0.5	0.5	0.5	0.5	0.6	0.7	0.7	0.8	0.8	1.0	1.0
	0.6	0.6	0.6	0.6	0.6	0.6	0.7	0.8	0.8	1.0	1.0	1.2	1.2
	0.7	0.7	0.7	0.7	0.7	0.7	0.8	1.0	1.0	1.2	1.2	1.4	1.4
	0.8	0.8	0.8	0.8	0.8	0.8	1.0	1.2	1.2	1.4	1.4	1.6	1.6
	1.0	1.0	1.0	1.0	1.0	1.0	1.2		1.4				

Table G.1: Configuration matrix Missile Datcom for small launch vehicles.

Length [m]	20.0	22.5	25.0	27.5	30.0	32.5	35.0	40.0	45.0	50.0
Diameter [m]	1.6	1.6	1.6	1.6	1.6	1.6	1.8	1.8	2.0	2.0
	1.8	1.8	1.8	1.8	1.8	1.8	2.0	2.0	2.25	2.25
	2.0	2.0	2.0	2.0	2.0	2.0	2.25	2.25	2.5	2.5
	2.25	2.25	2.25	2.25	2.25	2.25	2.5	2.5	2.75	2.75
	2.5	2.5	2.5	2.5	2.5	2.5	2.75	2.75	3.0	3.0
	2.75	2.75	2.75	2.75	2.75	2.75	3.0	3.0	3.25	3.25
	3.0	3.0	3.0	3.0	3.0	3.0	3.25	3.25	3.5	3.5
					3.5	3.25	3.5	3.5	4.0	4.0
						3.5	4.0	4.0	4.5	4.5

Table G.2: Configuration matrix Missile Datcom for large launch vehicles.

Length [m]	20.0	22.5	25.0	27.5	30.0	32.5
Chord length wing root [m]	3.5	3.5	5.0	5.0	5.0	5.0
	5.0	5.0	6.5	6.5	6.5	6.5
	6.5	6.5	8.0	8.0	8.0	8.0

Table G.3: Configuration matrix Missile Datcom for winged large launch vehicles (diameters in the database are the same as in Table G.2).

Appendix H

Cost Model Validation Data

In this appendix the data are given that are used for the validation of the cost model. The launch vehicle characteristics originates from the user manuals [80, 79], ESA's Launch Vehicle Catalog [33] and the International Reference Guide to Space Launch Systems [47]. The fairing volume is calculated based on a simplified geometry of the fairing (conical nose and cylindrical fairing) and is calculated by:

$$Volume_{fairing} = \frac{\pi}{3} \cdot \left(\frac{D_{fairing}}{2}\right)^2 \cdot L_{nose} + \pi \cdot \left(\frac{D_{fairing}}{2}\right)^2 \cdot L_{fairing} \quad (H.1)$$

Where $D_{fairing}$ is the diameter of the cylindrical section of the fairing, $L_{fairing}$ the length of the cylindrical part of the fairing and L_{nose} the length of the nose.

In Chapter 9 a new CER is introduced for the production cost of a SRM with a propellant mass smaller than 13,000 kg. The cost data presented in Table H.1 is used to develop this CER. The data from Table H.1 originates from [107] and [94] and the price of the TFU is based on the estimation of the number of motors sold.

Launch vehicle	Propellant mass	Cost TFU
	[kg]	[€M FY 2012]
Star 5	2.29	0.2752
Star 12 GV	32.9	0.7512
Star 17	120	1.2701
Star 30E	631	1.2905
Star 48B	2010	2.349

Table H.1: Cost data used for the development of a CER for the production cost of small SRMs [107, 94].

Launch vehicle characteristic	Vega	Taurus	Minotaur I	Pegasus	Pegasus XL
Fairing					
Total fairing length	7.88	5.50	4.40	4.40	4.40
Fairing volume	31.3	9.05	4.39	4.39	4.39
Stage 1					
Propellant mass	88,000	48,700	20,785	12,152	15,000
Inert mass	7,330	4,400	2,248	1,759	2,800
TVC	Yes	Yes	Yes	No	No
Stage 2					
Propellant mass	24,000	12,154	6,237	3,025	3,915
Inert mass	1,950	1,088	691	343	416
TVC	Yes	Yes	No	Yes	Yes
Stage 3					
Propellant mass	10,500	3,027	3,915	782	770
Inert mass	915	352	416	126	126
TVC	Yes	Yes	Yes	Yes	Yes
Stage 4					
Propellant mass	AVUM	771	771	-	-
Inert mass	AVUM	104	104	-	-
TVC	AVUM	Yes	Yes	-	-

Table H.2: Launch vehicle characteristics for the validation of the cost model.

Launch vehicle characteristic	Vega	Taurus	Minotaur I	Pegasus	Pegasus XL
Total number of flights	120	40	30	40	40
Annual flight rate	6	2	2	2	2
Development					
System engineering factor f_0	1.4	1.4	1.4	1.4	1.4
Development standard factor f_1	0.9	0.8	0.8	1.0	1.0
Aircraft development cost $DC_{aircraft}$	0.0	0.0	0.0	122.0	122.0
Production					
System engineering factor f_0	1.05	1.05	1.05	1.05	1.05
Learning factor p	0.90	0.90	0.85	0.85	0.85
Factor for series production f_4	0.566	0.663	0.600	0.536	0.536
Operations					
Propellant mass GTOW	137	73.0	36.2	18.5	23.0
Launch vehicle type f_v	0.4	0.3	0.3	0.5	0.5
Processing type f_p	0.7	0.5	0.5	0.5	0.5
Complexity stage 1	0.15	0.15	0.15	0.4	0.4
Complexity stage 2	0.15	0.15	0.15	0.15	0.15
Complexity stage 3	0.15	0.15	0.15	0.15	0.15
Complexity stage 4	0.40	0.15	0.15	0.15	0.15
Air launch correction factor $f_{aircraft}$	1.0	1.0	1.0	0.5	0.5
Carrier aircraft cost $CO_{aircraft}$	0.0	0.0	0.0	1.75	1.75

Table H.3: Correction factors and additional elements used for the validation of the cost model.

The correction factors chosen for the launch vehicles follow the general guidelines described in Chapter 9. The total number of flights and launch rates are based on the actual launches in combination with estimated launch rates from [47]. Vega has a development standard factor 0.9 because the fourth stage has a liquid rocket engine. The cost of the fourth stage of Vega is not calculated but is taken from [61]: 149.7 million euro. Also the launch vehicle type correction factor for Vega is changed from 0.3 to 0.4 because of its liquid propelled 4th stage.

For the smaller launch vehicles (Minotaur I, Pegasus and Pegasus XL) a learning factor of 0.85 is used and for the larger launch vehicle (Vega and Taurus) 0.9. This is done because a lower vehicle mass results in a lower learning factor.

Launch vehicle	Cost	TransCost	Martino's model	Final model
Vega	Development cost amortized	9.298	5.765	5.765
	Average production cost	29.97	20.86	20.82
	Operations cost	10.01	10.01	10.01
	Total cost	49.28	36.64	36.59
	Advertised cost	32.00 [15, 61]		
	Difference [%]	+54.0	+14.5	+14.4
Taurus	Development cost amortized	16.72	6.508	6.508
	Average production cost	24.03	15.67	14.05
	Operations cost	9.378	9.378	9.378
	Total cost	50.12	31.56	29.93
	Advertised cost	24.00 [96]		
	Difference [%]	+109	+31.5	+24.7
Minotaur I	Development cost amortized	17.70	6.455	6.455
	Average production cost	20.83	11.389	9.815
	Operations cost	5.991	5.991	5.991
	Total cost	44.52	23.83	22.26
	Advertised cost	21.30 [47]		
	Difference [%]	+109	+11.9	+4.51
Pegasus	Development cost amortized	14.60	7.553	7.553
	Average production cost	12.99	7.650	6.353
	Operations cost	4.661	4.661	4.661
	Total cost	32.26	19.86	18.57
	Advertised cost	13.50 [112]		
	Difference [%]	+139	+47.1	+37.5
Pegasus XL	Development cost amortized	13.67	7.690	7.690
	Average production cost	11.82	7.803	6.589
	Operations cost	5.073	5.073	5.073
	Total cost	32.35	20.57	19.35
	Advertised cost	16.90 [10, 9, 112]		
	Difference [%]	+91.4	+21.7	+14.5

Table H.4: Outcome of the validation of the three cost models for existing launch vehicles.

The cost of the development of the carrier aircraft is based on the values from NASA's

HLS for a Boeing 747-400F [6]. These cost are corrected for the empty mass of the Stargazer (Lockheed L-1011) and the Boeing 747-400F [48]. The estimated annual fixed cost for the Stargazer can be found in [19].

The details of the three cost models for the five launch vehicles are shown in Table H.4.

Appendix I

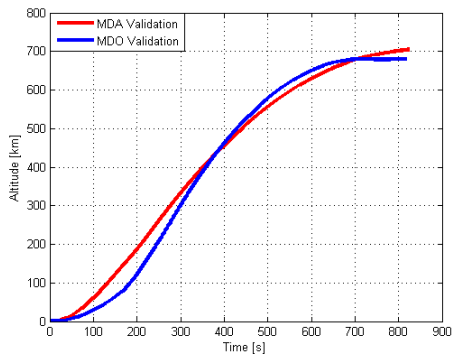
Multidisciplinary Design Optimization Validation Data

In this appendix the validation data for the MDA and MDO validation of Taurus and Pegasus is given. This data is only given to provide the reader additional information and insight and, therefore, the tables and figures in this Appendix are explained in Chapter 2.

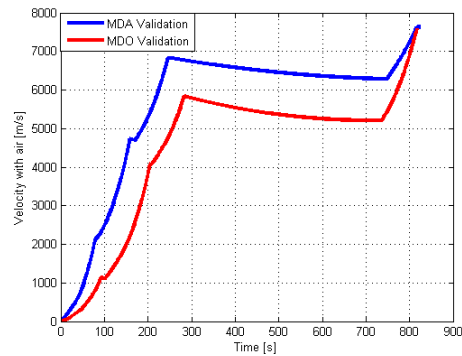
I.1 Taurus

Stage	Element	Value	Stage	Element	Value
Stage 1	Chamber pressure [bar]	85.9	Stage 3	Chamber pressure [bar]	55.8
	Exit pressure [bar]	0.718		Exit pressure [bar]	0.114
	Diameter case [m]	2.36		Diameter case [m]	1.27
	Diameter nozzle [m]	1.52		Diameter nozzle [m]	0.860
	Burn time [s]	79.5		Burn time [s]	75.6
	TVC [-]	Yes		TVC [-]	Yes
Stage 2	Chamber pressure [bar]	58.6	Stage 4	Chamber pressure [bar]	39.4
	Exit pressure [bar]	0.268		Exit pressure [bar]	0.0866
	Diameter case [m]	1.27		Diameter case [m]	0.965
	Diameter nozzle [m]	1.21		Diameter nozzle [m]	0.526
	Burn time [s]	75.0		Burn time [s]	67.7
	TVC [-]	Yes		TVC [-]	Yes

Table I.1: Input parameters MDA validation Taurus.

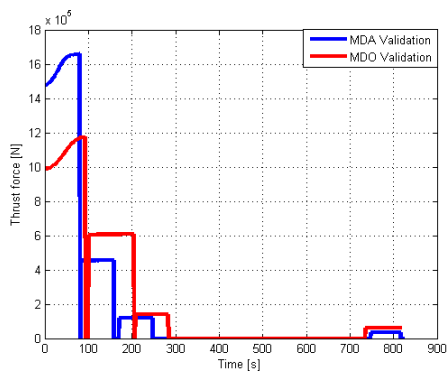


(a) Altitude versus time

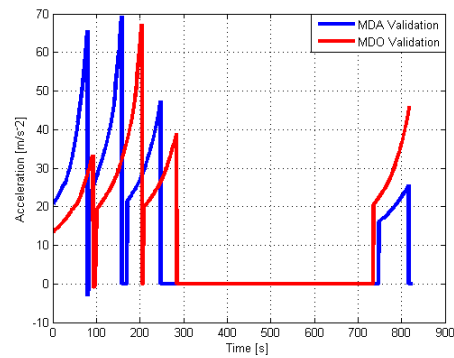


(b) Velocity versus time

Figure I.1: Comparison of the altitude and velocity versus time for the MDA and MDO validation of Taurus.

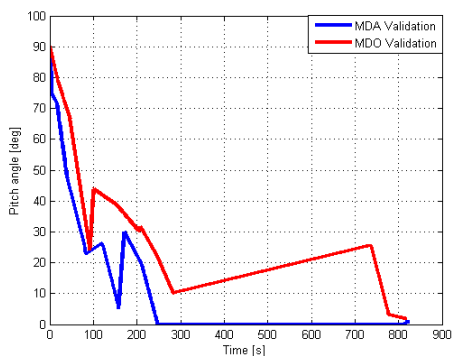


(a) Thrust versus time

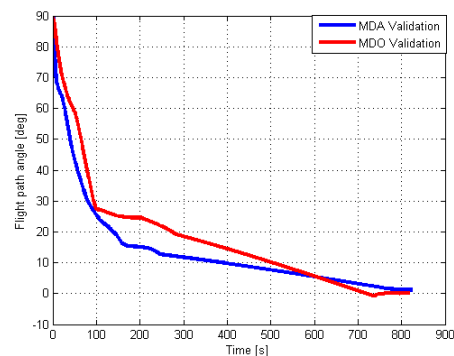


(b) Acceleration versus time

Figure I.2: Comparison of the thrust and acceleration versus time for the MDA and MDO validation of Taurus.



(a) Pitch angle versus time



(b) Flight path angle versus time

Figure I.3: Comparison of the pitch and flight path angle versus time for the MDA and MDO validation of Taurus.

Stage	Element	Value	Stage	Element	Value
Stage 1	Vacuum thrust [kN]	1,180	Stage 3	Vacuum thrust [kN]	140.4
	Vacuum Isp [s]	284.3		Vacuum Isp [s]	305.8
	Chamber pressure [bar]	70.5		Chamber pressure [bar]	44.5
	Exit pressure [bar]	0.458		Exit pressure [bar]	0.0615
	Diameter case [m]	1.38		Diameter case [m]	1.30
	Diameter nozzle [m]	1.55		Diameter nozzle [m]	1.24
	Length [m]	17.7		Length [m]	3.72
	Inert mass [kg]	2,339		Inert mass [kg]	255
	Propellant mass [kg]	40,216		Propellant mass [kg]	3,622
Stage 2	Vacuum thrust [kN]	606 .0	Stage 4	Vacuum thrust [kN]	62.81
	Vacuum Isp [s]	299.0		Vacuum Isp [s]	306.5
	Chamber pressure [bar]	59.6		Chamber pressure [bar]	45.5
	Exit pressure [bar]	0.142		Exit pressure [bar]	0.0592
	Diameter case [m]	1.77		Diameter case [m]	1.32
	Diameter nozzle [m]	1.79		Diameter nozzle [m]	0.837
	Length [m]	8.10		Length [m]	2.41
	Inert mass [kg]	1,232		Inert mass [kg]	148
	Propellant mass [kg]	22,026		Propellant mass [kg]	1,750

Table I.2: Vehicle characteristics for the MDO validation for Taurus.

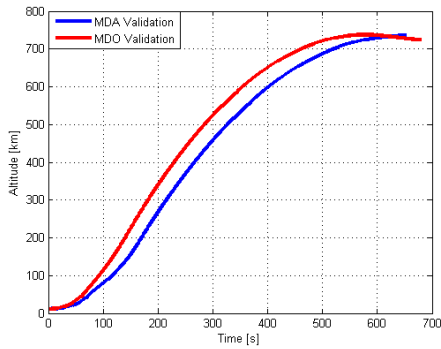
I.2 Pegasus XL

Stage	Element	Value	Stage	Element	Value
Stage 1	Chamber pressure [bar]	74.0	Stage 3	Chamber pressure [bar]	39.4
	Exit pressure [bar]	0.248		Exit pressure [bar]	0.0866
	Diameter case [m]	1.27		Diameter case [m]	0.965
	Diameter nozzle [m]	1.424		Diameter nozzle [m]	0.526
	Burn time [s]	69.1		Burn time [s]	67.7
	TVC [-]	Yes		TVC [-]	Yes
Stage 2	Chamber pressure [bar]	68.3			
	Exit pressure [bar]	0.173			
	Diameter case [m]	1.27			
	Diameter nozzle [m]	0.860			
	Burn time [s]	69.7			
	TVC [-]	Yes			

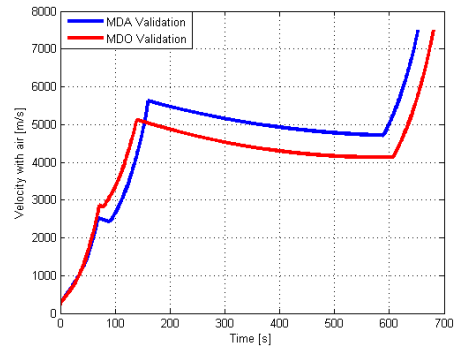
Table I.3: Input parameters MDA validation Pegasus XL.

Stage	Element	Value	Stage	Element	Value
Stage 1	Vacuum thrust [kN]	448.2	Stage 3	Vacuum thrust [kN]	32.77
	Vacuum Isp [s]	288.3		Vacuum Isp [s]	308.2
	Chamber pressure [bar]	46.8		Chamber pressure [bar]	47.6
	Exit pressure [bar]	0.229		Exit pressure [bar]	0.0546
	Diameter case [m]	1.73		Diameter case [m]	0.826
	Diameter nozzle [m]	1.31		Diameter nozzle [m]	0.621
	Length [m]	5.03		Length [m]	2.06
	Inert mass [kg]	1,025		Inert mass [kg]	79
	Propellant mass [kg]	11,544		Propellant mass [kg]	821
Stage 2	Vacuum thrust [kN]	109.4			
	Vacuum Isp [s]	297.0			
	Chamber pressure [bar]	42.1			
	Exit pressure [bar]	0.112			
	Diameter case [m]	1.03			
	Diameter nozzle [m]	0.865			
	Length [m]	3.10			
	Inert mass [kg]	200			
Propellant mass [kg]	2,339				

Table I.4: Vehicle characteristics for the MDO validation for Pegasus XL.

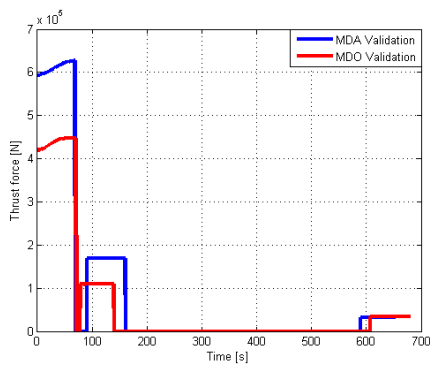


(a) Altitude versus time

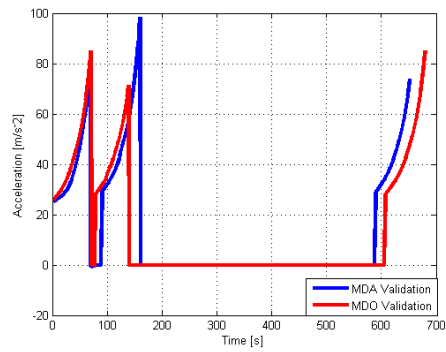


(b) Velocity versus time

Figure I.4: Comparison of the altitude and velocity versus time for the MDA and MDO validation of Pegasus XL.

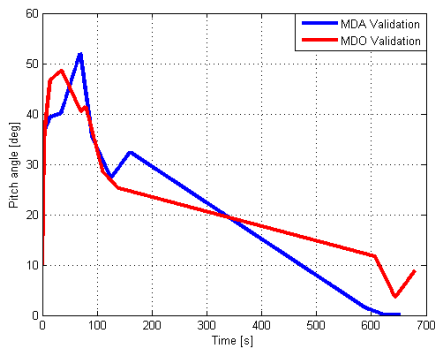


(a) Thrust versus time

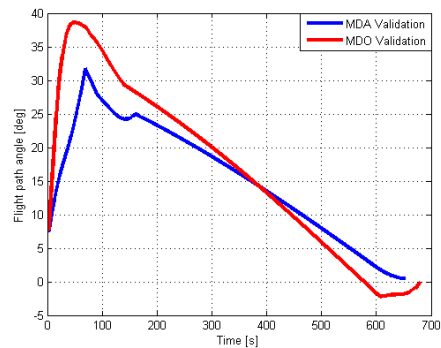


(b) Acceleration versus time

Figure I.5: Comparison of the thrust and acceleration versus time for the MDA and MDO validation of Pegasus XL.



(a) Pitch angle versus time



(b) Flight path angle versus time

Figure I.6: Comparison of the pitch and flight path angle versus time for the MDA and MDO validation of Pegasus XL.

Appendix J

Appendix to the Results

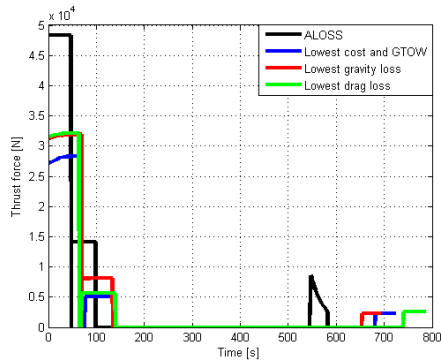
In this Appendix tables and figures are given to support the results presented in Chapter 11. The tables contain the detailed characteristics of the optimized launch vehicles for the various release conditions and configurations. Furthermore, figures that show the history of several trajectory parameters are included in this chapter. The outline of this Appendix is identically to the outline of Chapter 11. The characteristics of the optimized vehicle for regressive thrust will be addressed in Section J.4. Also the characteristics of the optimized vehicles with a constraint for the ratio web thickness motor case are given in Section J.5.

J.1 10 kg Payload Class

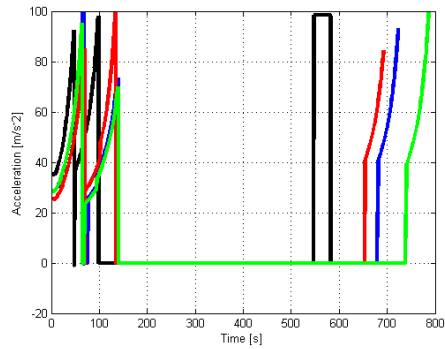
In this section the characteristics of all optimized vehicles for the 10 kg payload class are given. The figures that are already shown in Section 11.1 will not be repeated again in this appendix.

J.1.1 Optimized ALOSS Launch Vehicle

The figures for the altitude and velocity (Figure 11.4), pitch and flight path angle (Figure 11.5) and drag and lift force (Figure 11.6) are already given in Chapter 11.

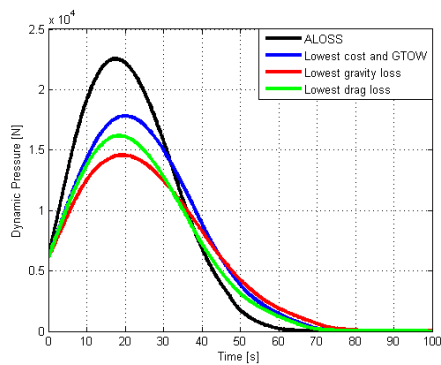


(a) Thrust force versus time

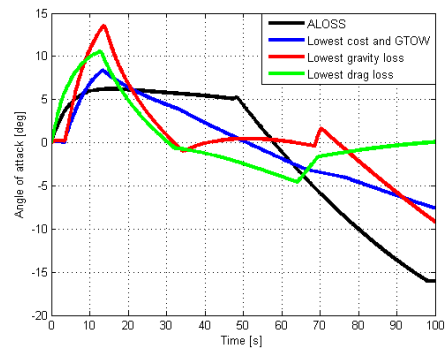


(b) Acceleration versus time

Figure J.1: Thrust force and acceleration versus time for the optimized vehicles for the ALOSS case.

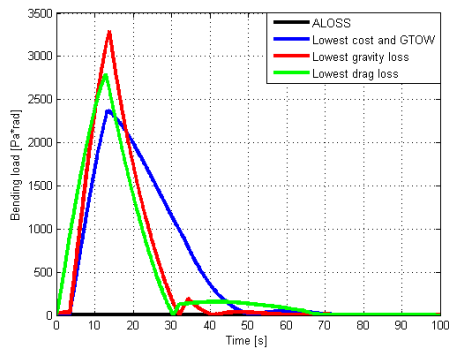


(a) Dynamic pressure versus time

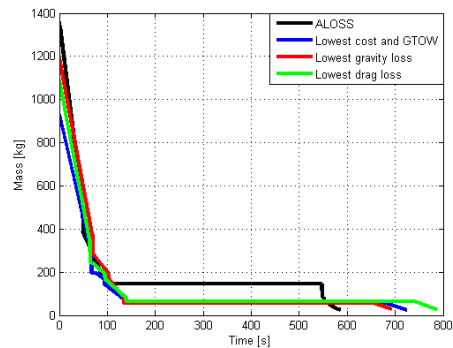


(b) Angle of attack versus time

Figure J.2: Dynamic pressure and angle of attack versus time for the optimized vehicles for the ALOSS case.



(a) Bending load versus time



(b) Mass versus time

Figure J.3: Bending load and mass versus time for the optimized vehicles for the ALOSS case.

Parameter	Unit	ALOSS	Cost and GTOW	Gravity loss	Drag loss	Search space
Cost per flight	€M	2.181	1.890	2.051	2.003	-
GTOW	kg	1,380	930.6	1,194	1,091	-
Vehicle length	m	~5.5	5.422	5.437	5.410	-
Vehicle diameter	m	0.66	0.5605	0.6467	0.5725	-
Vacuum thrust stage 1	kN	48.3	28.32	31.93	32.16	-
Vacuum thrust stage 2	kN	14.1	5.048	8.079	5.643	-
Vacuum thrust stage 3	kN	8.6	2.242	2.323	2.505	-
Isp stage 1	s	284.0	295.8	272.1	278.1	-
Isp stage 2	s	294.0	300.7	292.9	288.8	-
Isp stage 3	s	294.0	308.3	310.1	303.8	-
Inert mass stage 1	kg	128.1	65.01	63.47	69.28	-
Propellant mass stage 1	kg	862.8	666.7	844.4	777.0	-
Inert mass stage 2	kg	56.5	10.19	18.61	12.31	-
Propellant mass stage 2	kg	244.8	108.7	184.3	143.0	-
Inert mass stage 3	kg	26.5	3.976	4.614	4.230	-
Propellant mass stage 3	kg	60.7	32.13	32.89	40.39	-
Chamber pressure stage 1	bar	30.0	58.98	34.01	50.74	[30.0,70.0]
Exit pressure stage 1	bar	0.120	0.1768	0.4312	0.4712	[0.05,0.50]
Diameter case stage 1	m	0.660	0.5605	0.6467	0.5725	[0.30,0.67]
Diameter nozzle exit stage 1	m	0.606	0.3545	0.2873	0.2645	[0.20,0.67]
Burn time stage 1	s	47.4	66.32	68.55	63.99	[40.0,70.0]
Chamber pressure stage 2	bar	30.0	42.87	57.63	42.62	[30.0,70.0]
Exit pressure stage 2	bar	0.05	0.08734	0.21059	0.2009	[0.05,0.25]
Diameter case stage 2	m	0.630	0.4163	0.4402	0.4503	[0.30,0.67]
Diameter nozzle exit stage 2	m	0.440	0.204596	0.1774	0.1565	[0.10,0.67]
Burn time stage 2	s	49.4	61.70	63.62	69.68	[30.0,70.0]
Chamber pressure stage 3	bar	20.0	61.84	92.34	50.10	[30.0,70.0]
Exit pressure stage 3	bar	0.05	0.07174	0.09506	0.0816	[0.05,0.15]
Diameter case stage 3	m	34.0	0.2652	0.2415	0.2924	[0.20,0.60]
Diameter nozzle exit stage 3	m	0.380	0.1417	0.1236	0.1456	[0.10,0.50]
Burn time stage 3	s	0.340	42.08	41.81	46.65	[20.0,50.0]
Length stage 1	m	2.59	2.229	2.032	2.258	-
Length stage 2	m	1.13	0.9060	1.1078	0.9024	-
Length stage 3	m	0.84	0.6423	0.6884	0.6660	-
Coasting time stage 1	s	1.0	9.993	1.543	5.470	[1.00, 50.0]
Coasting time stage 2	s	455.0	543.6	520.3	601.2	[100.0,650.0]
Gravity loss	m·s ⁻¹	1,920	1,673	1,583	1,773	-
Drag loss	m·s ⁻¹	165.8	176.4	171.6	142.9	-
Steering loss	m·s ⁻¹	56.91	61.97	33.28	167.5	-
Maximum dynamic pressure	kPa	21.38	17.82	14.57	16.17	-
Maximum bending load	Pa·rad	2,403	2,365	3,293	2,798	-
Fairing separation	s	-	94.60	102.0	94.70	-
Semi-major axis	[km]	708.8	780.9	775.3	782.6	-
Eccentricity	[-]	0.02600	0.008682	0.003257	0.002067	-
ΔV	m·s ⁻¹	8,793	8,633	8,559	8,754	-

Table J.1: Characteristics for the optimized vehicles for the ALOSS case.

J.1.2 Ground launch and Release Flight Path Angle

The initial pitch angle, angle of attack, drag force and lift force are already shown in Figure 11.7 and 11.8.

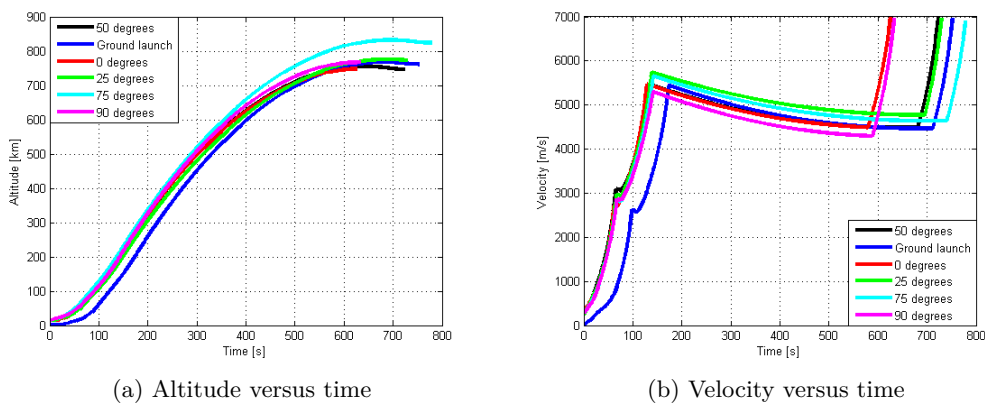


Figure J.4: Altitude and velocity versus time for the optimized ground launched vehicle and optimized air launched vehicles for various release flight path angles.

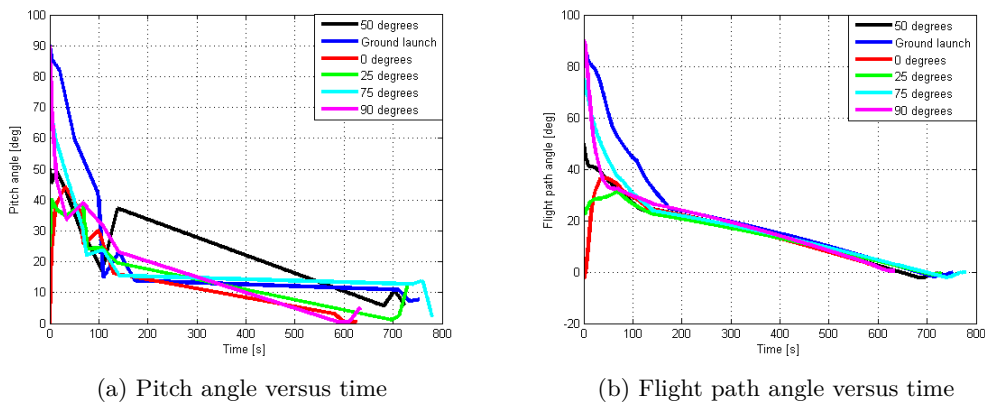
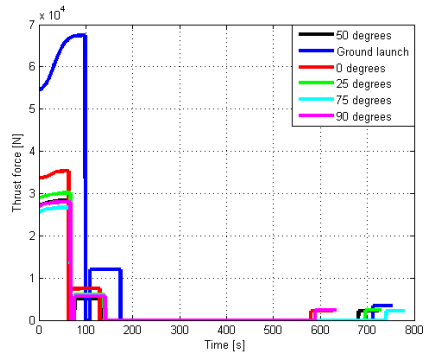
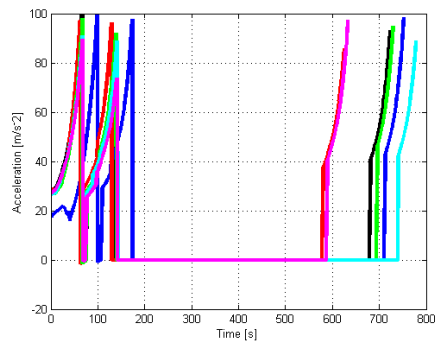


Figure J.5: Pitch angle and flight path angle for the optimized ground launched vehicle and optimized air launched vehicles for various release flight path angles.

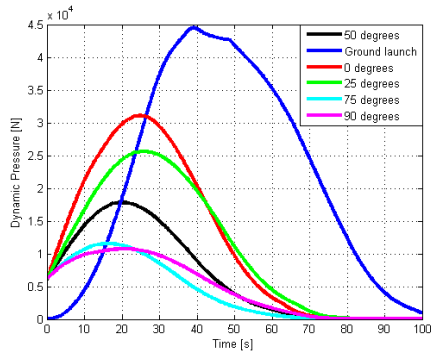


(a) Thrust force versus time

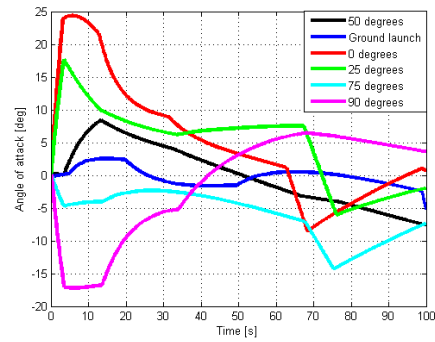


(b) Acceleration versus time

Figure J.6: Altitude and velocity versus time for the optimized ground launched vehicle and optimized air launched vehicles for various release flight path angles.

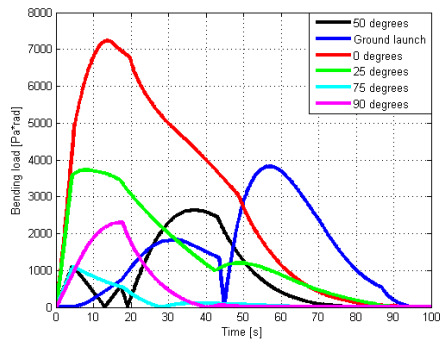


(a) Dynamic pressure versus time

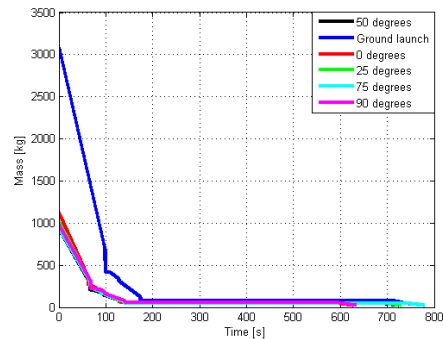


(b) Angle of attack versus time

Figure J.7: Dynamic pressure and angle of attack versus time for the optimized ground launched vehicle and optimized air launched vehicles for various release flight path angles.



(a) Bending load versus time



(b) Mass versus time

Figure J.8: Bending load and mass versus time for the optimized ground launched vehicle and optimized air launched vehicles for various release flight path angles.

Parameter	Unit	Ground launch	0°	25°	75°	90°
Cost per flight	€M	2.628	2.011	1.930	1.902	1.940
GTOW	kg	3,087	1,128	1,017	923.8	976.8
Vehicle length	m	6.745	5.469	5.440	5.395	5.482
Vehicle diameter	m	0.9126	0.6571	0.6102	0.6172	0.5801
Vacuum thrust stage 1	kN	67.46	35.34	30.14	26.65	27.97
Vacuum thrust stage 2	kN	11.98	7.404	5.996	5.788	5.658
Vacuum thrust stage 3	kN	3.415	2.145	2.261	2.074	2.446
Isp stage 1	s	281.2	293.4	290.7	285.2	290.8
Isp stage 2	s	293.9	291.4	297.6	299.6	298.9
Isp stage 3	s	302.7	309.5	306.1	310.9	309.0
Inert mass stage 1	kg	175.7	74.05	65.44	53.95	63.93
Propellant mass stage 1	kg	2,487	792.0	732.9	662.9	685.3
Inert mass stage 2	kg	33.53	14.89	11.722	11.862	11.776
Propellant mass stage 2	kg	277.2	163.1	133.1	134.5	129.5
Inert mass stage 3	kg	5.886	4.077	3.867	4.030	4.692
Propellant mass stage 3	kg	49.13	33.26	26.49	26.71	37.03
Chamber pressure stage 1	bar	52.92	48.36	48.51	37.17	55.63
Exit pressure stage 1	bar	0.4086	0.1685	0.2031	0.2179	0.2341
Diameter case stage 1	m	0.9126	0.6571	0.6102	0.5999	0.5801
Diameter nozzle exit stage 1	m	0.4020	0.4130	0.3546	0.3352	0.3182
Burn time stage 1	s	98.75	62.61	67.33	67.57	67.85
Chamber pressure stage 2	bar	89.44	38.58	39.08	43.35	45.42
Exit pressure stage 2	bar	0.3145	0.1510	0.09903	0.09594	0.10587
Diameter case stage 2	m	0.4851	0.4675	0.3750	0.3483	0.3854
Diameter nozzle exit stage 2	m	0.1757	0.2025	0.2144	0.2109	0.1995
Burn time stage 2	s	64.78	61.13	62.91	66.33	65.17
Chamber pressure stage 3	bar	72.69	66.58	77.17	81.64	77.95
Exit pressure stage 3	bar	0.1330	0.07051	0.10871	0.07759	0.08683
Diameter case stage 3	m	0.2658	0.2426	0.2562	0.2616	0.2651
Diameter nozzle exit stage 3	m	0.1345	0.1385	0.1178	0.1283	0.1338
Burn time stage 3	s	41.48	45.69	34.167	38.15	44.546
Length stage 1	m	3.017	2.120	2.120	1.980	2.117
Length stage 2	m	1.2963	0.9952	1.1243	1.2307	1.0605
Length stage 3	m	0.8013	0.7078	0.5666	0.5778	0.6846
Coasting time stage 1	s	9.919	5.572	8.635	7.624	7.798
Coasting time stage 2	s	538.7	450.8	556.9	599.1	448.3
Gravity loss	m·s ⁻¹	2,215	1,589	1,586	1,875	1,820
Drag loss	m·s ⁻¹	558.5	460.9	346.7	125.2	147.6
Steering loss	m·s ⁻¹	126.8	64.71	54.77	77.88	36.95
Maximum dynamic pressure	kPa	44.49	31.07	25.62	11.55	10.76
Maximum bending load	Pa·rad	1,250	9,116	3,533	807.9	3,020
Fairing separation	s	127.5	99.5	103.9	89.4	97.9
Semi-major axis	[km]	774.8	772.3	782.4	771.6	771.5
Eccentricity	[-]	0.003572	0.008334	0.002740	0.7564	0.8295
ΔV	m·s ⁻¹	9,858	8,851	8,687	8,718	8,716

Table J.2: Characteristics for the optimized ground launched vehicle and the optimized vehicles for various release flight path angles.

J.1.3 Release Altitude and Velocity

The figures for the thrust force and pitch path angle are already shown in Figure 11.9.

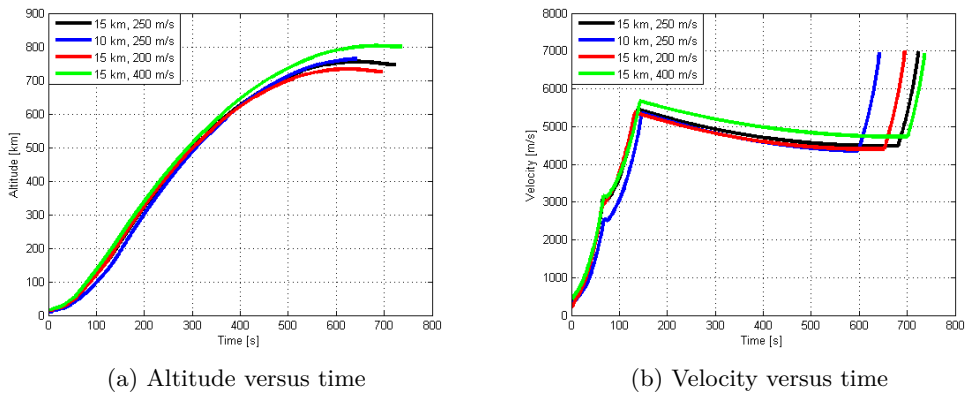


Figure J.9: Altitude and velocity versus time for the optimized air launched vehicles for various release altitudes and velocities.

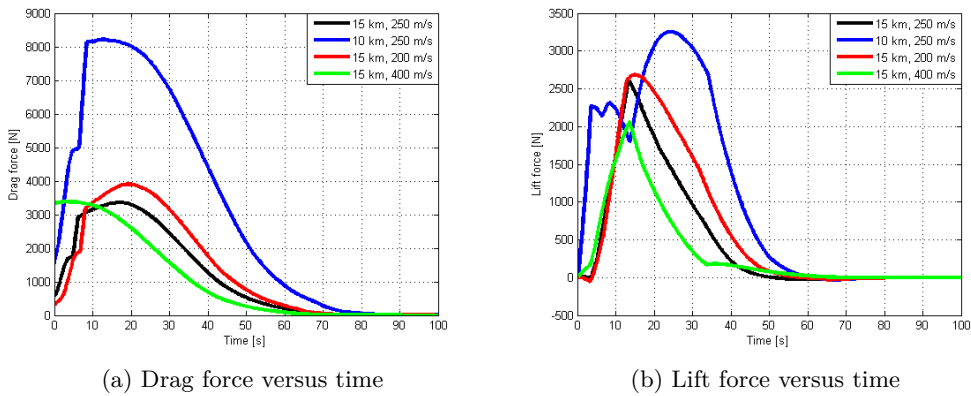
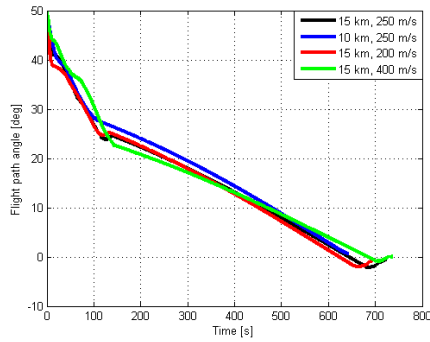
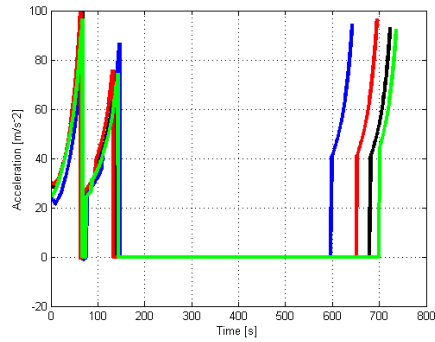


Figure J.10: Drag and lift force for the optimized air launched vehicles for various release altitudes and velocities.

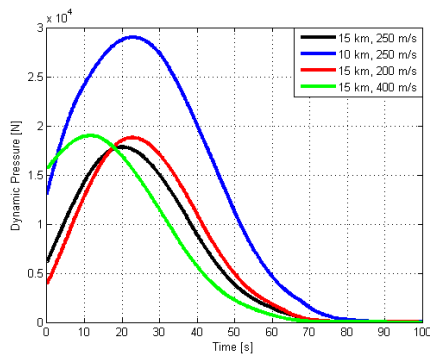


(a) Flight path angle versus time

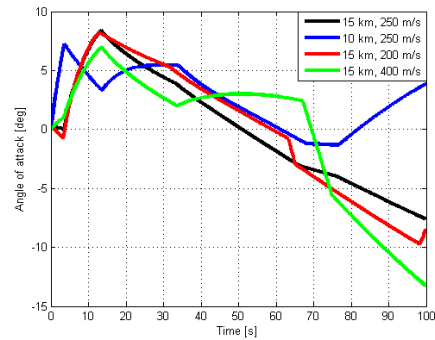


(b) Acceleration versus time

Figure J.11: Flight path angle and acceleration versus time for the optimized air launched vehicles for various release altitudes and velocities.

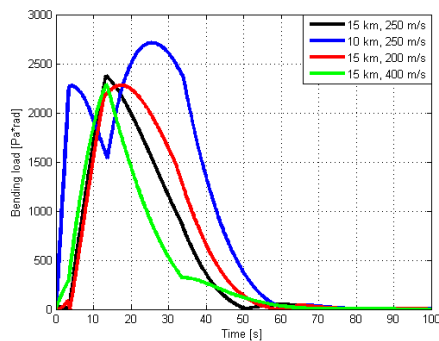


(a) Dynamic pressure versus time

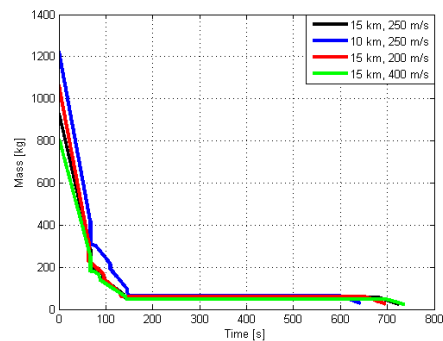


(b) Angle of attack versus time

Figure J.12: Dynamic pressure and angle of attack versus time for the optimized air launched vehicles for various release altitudes and velocities.



(a) Bending load versus time



(b) Mass versus time

Figure J.13: Bending load and mass versus time for the optimized air launched vehicles for various release altitudes and velocities.

Parameter	Unit	10 km, 250 m·s ⁻¹	15 km, 200 m·s ⁻¹	15 km, 400 m·s ⁻¹
Cost per flight	€M	2.080	1.973	1.813
GTOW	kg	1,225	1,064	807.3
Vehicle length	m	5.478	5.438	5.388
Vehicle diameter	m	0.6649	0.5947	0.5156
Vacuum thrust stage 1	kN	34.22	32.11	23.87
Vacuum thrust stage 2	kN	7.825	5.611	4.347
Vacuum thrust stage 3	kN	2.579	2.425	2.031
Isp stage 1	s	288.5	277.9	290.1
Isp stage 2	s	293.2	292.9	300.6
Isp stage 3	s	315.5	310.5	307.7
Inert mass stage 1	kg	72.29	69.47	48.24
Propellant mass stage 1	kg	844.7	765.4	577.7
Inert mass stage 2	kg	20.39	10.84	9.518
Propellant mass stage 2	kg	196.1	134.1	103.3
Inert mass stage 3	kg	5.195	4.445	3.278
Propellant mass stage 3	kg	38.54	35.28	24.44
Chamber pressure stage 1	bar	44.23	51.94	37.99
Exit pressure stage 1	bar	0.2128	0.4888	0.1625
Diameter case stage 1	m	0.6649	0.5947	0.5156
Diameter nozzle exit stage 1	m	0.3752	0.2600	0.3540
Burn time stage 1	s	67.82	63.09	66.88
Chamber pressure stage 2	bar	64.42	33.95	55.15
Exit pressure stage 2	bar	0.23297	0.11838	0.11525
Diameter case stage 2	m	0.4957	0.3852	0.3358
Diameter nozzle exit stage 2	m	0.1657	0.1966	0.1655
Burn time stage 2	s	69.97	66.65	68.01
Chamber pressure stage 3	bar	88.10	68.68	51.51
Exit pressure stage 3	bar	0.05656	0.06705	0.06173
Diameter case stage 3	m	0.2722	0.2813	0.2590
Diameter nozzle exit stage 3	m	0.1612	0.1498	0.1460
Burn time stage 3	s	44.901	43.025	35.283
Length stage 1	m	2.117	2.112	2.222
Length stage 2	m	1.011	1.0676	1.0318
Length stage 3	m	0.7257	0.6549	0.5759
Coasting time stage 1	s	8.756	1.808	7.740
Coasting time stage 2	s	452.1	521.1	558.5
Gravity loss	m·s ⁻¹	1,805	1,645	1,724
Drag loss	m·s ⁻¹	372.3	191.7	164.5
Steering loss	m·s ⁻¹	11.47	57.94	78.58
Maximum dynamic pressure	kPa	29.01	18.78	19.00
Maximum bending load	Pa·rad	2,711	2,279	2,293
Fairing separation	s	109.0	94.6	86.9
Semi-major axis	[km]	772.0	771.6	772.3
Eccentricity	[-]	0.009432	0.007595	0.004192
ΔV	m·s ⁻¹	8,904	8,686	8,482

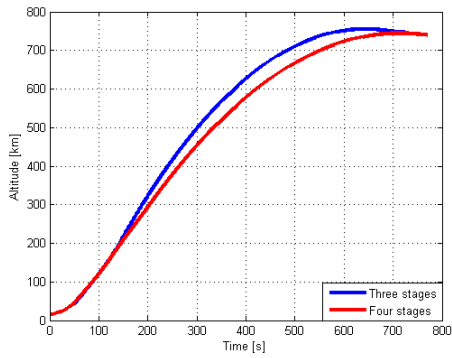
Table J.3: Characteristics for the optimized vehicles for different release altitude and velocities.

J.1.4 Number of Stages

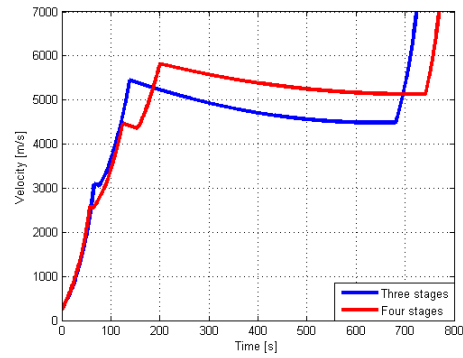
The pitch and flight path angle are already shown in Figure 11.11.

Parameter	Unit	Value	Parameter	Unit	Value
Cost per flight	€M	2.296	Diameter nozzle exit stage 2	m	0.2027
GTOW	kg	965.0	Burn time stage 2	s	59.94
Vehicle length	m	6.164	Chamber pressure stage 3	bar	37.05
Vehicle diameter	m	0.6210	Exit pressure stage 3	bar	0.07243
Vacuum thrust stage 1	kN	30.92	Diameter case stage 3	m	0.2875
Vacuum thrust stage 2	kN	6.046	Diameter nozzle exit stage 3	m	0.1546
Vacuum thrust stage 3	kN	2.406	Burn time stage 3	s	45.59
Vacuum thrust stage 4	kN	2.249	Chamber pressure stage 4	bar	30.85
Isp stage 1	s	290.3	Exit pressure stage 4	bar	0.05793
Isp stage 2	s	294.1	Diameter case stage 4	m	0.2259
Isp stage 3	s	301.1	Diameter nozzle exit stage 4	m	0.1665
Isp stage 3	s	301.4	Burn time stage 4	s	29.06
Inert mass stage 1	kg	73.92	Length stage 1	m	1.813
Propellant mass stage 1	kg	637.8	Length stage 2	m	1.007
Inert mass stage 2	kg	11.47	Length stage 3	m	0.6635
Propellant mass stage 2	kg	129.4	Length stage 4	m	0.6353
Inert mass stage 3	kg	3.719	Coasting time stage 1	s	7.378
Propellant mass stage 3	kg	38.24	Coasting time stage 2	s	30.35
Inert mass stage 4	kg	2.735	Coasting time stage 3	s	541.3
Propellant mass stage 4	kg	22.76	Gravity loss	m·s ⁻¹	1,617
Chamber pressure stage 1	bar	76.16	Drag loss	m·s ⁻¹	230.0
Exit pressure stage 1	bar	0.3382	Steering loss	m·s ⁻¹	53.88
Diameter case stage 1	m	0.6210	Maximum dynamic pressure	kPa	19.84
Diameter nozzle exit stage 1	m	0.2797	Maximum bending load	Pa·rad	2,431
Burn time stage 1	s	57.03	Fairing separation	s	93.8
Chamber pressure stage 2	bar	36.49	Semi-major axis	[km]	775.5
Exit pressure stage 2	bar	0.11790	Eccentricity	[-]	0.005458
Diameter case stage 2	m	0.4030	ΔV	m·s ⁻¹	8,637

Table J.4: Characteristics for the optimized four stage air launched vehicle.

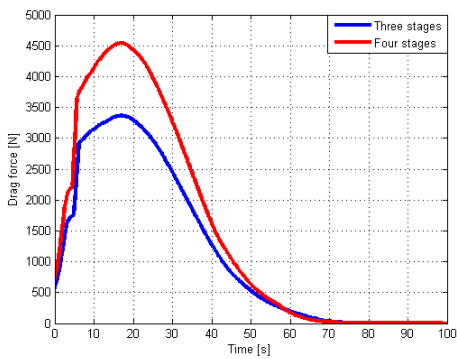


(a) Altitude versus time

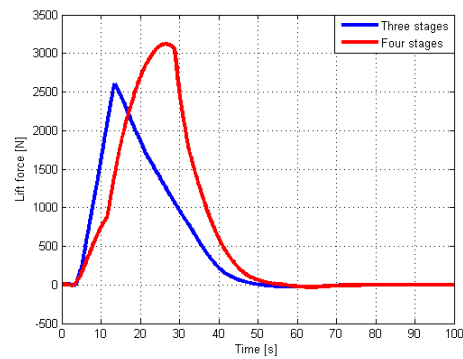


(b) Velocity versus time

Figure J.14: Altitude and velocity versus time for the three and four stage optimized air launched vehicle.

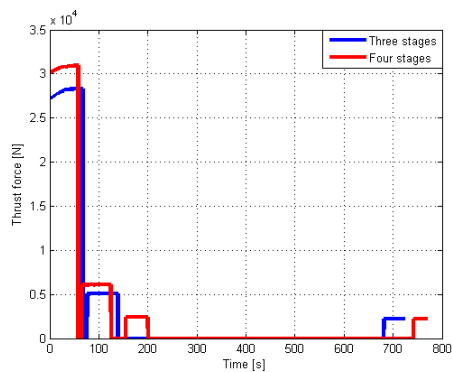


(a) Drag force versus time

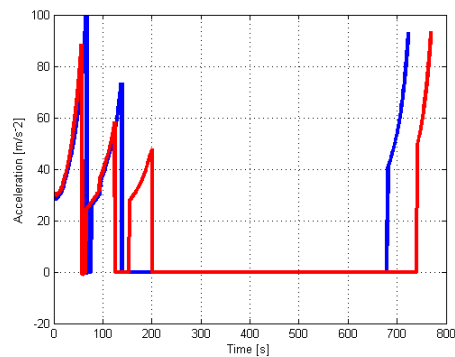


(b) Lift force versus time

Figure J.15: Drag and lift force for the three and four stage optimized air launched vehicle.

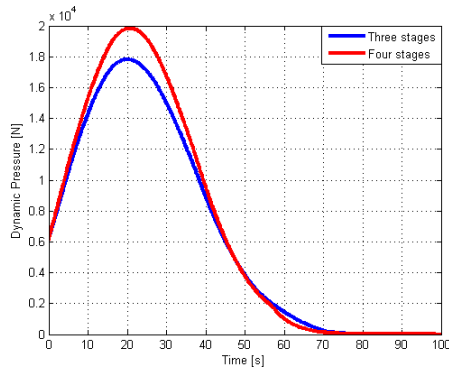


(a) Thrust force versus time

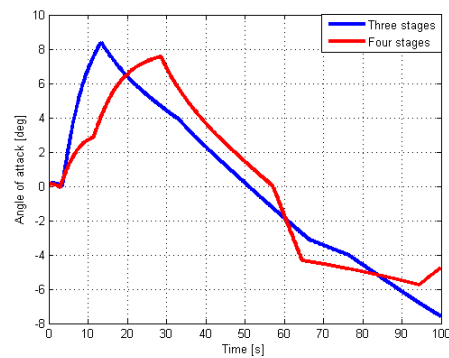


(b) Acceleration versus time

Figure J.16: Thrust force and acceleration versus time for the three and four stage optimized air launched vehicle.

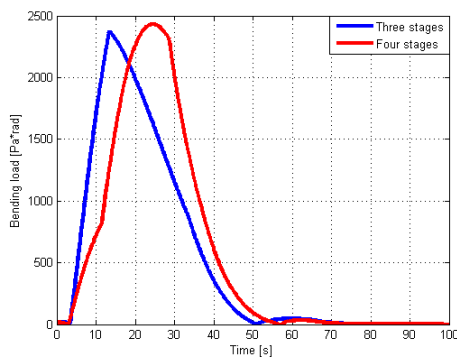


(a) Dynamic pressure versus time

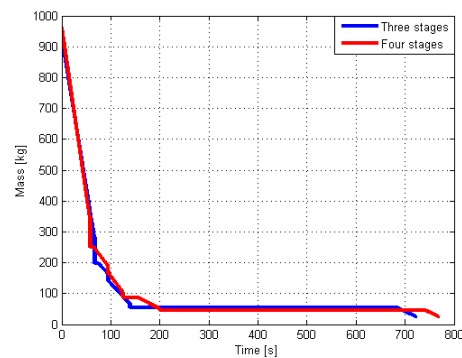


(b) Angle of attack versus time

Figure J.17: Dynamic pressure and angle of attack versus time for the three and four stage optimized air launched vehicle.



(a) Bending load versus time



(b) Mass versus time

Figure J.18: Bending load and mass versus time for the three and four stage optimized air launched vehicle.

J.2 2,000 kg Payload Class

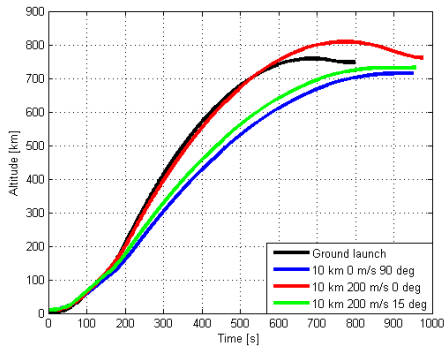
In this section the detailed characteristics of all optimized vehicles for the 2,000 kg payload class are given. The figures that are already shown in Section 11.2 will not be repeated in this appendix.

J.2.1 Ground Launch, Horizontal and Vertical Launch

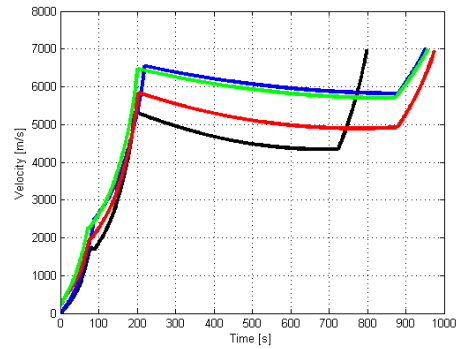
The figures for the angle of attack and bending load are already shown in Figure 11.12.

Parameter	Unit	Ground launch	10 km	10 km	10 km
			0 m·s ⁻¹	200 m·s ⁻¹	200 m·s ⁻¹
			90°	0°	15°
Cost per flight	€M	26.66	20.76	22.01	19.87
GTOW	kg	144,148	95,023	108,820	91,878
Vehicle length	m	35.41	32.21	29.65	29.00
Vehicle diameter	m	2.466	2.149	3.353	2.639
Vacuum thrust stage 1	kN	3,078	2,022	2,458	2,239
Vacuum thrust stage 2	kN	856.2	414.5	591.9	474.4
Vacuum thrust stage 3	kN	162.1	50.71	80.46	38.10
Isp stage 1	s	271.9	284.9	284.0	295.5
Isp stage 2	s	284.2	296.3	288.5	290.1
Isp stage 3	s	294.9	305.3	309.8	298.2
Inert mass stage 1	kg	8,262	4,625	5,481	5,669
Propellant mass stage 1	kg	92,702	65,857	68,280	58,310
Inert mass stage 2	kg	1,370	907.7	1,001	814.4
Propellant mass stage 2	kg	33,501	19,028	26,953	22,291
Inert mass stage 3	kg	328.6	129.9	212.6	108.3
Propellant mass stage 3	kg	4,350	1,238	2,641	1,176
Chamber pressure stage 1	bar	47.49	53.92	34.70	64.98
Exit pressure stage 1	bar	0.6230	0.3326	0.2188	0.1995
Diameter case stage 1	m	2.466	2.149	3.353	2.639
Diameter nozzle exit stage 1	m	2.355	2.374	3.242	2.974
Burn time stage 1	s	78.01	88.37	75.10	73.30
Chamber pressure stage 2	bar	34.80	42.84	31.05	28.63
Exit pressure stage 2	bar	0.2157	0.1207	0.1450	0.1316
Diameter case stage 2	m	1.972	1.664	1.894	1.763
Diameter nozzle exit stage 2	m	1.922	1.633	1.887	1.761
Burn time stage 2	s	105.9	129.5	125.1	129.8
Chamber pressure stage 3	bar	45.60	60.99	49.68	52.39
Exit pressure stage 3	bar	0.1424	0.0899	0.0500	0.1308
Diameter case stage 3	m	1.404	0.943	1.123	1.030
Diameter nozzle exit stage 3	m	0.9504	0.6170	1.0039	0.4690
Burn time stage 3	s	75.39	70.96	96.86	87.69
Length stage 1	m	14.26	13.84	9.240	10.72
Length stage 2	m	9.163	7.693	8.395	7.945
Length stage 3	m	3.360	2.234	3.348	1.858
Coasting time stage 1	s	10.49	2.020	3.193	1.616
Coasting time stage 2	s	528.7	660.6	675.2	704.6
Gravity loss	m·s ⁻¹	2,147	1,576	1,613	1,370
Drag loss	m·s ⁻¹	124.4	82.72	459.1	302.7
Steering loss	m·s ⁻¹	109.0	41.67	244.5	82.13
Maximum dynamic pressure	kPa	78.15	31.31	82.36	84.09
Maximum bending load	Pa·rad	3,875	2,924	17,931	15,224
Fairing separation	s	143.9	159.9	141.3	147.6
Semi-major axis	[km]	775.0	772.6	771.1	772.6
Eccentricity	[-]	0.008851	0.008745	0.008328	0.009035
ΔV	m·s ⁻¹	9,327	8,703	9,025	8,534

Table J.5: Characteristics for the optimized vehicles for ground launch and horizontal and vertical air launch conditions for the 2,000 kg payload class.

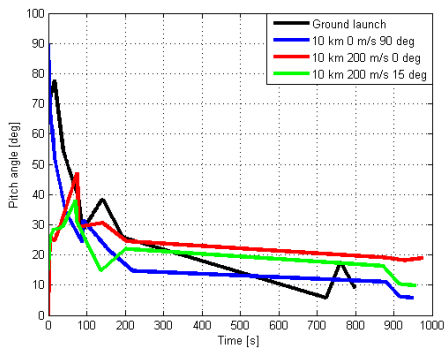


(a) Altitude versus time

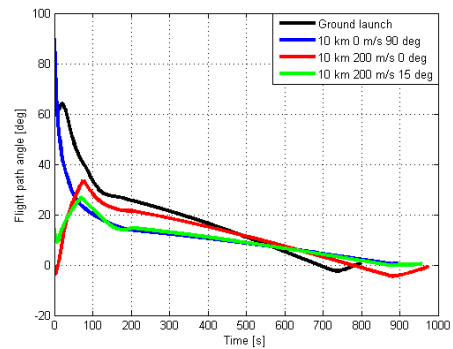


(b) Velocity versus time

Figure J.19: Altitude and velocity versus time for the optimized vehicles for ground launch and horizontal and vertical air launch conditions for the 2,000 kg payload class.

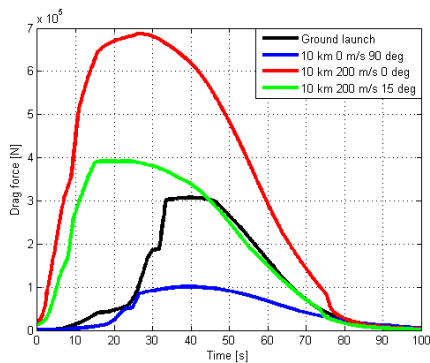


(a) Pitch angle versus time

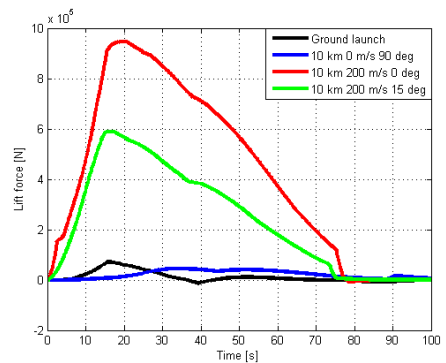


(b) Flight path angle versus time

Figure J.20: Pitch angle and flight path angle for ground launch and horizontal and vertical air launch conditions for the 2,000 kg payload class.



(a) Drag force versus time



(b) Lift force versus time

Figure J.21: Drag and lift force for the optimized vehicles for ground launch and horizontal and vertical air launch conditions for the 2,000 kg payload class.

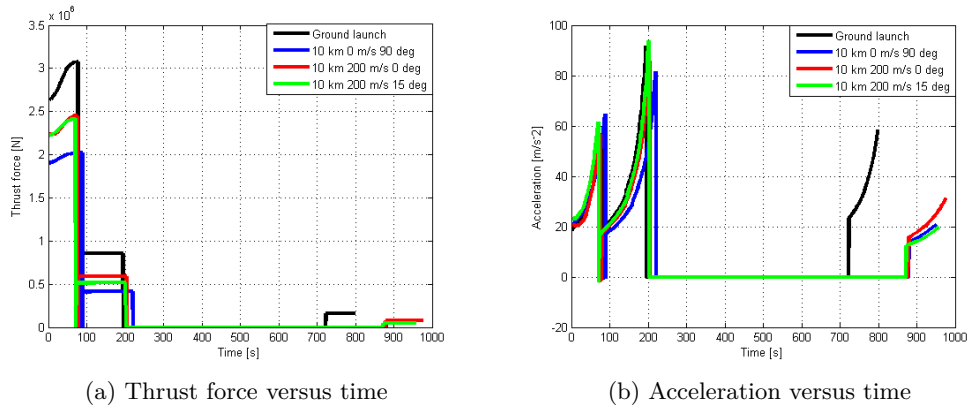


Figure J.22: Thrust force and acceleration versus time for the optimized vehicles for ground launch and horizontal and vertical air launch conditions for the 2,000 kg payload class.

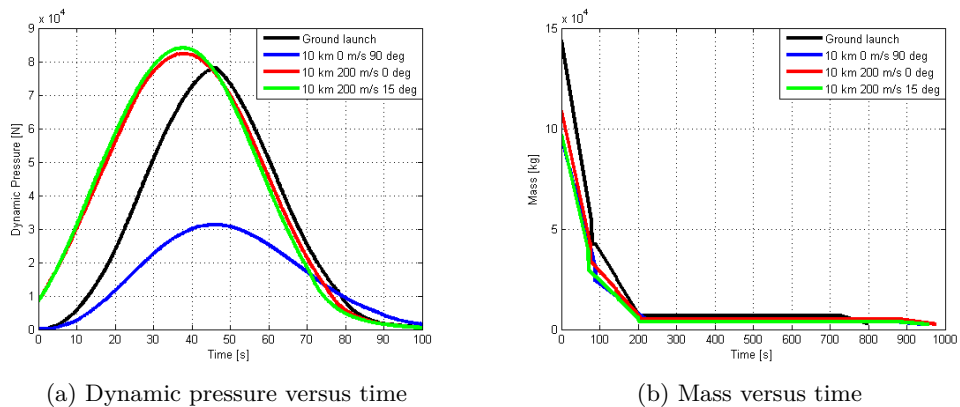


Figure J.23: Dynamic pressure and mass versus time for the optimized vehicles for ground launch and horizontal and vertical air launch conditions for the 2,000 kg payload class.

J.2.2 Release Altitude and Velocity

In this section the figures for the optimized vehicles for a different release altitude and velocity are given.

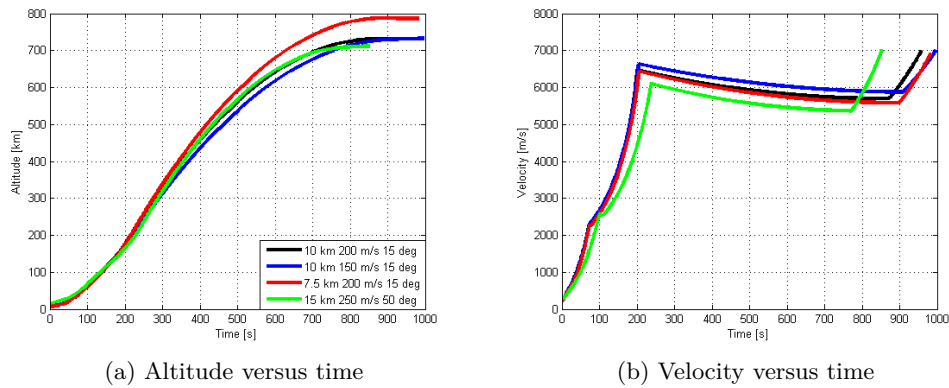


Figure J.24: Altitude and velocity versus time for the optimized air launched vehicles for various release altitudes and velocities for the 2,000 kg payload class.

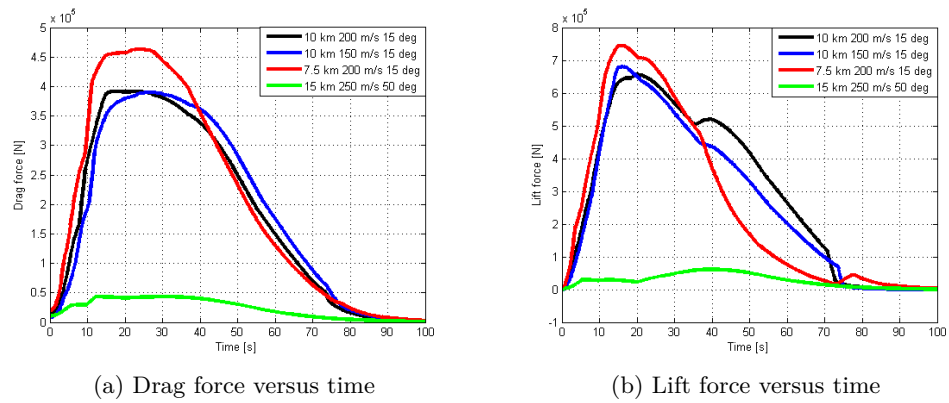


Figure J.25: Drag and lift force versus time for the optimized air launched vehicles for various release altitudes and velocities for the 2,000 kg payload class.

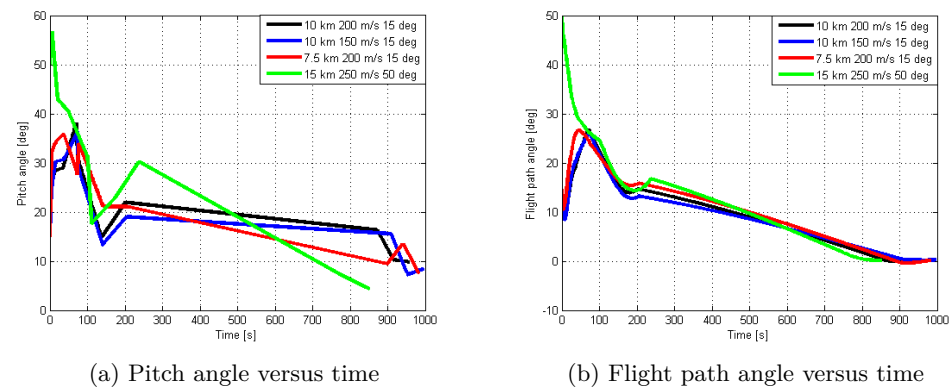
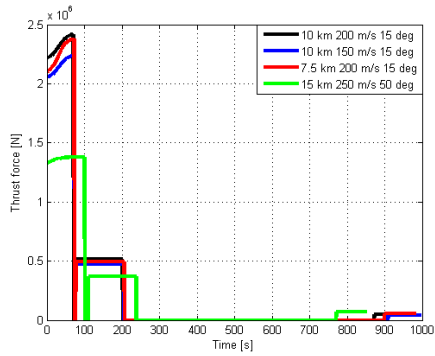


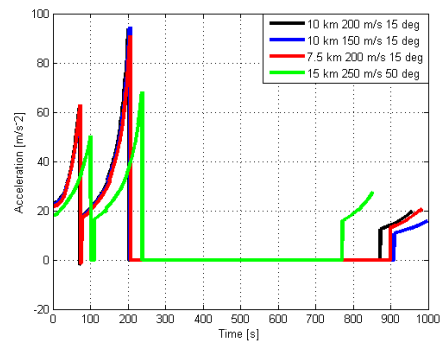
Figure J.26: Pitch angle and flight path angle versus time for the optimized air launched vehicles for various release altitudes and velocities for the 2,000 kg payload class.

Parameter	Unit	10 km	7.5 km	15 km
		150 m·s ⁻¹	200 m·s ⁻¹	250 m·s ⁻¹
		15°	15°	50°
Cost per flight	€M	20.35	20.56	18.30
GTOW	kg	95,938	97,236	75,182
Vehicle length	m	29.38	29.78	31.23
Vehicle diameter	m	2.698	2.678	2.035
Vacuum thrust stage 1	kN	2,325	2,382	1,380
Vacuum thrust stage 2	kN	502.0	494.6	371.3
Vacuum thrust stage 3	kN	41.47	51.19	67.00
Isp stage 1	s	295.3	295.7	295.0
Isp stage 2	s	288.9	288.9	291.7
Isp stage 3	s	298.3	298.0	308.8
Inert mass stage 1	kg	6,017	6,267	3201
Propellant mass stage 1	kg	60,981	61,833	49,110
Inert mass stage 2	kg	844.9	845.3	729.9
Propellant mass stage 2	kg	23,178	23,104	16,953
Inert mass stage 3	kg	112.1	131.4	157.6
Propellant mass stage 3	kg	1,259	1,507	1,843
Chamber pressure stage 1	bar	64.58	66.12	63.50
Exit pressure stage 1	bar	0.2019	0.2002	0.2010
Diameter case stage 1	m	2.698	2.678	2.035
Diameter nozzle exit stage 1	m	3.019	3.058	2.334
Burn time stage 1	s	73.76	73.11	99.98
Chamber pressure stage 2	bar	29.17	29.44	33.80
Exit pressure stage 2	bar	0.1448	0.1459	0.1282
Diameter case stage 2	m	1.758	1.763	1.575
Diameter nozzle exit stage 2	m	1.743	1.723	1.551
Burn time stage 2	s	127.1	128.5	126.9
Chamber pressure stage 3	bar	52.55	53.21	51.16
Exit pressure stage 3	bar	0.1303	0.1349	0.0561
Diameter case stage 3	m	0.976	0.968	0.874
Diameter nozzle exit stage 3	m	0.4898	0.5361	0.8723
Burn time stage 3	s	86.29	83.53	80.89
Length stage 1	m	10.80	11.02	12.27
Length stage 2	m	8.143	8.074	7.451
Length stage 3	m	2.012	2.268	3.284
Coasting time stage 1	s	4.508	4.392	10.585
Coasting time stage 2	s	704.7	693.4	534.5
Gravity loss	m·s ⁻¹	1,359	1,521	1,624
Drag loss	m·s ⁻¹	304.8	312.4	41.17
Steering loss	m·s ⁻¹	92.83	95.63	111.5
Maximum dynamic pressure	kPa	79.23	86.67	11.20
Maximum bending load	Pa·rad	15,670	17,573	2,072
Fairing separation	s	147.6	151.8	142.7
Semi-major axis	[km]	770.4	770.5	772.8
Eccentricity	[-]	0.004702	0.003591	0.002584
ΔV	m·s ⁻¹	8,600	8,641	8,530

Table J.6: Characteristics for the optimized air launched vehicles for different release altitudes and velocities for the 2,000 kg payload class.

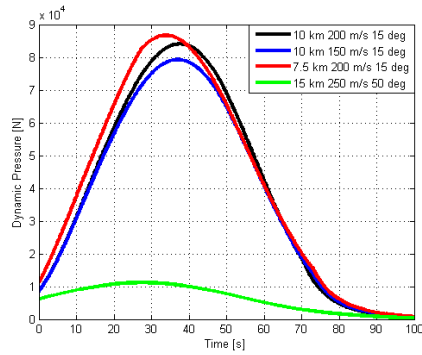


(a) Thrust force versus time

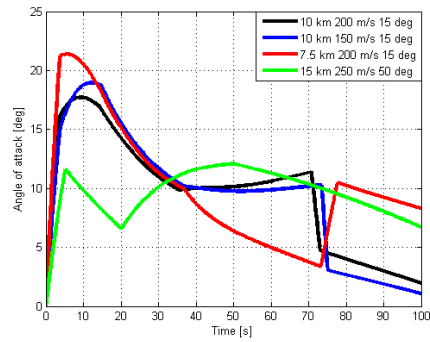


(b) Acceleration versus time

Figure J.27: Thrust force and acceleration versus time for the optimized air launched vehicles for various release altitudes and velocities for the 2,000 kg payload class.

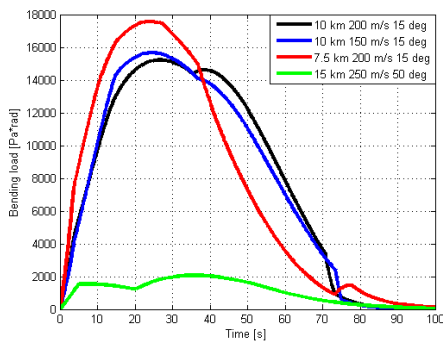


(a) Dynamic pressure versus time

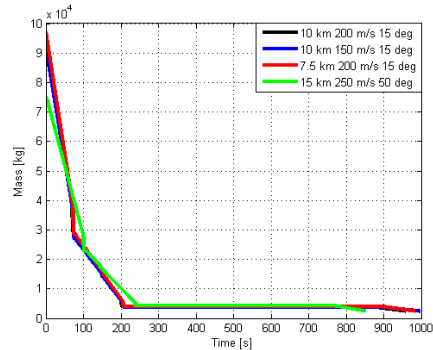


(b) Angle of attack versus time

Figure J.28: Dynamic pressure and angle of attack versus time for the optimized air launched vehicles for various release altitudes and velocities for the 2,000 kg payload class.



(a) Bending load versus time



(b) Mass versus time

Figure J.29: Bending load and mass versus time for the optimized air launched vehicles for various release altitudes and velocities for the 2,000 kg payload class.

J.2.3 Winged Vehicles

The figures for the dynamic pressure and angle of attack and the drag and lift force are already given in Figure 11.14 and 11.14.

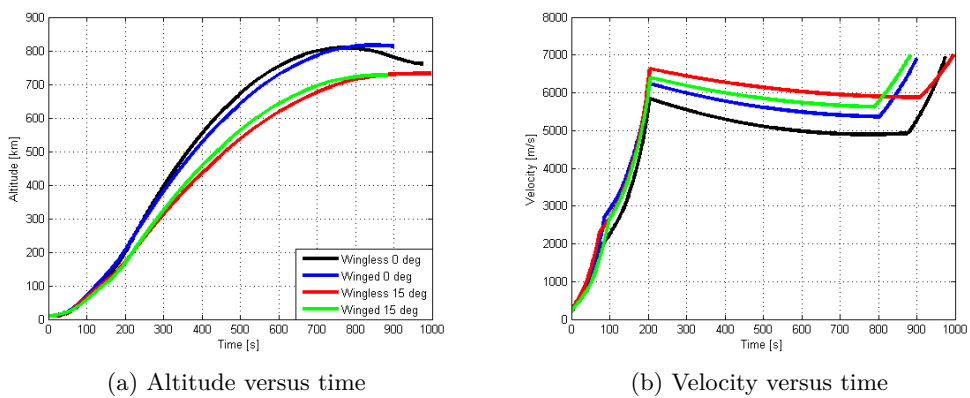


Figure J.30: Altitude and velocity versus time for the optimized winged air launched vehicles for the 2,000 kg payload class.

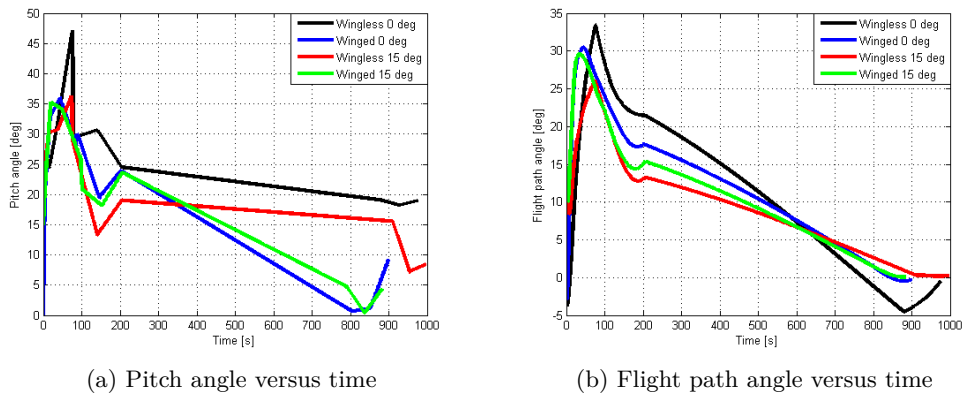


Figure J.31: Pitch angle and flight path angle versus time for the optimized winged air launched vehicles for the 2,000 kg payload class.

Parameter	Unit	10 km	10 km
		200 m·s ⁻¹	200 m·s ⁻¹
		0°	15°
Cost per flight	€M	21.43	20.79
GTOW	kg	87,206	83,173
Vehicle length	m	30.21	30.67
Vehicle diameter	m	2.281	2.121
Vacuum thrust stage 1	kN	1,942	1,605
Vacuum thrust stage 2	kN	393.7	440.5
Vacuum thrust stage 3	kN	51.71	45.70
Isp stage 1	s	286.6	288.2
Isp stage 2	s	301.4	298.5
Isp stage 3	s	304.6	305.6
Inert mass stage 1	kg	4,254	3,540
Propellant mass stage 1	kg	61,120	57,350
Inert mass stage 2	kg	899.7	885.7
Propellant mass stage 2	kg	15,706	16,526
Inert mass stage 3	kg	154.2	128.7
Propellant mass stage 3	kg	1,718	1,474
Chamber pressure stage 1	bar	46.94	49.72
Exit pressure stage 1	bar	0.2567	0.2459
Diameter case stage 1	m	2.281	2.121
Diameter nozzle exit stage 1	m	2.611	2.397
Burn time stage 1	s	85.91	98.10
Chamber pressure stage 2	bar	49.08	44.25
Exit pressure stage 2	bar	0.09614	0.1062
Diameter case stage 2	m	1.715	1.767
Diameter nozzle exit stage 2	m	1.714	1.763
Burn time stage 2	s	114.5	106.7
Chamber pressure stage 3	bar	60.22	53.37
Exit pressure stage 3	bar	0.09380	0.07619
Diameter case stage 3	m	1.025	0.9878
Diameter nozzle exit stage 3	m	0.6134	0.6346
Burn time stage 3	s	96.40	93.89
Mean chord length	m	3.504	3.567
Wing mass	kg	154.4	160.4
Length stage 1	m	12.35	12.85
Length stage 2	m	6.772	6.773
Length stage 3	m	2.445	2.368
Coasting time stage 1	s	1.779	1.179
Coasting time stage 2	s	601.0	583.8
Gravity loss	m·s ⁻¹	1,609	1,483
Drag loss	m·s ⁻¹	271.0	234.9
Steering loss	m·s ⁻¹	34.14	36.03
Maximum dynamic pressure	kPa	48.84	36.83
Maximum bending load	Pa·rad	6,544	5,481
Fairing separation	s	134.6	157.3
Semi-major axis	[km]	771.0	773.2
Eccentricity	[-]	0.007927	0.0008143
ΔV	m·s ⁻¹	8,609	8,550

Table J.7: Characteristics for the optimized winged air launched vehicles for the 2,000 kg payload class.

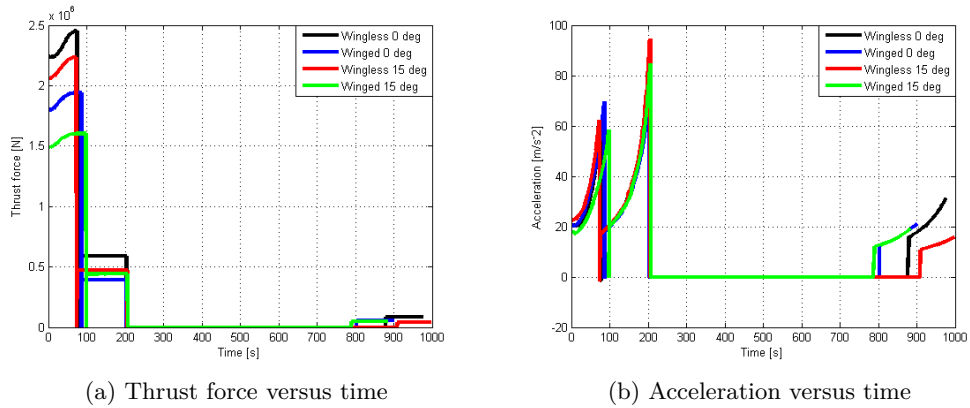


Figure J.32: Thrust force and acceleration versus time for the optimized winged air launched vehicles for the 2,000 kg payload class.

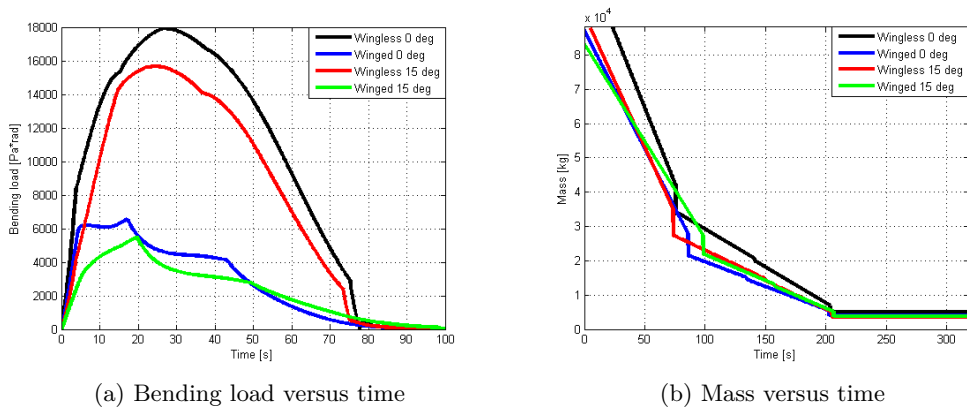
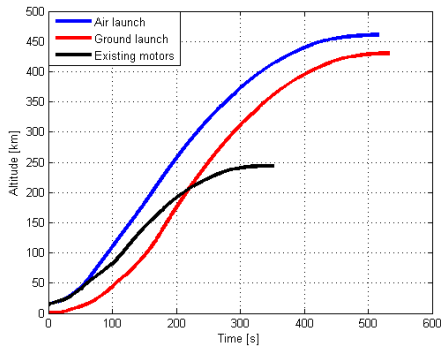


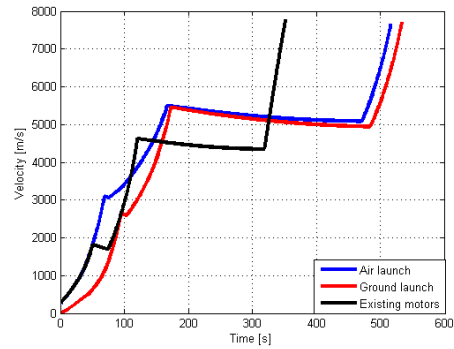
Figure J.33: Bending load and mass versus time for the optimized winged air launched vehicles for the 2,000 kg payload class.

J.3 Launch from Andøya

In this section the figures for the launch from Andøya are given. This also includes the figures for the launch vehicle that is based on COTS SRMs.

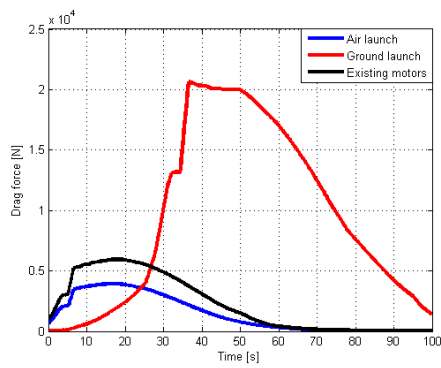


(a) Altitude versus time

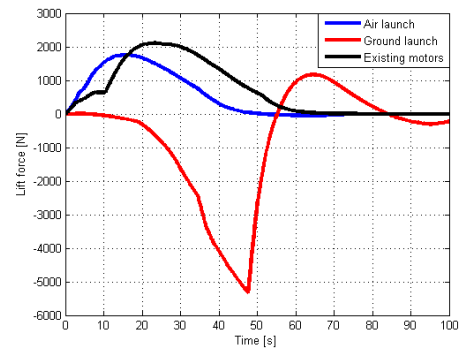


(b) Velocity versus time

Figure J.34: Altitude and velocity versus time for the optimized vehicles for the launch from Andøya.

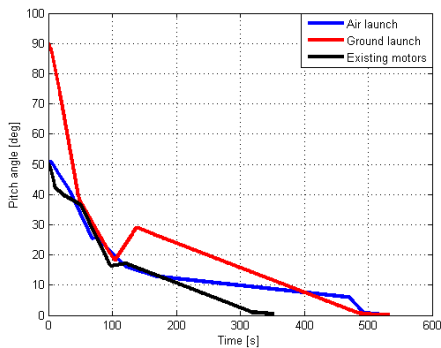


(a) Drag force versus time

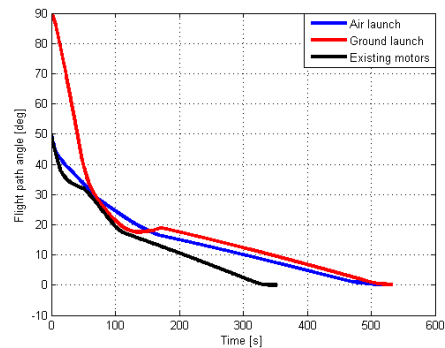


(b) Lift force versus time

Figure J.35: Drag and lift force versus time for the optimized vehicles for the launch from Andøya.



(a) Pitch angle versus time

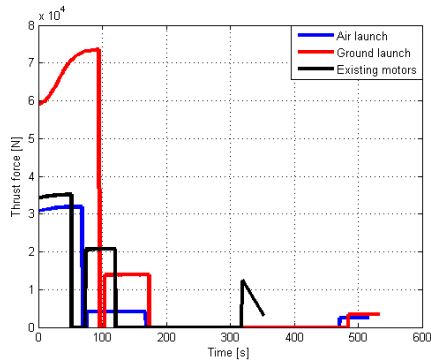


(b) Flight path angle versus time

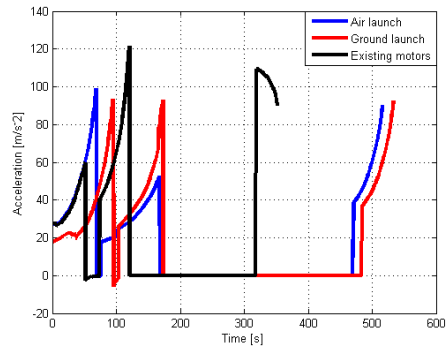
Figure J.36: Pitch angle and flight path angle versus time for the optimized vehicles for the launch from Andøya.

Parameter	Unit	Air launch	Ground launch	Existing motors
Payload	kg	12.50	12.50	10.00
Cost per flight	€M	1.999	2.730	2.131
GTOW	kg	1,107	3,325	1,197
Vehicle length	m	5.471	8.620	5.221
Vehicle diameter	m	0.6222	0.6711	0.763
Vacuum thrust stage 1	kN	31.89	73.55	35.14
Vacuum thrust stage 2	kN	4.103	13.86	20.68
Vacuum thrust stage 3	kN	2.459	3.507	[3.105 , 12.46]
Isp stage 1	s	284.2	277.3	290.4
Isp stage 2	s	293.4	292.9	291.4
Isp stage 3	s	307.7	302.0	281.8
Inert mass stage 1	kg	65.37	170.4	42.50
Propellant mass stage 1	kg	808.5	2646	631.4
Inert mass stage 2	kg	9.006	42.98	29.98
Propellant mass stage 2	kg	134.1	340.5	337.8
Inert mass stage 3	kg	4.223	7.025	14.02
Propellant mass stage 3	kg	38.46	60.62	79.60
Chamber pressure stage 1	bar	39.35	43.87	37.02
Exit pressure stage 1	bar	0.2472	0.4210	0.06589
Diameter case stage 1	m	0.6222	0.6711	0.7620
Diameter nozzle exit stage 1	m	0.3470	0.4252	0.6000
Burn time stage 1	s	68.61	95.01	51.1
Chamber pressure stage 2	bar	32.98	89.86	41.02
Exit pressure stage 2	bar	0.1111	0.3385	-
Diameter case stage 2	m	0.3950	0.6239	0.6934
Diameter nozzle exit stage 2	m	0.1729	0.1835	0.5052
Burn time stage 2	s	91.35	68.57	46.3
Chamber pressure stage 3	bar	54.37	73.52	61.02
Exit pressure stage 3	bar	0.0653	0.1417	-
Diameter case stage 3	m	0.2792	0.3209	0.3820
Diameter nozzle exit stage 3	m	0.1563	0.1327	0.2062
Burn time stage 3	s	45.83	49.72	33.3
Length stage 1	m	2.178	5.018	1.684
Length stage 2	m	1.016	1.149	1.219
Length stage 3	m	0.6933	0.7475	0.8019
Coasting time stage 1	s	7.519	8.961	23.04
Coasting time stage 2	s	303.5	311.6	198.3
Gravity loss	m·s ⁻¹	1,186	1,417	848.3
Drag loss	m·s ⁻¹	183.0	588.2	269.3
Steering loss	m·s ⁻¹	14.54	35.77	7.916
Maximum dynamic pressure	kPa	16.56	67.85	17.61
Maximum bending load	Pa·rad	1,541	3,957	1,476
Fairing separation	s	101.0	165.9	120.4
Semi-major axis	[km]	496.8	490.1	244.0
Eccentricity	[-]	0.004457	0.002952	0.0004186
ΔV	m·s ⁻¹	8,813	9,748	8,654

Table J.8: Characteristics for the optimized vehicles for the launch from Andøya.

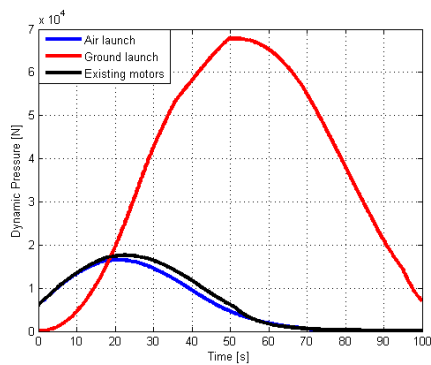


(a) Thrust force versus time

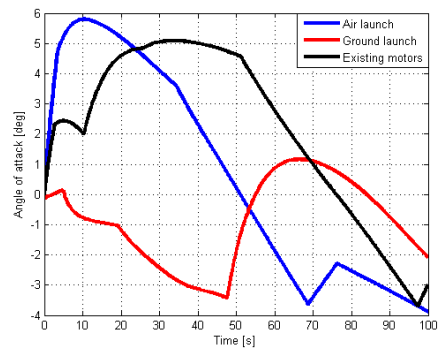


(b) Acceleration versus time

Figure J.37: Thrust force and acceleration versus time for the optimized vehicles for the launch from Andøya.

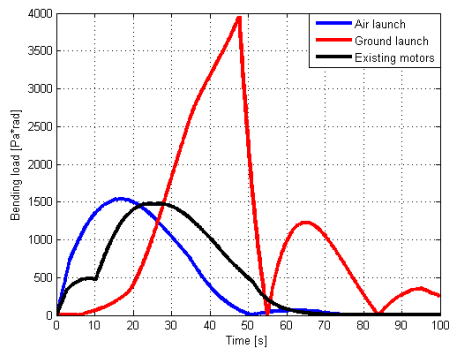


(a) Dynamic pressure versus time

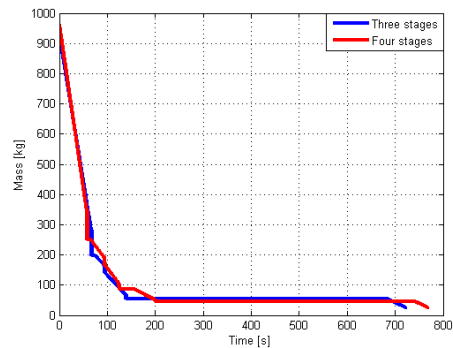


(b) Angle of attack versus time

Figure J.38: Dynamic pressure and angle of attack versus time for the optimized vehicles for the launch from Andøya.



(a) Bending load versus time



(b) Mass versus time

Figure J.39: Bending load and mass versus time for the optimized vehicles for the launch from Andøya.

J.4 Effects of a Regressive Burning Grain

The thrust force and acceleration versus time are already shown in Figure 12.5.

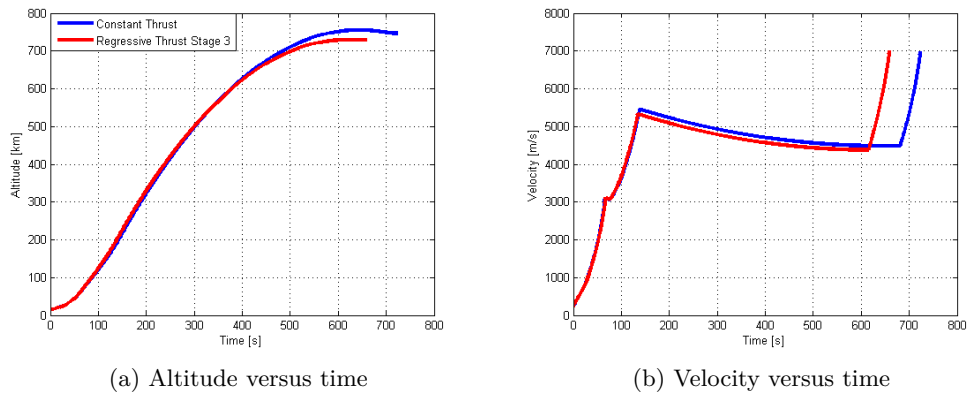


Figure J.40: Altitude and velocity versus time for the optimized air launched vehicle with a regressive burning third stage.

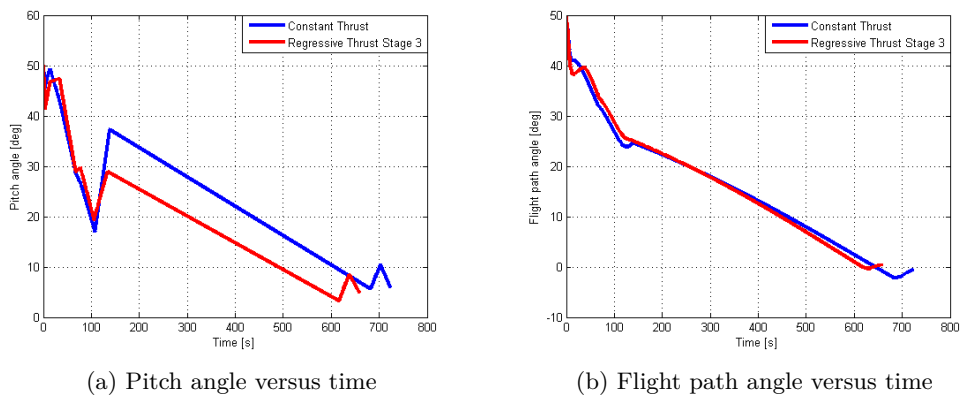
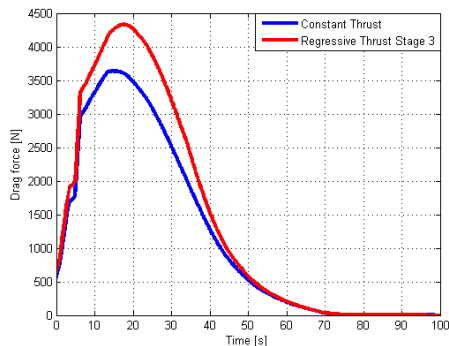


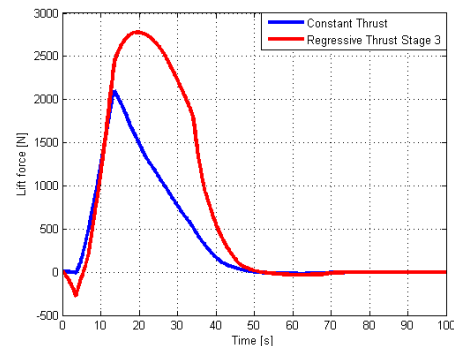
Figure J.41: Pitch angle and flight path angle for the optimized air launched vehicle with a regressive burning third stage.

Parameter	Unit	Value	Parameter	Value	Regressive thrust
Cost per flight	€M	2.034	Diameter nozzle exit stage 2	m	0.1809
GTOW	kg	1,170	Burn time stage 2	s	57.37
Vehicle length	m	5.744	Chamber pressure stage 3	bar	52.69
Vehicle diameter	m	0.5950	Exit pressure stage 3	bar	0.07828
Max. vacuum thrust stage 1	kN	35333	Diameter case stage 3	m	0.3134
Max. vacuum thrust stage 2	kN	6582	Diameter nozzle exit stage 3	m	0.1612
Max. vacuum thrust stage 3	kN	3007	Burn time stage 3	s	43.47
Isp stage 1	s	295.1	Length stage 1	m	2.535
Isp stage 2	s	292.6	Length stage 2	m	0.9029
Isp stage 3	s	305.1	Length stage 3	m	0.6864
Inert mass stage 1	kg	75.40	Coasting time stage 1	s	9.068
Propellant mass stage 1	kg	849.4	Coasting time stage 2	s	481.8
Inert mass stage 2	kg	13.47	Gravity loss	m·s ⁻¹	1,672
Propellant mass stage 2	kg	135.5	Drag loss	m·s ⁻¹	166.5
Inert mass stage 3	kg	4.754	Steering loss	m·s ⁻¹	39.57
Propellant mass stage 3	kg	44.98	Maximum dynamic pressure	kPa	18.57
Chamber pressure stage 1	bar	48.10	Maximum bending load	Pa·rad	2,726
Exit pressure stage 1	bar	0.1483	Fairing separation	s	92.8
Diameter case stage 1	m	0.5950	Semi-major axis	[km]	773.5
Diameter nozzle exit stage 1	m	0.4341	Eccentricity	[-]	0.009562
Burn time stage 1	s	67.58	ΔV	m·s ⁻¹	8,623
Chamber pressure stage 2	bar	45.20	Thrust fraction of stage 1	[-]	0.9737
Exit pressure stage 2	bar	0.1653	Thrust fraction of stage 2	[-]	0.9591
Diameter case stage 2	m	0.4538	Thrust fraction of stage 3	[-]	0.7918

Table J.9: Characteristics for the optimized air launched vehicle with a regressive burning third stage.



(a) Drag force versus time



(b) Lift force versus time

Figure J.42: Drag and lift force for the optimized air launched vehicle with a regressive burning third stage.

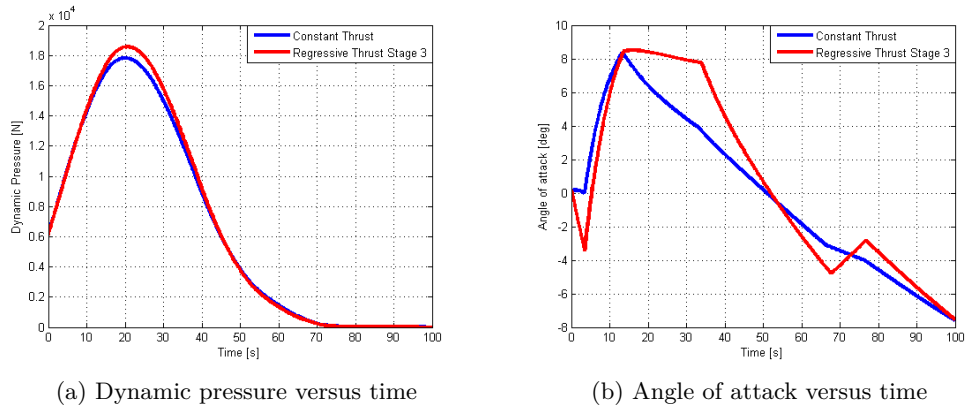


Figure J.43: Dynamic pressure and angle of attack versus time for the optimized air launched vehicle with a regressive burning third stage.

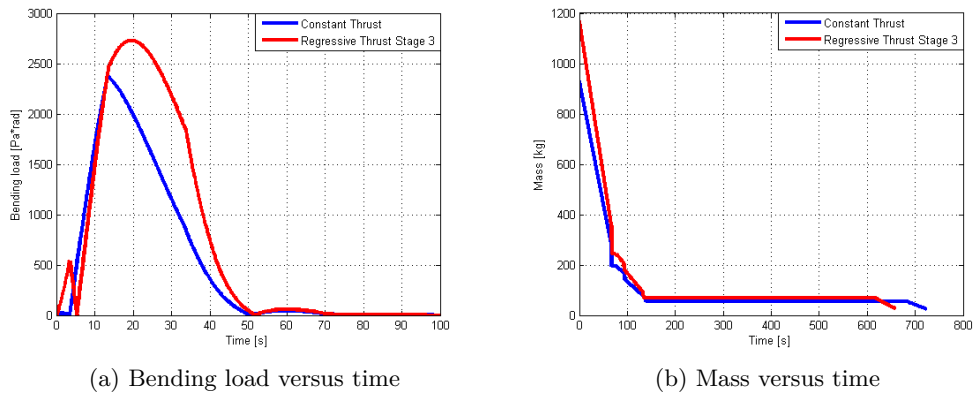
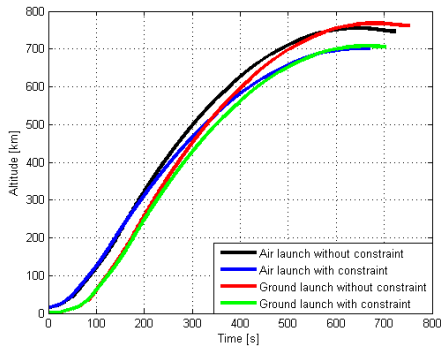


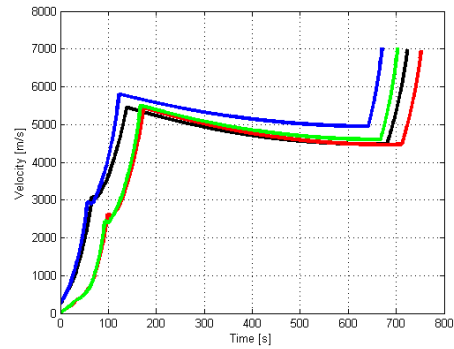
Figure J.44: Bending load and mass versus time for the optimized air launched vehicle with a regressive burning third stage.

J.5 Effect of the Implementation of a Constraint for the Web Thickness Case Diameter Ratio

In this section the detailed vehicles characteristics and figures for the optimized vehicles after the implementation of a constraint for the web thickness case diameter ratio.

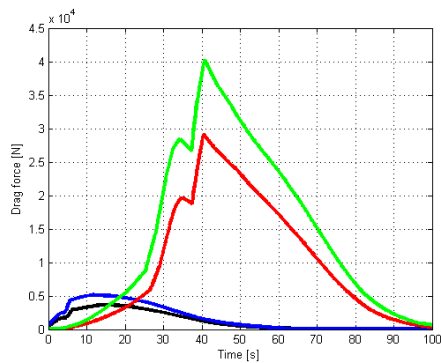


(a) Altitude versus time

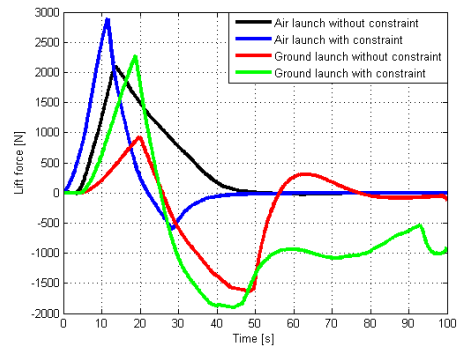


(b) Velocity versus time

Figure J.45: Altitude and velocity versus time for the optimized vehicles with or without the $\frac{2 \cdot w}{D_{case}}$ constraint.

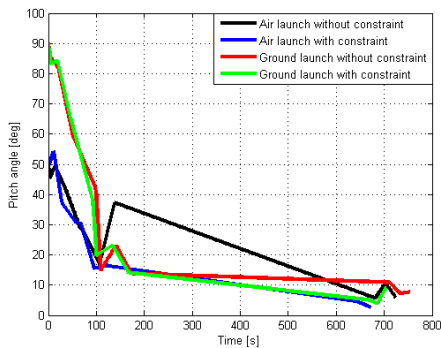


(a) Drag force versus time

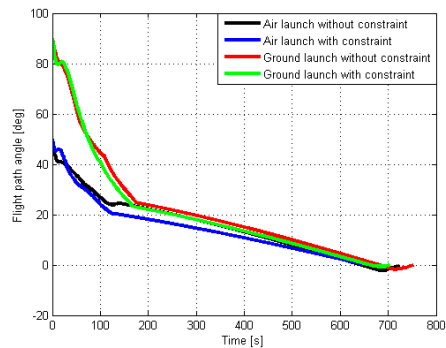


(b) Lift force versus time

Figure J.46: Drag and lift force versus time for the optimized vehicles with or without the $\frac{2 \cdot w}{D_{case}}$ constraint.



(a) Pitch angle versus time

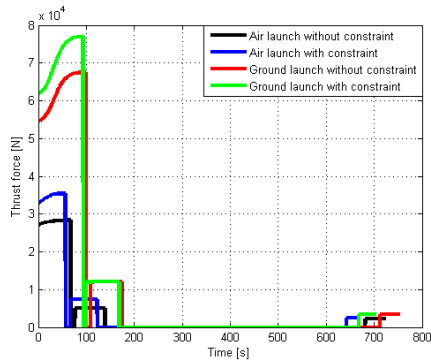


(b) Flight path angle versus time

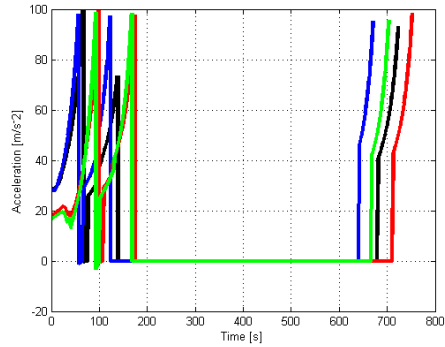
Figure J.47: Pitch angle and flight path angle versus time for the optimized vehicles with or without the $\frac{2 \cdot w}{D_{case}}$ constraint.

Parameter	Unit	Air launch	Ground launch
Cost per flight	€M	1.937	2.691
GTOW	kg	1,017	3393
Vehicle length	m	5.301	5.890
Vehicle diameter	m	0.6696	1.113
Vacuum thrust stage 1	kN	36,493	76,979
Vacuum thrust stage 2	kN	7,448	11,934
Vacuum thrust stage 3	kN	2,414	3,382
Isp stage 1	s	293.9	269.5
Isp stage 2	s	296.7	281.4
Isp stage 3	s	290.9	296.7
Inert mass stage 1	kg	65.29	163.7
Propellant mass stage 1	kg	734.7	2,785
Inert mass stage 2	kg	16.12	27.27
Propellant mass stage 2	kg	150.1	299.8
Inert mass stage 3	kg	3.418	4.929
Propellant mass stage 3	kg	26.54	42.90
Chamber pressure stage 1	bar	31.28	32.37
Exit pressure stage 1	bar	0.1015	0.4720
Diameter case stage 1	m	0.6689	1.1126
Diameter nozzle exit stage 1	m	0.5375	0.4345
Burn time stage 1	s	56.35	92.88
Chamber pressure stage 2	bar	30.25	30.00
Exit pressure stage 2	bar	0.08037	0.21845
Diameter case stage 2	m	0.6686	0.7947
Diameter nozzle exit stage 2	m	0.2670	0.2301
Burn time stage 2	s	56.94	67.34
Chamber pressure stage 3	bar	30.80	30.26
Exit pressure stage 3	bar	0.12256	0.08036
Diameter case stage 3	m	0.3748	0.4245
Diameter nozzle exit stage 3	m	0.1287	0.1799
Burn time stage 3	s	30.457	35.837
Length stage 1	m	2.125	2.532
Length stage 2	m	0.8795	0.9590
Length stage 3	m	0.4613	0.5883
Coasting time stage 1	s	9.837	7.211
Coasting time stage 2	s	514.2	500.2
Gravity loss	m·s ⁻¹	1,496	2,086
Drag loss	m·s ⁻¹	233.4	790.7
Steering loss	m·s ⁻¹	27.23	79.23
Maximum dynamic pressure	kPa	18.54	42.53
Maximum bending load	Pa·rad	2,421	1,175
Fairing separation	s	93.10	130.6
Semi-major axis	[km]	770.9	770.4
Eccentricity	[-]	0.009657	0.009046
ΔV	m·s ⁻¹	8,542	9,981

Table J.10: Characteristics for the optimized vehicles with the $\frac{2 \cdot w}{D_{case}}$ constraint.

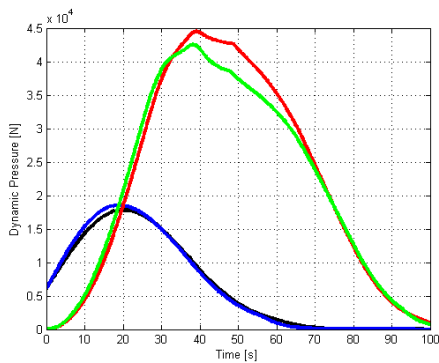


(a) Thrust force versus time

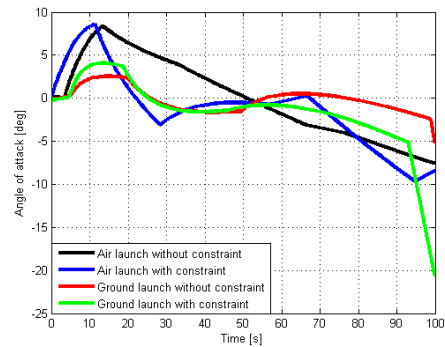


(b) Acceleration versus time

Figure J.48: Thrust force and acceleration versus time for the optimized vehicles with or without the $\frac{2 \cdot w}{D_{case}}$ constraint.

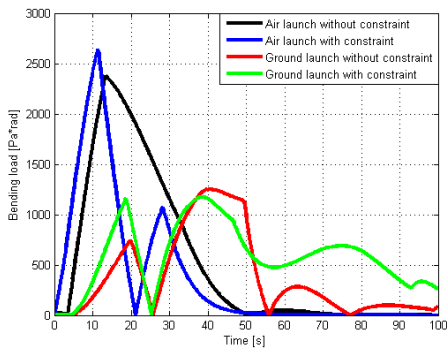


(a) Dynamic pressure versus time

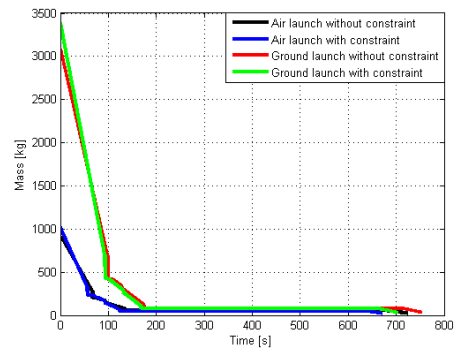


(b) Angle of attack versus time

Figure J.49: Dynamic pressure and angle of attack versus time for the optimized vehicles with or without the $\frac{2 \cdot w}{D_{case}}$ constraint.



(a) Bending load versus time



(b) Mass versus time

Figure J.50: Bending load and mass versus time for the optimized vehicles with or without the $\frac{2 \cdot w}{D_{case}}$ constraint.

References

- [1] M.A. Aldheeb, R. Kafafy, M. Idres, H.M. Omar, and M.A. Abido. Design Optimization of Micro Air Launch Vehicle Using Differential Evolution. *Journal of Aerospace Technology and Management*, Vol. 4, No. 2, pp. 185-196, 2012.
- [2] B.A.C. Ambrosius and H. Wittenberg. *AE4870A - Rocket Motion*. Lecture Notes, TU Delft, 2009.
- [3] Andøya Rocket Range. *Andøya Rocket Range The Cost-effective Entrance to Space*. Andøya Rocket Range, 2013. Web site: <http://www.rocketrange.no/> [Last accessed: September18th, 2013].
- [4] ATK. *ATK Space Propulsion Products Catalog*. ATK, 2008.
- [5] M. Balesdent. *Multidisciplinary Design Optimization of Launch Vehicles*. PhD dissertation, Ecole Centrale de Nantes, 2011.
- [6] P.A. Bartolotta, E. Buchen, W.C. Engeland, L.D. Huebner, P.L. Moses, M. Schaffer, R.T. Volland, D.F. Voracek, and A.W. Wilhite. *Horizontal launch: versatile concept for assured space access*. NASA, SP 2011-215994, 2011.
- [7] D.J. Bayley. *Design Optimization of Space Launch Vehicles Using a Genetic Algorithm*. PhD dissertation, Auburn University, 2007.
- [8] J.T. Betts. Survey of Numerical Methods for Trajectory Optimization. *Journal of Guidance, Control and Dynamics*, Vol. 21, No. 2, pp. 193-207, 1998.
- [9] M.A. Bille and R. Kayne. Practical Microsat Launch Systems: Economics and Technology. *Proceedings of 17th Annual AIAA/USU Conference on Small Satellites*, 2003.
- [10] M.A. Bille and E. Lishock. Smallsat Launch Options: Choices and Challenges. *Proceedings of 10th Annual AIAA/USU Conference on Small Satellites*, 1996.
- [11] W.B. Blake. Missile Datcom: 1997 Status and Future Plans. *AIAA Paper 97-2280*, 1997.

- [12] W.B. Blake. *Missile DATCOM User Manual - 1997 FORTRAN 90 Revision*. Wright Patterson Air Force Base, AFRL-VA-WP-TR-1998-3009, 1998.
- [13] F.W. Boltz. Optimal Ascent Trajectory for Efficient Air Launch into Orbit. *Journal of Spacecraft and Rockets*, Vol. 41, No. 1, pp. 153-157, 2004.
- [14] R.D. Braun, R.W. Powell, R.A. Lepsch, and D.O. Stanley. Comparison of Two Multidisciplinary Optimization Strategies for Launch-Vehicle Design. *Journal of Spacecraft and Rockets*, Vol. 32, No. 3, pp. 404-410, 1995.
- [15] F. Castellini. *Multidisciplinary Design Optimization for Expendable Launch Vehicles*. PhD dissertation, Politecnico di Milano, 2012.
- [16] F. Castellini and M.R. Lavagna. Comparative Analysis of Global Techniques for Performance and Design Optimization of Launchers. *Journal of Spacecraft and Rockets*, Vol. 49, No. 2, pp. 274-285, 2012.
- [17] A.C. Charania. *Generation Orbit*. Team Phoenicia/Techshop Nanosat Launcher Seminar, 2011. Web site: <http://www.youtube.com/watch?v=Ib-vgzNW7RY> [Last accessed: March 15th, 2013].
- [18] A.C. Charania, D. DePasquale, S. Matsuda, and H. Kanayama. Analysis of the Earth-to-Orbit Launch Market for Nano and Microsatellites. *61st International Astronautical Congress 2010, IAC 2010 7*, pp. 5791-5801, 2010.
- [19] M. Burnside Clapp. Airborne Launch Assist Space Access (ALASA). DARPA, March 27th 2012. Web site: http://www.darpa.mil/WorkArea/DownloadAsset.aspx/04_20120327_SeeMeID_ALASA-1 [Last accessed: March 11th, 2013].
- [20] COESA. *1976: U.S. Standard Atmosphere*. NOAA, 1976.
- [21] J.W. Cornelisse, H.F.R. Schroyer, and K.F. Wakker. *Rocket Propulsion and Spaceflight Dynamics*. Pitman, 1979.
- [22] K.B. Dahle. North Star - The Flexible, Green and Safe Sounding Rocket and Satellite Launch Service. *Andøya Rocket Range*, 23 January 2013. Web site: <http://www.rocketrange.no/?p=1513> [Last accessed: September 29th, 2013].
- [23] B. D'Andrea. *Solid Rocket Motor Materials and Processes*. 12th Edition CVA Summer School, Avia SpA, July 8th 2011. Web site: <http://w3.uniroma1.it/summerschool2011/Materiali/D> [Last accessed: March 25th, 2013].
- [24] D. DePasquale and J. Bradford. Nano/Microsatellite Market Assessment. *Spaceworks Enterprises, Inc.*, February 2013. Web site: http://www.sei.aero/eng/papers/uploads/archive/SpaceWorks_NanoMicrosat_Market_Feb2013.pdf [Last accessed: October 5th, 2013].
- [25] D. DePasquale, A.C. Charania, S. Matsuda, and H. Kanayama. NanoLauncher: An Affordable and Dedicated Air-Launch Transportation Service for Nanosatellites. *AIAA Space 2010 Conference and Exposition, AIAA Paper 2010-8629*, 2010.

- [26] B.B. Donahue. Air-Launched Mini-Shuttle. *37th AIAA/ASME/SAE/ASEE Joint Propulsion Conference & Exhibit, AIAA Paper 2001-3963*, 2001.
- [27] B.B. Donahue. Beating the Rocket Equation: Air Launch with Advanced Chemical Propulsion. *Journal of Spacecraft and Rockets, Vol. 41, No. 2, pp. 302-309*, 2004.
- [28] Dutch Space B.V. *Ariane Interstages*. Dutch Space B.V., 2007. Web site: http://www.dutchspace.nl/pages/products/content.asp?id=157&P=2_7_2 [Last accessed: July 11th, 2013].
- [29] R. Eerkens. *The air launch of micro satellites to low Earth orbit*. Literature Study, TU Delft, 2012.
- [30] A. Elias. Q&A thread to Pegasus Designer Dr. Antonio Elias. *NASA Spaceflight Forum*, August 20th 2006. Web site: <http://forum.nasaspaceflight.com/index.php?topic=3911.15> [Last accessed: November 24th, 2012].
- [31] F.M. Engelen. *Quantitative risk analysis of unguided rocket trajectories*. MSc thesis, TU Delft, 2012.
- [32] R.R.L. Ernst. *Liquid Rocket Analysis (LiRA): Development of a Liquid Bi-Propellant Rocket Engine Design, Analysis and Optimization Tool*. Mid-term report MSc thesis, TU Delft, 2013.
- [33] ESA. *Launch Vehicle Catalogue*. Revision 15, European Space Agency, 2004.
- [34] European Launch Vehicle S.p.A. *Launcher Composition*. European Launch Vehicle S.p.A., 2013. Web site: <http://www.elv.it/en/launcher-vega/composizione-lanciatore/> [Last accessed: July 11th, 2013].
- [35] G. Fasano and J.D. Pinter. *Modeling and Optimization in Space Engineering*. Springer Optimization and Its Applications, Vol. 73, 2013.
- [36] Federal Aviation Authority. *Commercial Space Transportation: 2011 Year in Review*. Federal Aviation Authority, 2012.
- [37] E.L. Fleeman. *Missile Design and System Engineering*. AIAA Education Series, 2012.
- [38] J. Foust. New opportunities for smallsat launches. *The Space Review*, 22 August 2011. Web site: <http://www.thespacereview.com/article/1913/1> [Last accessed: June 22nd, 2013].
- [39] W. Frick, J. Guerci, and B. Horais. Responsive Air Launch. *2nd Responsive Space Conference, RS2-2004-8003*, 2004.
- [40] E.K.A. Gill. *Micro-Satellite Engineering*. Lecture Slides, V.1.4, TU Delft, 2010.
- [41] E.K.A. Gill. *Verifying and Validating*. Lecture Slides, Space Systems Engineering, V.1.0, TU Delft, 2012.

- [42] S. Gordon and B.J. McBride. *Computer Program for Calculation of Complex Chemical Equilibrium Compositions and Applications: I Analysis*. NASA Reference Publication 1311, 1994.
- [43] W.E. Hammond. *Design Methodologies for Space Transportation System*. AIAA Education, 2001.
- [44] D.Y. Hsu. Comparison of four gravity models. *Position Location and Navigation Symposium, IEEE*, 1996.
- [45] R.W. Humble, G.N. Henry, and W.J. Larson. *Space Propulsion Analysis and Design*. 1st edition, Learning Solutions, 1995.
- [46] T. Hunsaker, M.A. Bille, and P. Kolodziejwski. Nanosat Launch Vehicles: A Global Perspective and Business Case. *AIAA SPACE 2013 Conference and Exposition, AIAA Paper 2013-5513*, 2013.
- [47] S.J. Isakowitz, J.B. Hopkins, and J.P. Hopkins Jr. *International Reference Guide to Space Launch Systems*. 4rd edition, AIAA, 2004.
- [48] Jane's IHS. *All the World's Aircraft: Development & Production*. Online version, IHS Jane's, 2013. Web site: <http://janes.ihs.com> [Last accessed: July 9th, 2013].
- [49] G.E. Jensen and D.W. Netzer. *Tactical Missile Propulsion*. Progress in Astronautics and Aeronautics, Vol. 170, 1996.
- [50] Y. Kamm and A. Gany. Solid Rocket Motor Optimization. *44th AIAA/ASME/SAE/ASEE Joint Propulsion Conference & Exhibit, AIAA Paper 2008-4695*, 2008.
- [51] D.E. Koelle. Cost Engineering: The New Paradigm for Space Launch Vehicle Design. *Journal of Reducing Space Mission Cost, Vol. 1, pp. 73-86*, 1998.
- [52] D.E. Koelle. *TransCost 6.2 Statistical-Analytical Model for Cost Estimation and Economical Optimization of Space Transportation Systems*. TransCostSystems, 1998.
- [53] G.D. Krebs. *Gunter's Space Page*. G.D. Krebs, 2013. Web site: <http://space.skyrocket.de> [Last accessed: July 5th, 2013].
- [54] P. Kunhikrishnan, L. Sowmianarayanan, and M. Vishnu Nampoothiri. PSLV-C19/RISAT-1 Mission: the Launcher Aspects. *Current Sciences, Vol. 104, No. 4, pp. 472-476*, 2013.
- [55] W. Lan. *Poly Picosatellite Orbital Deployer Mk III ICD*. The CubeSat Program, California Polytechnic State University, 2007.
- [56] J. Lee, B. Park, and K. Jeon. Mission and Trajectory Optimization of the Air-Launching Rocket System Using MDO Techniques. *9th AIAA/ISSMO Symposium on Multidisciplinary Analysis and Optimization, AIAA Paper 2002-5492*, 2002.

- [57] K.S. Lee and N. Sarigul-Klijn. Computational Prediction and Comparison of Ground versus Air Launched Rocket Noise. *43rd AIAA/ASME/SAE/ASEE Joint Propulsion Conference & Exhibit, AIAA 2007-5756*, 2007.
- [58] Lockheed Martin Astronautics. *Atlas Launch System Mission Planners Guide*. Revision 7, 1998.
- [59] E. Louaas, C. Talbot, J. Berenbach, P. Gonzalez Gotor, A. Ruiz Merino, J. Longo, M. Sippel, and L. Frobel. Aldebaran: A "System" Demonstrator Project for New Generations of Space Transportation, Now Entering in the Phase A. *60th International Astronautical Congress, IAC-09-D2.6.7*, 2009.
- [60] A.W. Markl. *An Initial Guess Generator for Launch and Reentry Vehicle Trajectory Optimization*. PhD dissertation, Universtat Stuttgart, 2001.
- [61] P. Martino. *Costs and Risks Analysis Tool for Conceptual Launch Vehicle MDO*. MSc thesis, Politecnico di Milano, 2010.
- [62] J.R.R.A. Martins and A.B. Lambe. Multidisciplinary design optimization: A Survey of architectures. *AIAA Journal*, in press, 2013.
- [63] A.F. Maurice. *Aerodynamic Performance Predictions of a SA-2 Missile using Missile Datcom*. MSc thesis, Naval Post Graduate School Monterey, 2009.
- [64] B.J. McBride and S. Gordon. *Computer Program for Calculation of Complex Chemical Equilibrium Compositions and Applications: I Users Manual and Program Description*. NASA Reference Publication 1311, 1996.
- [65] S. McParlin. *Personal communication*. Lecturer in Aerodynamics, London City University, 2013.
- [66] M.R. Mendenhall, H.S.Y. Chou, and J.F. Love. Computational Aerodynamic Design and Analysis of Launch Vehicles. *38th Aerospace Sciences Meeting & Exhibit, AIAA Paper 2000-0385*, 2000.
- [67] M.R. Mendenhall, D.J. Lesieutre, C.H. Whittaker, R.E. Curry, and B. Moulton. Aerodynamic analysis of Pegasus - Computations vs reality. *31st Aerospace Sciences Meeting and Exhibit, AIAA Paper 93-0520*, 1993.
- [68] D. Messier. Generation Orbit Wins NASA Contract for Dedicated CubeSat Launch. *Parabolic Arc*, September 30th 2013. Web site: <http://www.parabolicarc.com/2013/09/30/generation-orbit-wins-nasa-contract-dedicated-cubesat-launch/> [Last accessed: November 5th, 2013].
- [69] E. Mooij. *The motion of a vehicle in a planetary atmosphere*. Delft University Press, 1997.
- [70] E. Mooij. *Re-entry Systems*. Lecture Notes, TU Delft, 2011.
- [71] M. Mosier and E. Rutkowski. Pegasus XL Development and L-1011 Pegasus Carrier Aircraft. *Proceedings of 7th Annual AIAA/USU Conference on Small Satellites*, 1993.

- [72] J.A. Mulder, W.H.J.J. van Staveren, J.C. van der Vaart, and E. de Weert. *Flight Dynamics AE3-302*. Lecture Notes, TU Delft, 2007.
- [73] NASSA. *None Cone Design*. Nevada Aerospace Science Associates, 2009.
- [74] Nationaal Lucht- en Ruimtevaartlaboratorium. Norway and Netherlands sign Technical Arrangement Military Use of Space. *Nationaal Lucht- en Ruimtevaartlaboratorium*, September 24th 2013. Web site: <http://wp.nlr.nl/en/2013/09/24/noorwegen-en-nederland-ondertekenen-technical-arrangement-military-use-of-space/> [Last accessed: September 29th, 2013].
- [75] G.K. Noffz, R.E. Curry, E.A. Haering, and P. Kolodziej. *Aerothermal Test Results from the First Flight of the Pegasus Air-Launched Space Booster*. NASA Technical Memorandum 4330, 1991.
- [76] R. Noomen. *AE4-878 Space Mission Design: Integrators*. Lecture slides, V. 4-1, TU Delft, 2012.
- [77] R. Noomen. *AE4-878 Space Mission Design: Optimization*. Lecture slides, V. 4-4, TU Delft, 2012.
- [78] R.A. O’Leary and J.E. Beck. Nozzle Design. *Pratt & Whitney Rocketdyne’s Engineering Journal of Power Technology*, 1992. Web site: <http://www.pwrengineering.com/articles/nozzledesign.htm> [Last accessed: April 2nd, 2013].
- [79] Orbital. *Taurus Launch System Payload User Guide*. Release 4.0, 2006.
- [80] Orbital. *Pegasus User Guide*. Release 7.0, 2010.
- [81] T.L. Paez. Introduction to Model Validation. *Proceedings of the IMAC-XXVII*, 2009.
- [82] A. Pagano. *Global Launcher Trajectory Optimization for Lunar Base Settlement*. MSc thesis, TU Delft, 2010.
- [83] PaGMO/PyGMO. *PaGMO/PyGMO Wiki*. SourceForge, 2013. Web site: http://sourceforge.net/apps/mediawiki/pagmo/index.php?title=Main_Page [Last accessed: June 24th, 2013].
- [84] R.C. Parkinson. The An-225/Interim Hotol Launch Vehicle. *3rd AIAA International Space Plane Conference, AIAA Paper 91-5006*, 1991.
- [85] A.F. Rafique, H. Lin Shu, A. Kamran, and Q. Zeeshan. Multidisciplinary design of air launched satellite launch vehicle: Performance comparison of heuristic optimization methods. *Acta Astronautica, Vol. 67, Is. 7 and 8, pp. 826-844*, 2010.
- [86] A.V. Rao. A Survey of Numerical Methods for Optimal Control. *AAS/AIAA Astrodynamics Specialist Conference, AAS Paper 09-334*, 2009.
- [87] L. Ridolfi, M. Pontan, and P. Teofilato. Effect of different flight conditions at the release of a small spacecraft from a high performance aircraft. *Acta Astronautica, Vol. 66, Is. 5-6, p. 665-673*, 2010.

- [88] R.R. Rohrschneider. *Development of a Mass Estimating Relationship Database for Launch Vehicle Conceptual Design*. AE 8900, Georgia Institute of Technology, 2002.
- [89] M. Sarigul-Klijn and N. Sarigul-Klijn. A Study of Air Launch Methods for RLVs. *AIAA Paper 2001-4619*, 2001.
- [90] M. Sarigul-Klijn, N. Sarigul-Klijn, G.C. Hudson, and C. Brown. A New Air Launch Concept: Vertical Air Launch Sled (VALS). *AIAA SPACE 2012 Conference and Exposition, AIAA Paper 2012-5156*, 2012.
- [91] M. Sarigul-Klijn, N. Sarigul-Klijn, G.C. Hudson, L. Holder, B. McKinney, L. Menzel, and E. Grasbow. Trade Studies for Air Launching a Small Launch Vehicle from a Cargo Aircraft. *AIAA Aerospace Sciences Meeting and Exhibit 2005, AIAA Paper 2005-0621*, 2005.
- [92] N. Sarigul-Klijn, C. Noel, and M. Sarigul-Klijn. Air-Launching Earth to Orbit: Effects of Launch Conditions and Vehicle Aerodynamics. *42nd AIAA Aerospace Sciences Meeting and Exhibit, AIAA Paper 2004-872*, 2004.
- [93] N. Sarigul-Klijn, M. Sarigul-Klijn, and C. Noel. Air-Launching Earth to Orbit: Effects of Launch Conditions and Vehicle Aerodynamics. *Journal of Spacecraft and Rockets, Vol. 42, No. 3, pp. 569-575*, 2005.
- [94] J.J. Sellers. *Investigation into Hybrid Rockets and Other Cost-Effective Propulsion Systems Options for Small Satellites*. PhD dissertation, University of Surrey, 1996.
- [95] T.J. Sooy and R.Z. Schmidt. Aerodynamic Predictions, Comparisons, and Validations Using Missile DATCOM (97) and Aeroprediction 98 (AP98). *Journal of Spacecraft and Rockets, Vol. 42, Is. 2, pp. 257-265*, 2005.
- [96] SPACEandTECH. Expendable Launch Vehicle Database Taurus - Specifications. *SPACEandTECH.com*, 2001. Web site: http://www.spaceandtech.com/spacedata/elvs/taurus_specs.shtml [Last accessed: June 7th, 2013].
- [97] StratoLaunch Systems. *StratoLaunch Systems*. StratoLaunch Systems Inc., 2013. Web site: <http://www.stratolaunch.com> [Last accessed: September 11th, 2013].
- [98] G.P. Sutton and O. Biblarz. *Space Propulsion Elements*. 7th edition, John Wiley & Sons, 2001.
- [99] O. Trivailo, M. Sippel, and Y.A. Sekercioglu. Review of hardware cost estimation methods, models and tools applied to early phases of space mission plannings. *Progress in Aerospace Sciences, Vol. 53, pp. 1-17*, 2012.
- [100] TU Delft. *TU Delft Astrodynamics Toolbox*. TU Delft, 2012. Web site: <http://tudat.tudelft.nl> [Last accessed: July 20th, 2013].
- [101] M.J.L. Turner. *Rocket and Spacecraft Propulsion: Principles, Practice and New Developments*. 2nd edition, Springer, 2005.

- [102] Ministerie van Defensie (Ministry of Defense). *Strategie-, kennis- en innovatieagenda Defensie: anticiperen en innoveren in een veranderlijke wereld*. Ministerie van Defensie (Ministry of Defense), 2011. (in Dutch).
- [103] M.W. van Kesteren. *Air Launch versus Ground Launch*. Literature Study, TU Delft, 2013.
- [104] M.W. van Kesteren. *Research Plan - Influence of Launch Conditions on the Design and Performance of an Air Launched Vehicle*. TU Delft, 2013.
- [105] A.J.P. van Kleef. *Personal communication*. R&D Space Engineer at Nationaal Lucht- en Ruimtevaart Laboratorium, 2013.
- [106] A.J.P. van Kleef and B.A. Oving. *Affordable Launch Opportunities for Small Satellites (ALOSS)*. Nationaal Lucht- en Ruimtevaartlaboratorium, Report no. NLR-TR-2012-136, 2012.
- [107] M. van Pelt. *Personal communication*. Cost Engineer ESA/ESTEC, 2013.
- [108] J. Vandamme. *Assisted-Launch Performance Analysis Using Trajectory and Vehicle Optimization*. MSc thesis, TU Delft, 2012.
- [109] J. Vandamme. *Study on the Effect of Assisted Launch on Launch Vehicle Performance*. Literature Study, TU Delft, 2012.
- [110] H.G. Visser. *AE4212 Aircraft Performance Optimization*. Lecture Notes, TU Delft, 2010.
- [111] S.R. Vukelich, S.L., Stoy, K.A. Bruns, J.A. Castillo, and M.E. Moore. *Missile Datcom, Volume I - Final Report*. Air Force Flight Dynamics Laboratory, AFWAL-TR-86-3091, 1986.
- [112] M. Wade. *Encyclopedia Astronautica*. M. Wade, 2013. Web site: <http://www.astronautix.com> [Last accessed: March 23th, 2013].
- [113] K.F. Wakker. *Astrodynamics I - AE4-874, Part I*. Lecture Notes, TU Delft, 2007.
- [114] K.F. Wakker. *Astrodynamics I - AE4-874, Part II*. Lecture Notes, TU Delft, 2007.
- [115] G. Webb, E. Motorny, N. Pestmal, and O. Sokolov. The Market for Launching Small Satellite in Russia, its Present Situation and Likely Future Trends. *CommercialSpace.co.uk*, 2007. Web site: <http://www.commercialspace.co.uk/rus/wp-content/uploads/2011/06/THE-MARKET-FOR-LAUNCHING-SMALL-SATELLITE-IN-RUSSIA-ITS-PRESENT.pdf> [Last accessed: February 26th, 2013].
- [116] J.C. Whitehead. How Small Can a Launch Vehicle Be? *41st AIAA/ASME/SAE/ASEE Joint Propulsion Conference & Exhibit, AIAA Paper 2005-4506*, 2005.
- [117] J.C. Whitehead. Air Launch Trajectories to Earth Orbit. *42nd AIAA/ASME/SAE/ASEE Joint Propulsion Conference & Exhibit, AIAA Paper 2006-4785*, 2006.

-
- [118] R.L. Willer, M.S. Chi, R. Gleeson, and J.C. Hill. Diaminoglyoxime and diamino-furazan in propellants based on ammonium perchlorate. *US Patent 5071495 A*, 1990.
- [119] D.H. Wolpert and W.G. Macready. No Free Lunch Theorems for Optimization. *IEEE Transactions on Evolutionary Computation*, Vol. 1, No. 1, pp. 67-82, 1997.
- [120] B.T.C. Zandbergen. *AE4-S01 Thermal Rocket Propulsion*. Lecture Notes, Version 2.04, TU Delft, 2010.
- [121] B.T.C. Zandbergen. *AE1222-II: Aerospace Design & Systems Engineering Elements I, Launcher design and sizing*. Lecture Notes, TU Delft, 2012.
- [122] B.T.C. Zandbergen. *Personal communication*. Senior Lecturer, TU Delft, 2013.

